FU JEN STUDIES

SCIENCE AND ENGINEERING

NO. 26 1992

目 次 CONTENTS

續 (Continued)

Fu Jen Catholic University
Taipei, Taiwan, Republic of China

目 次（續） CONTENTS (Continued)

GENERALIZED BERNSTEIN-BEZIER TRIANGULAR PATCHES AND GEOMETRIC PROPERTIES OF CURVES

CHING-HER LIN

Graduate Institute of Mathematics
Fu Jen University
Taipei, Taiwan 24205, R.O.C.

ABSTRACT

The generalized Bernstein-Bezier curve possesses geometric construction algorithm and subdivision algorithm as the blending functions are chosen suitably. In addition, the triangular patches of the generalized Bernstein-Bezier polynomial are studied. The conditions of C^r and visual C^1 continuity across the common boundary of two patches are investigated as well.

1. INTRODUCTION

Over a dozen geometric properties have been considered to be desirable for computer aided geometric design (CAGD)[3~5]. Some of the geometric properties of generalized Bernstein-Bezier curve and surface have been discussed in Goldman's papers[3,4], where the two features, geometric construction algorithm and subdivision algorithm, are not given. The first part of this paper provides specific conditions for the blending functions to ensure that the generalized Bernstein-Bezier curve possesses these two geometric properties.

In addition, triangular generalized Bernstein-Bezier patch is defined. Triangles are more appropriate than rectangles for interpolation since the latter can only be used in the tensor product sets of points. Some surfaces, in particular, have intrinsically triangular parts in the rounded corner. Furthermore, it is important to ensure smoothness between composed patches. The C^r continuity across the common edge of two triangular patches and visual C^1 continuity connect triangular patches with rectangular ones are investigated.

2. GEOMETRIC PROPERTIES

The generalized Bernstein-Bezier curve is given by [6]

$$P(u)=\sum_{j=0}^{n}[\sum_{i=0}^{n} b_{ij}B_i^n(u)]V_j, \qquad 0\le u\le 1 \quad (1)$$

where V_0, V_1, ···, V, V_n are $n+1$ $3D$ points of a characteristic polygon, $b_{ij}\in IR$, $0\le i, j\le n$ and $B_i^n(u)$ are the classical Bernstein polynomials. The generalized Bernstein-Bezier curve studied in [3,4] are symmetric, possesses well-defined, convex hull and variation diminishing properties. Here, specific conditions are required for $\{b_{ij}: 0\le i, j\le n\}$ to guarantee the curve having geometric construction algorithm and subdivision algorithm.

(1) Geometric construction algorihm

A geometric construction algorithm provides a simple, numerically stable technique for evaluating $P(u)$ for any parameter u. The idea is to construct the auxiliary points.

$$V_j^k(u)=f_j^{n-1}(u)V_j^{k-1}(u)+s_j^{n-1}(u)V_{j+1}^{k-1}(u), \qquad k+j\le n$$

where $V_j^0(u)=V_j$ and $f_j^{n-1}(u)+s_j^{n-1}(u)=1$.

Equation (1) can be written as

$$P(u)=\sum_{j=0}^{n} D_j^n(u)V_j, \qquad 0\le u\le 1 \quad (2)$$

where

$$D_j^n(u)=\sum_{i=0}^{n} b_{ij}B_i^n(u), \qquad j=0, 1, \cdots, n \quad (3)$$

and

$$D_j^n(u)\equiv 0, \qquad \text{for } j<0 \text{ or } j>n \quad (4)$$

Lemma 1

If

$$\begin{cases} b_{(i+1)j}=\left(1-\dfrac{b_{(j+1)(j+1)}}{b_{jj}}\right)b_{ij}+\left(\dfrac{b_{jj}}{b_{(j-1)(j-1)}}\right)b_{i(j-1)}, & 0\le j\le i\le n-1 \\ b_{ij}=0, & 0\le i<j\le n \end{cases} \quad (5)$$

where $b_{11}, b_{22}, \cdots, b_{nn}$ are arbitrarily given n real numbers, $b_{00}=1$ and $b_{ij}=0$ if either $i<0$ or $j>0$, then

$$D_j^k(u)=f_j^{n-1}(u)D_j^{n-1}(u)+s_{j-1}^{n-1}(u)D_{j-1}^{n-1}(u), \qquad j=0, 1, \cdots, n \quad (6)$$

where

$$\left.\begin{aligned} f_j^n(u)&=1-\left(\frac{b_{(j+1)(j+1)}}{b_{jj}}\right)u, \\ s_j^n(u)&=\left(\frac{b_{(j+1)(j+1)}}{b_{jj}}\right)u, \qquad j=0, 1, \cdots, n-1 \end{aligned}\right\} \quad (7)$$

and

$$f_j^n(u)=s_j^n(u)=0, \qquad \text{for } j<0 \text{ or } j>n-1 \quad (8)$$

Proof

It follows from Eqs. (3), (5), (7) and the Properties of the Bernstein polynomials we can obtain Eq. (6). In fact,

$$\begin{aligned} &f_j^{n-1}(u)D_j^{n-1}(u)+s_{j-1}^{n-1}(u)D_{j-1}^{n-1}(u) \\ &=\sum_{i=0}^{n-1}[b_{ij}f_j^{n-1}(u)+b_{i(j-1)}s_{j-1}^{n-1}(u)]B_i^{n-1}(u) \\ &=\sum_{i=0}^{n-1}\left\{b_{ij}(1-u)+u\left[\left(\frac{1-b_{(j+1)(j+1)}}{b_{ij}}\right)b_{ij}+\left(\frac{b_{jj}}{b_{(j-1)(j-1)}}\right)\cdot b_{i(j-1)}\right]\right\}B_i^{n-1}(u) \\ &=\sum_{i=0}^{n-1}b_{ij}(1-u)B_i^{n-1}(u)+\sum_{i=0}^{n-1}b_{(i+1)j}uB_i^{n-1}(u) \\ &=\sum_{i=0}^{n}b_{ij}(1-u)B_i^{n-1}(u)+\sum_{i=0}^{n}b_{ij}uB_{i-1}^{n-1}(u) \\ &=\sum_{i=1}^{n}b_{ij}B_i^n(u)=D_j^n(u). \end{aligned}$$

Let

$$D[V_1, V_2, \cdots, V_n](u)=P(u)=\sum_{j=0}^{n}D_j^n(u)V_j.$$

Then the following results can be proved.

Lemma 2

Under condition (5), we have

$$D[V_0^1(u), \cdots, V_{n-1}^1(u)](u)=D[V_0, \cdots, V_n](u).$$

Proof

$$\begin{aligned}
D[V_0^1(u), \cdots, V_{n-1}^1(u)](u)&=\sum_{j=0}^{n-1} D_j^{n-1}(u)V_j^1(u)\\
&=\sum_{j=0}^{n-1} D_j^{n-1}(u)f_j^{n-1}(u)V_j+\sum_{j=0}^{n-1} D_j^{n-1}(u)s_j^{n-1}V_{j+1}\\
&=\sum_{j=0}^{n} [f_j^{n-1}(u)D_j^{n-1}(u)+s_{j-1}^{n-1}D_{j-1}^{n-1}(u)]V_j\\
&=\sum_{j=0}^{n} D_j^n(u)V_j=D[V_0, \cdots, V_n](u).
\end{aligned}$$

Lemma 3

Under condition (5), we obtain

$$D[V_0^k(u), \cdots, V_{n-k}^k(u)](u)=D[V_0, \cdots, V_n](u).$$

Proof

It follows from Lemma 2 and mathematical induction on k. In particular, if $k=n$ then $V_0^n(u)=P(u)$.

(2) **Subdivision algorithm**

Subdivision algorithms are important in computer aided design because they help trimming curves. In addition, they allow us to apply formulas, which are initially developed only for the end points of a curve where the parameter is 0 or 1, at arbitrary location along the curve.

The functions, $\{B_i^n(u)\}$ satisfy the identity

$$B_i^n(ru)=\sum_{k=0}^{n} B_{nik}(r)B_k^n(u)$$

where r and $B_{nik}(r)$ are constants[5]. Let det $M\neq 0$ where $M=(b_{ij})$ is an $(n+1)\times(n+1)$ matrix. Then the inverse M^{-1} of M is defined as

$$M^{-1}=(\det M)^{-1}\mathrm{adj}\ M$$

where adj M is the classical adjoint of M

$$(\text{adj}\, M)_{ij}=(-1)^{i+j}\det M(j\,|\,i)$$

where the scalar $(-1)^{i+j}\det M(j\,|\,i)$ is called the j, i cofactor of M. Let

$$W_j(r)=\sum_{k,h,\ell=0}^{n}(\det M)^{-1}(\text{adj}\, M)_{j\ell}B_{nh\ell}(r)b_{hk}(r)b_{hk}V_k, \qquad i=0,\ 1,\ \cdots,\ n.$$

Proposition 4

$$D[W_0(r),\ \cdots,\ W_n(r)](u)=D[V_0,\ \cdots,\ V_n](ru).$$

Proof

$$\begin{aligned}
&D[W_0(r),\ \cdots,\ W_n(r)](u)\\
&=\sum_{j=0}^{n}\Big(\sum_{i=0}^{n}b_{ij}B_i^n(u)\Big)W_j(r)\\
&=\sum_{k,h,i,\ell=0}^{n}\Big(\sum_{j=0}^{n}b_{ij}(\det M)^{-1}(\text{adj}\, M)_{j\ell}\Big)B_{nh\ell}(r)B_i^n(u)b_{hk}V_k\\
&=\sum_{k,h,i=0}^{n}B_{nhi}(r)B_i^n(u)b_{hk}V_k\\
&=\sum_{k=0}^{n}\sum_{h=0}^{n}b_{hk}B_h^n(ru)V_k=D[V_0,\ \cdots,\ V_n](ru).
\end{aligned}$$

Thus, if $\det M\neq 0$ then the points $W_0(r)$, $\cdots$, $W_n(r)$ subdivide the curve $P(u)$ from $P(0)$ to $P(r)$. By utilizing symmetry (i.e., $b_{(n-i)(n-j)}=b_{ij}$), we can subdivide the curve $P(u)$ from $P(r)$ to $P(1)$. Using these two subdivision algorithms one after the other, the curve $P(u)$ between any two points $P(r)$ and $P(s)$ can thus be subdivided.

3. TRIANGULAR PATCHES AND CONTINUITIES

Let $\boldsymbol{i}=(i_1,\ i_2,\ i_3)$, $\boldsymbol{j}=(j_1,\ j_2,\ j_3)$; where $i_k,\ j_k\geq 0$, $k=1,\ 2,\ 3$, $[\boldsymbol{i}]=i_1+i_2+i_3$; and a triangle $\boldsymbol{T}$ in the xy plane be defined by its three vertices P_1, P_2, P_3 in $\mathcal{R}^2$. Let $P\in\mathcal{R}^2$ be an arbitrary point, it has the unique representation

$$P=\sum_{i=1}^{3}u_iP_i, \qquad u_1+u_2+u_3=1.$$

P is said to have barycentric coordinates $\boldsymbol{u}=(u_1,\ u_2,\ u_3)$ with respect to

T. Triangular generalized Bernstein-Bezier patches can be defined as follows:

$$P(\boldsymbol{u})=\sum_{|j|=n} c_j[\sum_{|i|=n} b_i^j B_i^n(\boldsymbol{u})] \tag{9}$$

where

$$B_i^n(u)=\frac{n!}{i_1!i_2!i_3!}u_1^{i_1}u_2^{i_2}u_3^{i_3}$$

and $B_i^n(\boldsymbol{u})=0$ if at least one i_k violates the condition $0\leq i_k\leq n^{(2)}$. The polynomial Eq. (9) can be written as

$$P(\boldsymbol{u})=\sum_{|i|=n} d_i B_i^n(\boldsymbol{u})$$

where

$$d_i=\sum_{|j|=n} c_j b_i^j$$

(1) C^r continuity

Let $\hat{T}$ be an adjacent triangle to T with vertices $\hat{P}_1$, P_2, P_3 and denote barycentric coordinates in $\hat{T}$ by $\hat{u}$. The straight line P_2P_3 is the common boundary of these two triangles and corresponds to barycentric coordinates $\boldsymbol{u}_0=(0, u_2, u_3)$ and $\hat{\boldsymbol{u}}_0=(0, \hat{u}_2, \hat{u}_3)$. Let the vertex $\hat{P}_1$ have barycentric coordinates $\boldsymbol{v}=(v, v_2, v_3)$ with respect to T:

$$\hat{P}_1=v_1P_1+v_2P_2+v_3P_3; \qquad v_1+v_2+v_3=1.$$

Thus, $u_1=\hat{u}_1v_1$, $u_2=\hat{u}_1v_2+\hat{u}_2$, $u_3=\hat{u}_1v_3+\hat{u}_3$ where $v_1\neq 0$.

A polynomial $P(\boldsymbol{u})$ that is defined in terms of barycentric coordinates of T can also be defined over $\hat{T}$. That is,

$$P(u)=\sum_{|i|=n} d_i B_i^n(\boldsymbol{u})=\sum_{|i|=n} \hat{d}_i B_i^n(\hat{\boldsymbol{u}}).$$

Note that since T and $\hat{T}$ have a common boundary, we have

$$d_{i_0}=\hat{d}_{i_0}, \qquad |\boldsymbol{i}_0|=n,$$

where $\boldsymbol{i}_0=(0, i_2, i_3)$.

In order to determine the remaining d_i, we consider a direction not parallel to P_2P_3 and take directional derivatives up to order r with respect to it. Let this direction be expressed as $\boldsymbol{a}$ with respect to $\boldsymbol{T}$ and as $\hat{\boldsymbol{a}}$ with respect to $\hat{\boldsymbol{T}}$. Since the sth directional derivative of a Bernstein polynomial B_i^n is given by [2]

$$D_a^s B_i^n(\boldsymbol{u})=\frac{n!}{(n-s)!}\sum_{|k|=s} B_k^s(\boldsymbol{a})B_{i-k}^{n-s}(\boldsymbol{u}),$$

therefore

$$D_a^s P(\boldsymbol{u})=\frac{n!}{(n-s)!}\sum_{|i|=n-s}\Big[\sum_{|k|=s} d_{i+k}B_k^s(\boldsymbol{a})\Big]B_i^{n-s}(\boldsymbol{u}) \tag{10}$$

and

$$\sum_{|i|=n-s}\Big[\sum_{|k|=s} d_{i+k}B_k^s(\boldsymbol{a})\Big]B_i^{n-s}(\boldsymbol{u})=\sum_{|i|=n-s}\Big[\sum_{|k|=s} \hat{d}_{i+k}B_k^s(\hat{\boldsymbol{a}})\Big]B_i^{n-s}(\hat{\boldsymbol{u}}). \tag{11}$$

Specifically, evaluated Eq. (10) along P_2P_3, we obtain

$$D_a^s P(\boldsymbol{u}_0)=\frac{n!}{(n-s)!}\sum_{|i_0|=n-s}\Big[\sum_{|k|=s} d_{i_0+k}B_k^s(a)\Big]B_{i_0}^{n-s}(\boldsymbol{u}_0).$$

Therefore Eq. (11) becomes

$$\sum_{|i_0|=n-s}\Big[\sum_{|k|=s} d_{i_0+k}B_k^s(\boldsymbol{a})\Big]B_{i_0}^{n-s}(\boldsymbol{u}_0)=\sum_{|i_0|=n-s}\Big[\sum_{|k|=s} \hat{d}_{i_0+k}B_k^s(\hat{\boldsymbol{a}})\Big]B_{i_0}^{n-s}(\hat{\boldsymbol{u}}_0),$$
$$s=0,\ \cdots,\ r;\ 0\le r\le n. \tag{12}$$

Since $\boldsymbol{u}_0=\hat{\boldsymbol{u}}_0$, it follows from Eq. (12), we get

$$\sum_{|k|=s} d_{i_0+k}B_k^s(\boldsymbol{a})=\sum_{|k|=s} \hat{d}_{i_0+k}B_k^s(\hat{\boldsymbol{a}}), \qquad s=0,\ \cdots,\ r;\ 0\le r\le n. \tag{13}$$

Because

$$D_a^s\Big[\sum_{|k|=s} d_{i_0+k}B_k^s(\boldsymbol{u})\Big]=s!\sum_{|k|=s} d_{i_0+k}B_k^s(\boldsymbol{a}), \tag{14}$$

if follows from Eqs. (13) and (14) we have

$$D_a^s\Big[\sum_{|k|=s} d_{i_0+k}B_k^s(\boldsymbol{u})\Big]=D_a^s\Big[\sum_{|k|=s} \hat{d}_{i_0+k}B_k^s(\hat{\boldsymbol{u}})\Big], \qquad s=0,\ \cdots,\ r;\ 0\le r\le n$$

and hence

$$\sum_{|k|=r} d_{i_0+k}B_k^r(\boldsymbol{u})=\sum_{|k|=r} \hat{d}_{i_0+k}B_k^r(\boldsymbol{u}), \qquad 0\le r\le n.$$

Taking $\boldsymbol{u}=\boldsymbol{v}$, i.e., for $\hat{\boldsymbol{u}}=(1, 0, 0)$, we obtain

$$\sum_{|k|=r} d_{i_0+k}B_k^r(\boldsymbol{v})=\hat{d}_{i_0+(r,0,0)}, \qquad 0\leq r\leq n. \quad (15)$$

Having r on all values from 0 to n, Eq. (15) provides an algorithm to construct the desired $\hat{d}_i$ from the given d_i. Moreover, let $P(u)$ be defined over P_1, P_2, P_3 and $P(\hat{\boldsymbol{u}})$ be defined over $\hat{P}_1$, P_2, P_3. Then a necessary and sufficient condition for $P(\boldsymbol{u})$ and $P(\hat{\boldsymbol{u}})$ to be C^r across the common boundary is

$$\hat{d}_{i_0+(s,0,0)}=\sum_{|k|=s} d_{i_0+k}B_k^s(\boldsymbol{v}), \qquad 0\leq s\leq r.$$

That is,

$$\sum_{|j|=n} \hat{c}_j b^j_{i_0+(s,0,0)}=\sum_{|k|=s}\Big(\sum_{|j|=n} c_j b^j_{i_0+k}\Big)B_k^s(\boldsymbol{v}), \qquad 0\leq s\leq r.$$

(2) Visual C^1 continuity

In this subsection, we will connect triangular patches with rectangular ones. The smoothness condition between them, given by Farin[1] will be utilized. Let ϕ and ψ be two surface patches that have a common boundary curve $\xi(v)$, and $(D\xi)(v)$ denotes the tangent vector of $\xi(v)$. Let $(D_1\phi)(v)$ denote a cross boundary derivative of ϕ at $\xi(v)$, i.e., $(D_1\phi)(v)$ lies in the tangent plane of ϕ at $\xi(v)$ and is not collinear with $(D\xi)(v)$. And $(D_2\psi)(v)$ denotes for a cross boundary derivative of ψ at $\xi(v)$. A condition for visual C^1 continuity between ϕ and ψ is

$$\det[(D_1\phi)(v), (D_2\psi)(v), (D\xi)(v)]=0. \quad (16)$$

Let the rectangular patch ϕ be of degree n and the triangular patch ψ be of degree $n+1$. Then the common boundary curve ξ as a boundary for the rectangular patch ϕ must be of degree n, and as a boundary of the triangular patch ψ must be of degree $n+1$. The two patches, ϕ and ψ, are given as follows.

$$\phi(u,v)=\sum_{j=0}^{m}\sum_{k=0}^{n}\Big[\sum_{h=0}^{m} b_{hj}B_h^m(u)\Big]\Big[\sum_{i=0}^{n} b_{ik}B_i^n(v)\Big]V_{jk}, \qquad 0\leq u,\ v\leq 1$$

where the V_{jk} are vertices of the characteristic polyhedron that forms a $(m+1)\times(n+1)$ rectangular array of points, and

$$\psi(\boldsymbol{u})=\sum_{|i|=n+1} d_i B_i^{n+1}(\boldsymbol{u}).$$

The common boundary curve is

$$\xi(v)=\phi(0,\ v)=\psi(0,\ v,\ 1-v)$$

with the following forms

$$\xi(v)=\sum_{j=0}^{m}\sum_{k=0}^{n}(b_{0j}V_{jk})[\sum_{i=0}^{n} b_{ik}B_i^n(v)]=\sum_{|i0|=n+1} d_{i_0}B_{i_0}^{n+1}(0,\ v,\ 1-v).$$

Since

$$\sum_{|i|=n} d_i B_i^n(\boldsymbol{u})=\sum_{|i|=n+1}\hat{d}_i B_i^{n+1}(\boldsymbol{u})$$

where

$$\hat{d}_i=\frac{1}{n+1}\sum_{k=1}^{3} i_k d_{i-j_k},\qquad |i|=n+1,$$

and $\boldsymbol{j}_k=(j_1,\ j_2,\ j_3)$, $j_\ell=\begin{cases}0 & \ell\neq k\\ 1 & \ell=k,\end{cases}$ therefore, ϕ and ψ are continuous if and only if

$$d_{(0,i,n+1-i)}=\sum_{j=0}^{m}\sum_{k=0}^{n}\frac{1}{n+1}(ib_{(i-1)k}+(n+1-i)b_{ik})b_{0j}V_{jk}. \tag{17}$$

The first order partial derivatives of $\phi(u,\ v)$ at the common boundary are given by following formulas[6]

$$\phi_u(0,\ v)=m\sum_{i=0}^{n}(\sum_{j=0}^{m}\sum_{k=0}^{n}(b_{1j}-b_{0j})b_{ik}V_{jk})B_i^n(v) \tag{18}$$

$$\phi_v(0,\ v)=n\sum_{i=0}^{n-1}[\sum_{j=0}^{m}\sum_{k=0}^{n}(b_{(i+1)k}-b_{ik})b_{0j}V_{jk}]B_i^{n-1}(v). \tag{19}$$

For triangular patches, we shall consider a particular cross boundary derivative, i. e., taking $\boldsymbol{a}=(1,\ -v,\ v-1)$ in Eq. (10). Then

$$D_a\psi(0,\ v,\ 1-v)=(n+1)\sum_{i=0}^{n}(d_{(1,i,n-1)}-\sum_{j=0}^{m}\sum_{k=0}^{n}b_{ik}b_{0j}V_{jk})B_i^n(v). \tag{20}$$

The visual C^1 condition (16) is the form

$$\det[\phi_u(0, v),\ D_a\psi(0, v, 1-v),\ \phi_v(0, v)]=0.$$

Farin[1] proved that there exist constants μ, λ_0 and λ_1 such that

$$\mu\phi_u(0, v)+D_a\psi(0, v, 1-v)+[\lambda_0(1-v)+\lambda_1 v]\phi_v(0, v)=0. \tag{21}$$

It follows from Eqs. (18), (19), (20) and (21), we obtain

$$\sum_{i=0}^{n}\{(n+1)d_{(1,i,n-1)}-(n+1)\sum_{j=0}^{m}\sum_{k=0}^{n}b_{ik}b_{0j}V_{jk}$$
$$+m\mu\sum_{j=0}^{m}\sum_{k=0}^{n}(b_{1j}-b_{0j})b_{ik}V_{jk}+(n-i)\lambda_0\sum_{j=0}^{m}\sum_{k=0}^{n}(b_{(i+1)k}-b_{ik})b_{0j}V_{jk}$$
$$+i\lambda_1\sum_{j=0}^{m}\sum_{k=0}^{n}(b_{ik}-b_{(i-1)k})b_{0j}V_{jk}\}=0.$$

or

$$d_{(1,i,n-1)}=\sum_{j=0}^{m}\sum_{k=0}^{n}\left\{\left\{\left(\frac{i}{n+1}\right)\lambda_1 b_{(i-1)k}+\{1+[m\mu+(n-i)\lambda_0-i\lambda_1]\}b_{ik}\right.\right.$$
$$\left.\left.-\left(\frac{n-i}{n+1}\right)\lambda_0 b_{(i+1)k}\right\}b_{0j}-\left(\frac{m}{n+1}\right)\mu b_{ik}b_{1j}\right\}V_{jk}. \tag{22}$$

Therefore, Eqs. (17) and (22) are the conditions for the visual C^1 continuity connect triangular patches and rectangular ones at the common boundary.

4. CONCLUSIONS

The generalized Bernstein-Bezier curves, under conditions on $\{b_{ij}: 0\leq i,j\leq n\}$, holds the geometric construction algorithm and subdivision algorithm. The triangular patches of the generalized Bernstein-Bezier patches are defined. The smoothness conditions between patches are discussed.

REFERENCES

(1) G.E. Farin, "A Construction for the Visual C^1 Continuity of Polynomial Surface Patches", *Computer Graphics and Image Processing*, **20**, 272-282 (1982).

(2) G.E. Farin, "Smooth Interpolation to Scattered 3*D* Data", in: R.E. Barnhill and W. Boehm, eds., Surfaces in CAGD, North-Holland, Amsterdam.

(3) R.N. Goldman, "Markov Chains and Computer Aided Geometric Design: Part I—Problems and Contrains", *ACM Trans. Graph.*, **3**(3), 204-222 (1984).
(4) R.N. Goldman, "Markov Chains and Computer Aided Geometric Design: Part II—Examples and Subdivision Matrices", *ACM Trans. Graph.*, **4**(1), 12-40 (1985).
(5) R.N. Goldman, "Polya's urn Model and Computer Aided Geometric Design", *SIAM J. Alg. Discr. Meth.*, **6**(1), 1-28 (1985).
(6) C.H. Lin, "Generalized Bernstein-Bezier Curves and Surfaces", *Computer Aided Design*, **20**(5), 259-262 (1988).

推廣的伯恩斯坦-貝齊爾三角曲面片和曲線的幾何性質

林 清 河

輔仁大學數學研究所

摘 要

推廣的伯恩斯坦-貝齊爾曲線在適當的選擇混合函數下具有幾何結構算則和重分算則。本文中亦探討推廣的伯恩斯坦-貝齊爾三角曲面片在連接處具有連續性的條件。

HYPATIA OF ALEXANDRIA

YI-CHING YEN

Department of Mathematics

ABSTRACT

Flipping over the pages of world history, Hypatia of Alexandria in 370-415 A.D. clearly stands out as the first renowned woman mathemation, astronomer and philosopher.

Despite of her splendid career, she was brutally murdered by mobs of religious extremists.

Her tragic death marks the subsequent repression of intellectual women for as long as fifteen centuries.

"If you are inclined to lose faith in humanity, think of the brave of all times."

M. Deshumbert

Hypatia of Alexandria is the first famous woman mathematician, astronomer and philosopher that ever appeared in the world. We may find it out by reviewing the world history in the following:

In the ancient times, throughout the world, women rarely had the opportunity to receive education, let alone becoming well-known scholars.

Interestingly, however, we can find records of several famous woman scholars in the old China. One of the most representative women is Pan-Chau (ca. 49-120), a lady historian who continued to complete a classical historical volume "Hahnshu" after her father's and brother's death. Another example is Li Ching-Chau (1084-1151), a gifted poetess whose "tsyr", a form of Chinese lyric which resembles poems, is considered to be one of the best in the Chinese literature. Nonetheless, it was not until Ching Dynasty that a famous woman scientist was finally born. Wan Jen-Yi (1768-1797), a born scientist, who enjoyed investigating the nature with simple accessible tools had made some corrections to the recorded scientific observations of her Chinese predecessors. In addition, she was also skillful in both medicine and literature. Although she died at the young age of twenty nine, she had written several books in astronomy, geography, mathematics, medicine, poems and essays. Some

of the them are still extant. Historians praised her highly for her "versatility" and "virtuosity".

All these famous woman scholars came from intellecturl elite families and were educated at home. Their talents, dedication and accomplishments even outshone their contemporary male counterparts, lending the way to a new era of intellectually competitiveness for women.

In the west, science was a Greek invention, but its tools, writing and mathematics were developed in Egypt and Mesopotamia for some practical necessities.

It was from the great pyramid of Gizeh, erected at about 2900 B. C. that we found the first written history of science in Egypt. The Egyptians were interested in practical use of science. Priests and Priestesses, the most learned people of their times, developed such mathematics and astronomy as were applicable to problems at hand. Before 3000 B. C. medicine was already an established profession in Egypt and educated women engaged in its as doctors and surgeons. The Kahun medical papyrus (ca. 2500 B. C.), which might have been written by women, shows us the establishments of women surgeons[1]. The high level of training for the female physicians in Egypt suggests us the possibility of environment such that woman might have become a scientist[2].

The Babylonian history, which we studied from many tablets excavated at the site of ancient Nippur and the code of King Hammurabi (1728-1686 B. C.) tells us that the people of Mesopotamia—the Sumerians, Babylonians and Assyrians—were more advanced in science than Egyptians, particularly in observational astronomy. Even the oldest tablets (ca. 2100 B. C.) show a high level of computational ability of these people. They established sexagesimal positional system and made many computations in lists. One of the tablets called Plingtom 322 (ca. 1900-1600 B. C.) is a list of Pythagorean Triples. In those days women engaged in business, judges, elders and chemists, especially as perfumers. However, there were no records about other types of woman scientists.

Greek science began with Pythagoreans which brought women into the mainstream of developing natural philosophy and mathematics. Pythagoras (ca. 582-500 B. C.) of Samos had travelled all over the Mediterranean world and studied under many teachers. One of the

teachers was Delphic priestess Themistoclea, from whom, according to Greek philosopher Aristoxenus, that Pythagoras acquired most of his moral doctrines. It is likely for this reason that he had never refused women to study in the school he settled in the Greek colony of Croton between 540 to 520 B. C. There he founded a quasi-religious and quasi-political community, called Pythagorean Order, devoted to mathematical and philosophical investigation. The Pythagorean Order, included men and women in equal terms, had at least twenty eight woman teachers and students at that period of time. The most famous of them were his wife Theano and their two daughters. However, since all members of Pythagorean Order wrote under the name of Pythagoras, it is impossible to recognize individual contributions. Anyhow, women were indispensable part of the Order, it is reasonable to assume that women were involved in the research of this mathematical cosmology that so directly influenced the future development of science. After the democratic rebellion in Croton, Pythagorean School was destroyed. Still the offshoots of the Pythagorean School continued to include women throughout Greece and Egypt.

Outside of the Pythagorean Order, there were few opportunities for woman scientists in Greek society. In general, the Greeks were a patriarchal people and it was only in the militaristic city-state of Sparta that women had any degree of power. In Athens, the lawgiver Solon (ca. 683-599 B. C.) did not suggest educational equality between men and women and his attitude became the established situation of Athens. Thus, even most Athenian wealthy women were illiterate and were as secluded as the later women of Islam[3].

It was in classical Athens of fifth to fourth century B. C. that the natural philosophy, metaphysics, political ideology and mathematical thoughts of western civilization were first established. Then Athens entered a period of prosperity and intellectual greatness. The citizens of Athens (about ten per cent of the population) had enough time to take part in social activities of politics and culture, leaving the household chores to women and slaves. Attracted by the democratic form of the government in Athens, philosophers and mathematicians, many of them were Pythagoreans, gathered from everywhere of the Mediterranean area and they taught pupils knowledge and rhetoric with mathematical basis.

They were the first to make distinction between science and religion. They encouraged direct and careful observation of nature, and contributed to mathematics by making the use of whole notion of proofs, deduction and abstraction. "This is a discovery of unsuspected possibility of mind, which is one of the greatest steps in the development of human consciousness" (Sullivan, 1925).

Among the philosophers of that time, Socrates and Plato insisted that men and women are born equal and must have the same degree of education in order to support the whole society. But Aristotle, their most brilliant successor, believed that women were inferior to men, with their social position merely above slaves, not to mention receiving any kind of education. Aristotle's opinions of women, as on others, were to prevail in the western world for the next millennia. His bias against women resulted in a widespread belief that science was the region of the male[3].

Women, mostly foreigners from the Mediterranean world, in defiance of the law that forbade them to participate in public meetings, gathered to study at Plato's Academy in Athens, where the most important mathematical works of the fourth century B. C. were accomplished. Women in the Academy were used to dress as men in order to attend lectures unnoticed.

Since Athenian citizen could only marry another citizen's daughter by law, these foreign-born women who came to Athens for more study, formed a class in their own right as hetairae or courtesans, although they were well-educated, artistic and intellectual. The most famous among them was Aspasia (470-410 B. C.), born in Miletus of Ionia and daughter of Axiochus, a learned man who gave Aspasia good education. She came to Athens to take part in the intellectual life of the city. But on arrival, she found herself, as a foreigner, was classified as a courtesan. About 445 B. C., Aspasia lived with Pericules (495?-429 B. C.). She was said to have written many of his speeches, among them was his famous funeral oration (430 B. C.) for the the Athenians killed in the Peloponnesian War. In her salon the eminent people, among them was the astronomer Anaxagoras of Ionia, gathered to discuss about politics and science[3]. Plato in his "Dialogues" also tells us that she was a teacher of Socrates. It was her education and genius that won Aspasia her reputation.

Epicurus settled in Athens about 300 B. C., where he revived 'Atomism' of Democritus and Leucippus. His School was open to women and had educated some famous women.

Greece and the whole Mediterranean world were under the siege of Roman before 30 B. C. The Romans were less interested in science than the Greeks, and their culture never supported the development of mathematics. Women were inferior to men under the Roman law; yet their social status were far better than classic Athenean women and continued to improve over the five centuries of the Empire. Roman women learned to read and write, and upper-class matrons were educated by tutors. There were many women of strong character, mostly in politics and deeds, during the end of the first century and the beginning of the second century. After that, "the feminism" flourished in the imperial times which made women copy men's vices than in acquiring their strength. They seldom attended outdoor affairs. The ladies might devote themselves into music, literature, science, law or philosophy as a way of killing time, and men paid little attention to those so-called "blue-stockings".

Alexandria, a city of Egypt at the mouth of Nile, was founded by Alexander the Great (356-323 B. C.) in 332 B. C. and was designed by the eminent architect Dirocrates. In 306 B. C., Alexander's general Ptolemy Soter (or Ptolemy I, 367-283 B. C., ruled 323-285 B. C.), a Macedonian, began to reign Egypt. He selected Alexandria as the capital. As a disciple of Aristotle, he was distressed to find that scientific research in Egypt was hopelessly intertwined in established religion. He determined to change this situation, so he built a museum in Alexandria, which was a large institute devoted to research and teaching. The Museum contained lecture rooms, library, laboratories, gardens and living quarters. At about 300 B. C. he brought to Alexandria all the philosophers and scholars, among them was the famous mathematician Euclid, possible for him to invite. He then gave those scholars every effective encouragement, not only financially but also in plentiful books and manuscripts from Greece. The core of the Museum was its great library, which was the largest repository of learned works to be found anywhere in the world in nearly a millenary. Within forty years of its founding it boasted to have 600,000 papyrus rolls[4]. The later rulers of Egypt

continued to support the Museum until 30 B. C., when Ptolemy Dynasty was ended with the suicide of Queen Cleopatra who was defeated in the wars with Romans. This was also the end of the first period of intellectual activity in Alexandria, which was characterized by its nature as purely literary and scientific. After that Egypt was conquered by Romans, and the intellectual activities again became lively in Alexandria, which drew many Romans, Greeks and Jewish scholars to come there. This second school of thoughts was somewhat different from the first. The philosophy, blended different cultures, nationalities and varying personalities, develped into speculative philosophy of Neoplatonism[5]. Neoplatonism asserts that there is a supreme being or power, called the Absolute or One, mystic, remote and unapproachable by human beings in a direct way. It became a religion of many of the heathens[6]. Constantine the Great (ruled 306-337) was the first emperor who believed in Christianity and ordered it as the official religion in 313. He moved his capital from Rome to Byzantine in 330 and named it as Constantinople after his name. In 395 the Roman Empire was divided into the Eastern and the Western Empires, with Greece, Egypt and Asia Minor as the constituents of the eastern division. The economic structure of both empires was based on agriculture with a wide use of slave labor. The gradual decline of slave market effected on Roman economy, thereby reducing science to a mediocre level. The Alexandrian school gradually faded, along with the break up of the ancient society. Creative thinking gave way to compilation and commentarization. In 529 Emperor Justinian decreed to close the Alexandrian School. The Alexandrian library, as partly in existence at the hands of Christians, was put into fire at the fall of Alexadria to Arabs in 641.

The Roman authorities put a prefect, the governor; and a bishop, the head of Christian monks, in Alexandria. But the city of Alexandria in the fourth and fifth century was the most difficult place to rule in the whole Roman Empire. It consisted of many different nationalities, including Egyptians, Romams, Greeks and Jews, as well as various creeds such as pagans, Christians and Jews, and they all had opinions of their own, so that the people were stubborn, quick-tempered and suspicious. Especially Egyptians were hostile to Greco-Roman culture in their nature: they were ruled by Greeks and then by Romans for several centuries; they

even had to adore Greek deity Serapis brought to them by Ptolemy I, who built in Alexandria the most splendid and the best known temple of Serapis with a big library. Both of them were destroyed by Theodosius, the bishop of Alexandria, and his followers in 391 under the name of Roman Emperor Theodosius I. Owing to these reasons, there were numerous clashes, fights and tumults in the streets of Alexandria, not only between citizens and the soldiers, but also between different classes and religions of citizens themselves[7].

A slight scientific renaissance occurred in the fourth-century Alexandria and there flourished the most celebrated woman scientist Hypatia in the reign of about Arcadius (395-408). For fifteen centuries until the nineteen-century Hypatia was often considered to be the only female scientist in history[1].

Our knowledge of Hypatia is mainly from the celestial historians Socrates Scholastics (ca. 380-445)[8], Damascius (ca. 480-550)[9], Suidas (?-ca. 970)[10], Necephorus (806-815); her best known disciple Synesius of Cyrene (370-ca. 414)[11] and some other historians of her time. Hypatia was born about 370 in Alexandria and was murdered in March, 415. Her father Theon of Alexandria was a rather mediocre mathematician and astronomer, yet well-known for his extant commentaries on Ptolemy's "Almagest", "Handy Tables" and edition of Euclid's "Element" with rather unimportant additions and emendations[12]. We have no exact information about Hypatia's early life. However, being the daughter of Theon, who was associated with the Museum of Alexandria, we may assume that she was brought up in close touch with the Museum and that she received the greater part of her early education from Theon[13]. It was said that Theon intended to educate her to be 'a perfect human being', and in fact Theon must have labored much in teaching her, for Theon's biographers pointed out that all of his works were established in 360's and 370's and none thereafter, though he lived until 390's[12]. This record is an evidence against the assumption of some biographers who say that Hypatia was not born at 370, but twenty years earlier at 350. Another clue for Hypatia's correct birth year is that she was known to be still very attractive till her death in 415. It would be very unlikely for a woman of sixty five to remain very beautiful if she were born in 350. Also Synesius (370-ca. 414) said that she was of his age[14]. Hypatia

received a thorough training in arts, literature, science, philosophy and rhetoric of the time. However, it was not clear whether she had studied at Athens. Then she succeeded to the leadership of Platonic School of Alexandria. She was very beautiful, graceful and virtuous, but her fame rest on the manner she conducted at school. Everyone of that time praised her extraordinary eloquence and agreeable discourse in her lectures. She taught not only philosophy, but also scientific subjects such as mathematics, astronomy and physics[8]. Suidas said that she exceeded her father in mathematics and astronomy[10]. We may also assume that she taught some fundamentals of mechanics, because in one of Synesius' letters, he attributed to her for constructing an astrolable and in another letter, he asked her to order a hydroscope at Alexandria for him[14].

According to Suidas, she composed commentaries on Ptolemy's "Almagest", Diophantus' "Arithematica" and Appolonius' "Conic Sections"[10]. None of them survived. It was said that a portion of her original treatise "on the astronomical cannon of Diophantus" was found during the fifteenth century in the Vatican library, which was most likely taken there by the Turks, after the fall of Constantinople[3]. She is also credited for the revision of Book III of Theon's commentary on "Almagest" and she might have helped her father in the revision of Euclid's "Elements"[15]. All of the subjects she dealt with were the most advanced mathematical and astronomical topics of her time. It is a reasonable assumption that she had taught pupils on those scientific themes. For all her accomplishments described above, Hypatia has been considered as the first renowned woman mathematician and astronomer in the world.

Hypatia's philosophical lectures were on Plato, Aristotle and other philosophers. The contents of them were more scholarly and more scientific in their interests with less emphasis on the metaphysical and religious matters. Her philosophical acumen was reputed to have surpassed the best known philosophers of her time. People of all religions came from Europe, Africa and Asia to Alexandria to attend her lectures[14]. But her historical position in the sequence of Alexandrian thinkers does not quite match her fame[5], possibly due to the fact that her philosophical writings were not extant and she had not excellent disciples in philosophy in spite of having some brilliant disciples in literature, science and politics. It is strange why Suidas did not mention any of Hypatia's

works on philosophy, which might have many coexisted with her mathematical and astronomical ones in the library and were lost in the destruction and fires of the library caused by the mobs and later the fall of Alexandria to the Turks. Still Hypatia had acquired the name of the most famous woman philosopher of the world.

Among the most distinguished pupils of Hypatia are Synesius of Cyrene, Troillus, the teacher of Sorates Scholastics, Euoptius, the brother of Synesius and probably later Bishop of Tolemis, Olimpius, Hesychius the Jew and Herocles, the successor of Hypatia in the Platonic School of Alexandria. Above all, Synesius is the best known. He was a man of wide interests, a gifted and sensitive pupil of Hypatia[10]. Later he became a wealthy Bishop of Ptolemius. His essays, letters and hymns are extant and have been carefully studied. He was deeply interested in not only theoretical aspects of science but also its practical applications[11]. For example, once in his sick-bed, Synesius still requested Hypatia to have Alexandrian metal workers make him a hydroscope. He had made a silver astrolabe to present to his friend and also thought about to construct missiles which could hurl stones from the turrets[14]. About all these interesting ideas he had always consulted with Hypatia. To him she was his 'sister, mother, teacher and benefactress', as he called her in one letter. Once he sent her two books which he had written during that year. One was about debates, and he inquired her opinions about whether to publish the book. Another was completed by him in a single night under religious visions. It seemed that Hypatia was his best consultant in many fields. On his letter to his brother from his visit to Athens, Synesius wrote that "Today Egypt has received and cherished the fruitful wisdom of Hypathia. Athens was aforetime the dwelling place of the wise; today the beekeepers alone bring its honor, ..."[14]. His high praises for Hypatia were consistent with those of the people who were in contact with her[8].

Hypatia not only lectured in Museum but also had some kind of public position. She was a well-known public figure. Wearing the philosopher's tattered cloak, she would appear without fear in the center of Alexandria among men to hold open discussions. As a public speaker, she was always fluent and skillful. In her deeds she revealed her wisdom and statesmanship[9]. The citizen in general, admired and respected her

exceedingly, and it was to her house that new governors of Alexandria paid their first visits on their arrival at Alexandria. One of the officials closely associated with Hypatia toward the end of her life was Orestes, the Roman Prefect of Alexandria, a former student and long time friend of Hypatia[17].

On October 18, 412, Cyril (ca. 375-444) succeeded his uncle Theophilus to become Bishop of Alexandria. Soon after taking power, Cyril began prosecuting Jews, driving thousands of them from the city. Then he turned his attention to ridding the city of Neoplatonists, a group of scholars. His conducts began to infringe upon the civil authorities belonging to the Prefect Orestes and arose his anger. Frictions continued between these two until there was a definite break in their relation. Due to her intimacy with Orestes, many Christians charged that Hypatia was to blame for the odds between Orestes and Cyril, so she became an object of fear and hatred of those people. In March, in a holy season of Lent, a mob of Nitrian monks and the fanatical Christians carried her from her carriage on her way home from the Museum, dragged her to the Casareum, then a Christian church, stripped her naked, Peter the reader, a follower of Cyril, began to scrape her flesh from her bones with sharp oyster-shells and so did the merciless fanatical mobs. They tore her body to pieces, took the mangled limbs to a place called Cinaron and burned them to ashes with rice straws. Orestes, astonished at the brutal murder of Hypatia, reported the affair to Rome and requested an investigation. He then resigned and fled from Alexandria[8]. The investigation was repeatedly postponed for 'lack of witnesses' and eventually Cyril proclaimed that there had been no mob and no tragedy occurred, Hypatia was still alive and lived in Athens. Historians say that Cyril was responsible for Hypatia's death even if he did not take part in it. Certainly he could have prevented the mobs' violence had he made the slightest effort[17].

Hypatia was a virgin until her death. She was so beautiful and elegant that she might have had many admirers and suiters. But, according to the legend, she rejected all her persistent pursuers by saying that she married to "the truth"[7].

In an era when intellectual and political regions were monopolized by the male, Theon was a liberated person to teach and encourage his

unusually gifted daughter Hypatia to achieve things which no woman before her would have even dreamed of. She played her role splendidly and bravely, yet her life ended with a great tragedy. Her death also represented the end of an era in the ancient world when a brave woman could outshine her peers with her talents and dedication.

The martyrdom of Hypatia has been an inspiration and a source for many writers. There have been many novels and plays written in the name of Hypatia. One of the most famous books is written by Charles Kingsley in 1907[18]. There appeared in 1945 a book of Hypatia named "The Way of Life"[19], which is said to be compiled and transcribed from ancient records with the aid of Psychical Researcher Dr. John S. King. The contents of it was vividly and clearly written.

REFERENCES

(1) Alic, Margarett, "Hypatia's Heritage: A History of Women in Science from Antiquity Through the Nine-teenth Century", Beacon Press (1986).
(2) G. Clark, "Women in the Ancient World", Oxford Univ. Press, N.Y. (1989).
(3) M.B. Ogilivie "Women in Science: Antiquity Through the Nine-teenth Century", Cambridge, Mass., MIT Press (1986).
(4) H. Eves, "An Introduction to the History of Mathematics", Fourth ed., Holt, Rinehart and Winston, N.Y. (1953).
(5) Rist, John, "Hypatia", Phoenix, **19**, 214-225 (1965).
(6) A.W. Richeson, "Hypatia of Alexandria", *The Amer. J. of Math.*, **40**, 72-82 (1945).
(7) M.M. Mangasarian, "The Martyrdom of Hypatia", Pioneer Press, London (1921).
(8) Socrates Scholastics, "The Ecclessiastical History", Trans. by Henry Bohn (1853).
(9) "Hypatia, Dictionary of Greek and Roman Biography and Mythology", AMS Plus Inc. (1967).
(10) Suidas, Lexicon, ed. Ada Adler, Trans. by B.G. Teubner, I, Leipzig (1935).
(11) K.H. Dannenfeldt, "Synesius of Cyrene, Dictionary of Scientific Biography", Charles Scriber's Sons, N.Y. (1976).
(12) G.J. Toomer, "Theon of Alexandria, Dictionary of Scientific Biography", Charles Scriber's Sons, N.Y. (1976).
(13) E.E. Kramer, "Hypatia, Dictionary of Scientific Biography", Charles Scriber's Sons, N.Y. (1976).
(14) Synesius of Cyrene, "Letters of Synesius of Cyrene", Trans. by A. Fitzgerald, Oxford, 1926. Letters 10, 15, 16, 33, 81, 124 and 154 are to Hypatia, and are referred to her in 133, 136, 137 and 159.

(15) L.M. Osen, "Hypatia, Women in Mathematics", Cambridge, Mass., MIT Press (1974).
(16) J. Bregman, "Synesius of Cyrene", Berkeley, The Univ. of California Press (1982).
(17) Muller, Ian, "Hypatia, Women of Mathematics: A Bibliographic Source Book", ed., by L.S. Grinstein and P.J. Campbell, Greenwood Press, N.Y. (1987).
(18) Kingsley, Charles, "Hypatia, or New Foes with an Old Face", E.P. Dutton, N.Y. (1907).
(19) Hypatia, "The Way of Life: Compiled and Transcribed from Ancient Records", by Rev. Julius Joseph Schnell, Eagle Rock District, LA (1945).

亞歷山大城的海巴夏

顏 一 清
輔仁大學數學系

摘 要

本文釋明西元三七〇年至四一五年，在埃及亞歷山大城（Alexandria）的海巴夏（Hypatia）是中外歷史上出現的第一位傑出的女數學家、天文學家及哲學家。

在女子不易受教及不公開露面的那個時代，海巴夏由她的數學家兼天文學家的父親泰恩（Theon）栽培成人，加上她個人的才學她在博學院（The Museum）教授及著述當時最艱深的數學，天文學、物理學和哲學。她並且還是一位公衆人物，並受大衆景仰。但她也因此遭忌，而終於被一群狂徒殘殺。這個殘殺事件扼止了女子出頭的時間竟達十五世紀之久。

海巴夏才貌双絕，品德高超。爲了獨步她艱難的理想，她終身未婚。

有關她的事蹟，她當時的史學家略有記載。由於故事的淒測，至今小說家還喜歡把它寫成小說或戲劇。

THE PHASE OF LUNAR HARMONICS IN SCINTILLATION DATA

John R. Koster and H. Y. Lue

Department of Physics
Fu Jen University

ABSTRACT

Fourteen years of scintillation data were analyzed by Koster et al.[1] using lunar age superposition. They find that statistically significant lunar harmonics are present in the data at some hours of the day. They also find that the phase of these harmonics is not always an increasing function of time. The slope of a plot of harmonic phase versus hour is sometimes zero or negative. It is well known that lunar phases themselves increase with time. This paper shows that the observations can easily be explained if one remembers that the harmonic phase associated with scintillations depends on the place and time of the formation of the patch of irregularities which produces the scintillations, not on the place and time of the subsequent observation. If patch age and drift are taken into account, a zero or negative slope to the phase versus hour of observation plot is quite possible. Hence a negative slope to the harmonic phase versus hour of observation plot is not only possible. It provides useful information about the direction and magnitude of the drift of patches of irregularities in the ionosphere.

1. INTRODUCTION

If the amplitude of the radio signal transmitted by a satellite in synchronous orbit is recorded on a continuous basis at a ground station, the amplitude sometimes fluctuates rapidly with time. These variations in received signal strength are called scintillations, and are known to be due to irregular electron density structures in the ionosphere[2,3]. The intensity of scintillations over a 15-minute interval is characterized by a number known as the 'scintillation index'. Large data bases consisting of 15-minute scintillation indices covering many years on a continuous basis are in existence. One fruitful analysis method[1] searches for lunar harmonics in such data. Since scintillations are a function of season, each season must be analyzed separately. And since scintillations are

also a strong function of solar time, it is essential to analyze data for each hour of that season separately.

The method is called 'lunar age superposition'. The variable used is the probability that the scintillation index for a given hour is at or above some arbitrarily chosen level. Values of this probability for the specified season are accumulated in a 30×24 matrix, where the 30 rows represent the 30 days of the lunar month, and the 24 columns represent the 24 hours of the day. When a given column of the data matrix is subjected to Fourier analysis, significant lunar first and second harmonics are sometimes found. These harmonics are described in terms of their amplitude and phase. The meaning of amplitude is obvious, and phase, as used here, is merely the lunar age at which the harmonic reaches its maximum value.

An unexpected result emerges when one compares results from the 24 columns in the data matrix for a given season. One intuitively expects that the phase for each hour should be somewhat larger than the phase of the previous hour. After all, lunar phase (i.e., lunar age) is always such an increasing function of time. But on some occasions the plot of experimental harmonic phase versus hour over a period of some hours has a negative slope. This paper wishes to address this problem, and to see whether something can be learned from this unexpected result. It will be tacitly assumed that lunar harmonics, if present in scintillation data, are due to lunar tides in the neutral air. There is a vast literature on lunar tides in the atmosphere, and here we merely give reference to one of the best summaries[4]. Since lunar tides are most easily analyzed using lunar time, it is necessary to find a simple method of determining lunar time at any given solar time during the month.

2. THE EARTH-MOON SYSTEM

We can readily convert from solar to lunar time and vice versa if we refer to a simple model, in which times, both lunar and solar, appear as an easily visualized angles. We explain the model.

(1) Time as measured by an angle

Solar and lunar times appear as angles in the diagram given in Fig. 1. Points of interest on the diagram are:

N The north pole of the earth.
G The longitude of Greenwich—i. e., zero longitude.
O The longitude of the observer.
H Heliocenter=center of the sun.
T Mean time reference; point opposite *H*, or anti solar point.
M The center of the moon.
L The anti-lunar point.
J Time origin. *J* will be 0 at the beginning of the month.

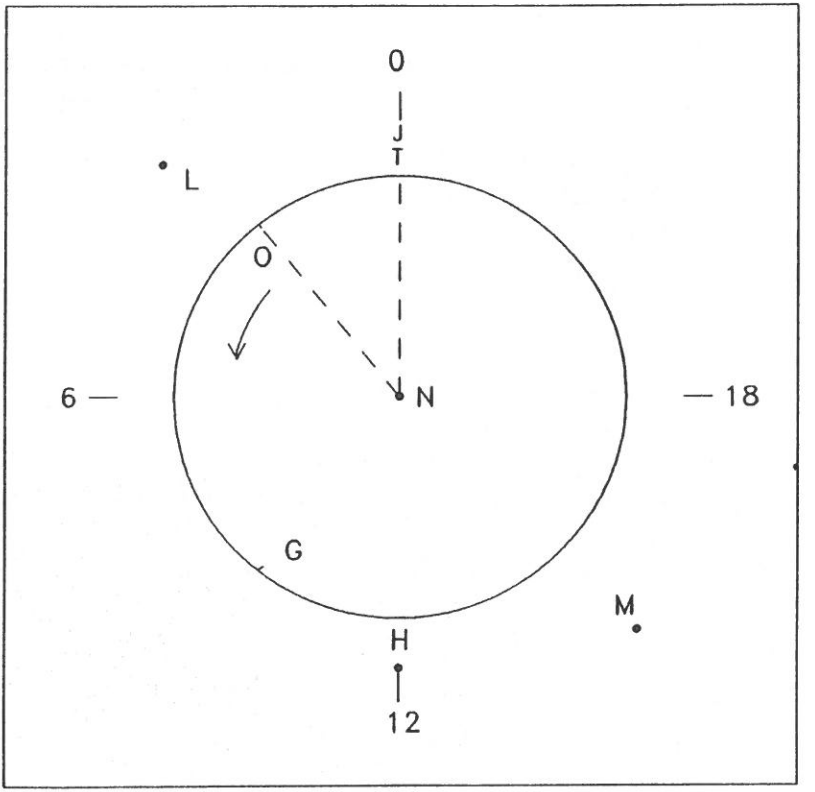

Fig. 1. Diagram of the earth-moon system. Solar time is equal to angle *TNO*; lunar time is angle *LNO*, and lunar age is angle *TNL*. See text for further explanation.

In this diagram, angles are described by a 3-letter sequence; e.g., TNO, where N is the apex, and T and O are the extremities. Angles will be measured in 'turns' (1 turn=360°) for convenience. If one goes from T to O in an anti-clockwise direction, angle TNO is positive; otherwise negative. An angle can always be written either as positive or as negative; e.g., $TNO=-ONT$. Adjacent angles can be combined; e.g., $TNL+LNO=TNO$; or $TNL-ONL=TNL+LNO=TNO$.

The earth rotates in the positive (anticlockwise) direction of the arrow at a constant rate of one turn per day. The moon moves uniformly around the diagram at a constant rate, executing one full turn in a lunar month (30 days, here) at a rate of 1/30 turns per day.

We will assume that, at the beginning of the month, M (the moon) is coincident with H, O (the observer) is at T, and J (our time origin) is set to zero. The rotation proceeds, and time can be described in terms of angles on the diagram. The following angles are worth noting:

TNG Universal time (GMT or UT).

TNO Observer's local time.

GNO Observer's longitude.

TNL Lunar age (=lunar phase)

LNO Observer's lunar time.

Note that $TNO=TNL+LNO$

i.e., solar time=lunar age+lunar time.

Hence: $LNO=TNO-TNL$

i.e., lunar time=solar time−lunar age

JNT An integer equal to the number of full days in the elapsed time.

JNO The total elapsed time.

$JNO=JNT+TNO$, where JNT is an integer; TNO is less than 1.

$TNL=JNO/30=(JNT+TNL)/30$

i.e., lunar age=elapsed time/30. It is always<1.

It will be noted that the hours of the day are shown around the periphery of the figure for convenience. Time=0.0 when the observer is at T, the center of the earth's shadow (midnight).

If we are investigating a lunar first harmonic, a tidal crest will be found under M and a trough under L. For a lunar second harmonic,

crests will exist under M and L; troughs 0.25 turns away from each. A suitable time lag may have to be introducd in either case, since it is well known that in ocean tides the crests and troughs often lag behind the sub-lunar or anti-lunar points by some hours.

(2) Examination of the earth-moon system

In what follows, we will restrict ourselves to a single clock, that of an observer at longitude O in the diagram. Hence, our time is always measured in terms of angle TNO, even when considering events at another longitude.

(A) Tides at the observer's longitude

In this section we wish to examine the simplified model of the earth-moon system shown in Fig. 1. Assume that there is a lunar first harmonic tide only (although it is well known that the 2nd harmonic tide is usually dominant) and that the tidal crest is exactly under the moon. For an observer at O, a tidal crest appears when the moon is directly over the observer, (angle $MNO=0$, or angle $LNO=0.5$), a trough appears when the anti-lunar point is at the observer's zenith (angle $LNO=0$).

We next consider the question: 'How many tidal troughs occur during the month, and when does each occur?' A study of our model shows us that angle LNO will be zero 29 times during the month; one trough occurs each day.

When the troughs occur is easy to see from the model, too. A trough occurs whenever angle $LNO=0$. Our diagram shows that:

$$LNO=TNO-TNL$$

where TNO is the observer's local time, and $TNL=JNO/30=(JNT+TNO)/30$ is the lunar age.

Hence, $LNO=0$ implies that:

$$TNO_0=\frac{JNT+TNO_0}{30}$$

where JNT takes values 0, 1, 2, ···, 28 and where TNO_0 is the clock time(s) when $LNO=0$.

Trough times are therefore given by:

$$TNO_0=\frac{JNT}{29} \tag{1}$$

where $JNT=0, 1, 2, \cdots, 28$.

Tidal crests occur when $TNO=TNM$. But angle $TNM=TNL+0.5$. We can easily show, therefore, that crests occur whenever:

$$TNO_{0.5}=\frac{JNT+15}{29} \tag{2}$$

where $TNO_{0.5}$ is the clock time when $LNO=0.5$.

(B) Tides at another longitude

Suppose now that an observer, still at O, wishes to determine times of tidal crests and troughs at another location, which we shall call longitude B. For a trough to appear at B, it is necessary that angle TNB be equal to TNL—i.e., that $BNL=0$. Now:

$$TNB=TNO+ONB$$

$$TNL=\frac{JNT+TNO}{30}$$

Equating the right sides of the two above equations, and solving for TNO, we get:

$$TNO_0=\frac{JNT+30\times ONB}{29} \tag{3}$$

where $JNT=0, 1, 2, \cdots, 28$, and we note this reduces to Eq. (1) when angle $ONB=0$.

For a crest to appear over point B, it is required that angle TNB be equal to angle TNM. Since we know that:

$$TNB=TNO+ONB$$

and

$$TNM=\frac{JNT+TNO}{30}+0.5$$

we equate the right sides of the two equations, and get:

$$TNO_{0.5}=\frac{JNT+15-30\times ONB}{29} \qquad (4)$$

and note again that this reduces to Eq. (2) when $ONB=0$.

(C) Making observations on an hourly basis

Since much of our analysis is done on an hourly basis, we wish to consider a case where data have been accumulated in a 30×24 matrix. Columns (IC) contain data for each of the 24 hours, and rows (IR) correspond to the 30 days of the month. Times of daily observations will be given as $(IC-1)/24$ turns. The corresponding lunar ages are $[(IC-1)/24+(IR-1)]/30$. We will want to analyze each column separately. Lunar time can be determined from:

$$LNO=TNO-TNL$$

But, for a given column in our data matrix, TNO is fixed. We refer to this as TNO_c, the fixed value of TNO. And for our column, we can write:

$$LNO=TNO_c-TNL \qquad (5)$$

where $TNL=JNL/30=(JNT+TNO_c)/30$, and JNT takes the values 0, 1, 2, ···, 29.

If we now plot the values of lunar time (LNO) for our column as a function of lunar age (TNL), we get 30 discrete points lying along a straight line. Such plots for each of the columns of our data matrix are given in Fig. 2. The line for column 1 is the lowest one on the plot, that for column 24 is at the top. The slope of each line is -1 days/month. Equation (5) tells us that this line must cross the $LNO=0$ line when $TNL=TNO_c$ (see Eq. (5)). This means that the phase for any column of data (i.e., the lunar age at which the lunar time is zero) is equal to TNO_c for that column. Hence we conclude that:

$$\text{Phase for a given column}=TNO_c \qquad (6)$$

and TNO_c is just the time associated with the column.

The lunar time corresponding to any entry in any of our columns can be obtained from:

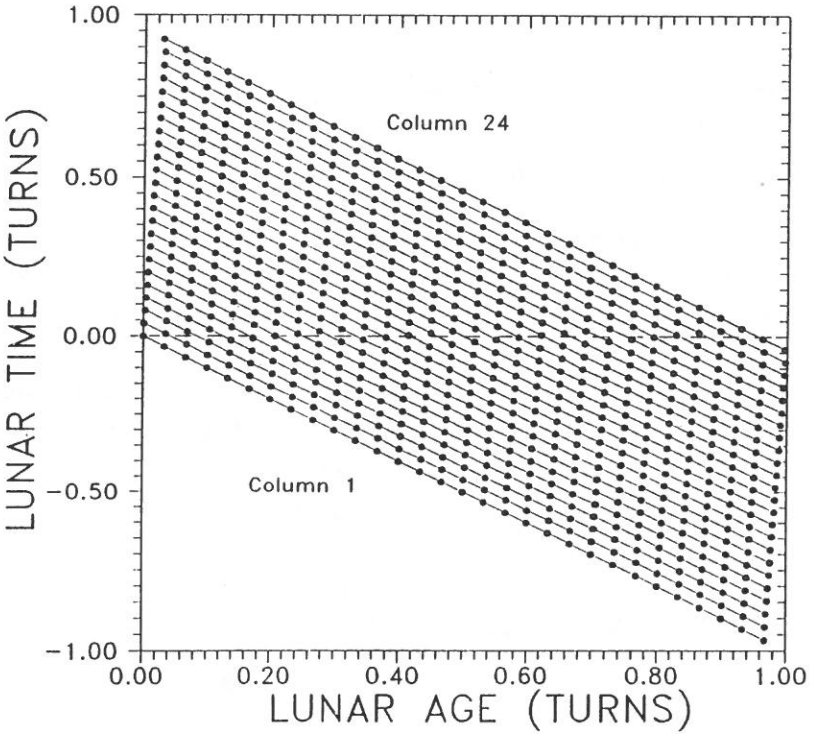

Fig. 2. Plots of lunar time versus lunar age for each column of a 30×24 data matrix. Column 1 is at the bottom, column 24 at the top. Note that for each column, lunar time crosses zero once only, at a lunar age which is equal to the observation time of the column in question. This is the phase for that column.

$$LNO=TNO_c-TNL=TNO_c-\frac{JNT+TNO_c}{30}$$

$$=TNO_c\times\frac{29}{30}-\frac{JNT}{30} \qquad (7)$$

This can be written in terms of our rows (IR), and columns (IC) in the form:

$$LNO=\frac{IC-1}{24}\times\frac{29}{30}-\frac{IR-1}{30} \qquad (8)$$

We summarize:

(a) The lunar time in any column decreases each day.

(b) The lunar time crosses zero once in each column, and

(c) The phase for any column is just TNO_c, the time the columnar observations are made. Note that the phases increase uniformly with hour.

3. A SIMPLE MODEL FOR SCINTILLATION PRODUCTION

The basic mechanism for the production of irregularities in our model will be the irregularity patch. Such a patch can be imagined as a cloud of ionospheric irregularities with horizontal dimensions of the order of a few hundred to some thousands of kilometers, and with a thickness of a few meters to several hundred kilometers. Patches, once formed, drift horizontally; and when the radio wave from a satellite in synchronous orbit passes through such an irregularity patch in the ionosphere, scintillations will be observed at a ground station. We shall assume that such patches appear—we do not specify the method of their production.

We shall further assume that, in our model, patches appear regularly every night at the same time. The only difference from night to night will be a relatively modest variation in the "intensity" of the patch, which will give rise to a small variation in the scintillation index, depending on the presence or absence of a lunar neutral air tide in the upper atmosphere at the place and time of patch formation. Patches, once formed, will slowly die out, so that the amplitude of the scintillations they produce will depend on the time interval between the formation of a patch and its observation. We will specify the time and place of the formation of the patch, and the velocity of its movement. If one takes hourly observations over one month, and arranges the resulting 720 scintillation indices in matrix form, it is possible to select one matrix column at a time and plot the 24 points. They should fit an expression of the form:

$$A = A(0) + A(1) \times \cos(LNO),$$

where $A(0)$ and $A(1)$ are constants for a given column; LNO is the

lunar time associated with the formation of the patch each day. We will want to determine the amplitude and phase of the above expression from the observational data.

We wish to call attention to three important properties of our scintillation model. These are:

(a) The amplitude of the scintillations observed depends on the elapsed time since formation of the patch. Scintillations diminish with time—at a rate which our model will specify.

(b) The phase associated with a column of our data matrix depends on the time of a patch's formation, not on the time of its observation. If, for example, a patch forms each evening of the month at exactly 19 hours local time, and the patch is observed at 19, 20, 21 and 22 hours, amplitudes will be smaller at the later hours, but the phase will be exactly the same at all four hours. The phase depends on the presence or absence of a lunar tide at the time the patch was formed.

(c) The phase associated with a column in our data matrix depends also on the place of formation of the patch in cases where the patches are moving. It depends on the presence or absence of a tide at the place where the patch was formed, not on its presence or absence at the subsequent place of observation.

If we observe drifting patches, therefore, our model must determine the lunar time prevailing at the time and place of patch formation in order to determine the appropriate phase for the column of data that we are analyzing.

4. KINDS OF PATCHES AND THEIR ASSOCIATED PHASE

(1) Specifying the properties of the patch

In order to simulate the phases produced when we have daily sampling of the scintillations due to an assumed irregularity production mechanism, we must specify certain properties of that mechanism. This is done by giving answers to a few relatively simple questions. Among the most basic questions to be answered are the following:

(A) When are the irregularities formed?

We shall consider hourly time periods. And for each hour we shall give a yes or no answer as to whether irregularities are formed at that hour or not.

(B) Once formed, how long do the irregularities last?

In our model, we shall assume that irregularities, once formed, decay exponentially. Thus we can specify what time constant is to be assigned to a given set of irregularities. We shall want to try situations where the time constant is relatively short, and irregularities formed at one hour do not persist long enough to be observed during the next hour. We sometimes may wish to try a longer time constant, so that irregularities once formed will be observed for a number of successive hours following their formation.

(C) Do the irregularities move?

We can specify whether irregularities formed over an observing station remain stationary relative to the observer, or whether they move eastward or westward with an assigned drift velocity.

(D) How is the probability of irregularity production at a given solar time affected by a lunar tide?

If production and tide are positively correlated, we might expect a scintillation index peak when the moon is directly over the observer—i. e., the local lunar time is 0.5 turns. If the correlation is negative, a probability maximum will occur when lunar time is 0.0. The method can easily be extended to deal with a possible second lunar harmonic, with two peaks and two troughs per lunar day, but we shall not consider that here.

Once we have specified our mechanism, we can produce a matrix (30×24 as usual) in which every entry has an easily calculable lunar time associated with it. That lunar time is a function of three things:

(a) The time at which the patch under consideration was formed. This is not necessarily the time it is observed.

(b) The place where the patch was formed. This is not necessarily the place where it is observed.
(c) The lunar age when the patch was formed.

(2) Demonstrating the results of a chosen mechanism

At this stage we wish to demonstrate the results we get from a variety of simple production mechanisms. Each mechanism is described in terms of the answers given to the four questions listed above.

(A) A single short-lived patch each day, no drift

We will start with a very simple mechanism, in which the four questions are answered as follows:

(a) Time of patch formation: 18 H each day only.
(b) Duration—not greater than one hour.
(c) Patch movement after formation? None.
(d) Correlation of SI with a lunar tide—negative.

If we proceed from the beginning of a lunar month, and make hourly observations, scintillations will be observed each day at 18 hours local time only (TNO=0.75). Arranging the hourly values of SI in a 30×24 matrix, we will get a matrix in which all the columns except column 19 will be filled with zeros. In this column, it is clear that on each successive day, the angle LNO decreases by 1/30 of one turn. LNO will be zero when time (TNO)=0.75 turns, the time at the head of the column. The value of SI is greatest when LNO=0.0; i. e., when a tidal trough is at the observers site. Hence we would expect a plot of SI versus month for this column of our table to be of the form:

$$SI=A+B\cos(LNO) \tag{9}$$

$$SI=A+B\cos(TNL-TNO_c) \tag{10}$$

where TNO_c is the value of TNO for the column, and TNL takes all values between 0.0 to 1.0, i. e., a DC term of amplitude A and a superimposed lunar harmonic of amplitude B where the phase of the harmonic is just the time of the patch's formation.

(B) A single patch lasting several hours, no drift

In this case, things are the same as in (A), but now the irregularity patch has a duration of, say, three hours. During the three hours, the amplitude of the scintillations will decrease in an exponential way. Hence, the value of B will be progressively smaller at hours 18, 19 and 20. The phase, however, will remain constant over these hours, having been fixed at the time of the irregularity formation. The value of the phase is equal to the formation time in turns=18/24=0.75 turns for all three columns. The plot of phase versus hour in this case is a horizontal straight line over a 3-hour period, i. e., a line with zero slope.

(C) New patches at subsequent hours, no drift

We here return to a patch duration of only one hour. But now we have new patches formed at successive hours 18, 19 and 20. It is evident that the phase is different for the three columns involved. It is determined by the time of the formation of the three patches. Initial times at the head of columns 19, 20, and 21 are 0.75, 0.792 and 0.833 respectively, and these are the three phases. In this case, the phase versus hour plot will have a positive slope of 1 lunar turn (month) per solar turn (day)=30 days/24 hours=1.25 days/hour. We emphasize again, that the phase is determined by the time of the formation of the patch, not of its observation.

(D) A single patch, lasting several hours, with drifts

We next consider a somewhat more complex case. A large patch is formed over the observer at 18 hours local time. No formation takes place before or after this time, but the patch, once formed, persists for a number of hours, with a slow exponential decrease in its amplitude with patch age. We further introduce a constant, non-zero drift velocity of the patch after it is formed. What will now happen?

If our observer makes his observations at 18 hours, patch formation place coincides with O, and the situation is no different than it was in (A), since observation time coincides with formation time. But if our observer now makes observations at 19 hours, he will see an irregularity patch which was formed at 18 hours his time, but at some longitude X,

where X is different from O. The position of longitude X relative to O, however, can be determined. Assume that V is the drift velocity given in terms of a fraction of the earth's rotational velocity—say 0.5. The irregularity was formed at a distance $V\times$(elapsed time) from the observer. Longitude X may be greater or less than longitude O, depending on whether the drift is westward (XNO is negative) or eastward (XNO is positive). The amplitude of the observed scintillations will decrease with time, of course, but what about the phase? The phase is determined by the place and time of formation of the irregularity patch which the observer is currently watching. The place was, of course X, and the time was 18 hours on the observer's clock. The time was:

$$TNX=TNO_f+ONX \tag{11}$$

where TNO_f is the observer's formation time.

The phase for a column of observations at this time is just:

$$\text{PHASE}=\text{Formation time}=TNO_f+ONX \tag{12}$$

Hence, the phase for such a column, although observed at a time when $TNO>TNO_f$, may easily be greater or less than the phase of the preceding hour, depending whether ONX is positive or negative.

If we want the lunar time, we can easily get it from:

$$LNX=TNX-TNL=TNO_f+ONX-TNL \tag{13}$$

where TNL is lunar age at formation time—a constant.

The required procedure is now clear. First determine ONX (velocity $\times$elapsed time since formation), then determine the phase for the column, from Eq. (12) and the appropriate lunar time LNX from Eq. (13). Lunar times for subsequent days of the month can be determined directly from Eq. (13) by giving TNL the appropriate value for each day, i.e., $(JNT+TNX)/30$, where JNT takes integer values.

(E) Summary of the four patch types considered above

As an example of all the above patch types, we consider an imaginary day on which the following things happen:

(a) For the first six hours, patches form at the beginning of each hour, vanish before the next hour.

(b) For the next six hours, a single patch forms, and persists until the end of the six hour period. No drifts occur.

(c) Same as (b), but a huge patch drifts eastward with velocity equal to 0.5× the earth's rotational velocity.

(d) Same as (c), but now the drift is westward.

Figure 3 shows the result when the above is run on a computer program which implements the equations derived above.

It is clear that freshly produced patches (points 1—6) result in a phase versus hour slope of 1.25 days/hour, which is the same as the slope for the moons phase. Long duration patches without drift (points 7—12) yield a slope of 0.0 days/hour. Westward drifting persistent patches give a slope somewhat larger than 0.0 days/hour (points 19—24) and eastward drifting persistent patches give a slope which is negative. (points 13—18)

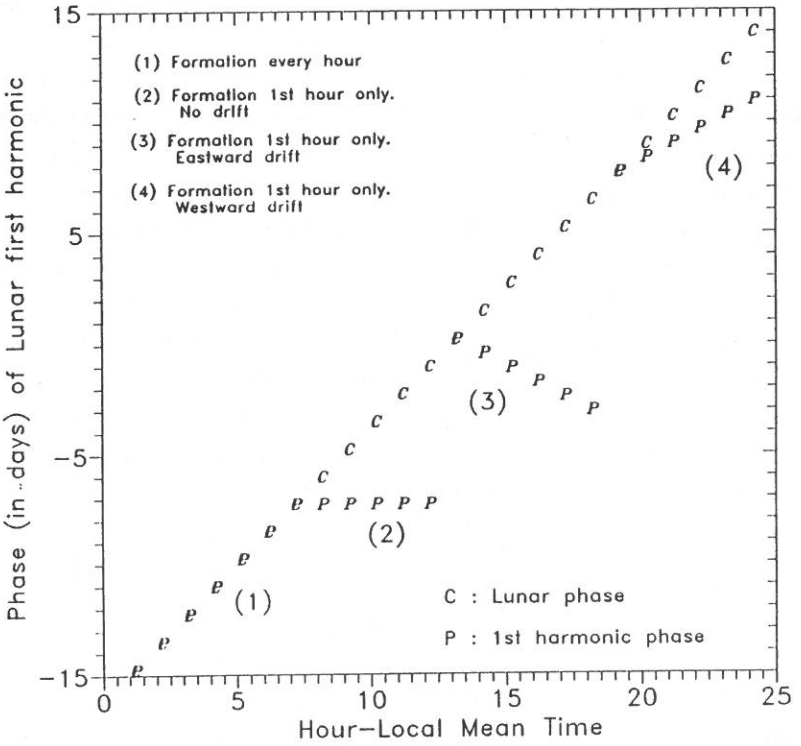

Fig. 3. Hourly values of lunar phase (*C*) and first harmonic phase from scintillation data (*P*) for 4 different types of irregularity patch. Each type covers six hours.

Our conclusion? A zero slope in phase versus hour plots will occur in even an extremely simple model if one has persistent patches of irregularities. The slope may become negative if the patch is large and there is an eastward drift.

5. DISCUSSION

We now address the question of the credibility of our model. It is clearly over-simplified. But it may not be as unrealistic as one might first expect. The most unrealistic assumption is the assumption that patches form at precisely the same time on each of 30 successive days. This clearly does not happen in real life. But the real data that is analyzed in Koster et al.[1] is not a single month's data—but data averaged over a 4-month period for 14 successive years. The averages are not wildly different from the values assumed in the model. Further, records show that patches of irregularities often persist for many hours, and drift velocities associated with such patches have frequently been measured. Values from 0.25 to 0.50× the earth's rotational velocity are not unusual. It is clearly possible to remove most of the simplifications in the above model, at the expense of making the computer simulation program progressively more complex. What we have shown here is that even in a very simple model, we would expect to find positive, zero and negative slopes when we plot phase versus hour for data with a lunar harmonic rather deeply buried in the noise. The slopes can be telling us something valuable about the drift speed, direction, and duration of the patches of irregularities. A much more complex model is worth developing, since even the simple one yields results that agree with the somewhat surprising results obtained in the original analysis of data.

6. CONCLUSION

When results rising from the analysis of experimental results do not agree with what seems to us to be intuitively obvious, there are a number of possibilities:

(a) Our analysis is wrong.

(b) Our intuition is wrong.

(c) Both analysis and intuition are wrong.

Our findings here show that (b) is true. Our intuition was in error. Even a simple model can given rise to a negative phase versus hour slope. It does not follow, unfortunately, that (a) is false. Further investigation is both justified and necessary.

7. ACKNOWLEDGMENT

This work has been supported by the National Science Council of the Republic of China under contract NSC80-0208-M030-12.

REFERENCES

(1) J.R. Koster, Y.N. Huang, H.Y. Lue and H.S. Wu, *J. Geophys. Res.* *(in the press)* (1993).

(2) B.H. Briggs, *Contemp. Phys.*, **16**, 469 (1971).

(3) J. Aarons, H.E. Whitney and R.S. Allen, *Proc. Inst. Elec. Electronic Engr.*, 59 (1971).

(4) R.S. Lindzen and S. Chapman, *Space Sci. Rev.*, **10**, 3 (1969-1970).

閃爍資料中的陰曆諧振相位

高士達 呂秀鏞

輔仁大學物理系

摘 要

高士達等人利用陰曆年代的疊加法分析了 14 年的閃爍資料。他們發現在一天中某些時段出現著陰曆諧振統計上的顯著。他們也發現在這些諧振中的相位並不是都隨時間而增加。在諧振相位相對於鐘點的圖形中，斜率有時是零或負值。然而陰曆相位隨時間之增加是一件已知之事實。本文證實能很容易地解釋所觀測的現象，若我們記住閃爍關聯的諧振相位是決定於造成閃爍的不規則碎片所發生的時間地點，而不是決定於隨後觀測的地點及時間。若考慮碎片年代和漂移，於相位相對於觀測鐘點的圖形，零或負斜率是完全可能的。因此在諧振相位相對於觀測鐘點的圖形中一個負斜率不僅是可能的，它亦提供了關於電漿不規則碎片漂移的方向及距離一有用的資訊。

RAYLEIGH-BRILLOUIN SCATTERING IN CALCIUM-ALUMINATE OXIDE GLASSES

LUU-GEN HWA

Department of Physics,
Fu Jen Catholic University
Taipei, Taiwan 242, R.O.C.

JOHN SCHROEDER

Department of Physics and Center for Glass Science
Rensselaer Polytechnic Institute
Troy, New York 12180, U.S.A.

ABSTRACT

Rayleigh-Brillouin scattering measurements on various multi-component Calcium-Aluminate (CA) oxide glasses have been performed as a function of composition. The Rayleigh-Brillouin scattering intensities and frequency shifts along with the measurements of index of refraction and density allowed the calculations of the Landau-Placzek ratio, sound velocities, elastic constants and Pockels' elasto-optic coefficients. On the basis of λ^{-4} scaling, some calcium-aluminate oxide glasses exhibit lower intrinsic scattering loss than the best silica glass and they are prime candidate as optical waveguide material for the near infrared regime.

1. INTRODUCTION

Rayleigh-Brillouin scattering measurements on various multi-component Calcium-Aluminate (CA) oxide glasses have been carried out as a function of composition. The Rayleigh-Brillouin scattering intensities and the Brillouin frequency shifts along with the measurements of index of refraction and density allowed the calculations of the Landau-Placzek ratio, sound velocities, elastic constants, Pockels' elasto-optic coefficients and the intrinsic scattering loss[1].

The typical Rayleigh-Brillouin scattering spectrum of glass has five spectral lines, two frequency shifted doublets consisting of longitudinal and transverse lines and a strong unshifted central Rayleigh line. Usually the Rayleigh line may be orders of magnitude greater than the shifted

doublets.

A recent paper by Lines et al.[2] proposed that the scattering is minimized by filling as many "holes" as possible in a three-dimensionally coordinated oxide network with cations smaller than divalent oxygen, and doing so in a manner which produces the fewest broken bonds in the network itself. This condition is well satisfied in the whole family of calcuim-aluminate based glasses, which should consequently be excellent ultra-low loss optical waveguide material at or near the "silica" wavelength of 1.55 μm.

We report here the first systematically experimental investigation of CA glasses by light scattering technique.

2. THEORETICAL BACKGROUND

Rayleigh scattering in dense disordered materials is brought about due to microscopic fluctuations in the dielectric susceptibility about its equilibrium value. For a multi-component liquid, the fluctuations in the dielectric susceptibility about its equilibrium value have the form[1,3,4]:

$$\langle\delta\epsilon_k^2\rangle=\left(\frac{\partial\epsilon}{\partial\rho}\right)^2_{T,\{C\}}\left(\frac{\partial\rho}{\partial S}\right)^2_{P,\{C\}}\langle\delta S_{red}^2\rangle+\left(\frac{\partial\epsilon}{\partial\rho}\right)^2_{T,\{C\}}\left(\frac{\partial\rho}{\partial S}\right)^2_{S,\{C\}}\langle\delta P^2\rangle$$
$$+\sum_{j=1}^{n-1}\sum_{k=1}^{n-1}\left(\frac{\partial\epsilon}{\partial C_j}\right)_{T,P,\{C'\}}\left(\frac{\partial\epsilon}{\partial C_k}\right)_{T,P,\{C'\}}\langle\delta C_j\delta C_k\rangle \qquad (1)$$

In this equation the subscript $\{C\}$ denotes the $n-1$ indepedent mass fraction C_1, C_2, $\cdots$, C_{n-1}, whereas the prime in $\{C'\}$ means that the mass fraction appearing in the partial derivative is omitted from the set $\{C\}$, where $\langle\delta P^2\rangle$ represent pressure fluctuations that manifest themselves as sound waves. These are propagating fluctuations, and they result in the inelastic scattering or Brillouin lines. $\langle\delta S_{red}^2\rangle$ and $\langle\delta C_j\delta C_k\rangle$ are entropy fluctuations and concentration fluctuations, respectively, with former being caused by thermal diffusion and the latter by mass diffusion. Both are diffusive modes; consequently they are non-propagating and will be found as quasi-elastic scattering or the Rayleigh line.

For a binary or pseudobinary liquid the above equation reduces to the form[1]:

$$\langle \delta \epsilon_k^2 \rangle \propto \left(\frac{\partial \epsilon}{\partial \rho} \right)_{C,T}^2 \langle \delta \rho_k^2 \rangle + \left(\frac{\partial \epsilon}{\partial C} \right)_{P,T}^2 \langle \delta C_k^2 \rangle \qquad (2)$$

where we have contribution only from density and concentration fluctuations, respectively. The scattering intensity that one measures in a Rayleigh-Brillouin experiment is proportional to the mean square fluctuation in the dielectric susceptibility.

A normalized intensity ratio, the Landau-Placzek ratio, is defined as the ratio of the Rayleigh intensity to the sum of the Brillouin intensities:

$$R_{LP} \equiv \frac{I_R}{2I_B} \qquad (3)$$

In Brillouin scattering for a given incident and scattered light direction in an isotropic solid, four possible scattered light components exist, namely, *VV*, *VH*, *HV* and *HH*. Here *V* denotes polarization perpendicular to the scattering plane and *H* denotes polarization parallel to the scattering plane. For the case of 90° scattering, the following equations give the Brillouin scattering cross section for scattering in glasses[5]:

$$\left(\frac{d\sigma}{d\Omega} \right)_{VV} = \epsilon_0 \left(\frac{\omega_0}{C} \right)^4 \frac{V k_B T}{32\pi^2} \frac{P_{12}^2}{C_{11}} \qquad (4)$$

$$\left(\frac{d\sigma}{d\Omega} \right)_{HH} = \epsilon_0 \left(\frac{\omega_0}{C} \right)^4 \frac{V k_B T}{32\pi^2} \frac{P_{44}^2}{C_{11}} \qquad (5)$$

$$\left(\frac{d\sigma}{d\Omega} \right)_{VH} = \epsilon_0 \left(\frac{\omega_0}{C} \right)^4 \frac{V k_B T}{32\pi^2} \frac{P_{44}^2}{2C_{44}} \qquad (6)$$

$$\left(\frac{d\sigma}{d\Omega} \right)_{HV} = \epsilon_0 \left(\frac{\omega_0}{C} \right)^4 \frac{V k_B T}{32\pi^2} \frac{P_{44}^2}{2C_{44}} \qquad (7)$$

The *VV* and *HH* components are due to scattering from longitudinal phonons and consequently depend on the normal strains, but the *HV* and *VH* components originate from the shear strains which act in planes normal to the scattering plane. The last two terms exhibit the reciprocity relations. Hence, the choice of polarization for the incident light and scattered light selects specfic acoustic modes. The two sets of material constants, the elastic constants C_{ij} and the Pockels' elasto-optic coefficients

P_{ij}, determine the Brillouin spectrum. P_{ij}^2 determines the intensity of each line, and C_{ij} determines the extent of the shift with respect to frequency from the incident light frequency.

In a glass the elastic strain produced by a small stress can be described by two independent elastic constants, C_{11} and C_{44}. Using the Cauchy relation that $2C_{44}=C_{11}-C_{12}$ allows one to determine C_{12}. For pure longitudinal waves

$$C_{11}=\rho V_L^2 \tag{8}$$

and for pure transverse waves

$$C_{44}=\rho V_T^2 \tag{9}$$

where ρ is the density, and V_L and V_T the longitudinal and transverse velocities, respectively. These sound velocities can be calculated with the aid of the Brillouin equation given as[6]:

$$V_{L,T}=\frac{C}{2\nu_0}\left(\frac{\Delta\nu_{L,T}}{\sin\frac{\theta}{2}}\right)\frac{1}{n} \tag{10}$$

where $\Delta\nu_{L,T}$ the appropriate Brillouin splitting (either longitudinal or transverse) in Gigahertz, ν the incident laser frequency, n the index of refraction at laser frequency, and θ the scattering angle, respectively. For a glass the velocity is independent of the direction of propagation and only one longitudinal and a doubly degenerate transverse acoustic branch exists.

The Brillouin intensities at the various polarization selections and Brillouin shifts coupled with the auxiliary parameters of density and refractive index gives the Pockels' elasto-optic coefficients for these glasses. The pockels' coefficients are determined for CA glasses with respect to the SiO_2 glass by the following equations[1,3,4]:

$$P_{12}=\left[\frac{I_B(VV)}{I_B(VV)_0}\right]^{1/2}\left[\frac{\Delta\nu_B^L}{\Delta\nu_B^L(O)}\right]\left[\frac{n(O)}{n}\right]^5\left[\frac{\rho}{\rho(O)}\right]^{1/2}P_{12}(O) \tag{11}$$

$$P_{44}=\pm P_{12}\frac{V_T}{V_L}\left[2\frac{I_B(VH)}{I_B(VV)}\right]^{1/2} \tag{12}$$

In the above equations $I_B(VV)_0$, $\Delta\nu_B^L$, $n(O)$, $\rho(O)$ and $P_{12}(O)$ refer to the

Brillouin intensity, Brillouin shift, refractive index, density and Pockels' coefficient of SiO_2, while the same quantities without the zero designator refer to sample parameters.

3. EXPERIMENTAL ASPECTS

The methods employed to obtain the Brillouin spectra of CA glasses are laser excitation (Argon-ion) operating at 4,880 Å coupled to a stablized multi-pass high contrast Fabry-Perot interferometer with a photon counting detection system and associated data handling electronics.

The entire Fabry-Perot is contained in a thermally stablized box, and the whole system is mounted on a vibration isolated optical table. The detector consists of an ITT-FW 130 photomultiplier tube with a small effective photocathode that is cooled to −20°C. The dark count of this photomultiplier tube in the cooled state is persistently approximately 0.4 count/sec, and it has a quantum efficiency of 10% at 4,880 Å. The current generated by the photomultiplier is shaped, amplified, discriminated, and converted to counts per second, and the data of each subsequent scan are stored in a 1,024 multi-channel analyzer of the Burleigh DAS-1 system. This Burleigh DAS-1 scans the Fabry-Perot and ensures long-term stability of the interferometer by providing servo-control for the piezoelectric stacks of the Fabry-Perot. The scattering experiment reported here was conducted in a three-pass mode with mirrors of 93% reflectivity, resulting in a finesse of 80, a contrast of 10^8, and an overall measured transmission of 0.40.

The sample is contained in a cubic cell, 7.5 cm on each side. The sides of the cell are optically polished. All samples are polished on three sides and then immersed in water-free paraffin oil in the scattering cell to minimized any parasitic scattering and also to protect the delicate surfaces from water vapor attack. The density was determined by an Archimedes technique for which *n*-hexadecane was the working fluid. The index of refraction of the sample was measured by determining the angle of minimum deviation of a sample.

4. RESULTS

Table 1 gives the exact compositions of Calcium-Aluminate-Oxide glass in mole % used in this study. Table 2 shows density, index of refraction and the results of the scattering loss measurements made at 4,880 Å in terms of the Landau-Placzek ratio for CA glasses. The values of SiO_2 is also given for comparison purposes.

Table 1. Summary of constituents of Calcium-Aluminate-Oxide glass in mole %

Glass I.D. #	Glass composition (%)							
	CaO	Al_2O_3	SiO_2	$CaCl_2$	GeO_2	MgO	BaO	Y_2O_3
CAS-p 25	56.7	28.3	15.0					
CAS-p 15	50.73	42.27	7.0					
CAG-3	31.32	26.8		4.98	36.9			
CAG-3.1	33.4	33.3			33.3			
CAG-3.2	43.09	31.91			25.00			
CAG-3.3	45.96	34.04			20.00			
GL-2289	47.97	32.43				9.19	7.70	2.70
CA-p 57	57.3	42.7						

Table 2. Density, index of refraction, Landau-Placzek ration R_{LP} and scattering loss in dB/km of Calcium-Alumate-Oxide glasses at 4,880 Å and 300 K

Sampple	ρ (g/cm³)	n (at 4,880 Å)	R_{LP}	α_S (dB/km)
CAS-p 25	2.877	1.662	56.90	8.48
CAS-p 15	2.847	1.652	51.28	13.01
CA-p 57	2.872	1.671	94.75	23.46
CAG-3	3.314	1.670	56.14	37.97
CAG-3.1	3.226	1.671	63.86	23.66
CAG-3.2	3.177	1.671	68.26	43.67
CAG-3.3	3.260	1.672	81.73	37.44
GL-2289	3.211	1.647	357.3	206.43
SiO_2	2.203	1.462	21.9	11.6

The scattering loss in dB/km is calculated from a combination of Rayleigh and Brillouin data. The Brillouin scattering loss α_S is given by[1]:

$$\alpha=\frac{8\pi^3}{3}\frac{kT}{\lambda_0^4}(n^4P_{12})^2\frac{1}{\rho V_L^2} \tag{13}$$

and the Rayleigh scattering loss becomes

$$\alpha=\alpha_B(R_{L.P.}+1) \tag{14}$$

where n, P_{12}, ρ, V_L, λ_0 and T are refractive index, Pockels' coefficient, density, longitudinal velocity, laser wavelength and lattice temperature, respectively.

The Brillouin shifts and sound velocities (both longitudinal and transverse) of CA glasses are given in Table 3. The calculated elastic constants and Pockels' elasto-optic coefficients are shown in Table 4.

The Brillouin shifts also allow determination of Poisson's ratio by using the following expression:

$$\sigma=\frac{(\Delta\nu_B^L)^2-2(\Delta\nu_B^T)^2}{2[(\Delta\nu_B^L)^2-(\Delta\nu_B^T)^2]} \tag{15}$$

where $\Delta\nu_B^L$ and $\Delta\nu_B^T$ are the longitudinal and transverse Brillouin shifts, respectively.

Table 3. Brillouin shifts and sound velocity (Both longitudinal and transverse) of Calcium-Aluminate-Oxide glasses at 4,880 Å and 300 K

Sample (mole %)	$\Delta\nu_B^L$ (GHz)	$\Delta\nu_B^T$ (GHz)	V_L (m/sec)	V_T (m/sec)
CAS-p 25	33.072	18.259	6,772.9	3,739.2
CAS-p 15	31.645	17.401	6,412.0	3,525.9
CA-p 57	33.269	17.964	6,733.2	3,635.7
CAG-3	30.741	16.776	6,287.9	3,431.4
CAG-3.1	30.04	16.676	6,130.1	3,402.9
CAG-3.2	31.41	17.491	6,375.6	3,550.3
CAG-3.3	32.033	17.439	6,456.5	3,515.0
GL-2289	32.694	17.863	6,659.8	3,638.7

Table 4. Elastic constant (C_{11}, C_{44}) and Pockels' elasto-optic coefficients of Calcium-Aluminate-Oxide glasses at 4,880 Å and 300 K

Sample (mole %)	C_{11} (GPa)	C_{44} (GPa)	P_{12}	P_{44}
CAS-p 25	132.0	40.2	0.114	0.045
CAS-p 15	117.1	35.4	0.143	0.041
CA-p 57	130.2	38.0	0.143	0.037
CAG-3	131.0	39.0	0.235	0.073
CAG-3.1	121.2	37.4	0.241	0.075
CAG-3.2	129.0	40.0	0.227	0.092
CAG-3.3	135.9	40.3	0.199	0.081
GL-2289	142.4	42.5	0.243	0.109

Lines suggested that the Calcium-Aluminate Oxide glasses exhibit the projected minimum intrinsic scattering loss at 1.9 μm[2,7]. Consequently, we use the λ^{-4} scaling and calculate the scattering loss for CA glass at 1.9 μm. Table 5 gives the Poisson's ratio and the converted scattering loss for CA glass.

Table 5. Poisson's ratio σ and scattering loss α_S in dB/km for Calcium-Aluminate-Oxide glasses SiO_2 glass at 300 K

Sample (mole %)	σ	α_S (at 1.9 μm)
CAS-p 25	0.281	0.0369
CAS-p 57	0.283	0.0566
CA-p 57	0.294	0.1020
CAG-3	0.288	0.1641
CAG-3.1	0.277	0.1030
CAG-3.2	0.271	0.1899
CAG-3.3	0.289	0.1629
GL-2289	0.287	0.8983
SiO_2	0.170	0.1140 (at 1.55 μm)

5. DISCUSSION AND CONCLUSION

We have successfully measured the intensity and spectral distribution of the various multicomponent Calcium-Aluminate oxide glasses. On the basis of λ^{-4} scaling, some of the Calcium-Aluminate oxide glasses exhibit less Rayleigh scattering loss than the best silica glasses as seen in Table 5 at their respective wavelength (1.9 μm for CA glass and 1.55 μm for silica glass) for minimum loss. Those CA glasses with low Rayleigh scattering losses are prime optical waveguide material for the near infra-red regime.

From Table 3, we find the CA glasses have very high values of Brillouin shifts and sound velocities. Consequently, the calculated elastic constants also have large values. This implied that the CA glasses possess the very rigid lattice structure.

The Pockels' elasto-optic coefficients will give us the information on the coupling of photon and phonon. The result in Table 4 shows the CA glasses with GeO_2 composition have the higher Pockels' coefficient then the rest of CA group. The reason for this difference is not a easy task. We need more study in order to understand this coupling constant[8~10]. CA glasses also show very clear and strong transverse Brillouin shifts which imply a low coordination number in their structure. This compares with the very weak transverse Brillouin shift for a high coordination number heavy metal fluoride glass[3].

The Poisson's ratio can give the bonding picture of the glass structure. When the Poisson's ratio is about 0.25, the glass tends to be ionic bond and central force fields seem to be the predominant effect in the glass[11,12]. In Table 5 the poisson's ratio of the Calcium-Aluminate oxide glasses is in the range of 0.271 to 0.294. Therefore, we can conclude that CA glasses have the ionic bond in their structure as compared to silica glass (the Poisson's ratio is 0.170), which is predominantly covalent.

From the result in Table 5, it seems that the Calcium-Aluminate-Silicate (CAS) glasses have lower scattering loss than the Calcium-Aluminate-Germanium (CAG) glasses. Consequently, further research on these Calcium-Aluminate oxide (especially CAS glasses) glasses for different mole percentage composition and processing condition is necessary.

REFERENCES

(1) J. Schroeder, *Treatise on Material Science and Technology*, Vol. 12, M. Tomozawa and R.H. Doremus, eds., pp. 157-222, Academic Press, New York (1977).
(2) M.E. Lines, J.B. MacChesney, K.B. Lyons, A.J. Bruce, A.E. Miller and K. Nassau, *J. Non-Crystalline Solids*, **107**, 251-260 (1989).
(3) J. Schroeder, M. Fox-Bilmont, B.G. Pazol, V. Tsoukala, M.G. Drexhage and O.H. El-Bayoumi, *Optical Engineering*, **24**, #4 (1985).
(4) Z. Pan and J.P. Wicksted, *Optical Engineering*, **31**, #1 (1992).
(5) M. Born and K. Huang, *Dynamical Theory of Crystal Lattices*, Oxford University Press (1954).
(6) L. Brillouin, *Ann. Phys. (Paris)*, **17**, 88 (1922).
(7) M.E. Lines, *J. Non-Crystalline Solids*, **103**, 279 (1988).
(8) H. Mueller, *Proc. R. Soc. (London)*, **166A**, 425 (1938).
(9) J.E. Sipe, *Can. J. Phys.*, **55**, 2169 (1977).
(10) J.E. Sipe, *Can. J. Phys.*, **56**, 199 (1978).
(11) M.P. Brassington, T. Halling, A.J. Miller and G.A. Saunders, *Mater. Res. Bull.*, **16**, 613 (1981).
(12) R. Ota and N. Soga, *J. Non-Crystalline Solids*, **56**, 105 (1983).

鈣-鋁氧化玻璃的瑞立-布里元散射

華 魯 根
輔仁大學物理系
史 瑞 德
壬色列理工學院物理系

摘 要

不同成分的鈣-鋁氧化玻璃之瑞立-布里元散射量度已經被執行。瑞立-布里元散射的強度和頻率位移以及折射率和密度的量度允許吾人計算藍道-普來切克比，聲速，彈性係數以及巴克爾光彈性係數。以和波長四次方成反比定律爲指標，一些鈣-鋁氧化玻璃展現較矽玻璃更低的本質散射損耗。它們是在近紅外光區用來做光波導材料最主要的候選者。

使用運算轉導放大器合成高性能濾波器

鄞 永 昌

輔仁大學電子工程系

摘 要

本文提出一個新的方法可應用於電流式或電壓式濾波器的設計。藉由既有帶通濾波器，在其左、右各串聯一個帶拒濾波器，進而形成一個具高性能增益的帶通濾波器。如此則可解決某些低增益帶通濾波器的缺點。最後，本文並以一個範例來做說明，以實驗來驗證所提方法之正確性與實用價值。

一、前 言

運算轉導放大器 (Operational Transconductance Amplifier，OTA) 是合成多種不同高頻主動濾波器的主要元件之一。許多用一個或多個運算轉導放大器的實體化二階濾波器網路早已出現[1~4]。因爲類比積體電路設計傳統上集中於電壓式訊號處理。但近幾年來，使用電流當變數，而非以電壓當變數的電流式訊號處理電路，由於具有較高的增益，較精準、較寬的頻率響應[5,6]，較大的動態範圍，較簡單的電路，較小的晶片面積[7]及較小的功率消耗等等優點，而受到很大的關注[5]。

由於電壓式的濾波器已發展的相當完整，所以互易定理[7]及對偶性[8]兩個重要電路理論，被提出作爲將現有電壓式濾波器轉換到相對的電流式濾波器的方法。本文所提出之高性能濾波器，即在於以既有的濾波器，無論其爲電壓式濾波器或是已被轉換成電流式之濾波器爲基礎，在高於與低於帶通濾波器中心頻率之處各設計一個適當帶拒濾波器 (Bandnotch (I)、(II))，並將此三個濾波器串聯如圖1。所得之高性能濾波器，在高、低頻處，因其可設計成較大斜率，所以去除雜訊功能較強。另外在增益方面則可提升 30 分貝以上。本文僅對運算轉導放大器做分析與實驗，至於如電流傳轉器 (Current Conveyor，CC)，運算電流放大器 (Translinear Operational Current Amplifier，TOCA)，電流式 MOSFET-C 濾波器等，也可應用本文所提之方法而獲得改良。

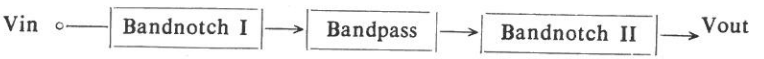

圖 1 兩個帶拒串一個帶通。

二、電路描述

方程式 $T(s)=\dfrac{a_1 s}{s^2+\dfrac{\omega_0}{Q}s+\omega_0^2}$ 是二階帶通濾波器的標準型式。其中 ω_0 是中心頻率，Q 是品質因素，a_1 是常數，中心頻率增益$=\dfrac{a_1 Q}{\omega_0}$；頻寬$=\dfrac{\omega_0}{Q}$。圖 2 表示出其特性曲線[9]。

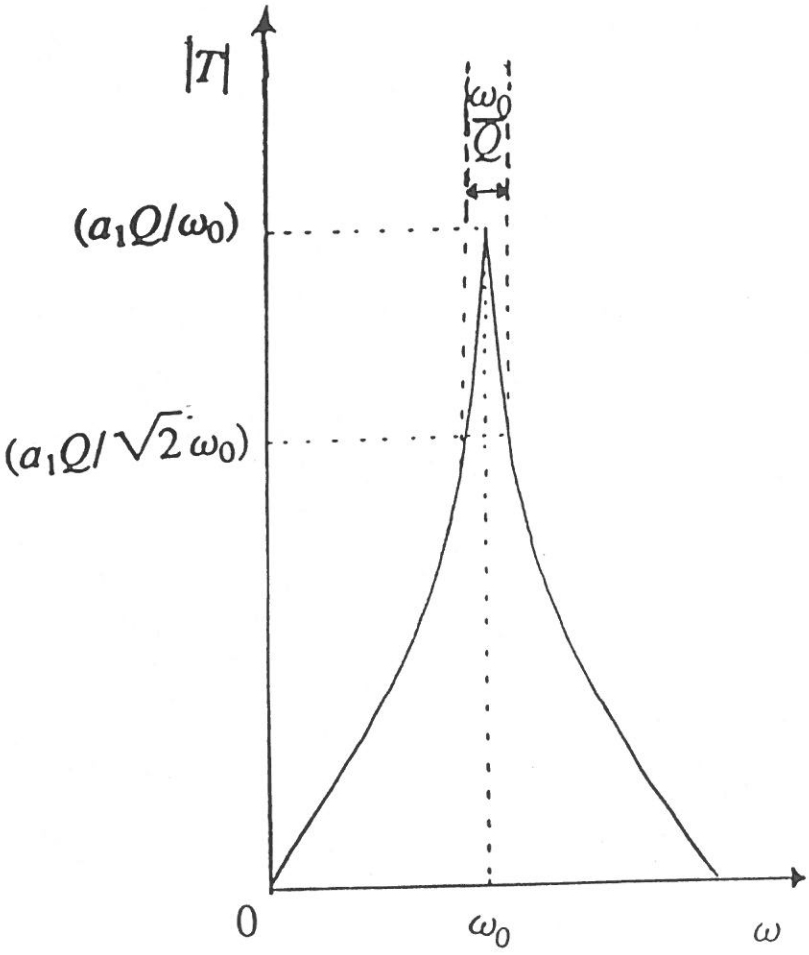

圖 2 帶通濾波器。

方程式 $T(s)=\dfrac{a_2s^2+\omega_0^2}{s^2+\dfrac{\omega_0}{Q}s+\omega_0^2}$ 是二階帶拒濾波器的標準型式。其中 ω_0 是中心頻率，Q 是品質因素，a_2 是常數，高頻增益$=a_2$；頻寬$=\dfrac{\omega_0}{Q}$。圖 3 表示出其特性曲線[9]。

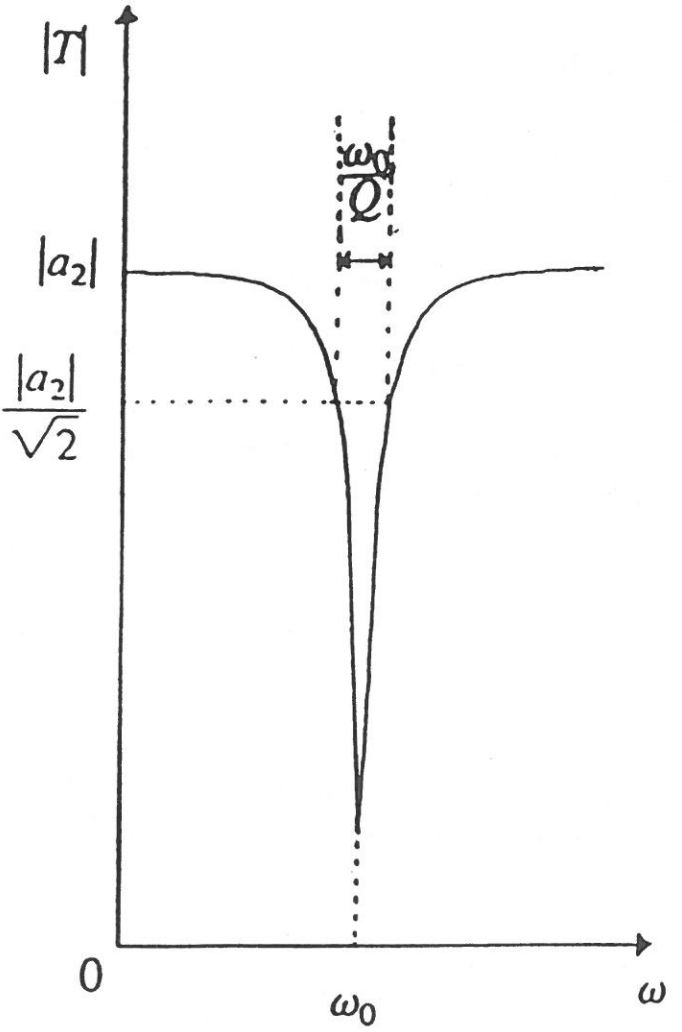

圖 3 帶拒濾波器。

假設 ω_0、ω_{01}、ω_{02} 分別是帶通濾波器、帶拒濾波器 (I) 及帶拒濾波器 (II) 之中心頻率。當帶通濾波器爲固定時，爲了提高整個濾波器之增益，可以設計兩個帶拒濾波器。其中帶拒濾波器 (I) 之中心頻率 $\omega_{01}<\omega_0$；另一個帶拒濾波器 (II) 之中心頻率 $\omega_{02}>\omega_0$。再將三個濾波器串聯如圖 1，高性能增濾波器即可合成。

帶拒濾波器 (I)、(II) 中心頻率 ω_{01}、ω_{02} 可任意選定。爲了得到具有對稱的濾波器。我們必須符合方程式：$\frac{\omega_0}{\omega_{01}}=\frac{\omega_{02}}{\omega_0}=K$，$K$ 是常數。K 值愈大，高性能濾波器的增益值愈大。

假設 $T_{BP}(s)$、$T_{NP1}(s)$、$T_{NP2}(s)$ 分別爲帶通濾波器、帶拒濾波器 (I)、(II) 之轉移方程式。三者串聯後之轉移方程式 $T(s)=T_{BP}(s)\times T_{NP1}(s)\times T_{NP2}(s)$。依據 $T(s)$ 方程式即可找出高性能濾波器的理想曲線圖。

三、實驗結果

從 1971 年之後，運算轉導放大器的積體電路已可在市場上買到[10]。1986 年 Nawrocki 和 Klein 提出第一個具有五種濾波功能的濾波器。如圖 4 所示[3]。它除了主動元件，採用八個 OTA 外，只用了兩個接地電容作被動元件。因此，特別適用於積體電路的製作。

觀察圖 4 的電路中各別元件的功能，可得到輸出-輸入電壓之間的函數關係爲：

$$H(s)=\frac{v_2}{v_1}=\frac{a_2s^2+a_1s+a_0}{b_2s^2+b_1s+b_0}$$

其中

$a_0=g_{a_0}g_1g_2$，$a_1=g_{a_1}g_2c_1$，$a_2=g_{a_2}c_1c_2$

$b_0=g_{b_0}g_1g_2$，$b_1=g_{b_1}g_2c_1$，$b_2=g_{b_2}c_1c_2$

低通：$a_1=a_2=0$

高通：$a_0=a_1=0$

帶通：$a_0=a_2=0$

帶拒：$a_1=0$

全通：$a_0=b_0$，$a_1=b-b_1$，$a_2=b_2$

本文挑選 CA 3080 型運算轉導放大器。而濾波器的實驗描述如下：

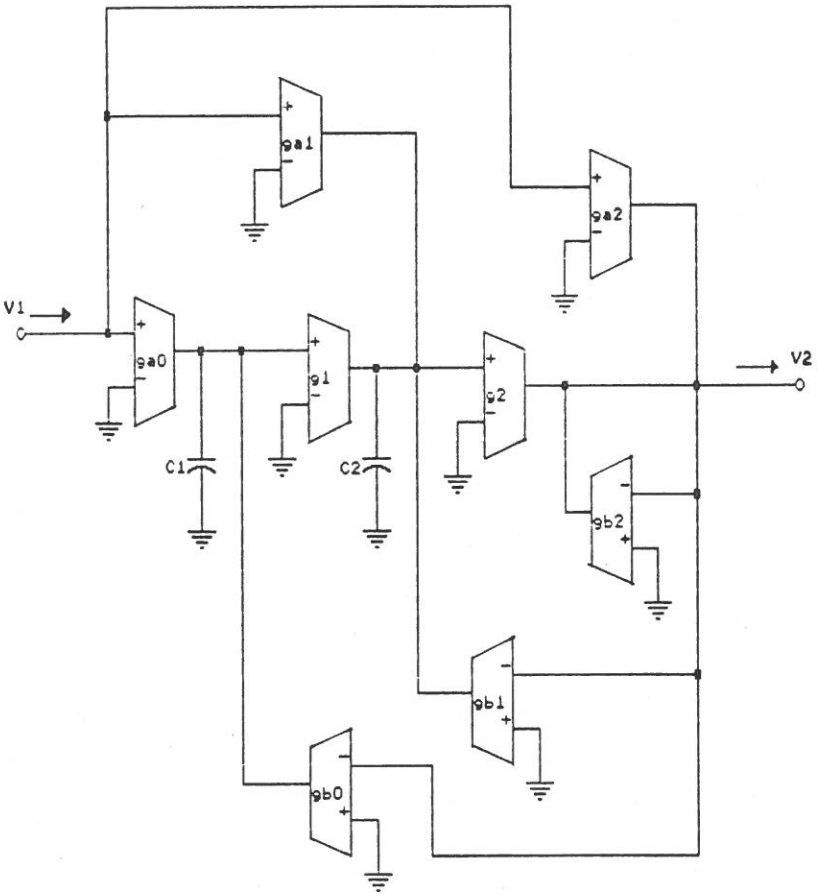

圖 4 Nawrocki 和 Klein 提出的濾波器[3]。

1. 一般帶通濾波器

選用圖 4 濾波器。爲了得到帶通濾波器，必須令 $a_2=a_0=0$。所以選擇的各項參數爲：$g_{b_0}=g_{b_2}=20$ ms，$g_{b_1}=g_{a_1}=2$ ms，$g_{a_0}=g_{a_2}=0$，$c=330$ nF，$g_1=g_2=2$ ms；品質因素 $Q=10$；中心頻率 $f_0=965$ Hz。實驗結果顯示在圖 5。

2. 高性能帶通濾波器

如圖 1，兩個帶拒濾波器 (I)、(II) 串聯一個帶濾波器 。爲了顯示出高性能帶通濾波器的高增益性能。我們選擇帶通濾波器的所有參數值如一般帶通濾波器

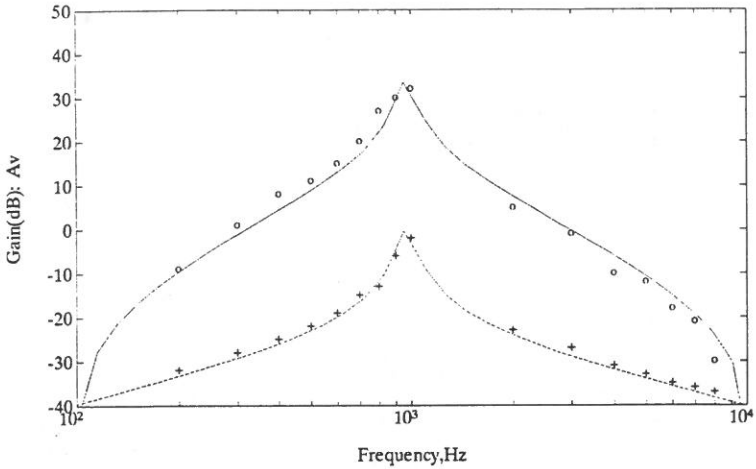

圖 5 實線表示兩個帶拒串聯一個帶通之理想曲線。
○ 表示兩個帶拒串聯一個帶通之測量值
點線 表示一個帶通之理想曲線
＋ 表示一個帶通之測量值

。另外，帶拒濾波器 (I) 和帶拒濾波器 (II) 仍採用圖 4 電路。爲了得到對稱形濾波器。我們任意選定 $K=10$。所以在 $\frac{\omega_0}{\omega_{01}}=\frac{\omega_{02}}{\omega_0}=10$ 的條件下，我們選擇帶拒濾波器 (I) 的中心頻率 $f_0=96$ Hz，$Q=0.1$，$g_{b_0}=g_{b_2}=g_{a_0}=g_{a_2}=2$ ms，$g_{a_1}=0$，$g_{b_1}=20$ ms，$g_1=g_2=0.2$ ms，$c=330$ nF。帶拒濾波器 (II) 的中心頻率 $f_0=9{,}644$ Hz，$Q=0.1$，$g_{b_0}=g_{b_2}=g_{a_0}=g_{a_2}=2$ms，$g_{b_1}=g_1=g_2=20$ ms，$g_{a_1}=0$，$c=330$ nF。實驗結果顯示在圖 5。

四、結　　論

本文提出改善帶通濾波器性能的方法。從實驗上，可以很清楚比較出，改善後之濾波器有極大的增益值。而理論和測量結果之小誤差。可能是被動元件之誤差造成。至於非使用運算轉導放大器做成之濾波器，也可用本文之方法獲得改善。

五、誌　　謝

本研究承蒙侯俊禮老師指導，陳邦家學長及劉岳乘助教在實驗上之協助，謹

致最高謝意。

參考文獻

(1) R.L. Geiger and J. Ferrell, "Voltage Controlled Filter Design Using Operational Transconductance Amplifiers", *Proceedings of the IEEE International Symposium on Circuits and Systems*, **2**, 594-597 (1983).

(2) S.H. Malvar, "Electronically Controlled Active-C Filter and Equalisers with Operational Transconductance Amplifiers", *IEEE Transaction on Circuits and Systems*, **31**, 645-649 (1984).

(3) R. Nawrocki and U. Klein, "New OTA-Capacitor Realisation of a Universal Biquad", *Electronics Letters*, **22**(1), 50-51 (1986).

(4) N.A. Shah and S.N. Ahmad, "Electronically Tunable OTA-Based All-Pass Circuit", *Int. J. Electron.*, **68**, 963-966 (1990).

(5) "Special Issue on Current-Mode Analogue Signal Processing Circuits", *IEE Proc.* **137**, pt. G, No. 2 (1990).

(6) S.I. Liu, "The Analysis and Design of Current-Mode Circuits", Ph.D. Dissertation, Nation Taiwan University (1991).

(7) G.W. Roberts and A.S. Sedra, "All Current-Mode Frequency Selective Circuits", *Electronics*, **25**(12), 759-761 (1989).

(8) M. Higashimura, "Realisation of Current-Mode Transfer Function Using Four-Terminal Floating Nullor", *ibid.*, **27**(2), 170-171 (1991).

(9) A.S. Sedra and K.C. Smith, "Microelectronic Circuit", Third Edition, pp. 776-786 (1991).

(10) A. Bialko and R.W. Newcomb, "Generation of All Finite Linear Circuits Using the Integrated DVCCs", *IEEE Transaction on Circuit Theory*, **18**, 733-736 (1971).

High Performance Bandpass Filter Using OTAs

YUNG-CHANG YIN
Electronic Engineering Department
Fu Jen Catholic University

ABSTRACT

A new design method for improving filter gain of current-mode and voltage-mode RC active bandpass filter is presented. A high performance bandpass filter can be constructed by using cascade connection of one bandpass and two bandnotch filters with adequate resonance frequencies. The designed filter can offer the merit of high current and voltage gain, and thus solve the low-gain problem of the traditional RC active filters. Finally, the experimental results of a designed typical bandpass filter is shown in order to verify the theoretical preciseness and practicability of the design method.

電力系統強健性激磁控制器之設計與分析

潘純新　　李永勳

輔仁大學電子系

摘　　要

本論文提出兩種線上調整控制法則來設計電力系統穩定器 (PSS)。所提比例積分控制器之初始增益利用模態控制理論 (modal control theory) 的極點指定法來設計。控制器的適應性增益 (adaptation gains) 是依據系統的量測值和線上調整演算法作即時調整。特徵值分析和非線性計算機動態模擬證明所提控制器較傳統的固定增益 PI 控制器能够在廣範圍的負載變化下提供更好的阻尼效果和强健性。同時具有線上調整之增益規劃型控制器在相同的阻尼要求下能够節省計算機記憶體容量。

一、引　　言

當電力系統發生突發狀況，如負載變動及開路、短路故障，或電力系統互連 (interconnection) 時，會產生內部自發性低頻振盪現象 (spontaneous low frequency oscillation) 的動態穩定度問題[1,2]。動態穩定度的低頻振盪現象代表發電機轉軸的動態行爲，其頻率大約在 0.5～2 Hz 之間，這種現象可用線性系統的頻率領域的特徵值來分析，相對於低頻振盪的特徵值稱爲系統機電模式 (electromechanical mode)。系統低頻振盪常導致系統運轉困難，嚴重則可能引起系統跳機、解聯等穩定度問題[2~5]。

電力系統在遭遇負載變動或故障等干擾後將會產生振盪現象，此時系統必須要有足够的阻尼使得干擾發生後發電機能迅速回復到穩定狀態。一般改善動態穩定度的方法有採用快速動作的靜態激磁系統 (static excitation system) 外加一個額外的輔助控制訊號如發電機角速度偏移量 $\Delta\omega$ 或發電機功率偏移量 ΔP 回授的電力系統穩定器 (power system stabilizer、PSS)[2,3] 來提供系統阻尼提高動態穩定度。傳統 PSS 採用相位領先-落後 (phase lead-lag) 控制器[4]，最近比例積分 (PI) 電力系統穩定器因其有結構簡單容易施行等特點而常被引用[5]。

固定增益型控制器之主要缺點是它的增益設定在某一特定的工作點，對其他的工作條件時就不能滿足系統的需要了。系統工作點由於負載條件的改變或遭遇故障後而產生的大幅的漂移，此時固定增益的控制器就不能提供足够的阻尼效果了。解決的方法是採用自調式 (self-tuning) 等適應控制器作線上自我調整控制器參數值以達到系統阻尼效果[7]。利用增益規劃 (gain scheduling) 法來設計一

種增益查看表 (look up table) 作線上調整的 PSS 也可以達到廣範圍的負載變化下的阻尼效果[6]。

本論文利用一種簡單的線上調整控制法則 (on-line tuning control algorithm) 來設計線上調整型 PSS 和具有線上調整之增益規劃型 PSS，線上調整型 PSS 之初始增益和增益規劃法之增益查表內的增益值是利用極點指定法來計算，查看表的增益是根據不同的 $P-Q$ 區域來設計然後儲存在記憶體內。數位計算機依據系統偵測到的量測值，然後在增益查看表選取對應的增益。因爲 $P-Q$ 區域之規劃受記憶體空間限制不可能切割成無限多的區間，而在每一區間增益的調整就需仰賴線上調整法則依據發電機轉軸的速度量測值在每一取樣瞬間作線上自我調整。在干擾狀態下發電機動態響應的計算機模擬顯示線上調整型和具有線上調整之增益規劃型 PSS 比固定增益型和增益規劃型 PSS 更具阻尼效果。在有限的記憶體容量下具線上調整之增益規劃型 PSS 更具有經濟效益。本論文同時比較各種不同法則的動態阻尼效果，用以驗證所提的線上調整型 PSS 之對負載條件變化之強健性。

二、電力系統數學模式之建立

在研究電力系統之動態穩定度和暫態穩定度問題時，必須先建立一適當且完整的數學模型，模型之複雜度視問題的定義和所要求的精確度來決定，在電力系統動態問題研究上根據不同的問題定義去選擇最適合的系統模型。

而在電力系統低頻振盪的動態問題，無論在何種干擾下，並非所有系統元件的特性都對動態問題有很大之關聯，只有其中一部分元件對動態特性影響非常重要而且直接，如汽渦輪調速機系統，同步發電機，和激磁系統等。而整個電力系統的動態行爲就由這些系統的非線性微分方程式來描述。爲方便在頻率領域上作系統特性分析和控制器之設計，將系統非線性微分方程式經過增量微分 (incremental differential)，可得在某一工作點的線性化微分方程式，此方程式經整理後可表示成狀態方程式，系統在工作點附近的動態行爲可由狀態方程式的特徵值來評估，由特徵值在 S 平面的位置可判斷系統的動態穩定度[1~3]。

本節將建立電力系統的非線性動態方程式，然後在工作點上將其線性化得一組高階的狀態方程式，利用此狀態方程式來作系統分析和控制器設計的理論依據。

圖 1 爲本研究的電力系統，包含一同步發電機經由一對並聯傳輸線連接到無限滙流排。同步發電機模型爲凸極式，每一軸上均有阻尼繞組，同時忽略次暫態效應，發電機動態行爲以雙軸模型 (two-axis model) 來描述[1]，發電機轉子電路的暫態電壓方程式爲：

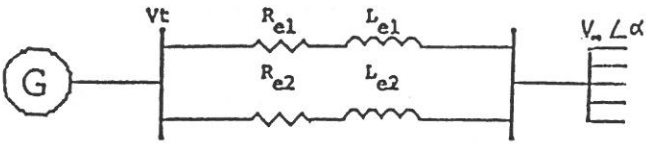

圖 1 單機無限滙流排系統。

$$\dot{E}'_d = \frac{-E'_d-(X_q-X'_q)I_q}{T'_{q0}} \tag{1}$$

$$\dot{E}'_q = \frac{E_{FD}-E'_q+(X_d-X'_d)I_d}{T'_{d0}} \tag{2}$$

式中 $T'_{q0}=L_q/r_q$、$T'_{d0}=L_f/r_f$ 分別爲交軸和直軸次暫態時間常數。

由發電機滙流排往發電機及雙並輸電線兩端看，其直軸和交軸電壓方程式爲：

$$V_d=E'_d-rI_d-X'_qI_q=-V_\infty \sin(\delta-\alpha)+R_eI_d+\omega L_eI_q \tag{3}$$

$$V_q=E'_q-rI_q+X'_dI_d=V_\infty \cos(\delta-\alpha)+R_eI_q-\omega L_eI_d \tag{4}$$

發電機的機械搖擺方程式 (swing equations) 爲：

$$\dot{\omega} \doteq \frac{T_m-D\omega-T_e}{M} \tag{5}$$

$$\dot{\delta}=\omega_b(\omega-1.0) \tag{6}$$

其中 T_m 爲調速機 (governor) 輸出的機械轉矩，$T_e=E'_dI_d+E'_qI_q$ 爲發電機內部的電磁轉矩。

同步發電機內激磁電壓由靜態激磁機來控制，圖 2 爲靜態激磁系統 (static excitation system) 方塊圖，激磁系統動態方程式爲：

$$\dot{E}_{FD} = \frac{-E_{FD}+K_{AE}(V_{ref}-V_t-V_s+U_{PSS})}{T_{AE}} \tag{7}$$

$$\dot{V}_s = \frac{K_F\dot{E}_{FD}-V_s}{T_F} \tag{8}$$

其中 U_{PSS} 爲電力系統穩定器 (PSS) 的輸出訊號，T_{AE} 及 T_F 分別爲激磁機和穩定變壓器的時間常數。

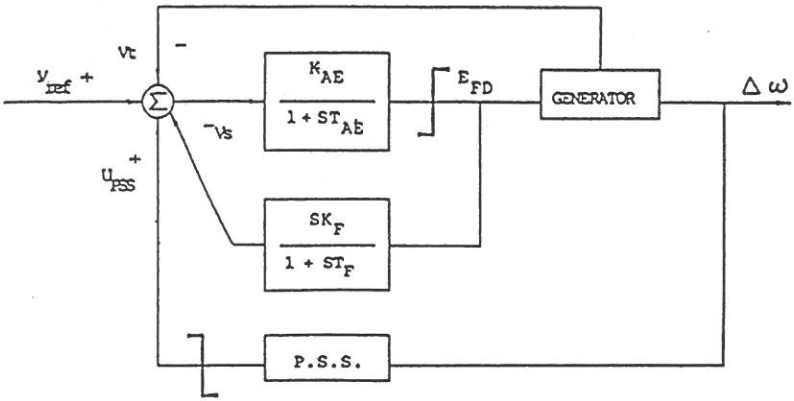

圖 2 激磁系統。

圖 3 爲發電機之調速機和再熱式渦輪機 (governor and reheat turbine) 方塊圖，其輸出 P_m 爲推動發電機之機械功率。調速機和渦輪機動態方程式爲：

$$\dot{P}_R=\frac{K_G(\omega_{ref}-\omega)-P_R}{T_{SR}} \tag{9}$$

$$\dot{P}_H=\frac{P_R-P_H}{T_{SM}} \tag{10}$$

$$\dot{P}_C=\frac{P_H-P_C}{T_{CH}} \tag{11}$$

$$\dot{P}_m=\frac{P_C+K_{RH}T_{RH}\dot{P}_C-P_m}{T_{RH}} \tag{12}$$

合併 (1)～(12) 式共 10 個一階非線性動態微分方程式，將這些方程式在工作點上線性化可得一組狀態方程式。利用頻域分析法，由狀態方程式的特徵值直接求得發電機的阻尼與低頻振盪模式。由系統狀態方程式和輸出方程式也可以判斷系統是否穩定以及設計所需要的電力系統穩定化設備。

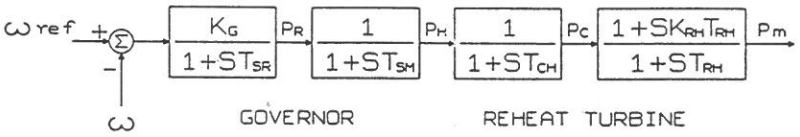

圖 3 渦輪機和調速機系統。

系統數如下[1]：

同步發電機 (p. u.)

$X_d=1.7$ $X_q=1.64$ $X'_d=0.245$ $X'_q=0.38$
$r=0.001096$ $T'_{d0}=5.9$ sec $T'_{q0}=0.075$ sec $M=4.4$

激磁系統

$K_{AE}=400$ $T_{AE}=0.05$ sec $K_F=0.025$ sec
$T_F=1$ sec $E_{FD\ max}=+7.3$ p. u. $E_{FD\ min}=-7.3$ p. u.

調速機

$K_G=3.5$ $T_{CH}=0.05$ sec $T_{RH}=8$ sec
$T_{SR}=0.1$ sec $T_{SM}=0.2$ sec $K_{RH}=0.3$

傳輸線 (p. u.)

$R_{e1}=R_{e2}=0.04$ $L_{e1}=L_{e2}=0.8$

電力系統穩定器

$T_W=0.125$ sec $U_{PSS\ max}=0.12$ p. u. $U_{PSS\ min}=-0.12$ p. u.

標稱工作點

$P_0=1.0$ p. u. $Q_0=0.2$ p. u. $V_t=1.0$ p. u.

三、控制器之設計

在電力系統穩定器參數值的計算上，首先須將非線性的系統動態方程式在工作點附近線性化以便獲得一組所需的線性模式，此系統的狀態方程式爲[9]：

$$\dot{X}(t)=AX(t)+BU(t) \tag{13}$$

$$Y(t)=CX(t) \tag{14}$$

其中 $X(t)=[\Delta\omega, \Delta\delta, \Delta E'_d, \Delta E'_q, \Delta E_{FD}, \Delta V_S, P_R, \Delta P_H, \Delta P_C, \Delta P_m]^T$ 爲系統狀態，$Y(t)=\Delta\omega$ 爲系統輸出訊號，$U(t)=U_{PSS}$ 爲電力系統穩定器的輸出控制訊號，A、B 和 C 爲系統常數矩陣。P_R、P_H、P_C 和 P_m 爲調速機和再熱式渦輪機的狀態變數。

表一、第二行爲本研究系統開路狀態，也就是未加電力系統穩定器時的系統特徵值，其代表低頻振盪的機電模式爲 $\lambda_0=-0.077\pm j10.13=-\alpha_0\pm j\omega_0$，阻尼比$=\alpha_0/\sqrt{\alpha_0^2+\omega_0^2}=0.007$，而一般低頻振盪阻尼比要求在 0.1-0.2 之間，這表示同步發電機的阻尼非常差，所以爲改善系統動態阻尼效果，必須外加一個以發電機轉軸轉速爲回授訊號的輔助控制器，也就是 PSS，來提供額外的阻尼訊號以改善系統的阻尼。

表一 系統特徵值

	$P_0=1.0$ p.u.** $Q_0=0.2$ p.u.		$P_0=1.2$ p.u. $Q_0=0.8$ p.u.		$P_0=0.8$ p.u. $Q_0=0.6$ p.u.	
	Open system	Fixed gain	Open system	Fixed gain	Open system	Fixed gain
Generator	$-0.077\pm j10.13$*	$-2.4\pm j10.2$*	$0.229\pm j8.83$*	$-2.097\pm j7.81$*	$-0.096\pm j8.42$*	$-1.611\pm j7.52$*
	$-1.535\pm j0.72$	$-2.349\pm j2.86$	-2.843 -1.401	$-3.075\pm j4.45$	-2.91 -1.31	$-3.902\pm j3.69$
Exciter	-41.96	-41.96	-42.02	-42.01	-41.83	-41.83
	-218.45	-218.59	-217.85	-217.97	-217.4	-217.48
Turbine and governor	-0.1249	-0.1249	-0.1249	-0.1249	-0.1248	-0.1248
	-4.9	-5.08	-4.85	-5.06	-4.86	-5.08
	-10.2	-10.07	-10.24	-10.07	-10.25	-10.09
	-19.94	-19.95	-19.94	-19.95	-19.93	-19.94
PI controller		-1.53		-1.26		-1.23

**: Nominal operating point.
*: Electromechanical mode.

1. 固定增益和增益規劃式 PI 型 PSS 之設計[6]

圖 4 爲固定增益的 PI 型 PSS，PI 控制器的參數是利用模態控制理論 (modal control theory) 的極點指定法來決定。將 (13) 和 (14) 式取拉氏轉換 (Laplace transformation)，可得：

$$SX(s)=AX(s)+BU(s) \tag{15}$$

$$Y(s)=CX(s) \tag{16}$$

控制訊號可以表示爲：

$$U(s)=H(s)Y(s)=\frac{ST_W}{1+ST_W}\left(K_P+\frac{K_I}{S}\right)Y(s) \tag{17}$$

其中 T_W 爲消去項時間常數 (washout term time constant)，K_P 和 K_I 爲待決定的控制器參數值。

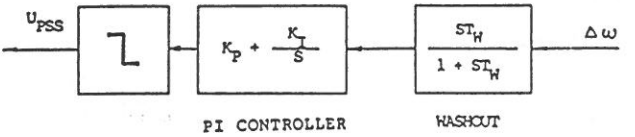

圖 4 固定增益 PI 型 PSS。

由 (15) 和 (16) 式可得閉回路系統的特徵方程式爲[6]：

$$1-C(SI-A)^{-1}BH(s)=0 \tag{18}$$

對任何閉回路特徵值入代入 (18) 式可得：

$$\left.\begin{aligned} &1-C(\lambda I-A)^{-1}BH(\lambda)=0 \\ &\text{或} \\ &H(\lambda)=[C(\lambda I-A)^{-1}B]^{-1}=\frac{\lambda T_W}{1+\lambda T_W}\left(K_P+\frac{K_I}{\lambda}\right) \end{aligned}\right\} \tag{19}$$

假設 λ_1 和 λ_2 爲預定的一對代表機電模式的特徵值，我們將 λ_1 和 λ_2 代入 (19) 式則可得一組由 K_P 和 K_I 所組成的代數方程式，解這些代數方程式可得所需要的 K_P 和 K_I 參數值。

由表一、第二行可知開路系統的機電模式必須藉 PI 控制器將它向左邊移到較合乎要求的位置。在本論文中機電模式特徵值被指定爲：

$$\lambda_1, \lambda_2=-2.4\pm j10.2 \quad \text{(阻尼比}=0.23\text{)}$$

從 (19) 式可獲得固定增益 PI 型 PSS 的控制器參數值爲：

$$K_P=13.97$$

$$K_I=-188.63$$

上述的預先指定特徵值是根據同步發電機阻尼的期望值而任意決定的。如果控制器參數值超出合理範圍時，則指定特徵值必須調整直到所要求的參數值落在適當的範圍。表一、第三行的系統特徵值爲加上所設計的固定增益 PI 型 PSS 時其機電模式恰如所指定的。

發電機低頻振盪的阻尼特性只要系統的負載條件不改變的話都能夠維持在相當的水準。不幸的，這對實際系統是永遠不可能達成的，因爲系統的負載條件會隨系統的干擾和負載的變動而改變。爲著驗證負載條件改變對系統特徵值之影響

，表一、第四～六行爲系統負載條件變化下的系統特徵，值在特徵值中可看出機電模式對負載變動較其他模式要靈敏。在 $P_0=1.2$ p. u.，$Q_0=0.8$ p. u. 時開路系統機電模式爲不穩定的，$P_0=0.8$ p. u.，$Q_0=0.6$ p. u. 時機電模式稍爲好一些但仍很差。表中第五行和第七行爲加上固定增益 PI 型 PSS 負載條件變化之系統特徵值，表中得知負載增加時其機電模式由 $(-2.4\pm j10.2)$ 變爲 $(-2.097\pm j7.81)$ 阻尼變差了，當負載減輕時機電模式變爲 $(-1.611\pm j7.52)$ 阻尼變得更差。所以固定增益的 PSS 在廣範圍負載變化下就很難維持系統良好的阻尼效果了。

爲著達到廣範圍負載條件變化下系統仍然有相同的阻尼效果，在文獻 (6) 提出利用增益規劃法來設計一可適性 PSS，圖 5 所示既爲其系統方塊圖，其設計的理論是將發電機之 P—Q 平面劃分爲許多小方塊，在 off-line 時每一小塊以上述極點指定法計算 PSS 參數值。這些參數值存在計算機記憶體中當查看表。在 on-line 時計算機在每一取樣時刻不停地偵測系統的實功率 P 和虛功率 Q，再從查看表中取得相對應的 PSS 參數值，因此 PSS 隨時根據偵測結果選取適當參數值，如此也可保證在任何工作點都能提供系統良好阻尼作用。表二爲系統在不同工作點下，機電模式維持在相同 $(-2.4\pm j10.2)$ 時所需要的 PI 型 PSS 參數值。

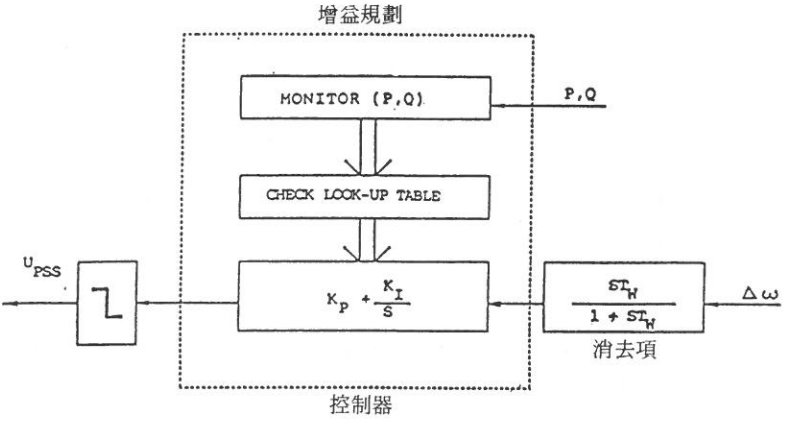

圖 5 增益規劃法 PI 型 PSS[6]。

表二 固定機電模式所求 PI 型 PSS 增益

Gains \ Operation condition	$P_0=$ 1.5 p.u. $Q_0=$ 0.9 p.u.	$P_0=$ 1.2 p.u. $Q_0=$ 0.8 p.u.	$P_0=$ 1.0 p.u.* $Q_0=$ 0.2 p.u.	$P_0=$ 0.8 p.u. $Q_0=$ 0.6 p.u.	$P_0=$ 0.6 p.u. $Q_0=$ 0.9 p.u.	$P_0=$ 0.4 p.u. $Q_0=$ 0.5 p.u.
K_P	35.72	30.73	13.97	29.97	54.45	56.82
K_I	−78.78	−109.94	−188.63	−97.59	− 3.77	71.70

*: Nominal operating point.

增益規劃法雖可提供在廣範圍負載條件變化下的阻尼效果，但是其計算機記憶體容量若 $P-Q$ 小方塊畫分得很細小時非常浪費，若小方塊劃分得太大時，其阻尼效果就會不理想，本論文提出下列兩方法來改善增益規劃法在使用上的一些限制。

2. 具有線上調整 PI 型 PSS 之設計

圖 6 爲具有線上調整 (on-line tuning) PI 型 PSS 方塊圖，誤差訊號鑑別器 (error signal conditioner) 的回授訊號爲發電機的速度誤差 $\Delta\omega$，其取樣週期爲 T_2，因爲線上調整 PI 控制器參數值 K_{PA} 及 K_{IA} 需要經過適應演算機構 (adaptation mechanism) 的計算，所以輔助控制訊號 U_{PSS} 之取樣週期 T_1 較 T_2 爲大，利用此種雙取樣之控制方式，可以減少零階保持取樣器的延遲誤差，而且回授訊號也能够維持最新狀態[9]。

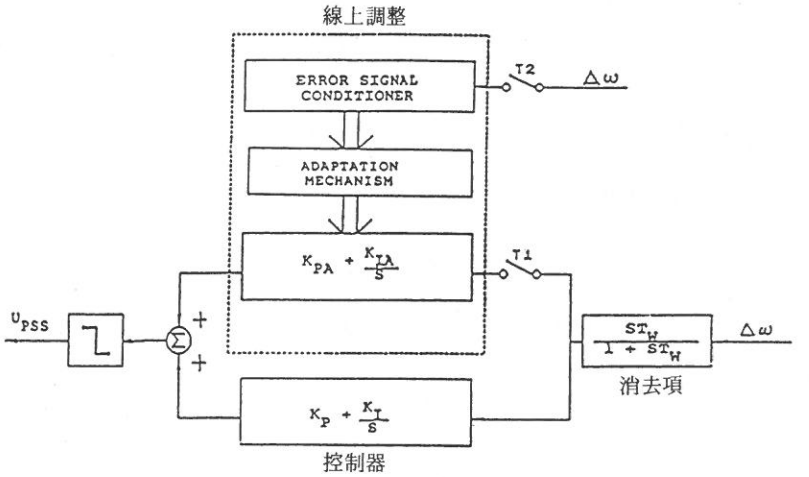

圖 6 具有線上調整 PI 型 PSS。

在系統動態期間，速度誤差訊 $\Delta\omega$ 是取樣瞬間直接量測，而速度誤差增量 $d\Delta\omega$ 是由誤差訊號鑑別器計算出來。線上調整 PI 控制器增益由適應機構 (adaptation mechanism) 根據一序列速率誤差量 $\Delta\omega$ 和速度誤差增量 $d\Delta\omega$ 資料來決定的。

圖 7 爲速度誤差和速度誤差增量所構成的誤差平面[8]，其中直線 L_α 爲止帶區 (dead-band area)，直線 L_β 爲垂直於 L_α 的另一直線，L_α 和 L_β 同時通過誤差平面原點。在取樣瞬間系動狀態爲 $(\Delta\omega_0, d\Delta\omega_0)$，假設 $(\Delta\omega, d\Delta\omega)$ 爲系統下的下一個狀態，令通過 $(\Delta\omega_0, d\Delta\omega_0)$ 和 $(\Delta\omega, d\Delta\omega)$ 且平行於直線 L_α 的直線斜率爲 $-m$，表示爲：

$$\frac{d\Delta\omega - d\Delta\omega_0}{\Delta\omega - \Delta\omega_0} = -m \tag{20}$$

則通過 $(\Delta\omega, d\Delta\omega)$ 和原點的直線方程式爲：

$$\frac{d\Delta\omega}{\Delta\omega} = \frac{1}{m} \tag{21}$$

將 (21) 式中 $d\Delta\omega$ 代入 (20) 式，可得：

$$\Delta\omega = m(m^2+1)^{-1}(m\Delta\omega_0 + d\Delta\omega_0) \tag{22}$$

$$d\Delta\omega = (m^2+1)^{-1}(m\Delta\omega_0 + d\Delta\omega_0) \tag{23}$$

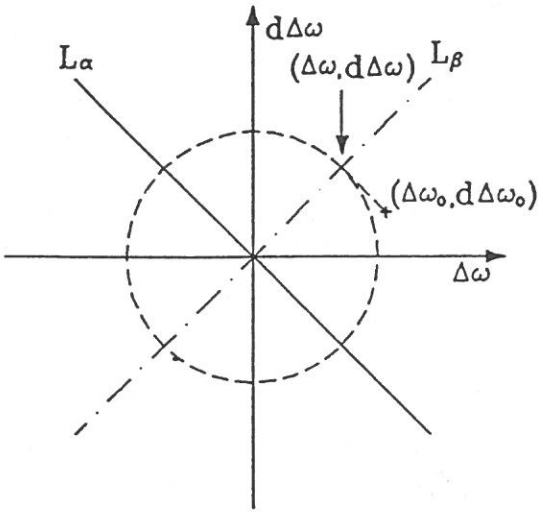

圖 7 回授訊號機構成之誤差平面。

由 $(\Delta\omega, d\Delta\omega)$ 至原點之距離爲：

$$[(\Delta\omega)^2+(d\Delta\omega)^2]^{1/2}=(m^2+1)^{-1/2}(m\Delta\omega_0+d\Delta\omega_0) \tag{24}$$

假設控制訊號偏移量 ΔU_{PSS} 爲線性且正比於上式的距離，則：

$$\Delta U_{PSS}=P(m^2+1)^{-1/2}m\Delta\omega_0+P(m^2+1)^{-1/2}d\Delta\omega_0 \tag{25}$$

其中 P 爲一比例常數，在 $t=K\Delta T$，$K=1, 2, 3, \cdots, n$，其中 ΔT 爲取樣週期，(25) 式可以重寫爲：

$$\Delta U_{PSS}(t)=P(m^2+1)^{-1/2}m\Delta\omega_0(t)+P(m^2+1)^{-1/2}d\Delta\omega_0(t) \tag{26}$$

將 (26) 式兩邊積分，可得：

$$\begin{aligned} U_{PSSA}&=P(m^2+1)^{1/2}m\sum_{t=0}^{\infty}\Delta\omega_0(t)\Delta t+P(m^2+1)^{-1/2}\Delta\omega_0(t) \\ &=K_{IA}\sum_{t=0}^{\infty}\Delta\omega_0(t)\Delta t+K_{PA}\Delta\omega_0(t) \end{aligned} \tag{27}$$

其中 K_{IA} 和 K_{PA} 爲線上調整 PI 型控制器參數[9]，表示爲：

$$K_{PA}=P(m^2+1)^{-1/2} \tag{28}$$

$$K_{IA}=P(m^2+1)^{-1/2}m=mK_{PA} \tag{29}$$

圖 6 具有線上調整 PI 型 PSS，其中 K_P 和 K_I 的參數值是在特定工作點下利用前面所敍述的極點指定法來決定的。而線上調整控制器參數值是由（28）和 (29) 式來決定，其中只有一個 P 的參數必須事先決定，K_{PA} 和 K_{IA} 的值能夠在每一取樣瞬間依據上述兩式來更新。

3. 具有線上調整之增益規劃式 PI 型 PSS 之設計

線上調整 PI 型 PSS 在工作點附近的負載變化下能夠維持非常好的阻尼效果，但是當負載條件在廣範圍變化下或是在大訊號干擾下系統阻尼效果就不是很理想了。圖 8 爲將上面所討論的線上調整式和增益規劃式兩控制法合併在一起的一種新的控制法則。

圖 8 的增益規劃式 PI 控制器增益是根據 $P-Q$ 偵測器偵測系統的 $P-Q$ 量測值，依據此量測值在計算機記憶體選取對應的參數值，使得 K_P 和 K_I 能夠隨系統負載條件和干擾訊號變化而隨時更新。另一組線上調整 PI 型控制器的參數值就根據系統速度誤差回授訊號利用 (28) 和 (29) 式在每一取樣瞬間隨時更新。將兩控制法則合併後使得系統獲相當好的強健性 (robustness)。

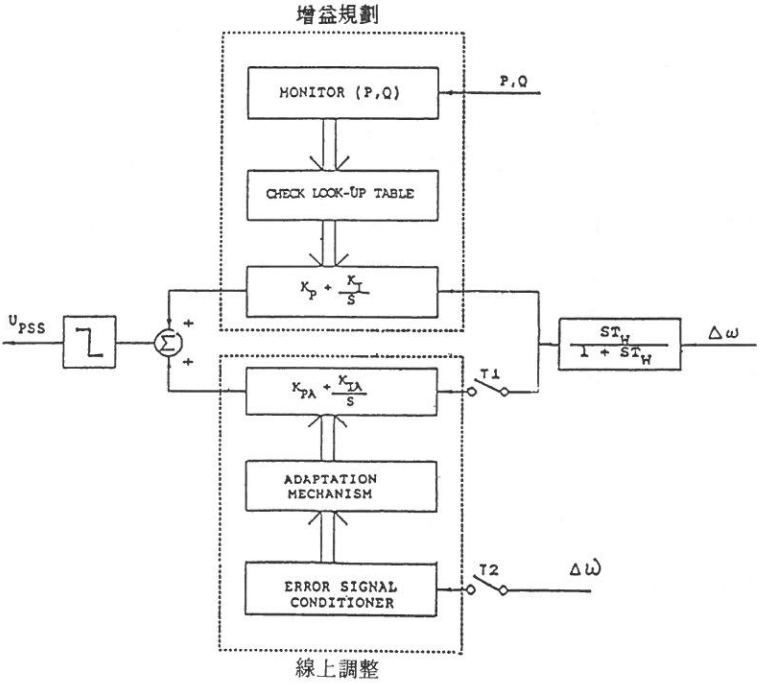

圖 8 具有線上調整之增益規劃式 PI 型 PSS。

四、系統動態模擬

爲了驗證所提控制器在各種不同干擾下和負載變化下的阻尼效果，利用系統非線性方程式，來作時間領域的動態模擬，模擬中線上調整的雙取樣週期爲 $T_1=5$ m sec 和 $T_2=20$ m sec，增益 P 經過適當調整和試驗取 $P=50$。而在增益規劃中 $P-Q$ 小方塊爲 0.1 p. u.×0.1 p. u. 和取樣週期爲 5 m sec。模擬時包含所有的非線性限制如激磁機的界限電壓(ceiling voltage)和控制訊號極限等。

圖 9 至圖 11 爲不同負載條件下系統遭遇 0.25 p. u. 的步階機械轉矩變化的動態響應，圖 9(a)、圖 9(b)、圖 9(c) 分別爲 $P_0=1.0$ p. u.，$Q_0=0.2$ p. u. 的同步發電機的速度、轉矩角和有效功率及無效功率等響應。圖 9(d)、圖 9(e)、圖 9(f) 分別爲增益規劃、線上調整和線上調整之增益規劃等 PSS 之控制器參數值響應，圖 10 及圖 11 分別爲 $P_0=1.2$ p. u.，$Q_0=0.8$ p. u. 及 $P_0=0.8$ p. u.，$Q_0=0.6$ p. u. 時的系統動態響應，表三爲系統在上述干擾時速度響應之穩定時間 (settling time)。圖 12 及圖 13 分別爲不同負載條件下系統遭遇 100 m sec 之雙饋線中單線開線故障的動態響應。由圖 9 至圖 13 和表三的動態響應可獲下列結果：

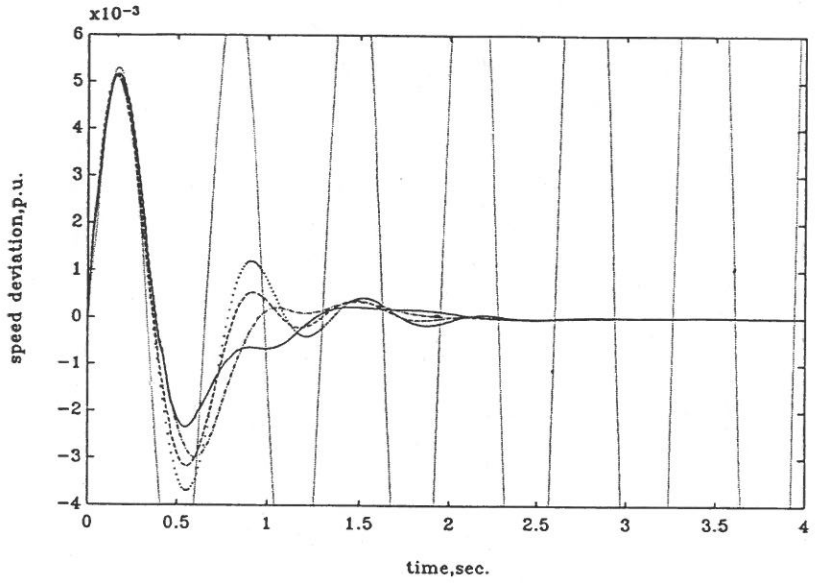
x10⁻³
speed deviation,p.u.
time,sec.

圖9(a)

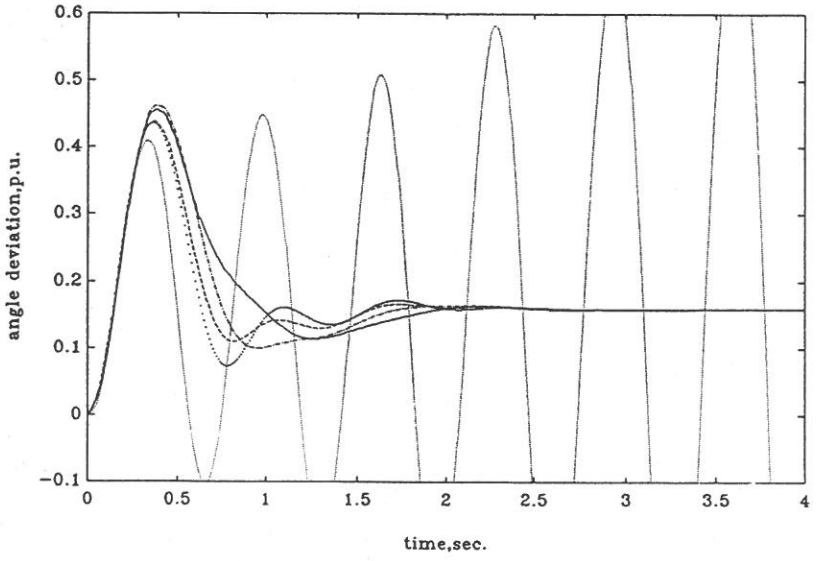
angle deviation,p.u.
time,sec.

圖9(b)

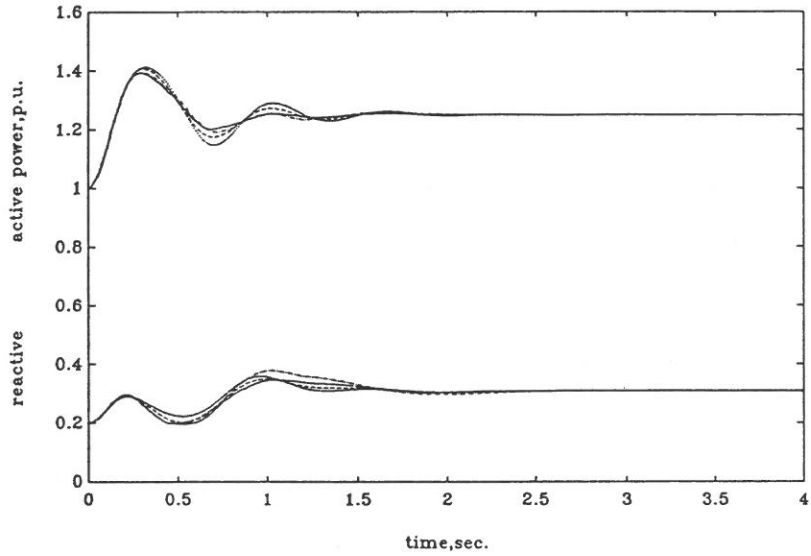

圖9(c)

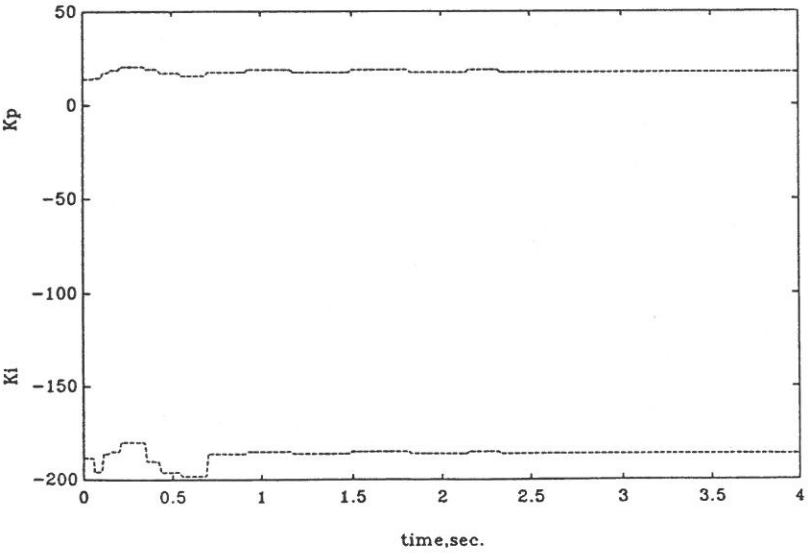

圖9(d)

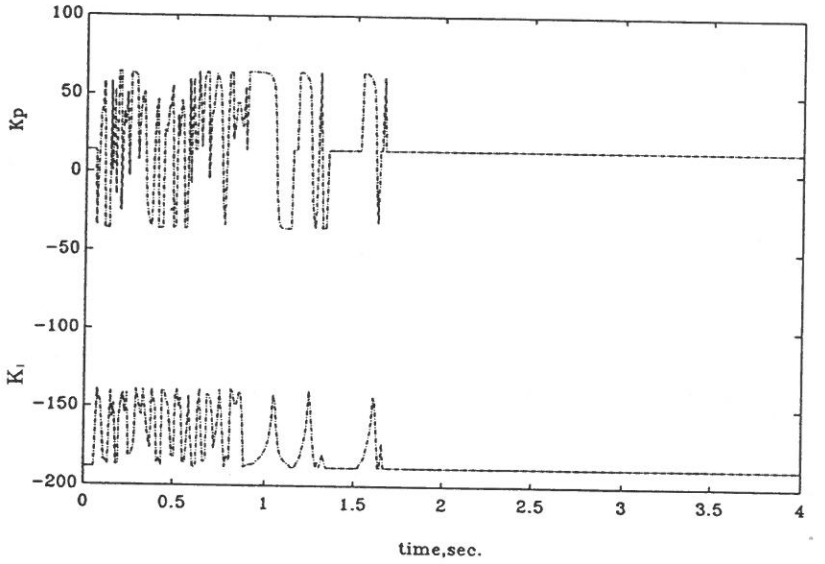

圖9(e)

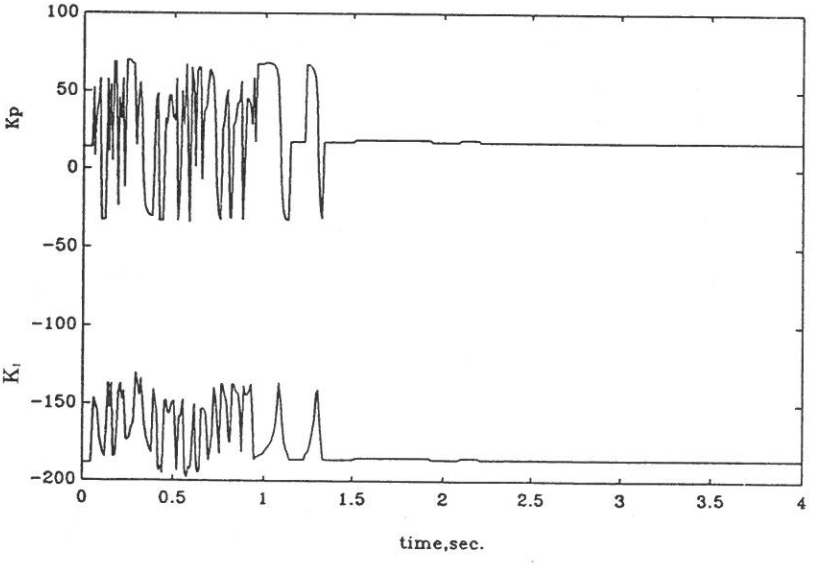

圖9(f)

圖 9 機械轉矩變化之系統動態響應 (P_0=1.0 p.u.，Q_0=0.2 p.u.)。

····· 開路系統　　-·-·-· 線上調整 PSS

· · · · 固定增益 PSS　　——— 具線上調整之增益規劃 PSS

- - - - 增益規劃 PSS

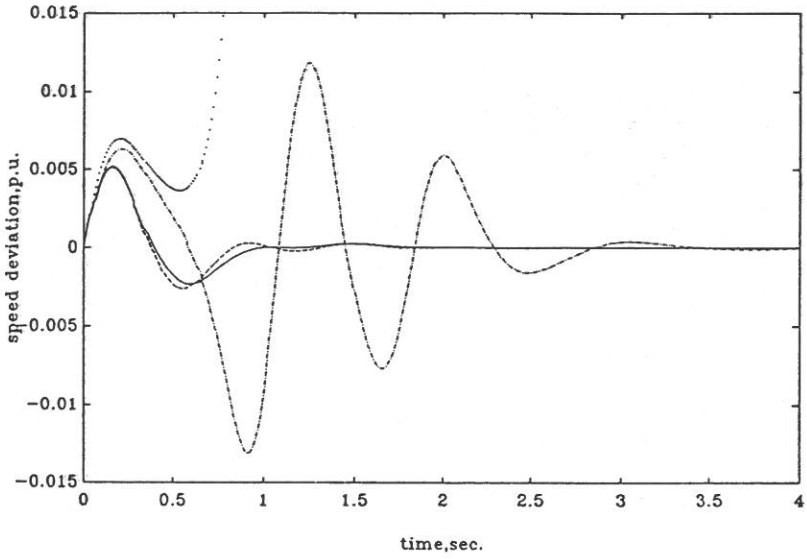

圖10(a)

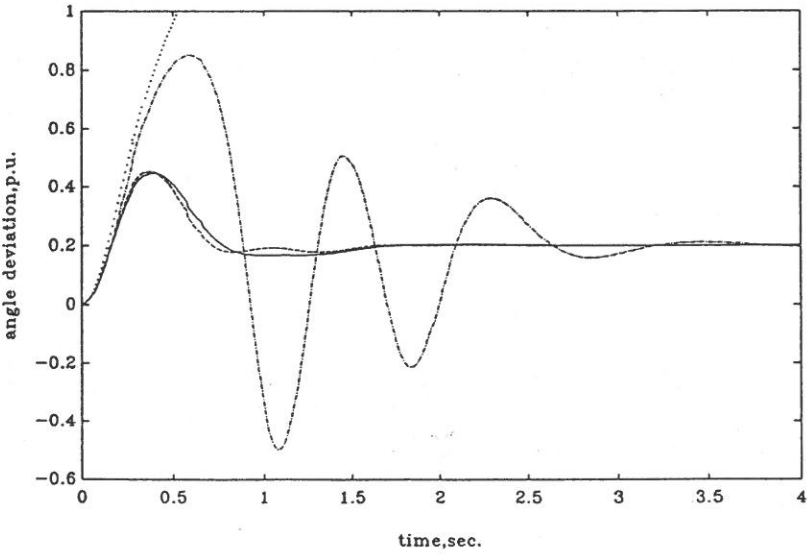

圖10(b)

圖10 機械轉矩變化之系統動態響應 ($P_0=1.2$ p.u.，$Q_0=0.8$ p.u.)。

- • • • 固定增益 PSS
- -•-•- 線上調整 PSS
- - - - 增益規劃 PSS
- ——— 具線上調整之增益規劃 PSS

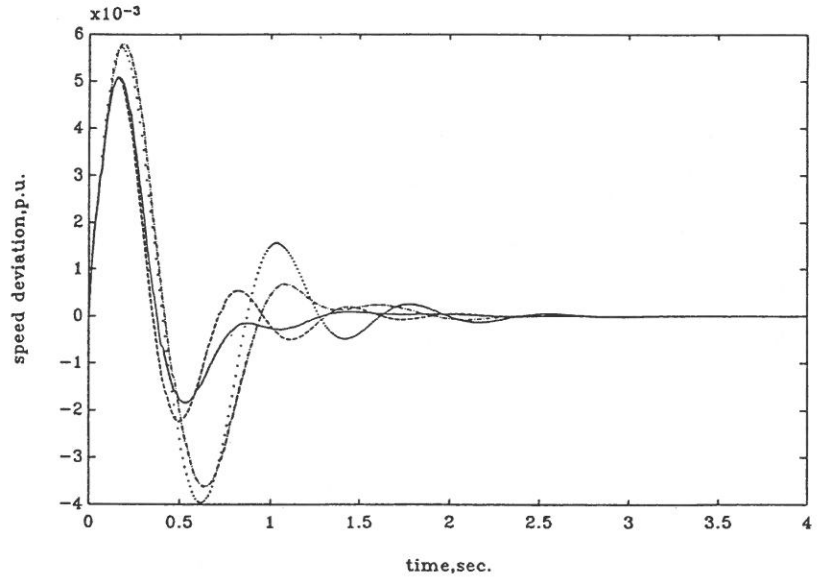

圖11(a)

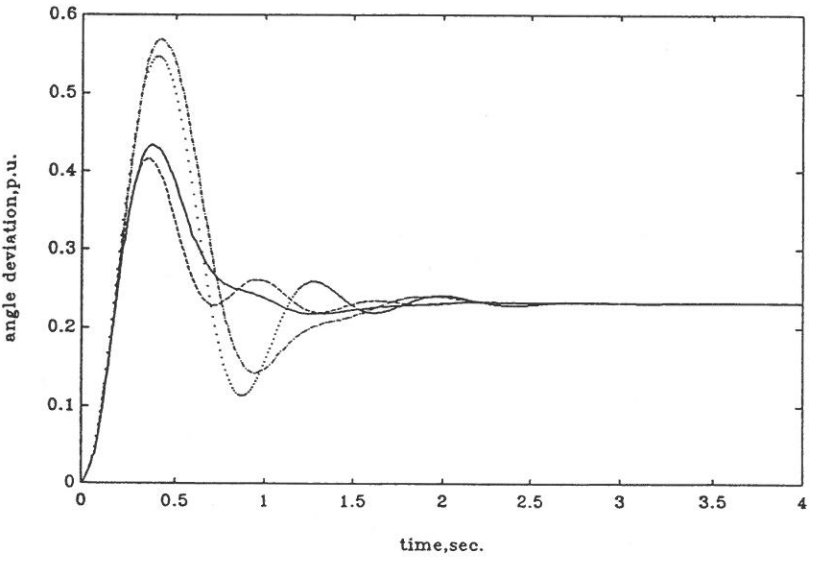

圖11(b)

圖11 機械轉矩變化之系統動態響應 (P_0=0.8 p.u.，Q_0=0.6 p.u.)。

- · · · · 固定增益 PSS
- - - - 增益規劃 PSS
- -·-·- 線上調整 PSS
- ——— 具線上調整之增益規劃 PSS

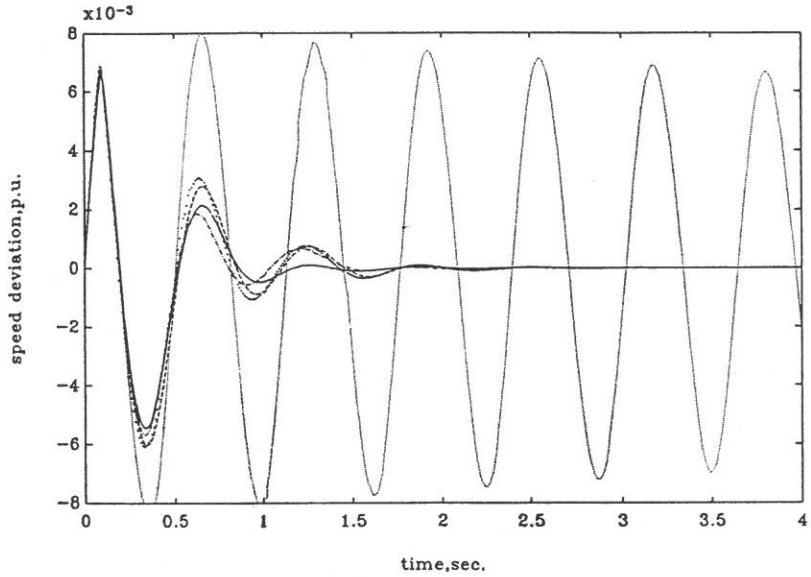

圖12(a)

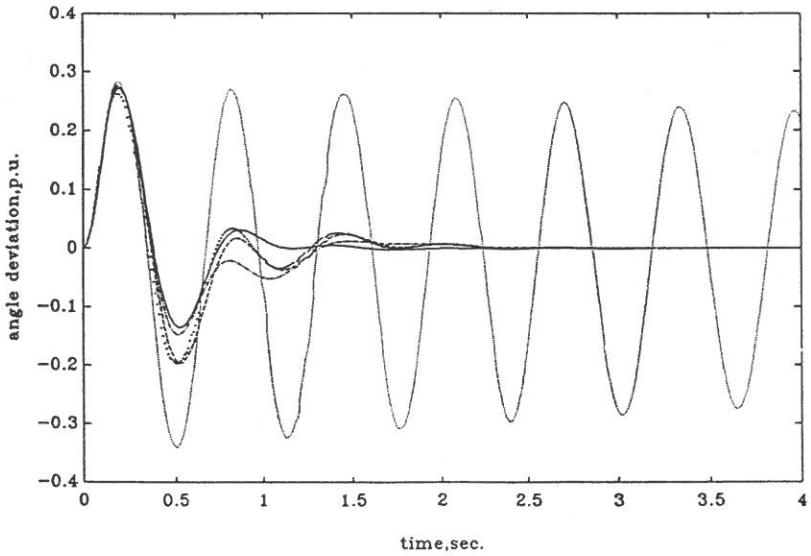

圖12(b)

圖12 系統開線故障之動態響應 (P_0=1.0 p.u.，Q_0=0.2 p.u.)。

····· 開路系統　　-·-·-· 線上調整 PSS

• • • • 固定增益 PSS　　——— 具線上調整之增益規劃 PSS

- - - - 增益規劃 PSS

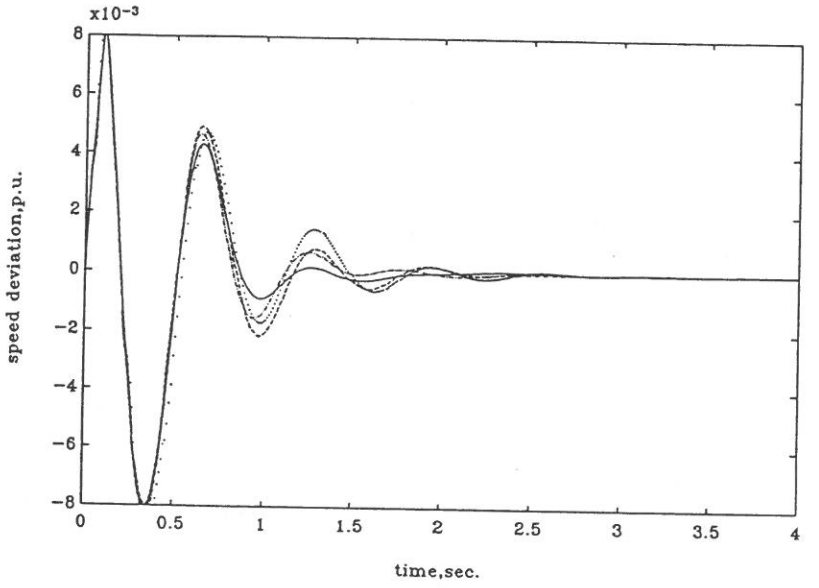

圖13(a)

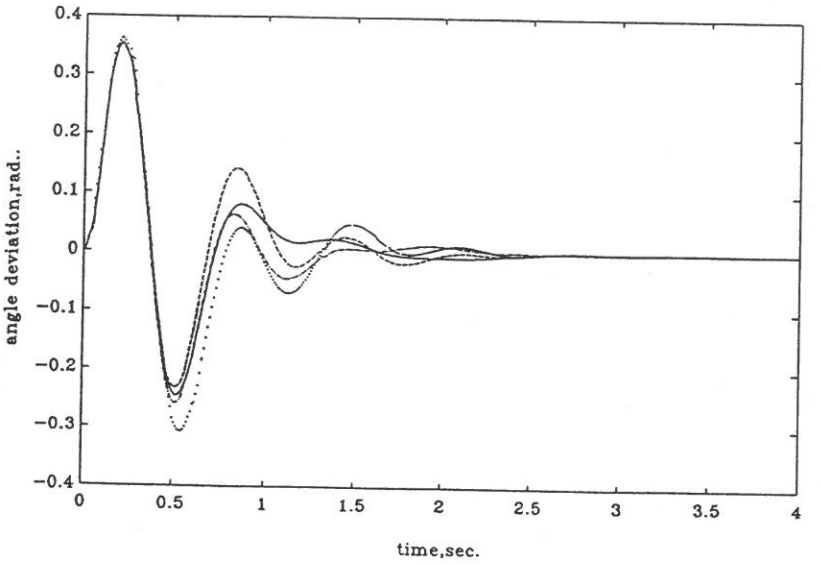

圖13(b)

圖13 系統開線故障之動態響應 (P_0=1.2 p.u.，Q_0=0.8 p.u.)。

- • • • 固定增益 PSS
- - - - 增益規劃 PSS
- -·-·- 線上調整 PSS
- —— 具線上調整之增益規劃 PSS

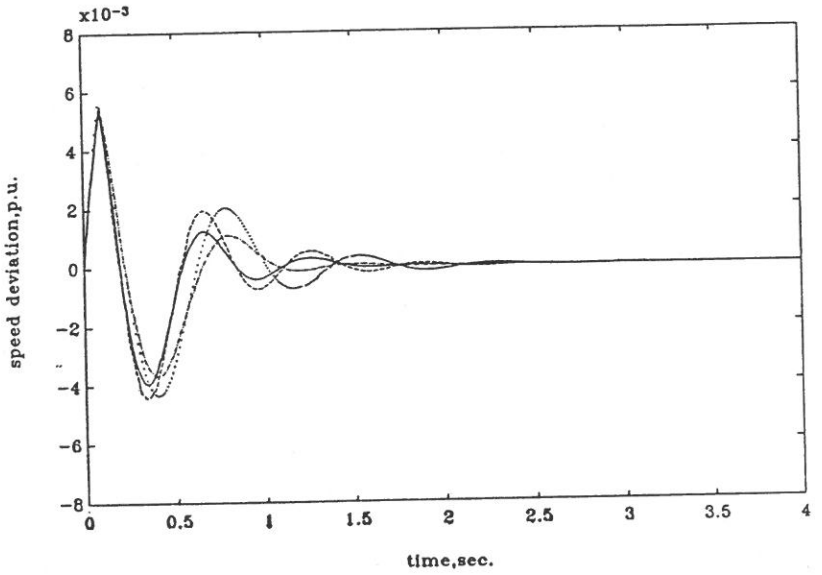

圖14(a)

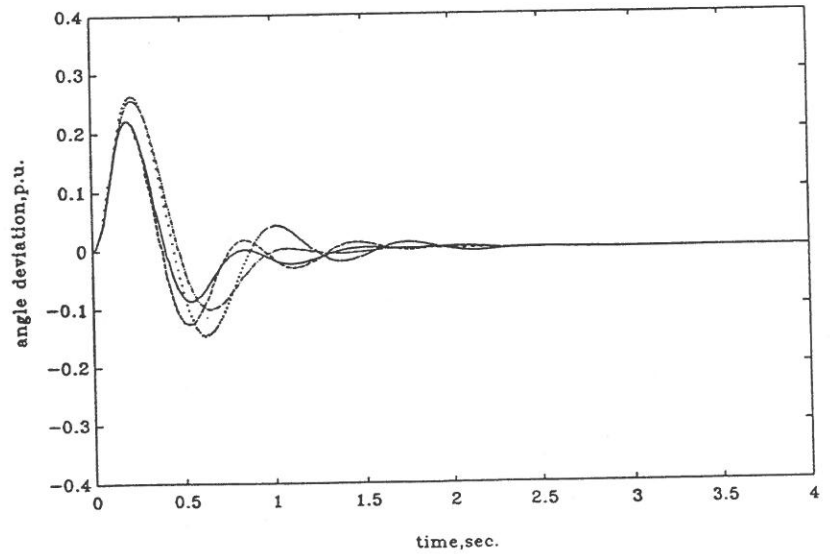

圖14(b)

圖14 系統開線故障之動態響應 (P_0=0.8 p.u.，Q_0=0.6 p.u.)。

· · · · 固定增益 PSS　　-·-·-· 線上調整 PSS

- - - - 增益規劃 PSS　　——— 具線上調整之增益規劃 PSS

表三 系統遭遇機械轉矩變化時動態響應之穩定時間

	$P_0=1.0$ p.u. $Q_0=0.2$ p.u.	$P_0=1.2$ p.u. $Q_0=0.8$ p.u.	$P_0=0.8$ p.u. $Q_0=0.6$ p.u.
Gain schedule with on-line tuning	0.88 sec	0.95 sec	0.75 sec
On-line tuning	0.95 sec	1.02 sec	1.13 sec
Gain scheduling	1.04 sec	2.75 sec	1.18 sec
Fixed gain	1.12 sec	∞	1.51 sec
Open system	∞	∞	>4 sec

* Settling time T is define by $|\Delta\omega|\leq 0.0005$ p.u. for $t\geq T$.

(1) 本論文所提的線上調整型和具有線上請整之增益規劃型 PSS 比固定增益型和增益規劃型 PSS 更能改善系統的動態阻尼效果。

(2) 線上調整型和具有線上調整之增益規劃型 PSS 的參數值能够依系統動態響應快速更新以反應系統的阻尼要求。

(3) 在 $P_0=1.2$ p. u.，$Q_0=0.8$ p. u. 時系統遭遇 0.25 p. u. 的機械轉矩變化時固定增益型 PSS 之系統響應爲不穩定的，而線上調整和增益規劃型 PSS 之系統響應爲穩定的。

(4) 負載變化時線上調整型 PSS 的動態響應較增益規劃和具線上調整之增益規劃型 PSS 來得差一點，但其具有節省計算機記憶容量的優點。

(5) 在開線故障時線上調整型和具有線上調整之增益規劃型 PSS 仍然能顯現其對系統的動態阻尼效果。

(6) 在廣範圍負載條件變化下，增益規劃型和具有線上調整之增益規劃型 PSS 在負載變化所產生的強健性要比其他控制器來得好。而具有線上調整之增益規劃型 PSS 爲達相同阻尼效果的條件下，其計算機記憶體的容量會較增益規劃型來得小一些。

五、結 論

利用簡單的線上調整演算法設計出兩種具有良好強健性的線上調整式 PI 電力系統穩定器，線上調整型和具有線上調整之增益規劃型電力系統穩定器在系統干擾之情況下能够提供比固定增益型 PSS 更好的阻尼效果，所以系統的動態穩定度能够更爲增進。具有線上調整之控制器參數值能够快速依系統響應而更新，同時更能節省儲存的記憶體容量。計算機動態模擬驗證在各種不同的干擾下，線上調整型和具有線上調整之增益規劃型 PSS 比固定增益型 PSS 更具阻尼效果。同時對負載條件變化所產生的靈敏度亦比較低，且由於於演算法簡單和很容易用微算機來施行，所以本論文所提的控制器爲一種架構簡單的強健法激磁控制器。

本論文爲電力系統強健性激磁控制器之設計與分析，未來還可以繼續討論利用頻域最佳化法和 H^{∞} 控制理論應用於強健性激磁控制器之設計。

六、誌　　謝

本研究計畫承聖言會單位之經費贊助得以順利完成，在此，致誠摯之謝意。

參考資料

(1) P.M. Anderson and A.A. Fouad, *Power System Control and Stability*, Ames. Iowa: Iowa State University Press (1977).

(2) F.P. DeMello and C. Concordia, "Concepts of Synchronous Machine Stability as Affected by Excitation Control", *IEEE Transactions on Power Apparatus and System*, **88**, 316-329 (1969).

(3) E.V. Larsen and D.A. Swann, "Applying Power System Stabilizers", *IEEE Transactions on Power Apparatus and System*, **100**, 3017-3046 (1981).

(4) A. Ghosh, G. Ledwich, G.S. Hope and O.P. Malik, "Power System Stabilizer for Large Disturbances", *Proceeding of the IEE*, **132**, 14-19 (1986).

(5) Y.Y. Hsu and C.Y. Hsu, "Design of a Proportional-Integral Power System Stabilizer", *IEEE Transactions on Power Systems*, **1**(2), 46-53 (1986).

(6) Y.Y. Hsu and C.J. Wu, "Adaptive Control of a Synchromous Machine Using the Auto-Searching Method", **3**(4), 1434-1440 (1988).

(7) C.J. Wu and Y.Y. Hsu, "Self-Tuning Excitation Control for Synchronous Machine", *IEEE Transactions on Aerospace and Electronic Systems*, **22**, 389-394 (1986).

(8) K.L. Tang and R.J. Mulholland, "Comparing Fuzzy Logic with Classical Controller Design", *IEEE Transactions on System, Man, and Cyberetics*, **SMC-17**, 1085-1087 (1987).

(9) R. Isermann, *Digital Control System*, Springer-Verlag Berlin, Heidelberg (1981).

Design and Analysis of On-Line Tuned Excitation Control for a Synchronous Machine

CHUN-HSIN PAN AND YUANG-SHUNG LEE

Electronic Engineering Department
Fu Jen Catholic University

ABSTRACT

The on-line tuning control schemes are presented for design of a power system stabilizer (PSS). The initial gains of the proposed proportional-integral (PI) controller are determined by pole-placement method based on modal control theory; the adaptation gains of the controller are adjusted in the real time using an on-line tuning algorithm based on the measured system operating conditions. Eigenvalues analysis and nonlinear computer simulations show that the proposed controller can offer better damping effect and robustness for synchronous generator electromechanical mode oscillations over a wide range of load conditions than conventional fixed-gain PI controller. The on-line tuning control shemes has an additional advantage of saving computer memory size.

COMPLETE CODES FOR ROE'S RIEMANN SOLVER AND THE EXACT SOLUTION TO THE SHOCK TUBE PROBLEM

JEN-ING HWANG AND REN-JYH LAN*

Department of Computer Science and Information Engineering
Fu Jen University

ABSTRACT

Sod (1978) surveyed a variety of finite-difference schemes for systems of nonlinear hyperbolic conservation laws on the basis of their performance on a standard shock tube problem. Roe (1981) proposed an approximate Riemann solver to replace the exact solution of the Riemann problem in the Godunov method. In this paper, a complete code for Roe's Riemann solver is presented for the solution of the shock tube problem. An approximate Jacobian matrix of the flux function is constructed to satisfy the "Property *U*". This treatment enables an efficient calculation. Also, a code of the exact solution to the shock tube problem is implemented. This work aids in understanding Roe's Riemann solver and the shock tube problem.

1. INTRODUCTION

During the past twenty years much effort has been paid to the numerical solution of systems of conservation laws. Sod[10] has discussed several finite difference methods for systems of nonlinear hyperbolic conservation laws, and he has also used the shock tube problem to test those finite difference methods.

Hyperbolic systems often possess weak solutions which are only piecewise smooth. A typical example is the occurrence of shock waves in fluid flow modeled by the Euler equations. For such cases, when a shock wave moves through a mesh point, the Taylor's series method breaks down, as derivatives do not exist at grid points which coincide with the shock position. In the past research directed to discovery of numerical algorithms which are robust in the presence of discontinuities

* Graduate Student, Department of Mathematics.

has proceeded in a somewhat heuristic manner. The Russian mathematician S. K. Godunov, proceeding from a physical standpoint and having knowledge of methods for solving the standard shock tube problem, applied this knowledge in a very clever way to obtain one of the first robust shock capturing algorithms[4]. The British aeronautical engineer P. L. Roe[7] has shown how to efficiently approximate the solution to the nonlinear Riemann problem utilized by Godunov. Roe goes even further in [8], giving a view of several classical finite difference schemes, which when coupled with his first result and applied to the Godunov approach obtains an even better approximation to the fluxes sought after when solving the Riemann problem. The study of Roe's scheme is given by Hwang[5].

The purpose of this paper is to implement a complete code of Roe's scheme, numerical results have been obtained for the shock tube problem as a test case. This leads a convenient way to compare with those methods in Sod's paper[10]. A code of the exact solution to the shock tube problem is also provided in the present paper.

Section 2 contains background material relevant to an understanding of later study. The Riemann problem for systems of conservation laws is presented, and the Rankine-Hugoniot is introduced. In section 3 the properties of the Riemann problem for the equations of gas dynamics for ideal polytropic gases are pointed out. Section 4 describes how to implement a complete code for Roe's Riemann solver to the shock tube problem and section 6 describes the exact solution. The relation between the shock tube and Riemann's problem is discussed in section 5. Finally, in section 7 illustrates the numerical results and gives the conclusions.

2. THE RIEMANN PROBLEM FOR SYSTEMS OF CONSERVATION LAWS

The initial-value problem for hyperbolic system of conservation laws has from

$$U_t+F(U)_x=0 \tag{1a}$$

$$U(x,\ 0)=U_0(x), \qquad -\infty<x<\infty \tag{1b}$$

Here $U(x, t)$ is a column vector of N unknowns, and the flux function $F(U)$ is a vector valued function of N components. Equation (1a) can be written in matrix from as

$$U_t+A(U)U_x=0, \qquad A(U)=\frac{\partial F(U)}{\partial U} \quad (2)$$

where $A(U)$ is the Jacobian matrix. The system Eq. (1) is called hyperbolic if all eigenvalues of $A(U)$ are real and $A(U)$ possesses a complete set of eigenvectors. It is assumed that the eigenvalues $\{\lambda_i(U)\}_{i=1}^N$ are distinct, nonzero, and arranged in an increasing order,

$$\lambda_1<\lambda_2<\cdots<\lambda_m<0<\lambda_{m+1}<\cdots<\lambda_N \quad (3)$$

with corresponding right eigenvectors $\{R^i(U)\}_{i=1}^N$. Let

$$R(U)=(R^1(U),\ R^2(U),\ \cdots,\ R^N(U)) \quad (4)$$

be a matrix with $R^i(U)$ as column i, $i=1, 2, \cdots, N$.

Then, $R^{-1}(U)$ has rows $\{L^i(U)\}_{i=1}^N$ which constitute consequently,

$$L^iR^j=\delta_{ij} \quad (5)$$

and

$$R^{-1}AR=\Lambda \quad (6a)$$

where

$$\Lambda_{ij}=\lambda_i\delta_{ij} \quad (6b)$$

To allow for discontinuous behavior, one admits weak solution which satisfy system Eq. (1) in the sense of distribution theory, i. e.,

$$\int_0^\infty\int_{-\infty}^{\infty}(G_tU+G_xF(U))dxdt+\int_{-\infty}^{\infty}G(x,\ 0)U(x,\ 0)dx=0 \quad (7)$$

for all C^∞ test functions $G(x, t)$ which vanish for large $|x|+|t|$. Thus, a piecewise smooth $U(x, t)$ is a weak solution of Eq. (1) if and only if

(i) U satisfies Eq. (1a) pointwise in each smooth region.

(ii) Across each curve of discontinuity the Rankine-Hugoniot relation

$$[F(U)]=S[U]$$

holds, where $S=dx/dt$ is the speed of propagation of the discontinuity, and [ ] is the conventional notation for jumps. In

the case where A is constant, the jump $[U]$ must be an eigenvector of A (see Ref. (2)), with S the corresponding eigenvalue, and discontinuities in the initial data $U_0(x)$ must propagate along characteristic curves: $dx/dt=\lambda_i$.

The Riemann problem for system Eq. (1) occurs when the initial data is only piecewise smooth, i.e.,

$$U_t+A(U)U_x=0 \tag{8a}$$

$$U(x,\ 0)=\begin{cases}U_L(x), & x<x_0\\ U_R(x), & x>x_0\end{cases} \tag{8b}$$

Here U_R and U_L are smooth functions, but $U(x,\ 0)$, $U_x(x,\ 0)$ may have a finite jump discontinuity at x_0.

When A is constant, the solution of system Eq. (8) is composed of constant states, separated by a fan of N characteristic lines[6] (see Fig. 1). Let

$$\lambda_0=-\infty,\quad \lambda_{N+1}=+\infty$$

and

$$U(x,\ t)=U_k,\qquad \text{for } \lambda_k<\frac{x}{t}<\lambda_{k+1},\ k=0,\ 1,\ 2,\ \cdots,\ N$$

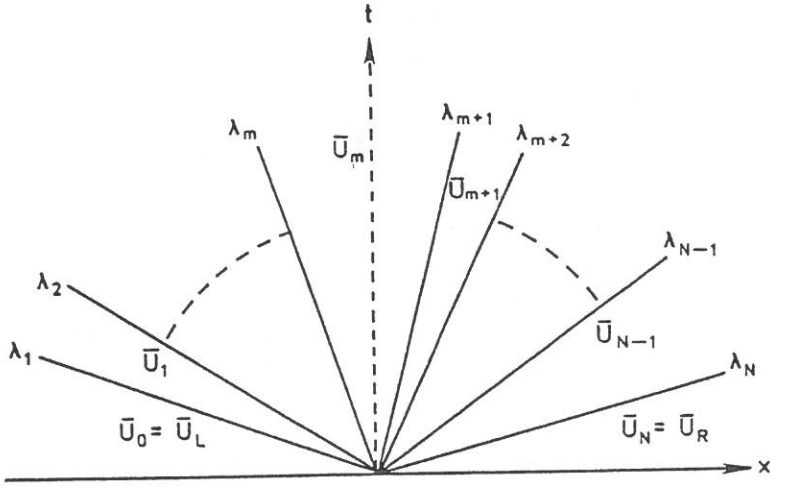

Fig. 1. Characteristics and constant state solution of the Riemann problem.

According to the Rankine-Hugoniot relations, the jumps across the characteristics must satisfy

$$[U_k]=U_k-U_{k-1}=\alpha^k R^k \tag{9}$$

for some α^k. Thus,

$$U_R-U_L=\sum_{k=1}^{N}\alpha^k R^k \tag{10}$$

and

$$\alpha^k=L^k(U_R-U_L) \tag{11}$$

3. THE RIEMANN PROBLEM IN GAS DYNAMICS

The one-dimensional equations of gas dynamics may be written in the conservation form

$$\rho_t+m_x=0 \tag{12a}$$

$$m_t+\left(\frac{m^2}{\rho}+p\right)_x=0 \tag{12b}$$

$$e_t+\left(\frac{m}{\rho}(e+p)\right)_x=0 \tag{12c}$$

where ρ is the density, u is the velocity, $m=\rho u$ is momentum, p is pressure, and e is energy per unit volume. It may be written

$$e=\rho\epsilon+\frac{1}{2}\rho u^2 \tag{13}$$

where ϵ is the internal energy per unit mass. Assume the gas is polytropic, in which case

$$\epsilon=\frac{p}{(\gamma-1)\rho} \tag{14}$$

where γ is the ratio of specific heats and it is a constant greater than one. Equations (12a)-(12c) may be written in vector form

$$U_t+F(U)_x=0 \tag{15}$$

where

$$U=\begin{pmatrix}\rho\\ m\\ e\end{pmatrix} \quad \text{and} \quad F(U)=\begin{pmatrix}m\\ \frac{m^2}{\rho}+p\\ \frac{m}{\rho}(e+p)\end{pmatrix}$$

Here $U(x, t)$ is the vector of conservative variables and $F(U)$ is the flux vector. The primitive variables are the density ρ, the velocity u, and the pressure p. System Eq. (15) can also be written in matrix form as

$$U_t+A(U)U_x=0, \qquad A(U)=\frac{\partial F(U)}{\partial U} \tag{16}$$

The eigenvalues of the Jacobian matrix $A(U)$ are

$$\lambda_1=u-c, \quad \lambda_2=u, \quad \lambda_3=u+c \tag{17}$$

where c is the sound speed, $c=(\gamma p/\rho)^{1/2}$.

The corresponding right eigenvectors of A form the matrix $R=(R^1, R^2, R^3)$ given by

$$R=\begin{pmatrix}1 & 1 & 1\\ u-c & u & u+c\\ H-uc & \frac{u^2}{2} & H+uc\end{pmatrix} \tag{18}$$

where $H=(e+p)/\rho=c^2/(\gamma-1)+u^2/2$ is the enthalpy. The inverse matrix of R is

$$R^{-1}=\begin{pmatrix}\frac{b_1+\frac{u}{c}}{2} & \frac{-b_2u-\frac{1}{c}}{2} & \frac{b_2}{2}\\ 1-b_1 & b_2u & -b_2\\ \frac{b_1-\frac{u}{c}}{2} & \frac{-b_2u+\frac{1}{c}}{2} & \frac{b_2}{2}\end{pmatrix} \tag{19}$$

with $b_1=b_2u^2/2$ and $b_2=(\gamma-1)/c^2$.

In order to solve system Eqs. (15) or (16) with an explicit time-stepping scheme, the domain of integration is discretized as (x_j, t^n), where $x_j=j\Delta x$, $j=1, 2, \cdots$, and $t^n=n\Delta t$, $n=1, 2, \cdots$. At a typical cell interface $x_{j+1/2}$, the local Riemann problem can be written:

$$U_t+A(U)U_x=0 \tag{20a}$$

$$U(x,\ 0)=\begin{cases}U_L=U_j^n, & x<x_{j+1/2}\\ U_R=U_{j+1}^n, & x>x_{j+1/2}\end{cases} \tag{20b}$$

where U_j^n is the average value in the computational cell centered on x_j at time t_n. Fixing attention on the interval $x_j\leq x\leq x_{j+1}$ and status $U_L=U_j^n$, $U_R=U_{j+1}^n$, let $U_{j+1/2}=V(U_L,\ U_R)$ be some symmetric average of the given data. For instance, $U_{j+1/2}=(U_L+U_R)/2$ is the simplest form. The system Eq. (20) can be locally ilnearized using the mean value Jacobian matrix $\hat{A}(U_L,\ U_R)=\hat{A}_{j+1/2}=\hat{A}(U_{j+1/2})$, and from Eqs. (10) and (11), one can write

$$\Delta U_{j+1/2}=\sum_{k=1}^{3}\alpha_{j+1/2}^k R_{j+1/2}^k \tag{21}$$

and

$$\alpha_{j+1/2}^k=L_{j+1/2}^k\Delta U_{f+1/2} \tag{22}$$

where $\alpha_{j+1/2}^k$ is the component of $\Delta U_{j+1/2}=U_{j+1}^n-U_j^n$ in the coordinate system of the right eigenvectors $\{R_{j+1/2}\}_{k=1}^3$ of $\hat{A}_{j+1/2}$. i. e.,

$$\begin{pmatrix}\alpha_{j+1/2}^1\\ \alpha_{j+1/2}^2\\ \alpha_{j+1/2}^3\end{pmatrix}=\begin{pmatrix}\dfrac{aa-bb}{2}\\ \Delta_{j+1/2}\rho-aa\\ \dfrac{aa+bb}{2}\end{pmatrix} \tag{23a}$$

where

$$aa=\frac{\gamma-1}{c_{j+1/2}^2}\left[\Delta_{j+1/2}e+\frac{u_{j+1/2}^2}{2}\Delta_{j+1/2}\rho-u_{j+1/2}\Delta_{j+1/2}m\right] \tag{23b}$$

$$bb=\frac{\Delta_{j+1/2}m-u_{j+1/2}\Delta_{j+1/2}\rho}{c_{j+1/2}} \tag{23c}$$

4. ROE'S SCHEME

Roe's scheme[7,8] for integration Eq. (20) has the conscrvation form

$$U_j^{n+1}=U_j^n-\frac{\Delta t}{\Delta x}(F^*_{j+1/2}-F^*_{j-1/2}) \tag{24}$$

here $F^*_{j+1/2}$ is a numerical flux-function across the $j+1/2$ cell interface and is obtained from the Roe linearization.

Roe's approximate Jacobian matrix $\tilde{A}(U_L, U_R)=\tilde{A}_{j+1/2}$ to the nonlinear system Eq. (20) is constructed such as to satisfy the "Property U"[6]:

(i) It constitutes a linear mapping from the vector space U to the vector space F.

(ii) As $U_L\to U_R\to U$, $\tilde{A}(U_L, U_R)\to A(U)$, where $A(U)=\partial F(U)/\partial F$.

(iii) For any U_L, U_R, $\tilde{A}(U_L, U_R)\times(U_L-U_R)=F_L-F_R$, where $F_L=F(U_L)$ and $F_R=F(U_R)$.

(iv) The eigenvectors of $\tilde{A}$ are linearly independent.

This special form of averaging has the computational advantage of perfectly resolving stationary discontinuities. Roe's averaging takes the following from

$$\tilde{u}_{j+1/2}=\frac{\bar{D}u_{j+1}+u_j}{\bar{D}+1} \tag{25a}$$

$$\tilde{H}_{j+1/2}=\frac{\bar{D}H_{j+1}+H_j}{\bar{D}+1} \tag{25b}$$

$$\tilde{c}_{j+1/2}=(\gamma-1)\left(\tilde{H}_{j+1/2}-\frac{\tilde{u}^2_{j+1/2}}{2}\right) \tag{25c}$$

$$\bar{D}=\sqrt{\frac{\rho_{j+1}}{\rho_j}} \tag{25d}$$

$$H=\frac{\gamma p}{(\gamma-1)\rho}+\frac{u^2}{2} \tag{25e}$$

The values $\tilde{u}_{j+1/2}$, $\tilde{H}_{j+1/2}$ and $\tilde{c}_{j+1/2}$ will help to calculate $\tilde{\lambda}^k_{j+1/2}$ in Eq. (17), $\tilde{R}^k_{j+1/2}$ in Eq. (18), and $\tilde{\alpha}^k_{j+1/2}$ in Eq. (23a). All these values ($\tilde{\lambda}^k_{j+1/2}$, $\tilde{R}^k_{j+1/2}$, and $\tilde{\alpha}^k_{j+1/2}$) are needed in Roe's approximate Riemann solver. Now, consider the numerical flux $F^*_{j+1/2}$ in Eq. (24), then the Riemann solver will be fully realized.

(1) A first approximate Riemann solver

In the first paper[7], Roe suggests that

$$F^*_{j+1/2}=F(U^*_{j+1/2}) \tag{26a}$$

where $U^*_{j+1/2}$ is the exact solution of the approximate Riemann problem at the $j+1/2$ interface for the locally linearized matrix $\tilde{A}_{j+1/2}$, and it is defined as

$$U^*_{j+1/2}=\frac{1}{2}(U^n_{j+1}+U^n_j)+\frac{1}{2}\sum_{\lambda^k<0}\tilde{\alpha}^k_{j+1/2}\tilde{R}^k_{j+1/2}-\frac{1}{2}\sum_{\lambda^k\geq 0}\tilde{\alpha}^k_{j+1/2}\tilde{R}^k_{j+1/2} \tag{26b}$$

(2) A second approximate Riemann solver

The second approximate Riemann solver is derived in [5,8] and is outlined in the following:

From (iii) of the "Property U" and Eq. (21), the flux difference is expressed as

$$\Delta F_{j+1/2}=\sum_{k=1}^{3}\tilde{\alpha}^k_{j+1/2}\tilde{\lambda}^k_{j+1/2}\tilde{R}^k_{j+2/1} \tag{27}$$

where

$$\Delta F_{j+1/2}=F_{j+1}-F_j=F(U^n_{j+1})-F(U^n_j).$$

This decomposition provides a means for finding the plus and minus flux increments across $j\pm 1/2$, i. e.,

$$\Delta F^+_{j+1/2}=\sum_{\lambda^k\geq 0}\tilde{\alpha}^k_{j+1/2}\tilde{\lambda}^k_{j+1/2}\tilde{R}^k_{j+1/2} \tag{28a}$$

$$\Delta F^-_{j+1/2}=\sum_{\lambda^k<0}\tilde{\alpha}^k_{j+1/2}\tilde{\lambda}^k_{j+1/2}\tilde{R}^k_{j+1/2} \tag{28b}$$

where $\Delta F^{\pm}_{j+1/2}$ are the increments of flux associated with positive and negative characteristic speeds respectively across the $j+1/2$ cell interface. Equation (28) leads to natural upwind differencing

$$U^{n+1}_j=U^n_j-\frac{\Delta t}{\Delta x}(\Delta F^-_{j+1/2}+\Delta F^+_{j-1/2}) \tag{29}$$

After some algebraic manipulations, scheme Eq. (29) with flux difference splitting Eq. (28) can be cast in conservation form Eq. (24) with the following numerical flux:

$$F^*_{j+1/2}=\frac{1}{2}(F_{j+1}+F_j)-\sum_{k=1}^{3}|\lambda^k_{j+1/2}|\alpha^k_{j+1/2}R^k_{j+1/2}.$$

5. THE SHOCK TUBE AND RIEMANN'S PROBLEM IN GAS DYNAMICS

A shock tube is sketched in Fig. 2(a). This is a tube closed at both sides, with a diaphragm separating two regions (regions 1 and 4). The initial conditions are also illustrated in Fig. 2(b). A diaphragm at x_0 separates these two regions which have different densities and pressures. The two regions are in a constant state. The initial conditions are $p_4 > p_1$, $\rho_4 > \rho_1$, and $u_4 = u_1 = 0$; i.e., both fluids are initially at rest.

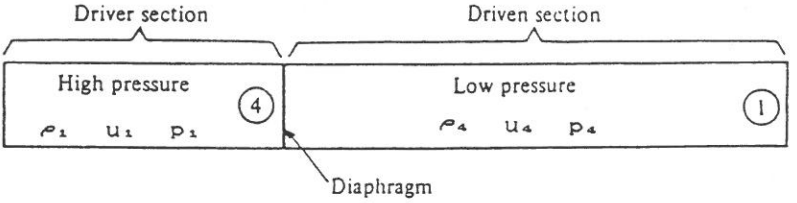

(a)

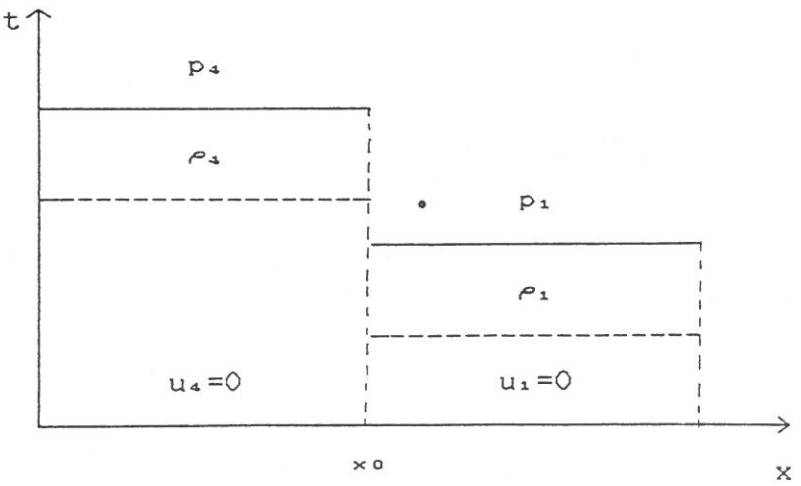

(b)

Fig. 2. Initial conditions in a pressure-driven shock tube.

At time $t=0$ (see Fig. 3) the diphram is broken. Upon rupture of the diaphragm, a normal shock wave moves into the low-pressure side (region 1), with a series of expansion waves propagating into the high-pressure gas (region 4). As the normal shock wave propagates to the right with velocity w, it increases the pressure of the gas behind it (region 2), and it induces a mass motion with velocity u_p. The interface between the driver and driven gases is called the contact surface, which also moves with velocity u_p. This problem was studied by Riemann. It is to determine the ensuing motion of the gas after breaking the diaphragm.

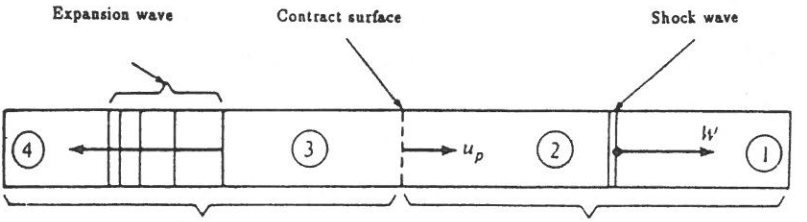

Fig. 3. Flow in a shock tube after the diaphargm is broken.

The Riemann problem for system Eqs. (12) or (16) with initial data of the form

$$U(x,\ 0)=\begin{cases}U_L(=U_4), & x<x_0\\ U_R(=U_1), & x>x_0\end{cases} \tag{30}$$

is the Riemann problem in gas dynamics, here

$$U_L=U_4=\begin{pmatrix}\rho_4\\ m_4\\ e_4\end{pmatrix} \quad \text{and} \quad U_R=U_1=\begin{pmatrix}\rho_1\\ m_1\\ e_1\end{pmatrix}$$

are two constant states of the gas.

The special case in which the velocity component vanishes, i.e., $u_4=u_1=0$, is then called the shock tube problem.

6. THE SHOCK TUBE PROBLEM

In this section the exact solution of the shock tube problem is described. Now, consider the case where $u_4=u_1=0$, $p_4>p_1$, and $\rho_4>\rho_1$ as mentioned in the preceding section (Figs. 2(a) and 2(b)). The solution[1,9] for some $t=t_1>0$ can be depicted graphically as in Fig. 4. It can be seen that the initial discontinuity breaks up into two discontinuities, the shock wave and the contact surface; these depend on the data. Figure 5 shows curves of u versus x, p versus x, and ρ versus x at $t=t_1>0$, points x_4 and x_3 represent the location of the head and tail of the expansion wave. The point x_2 is the position that an element of fluid initially at x_0 has reached by time $t=t_1>0$, i, e., point x_2 is the contact surface. It is seen that across a contact surface the pressure p and the normal component of velocity u are continuous. However, the density ρ and the specific energy ϵ are not continuous across a contact surface. Point x_1 is the location of the shock wave. Across a shock all of the quantities (ρ, u, ϵ, and p) will in general be discontinuous.

The analysis of the gas in a shock tube is discussed in [1,9]. It is outlined the discussion to relate the analysis to our code of the exact solution to the shock tube problem. Given the initial pressures p_4 and p_1.

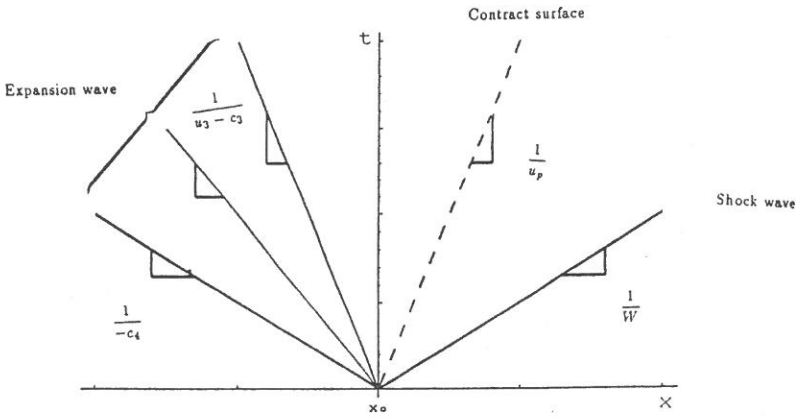

Fig. 4. Solution of the Riemann problem.

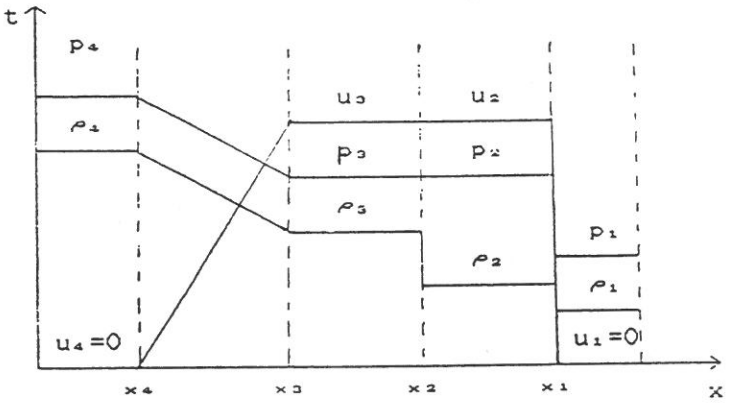

Fig. 5. Shock tube at $t>0$.

(i) Calculate p_2 from the following eqation:

$$1-\frac{(\gamma-1)\left(\frac{c_1}{c_4}\right)\left(\frac{p_2}{p_1}-1\right)}{\sqrt{2\gamma\left[(\gamma+1)\left(\frac{p_2}{p_1}\right)+\gamma-1\right]}}=\left(\frac{p_2}{p_4}\right)^{(\gamma-1)/2\gamma} \tag{31}$$

this defines the strength of the incident shock wave.

(ii) Calculate all other incident shock properties by using equations below:

$$\frac{\rho_2}{\rho_1}=\frac{1+\frac{\gamma+1}{\gamma-1}\frac{p_2}{p_1}}{\frac{\gamma+1}{\gamma-1}+\frac{p_2}{p_1}} \tag{32}$$

$$W=c_1\sqrt{\frac{\gamma+1}{2\gamma}\left(\frac{p_2}{p_1}-1\right)+1} \tag{33}$$

where W is the velocity of the gas ahead of the shock wave, relative to the wave.

$$u_2=u_p=\frac{c_1}{\gamma}\left(\frac{p_2}{p_1}-1\right)\sqrt{\frac{\frac{2\gamma}{\gamma+1}}{\frac{p_2}{p_1}+\frac{\gamma-1}{\gamma+1}}} \tag{34}$$

(iii) Apply $p_3=p_2$, and $u_3=u_2=u_p$.

(iv) The density ρ_3 behind the expansion wave can be found from the isentropic relation

$$\frac{p_3}{p_4}=\left(\frac{\rho_3}{\rho_4}\right)^{\gamma} \tag{35}$$

(v) Calculate locations of points 1, 2, 3, and 4 by the following equations (see Fig. 4):

$$x_1=Wt+x_0 \tag{36a}$$

$$x_2=u_p t+x_0 \tag{36b}$$

$$x_3=(u_3-c_3)t+x_0 \tag{36c}$$

$$x_4=-c_4 t+x_0 \tag{36d}$$

Equation (31) gives the formula to find p_2. However, it is difficult to determine by the equation. Dutt proposed a Riemann solver[3] based on a global existence proof[9] for the Riemann problem. He also coded a subroutine to find p_2 and u_2. The subroutine is used for the computer code of the exact solution to the shock tube problem instead of Eq. (31).

7. NUMERICAL RESULTS AND CONCLUSIONS

Results have been obtained for the shock tube problem used as a test case by Sod[10]. The initial conditions are: $\rho_1=0.125$, $p_1=0.1$, $u_1=0$, $\rho_4=1.0$, $p_4=1.0$, and $u_4=0.0$. The ratio of specific heats γ is chosen to be 1.4. The diaphragm is at $x_0=0.5$ when $t=0$ and in all of the calculations $\Delta x=0.01$. The program was run at a CFL number of 0.95.

Figure 6 indicates the results incorporating either the exact or the first approximate Riemann solver. The corners at the endpoints of the expansion wave are rounded. There is a slight undershoot at the right corner of the expansion wave. The constant state between the contact surface and the shock is only partly realized. The transition of the contact surface occupies thirteen to fourteen zones and the transition of the shock occupies three to four zones.

Figure 7 shows the results incorporating either the exact or the second approximate Riemann solver. The results are very similar to those of Fig. 6. However, the solution is oscillation free. In particular, there is no undershoot at the right corner of the expansion wave.

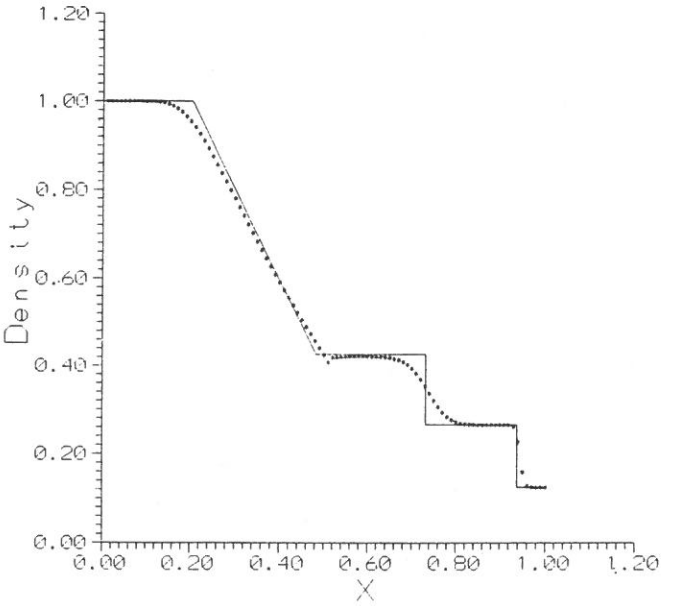
1.20
1.00
0.80
0.60
0.40
0.20
0.00
Density
0.00 0.20 0.40 0.60 0.80 1.00 1.20
X

Fig. 6(a)

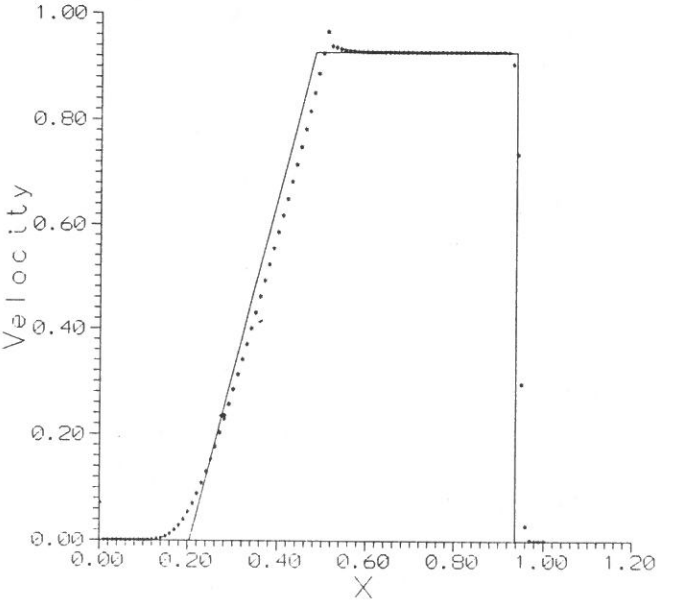
1.00
0.80
0.60
0.40
0.20
0.00
Velocity
0.00 0.20 0.40 0.60 0.80 1.00 1.20
X

Fig. 6(b)

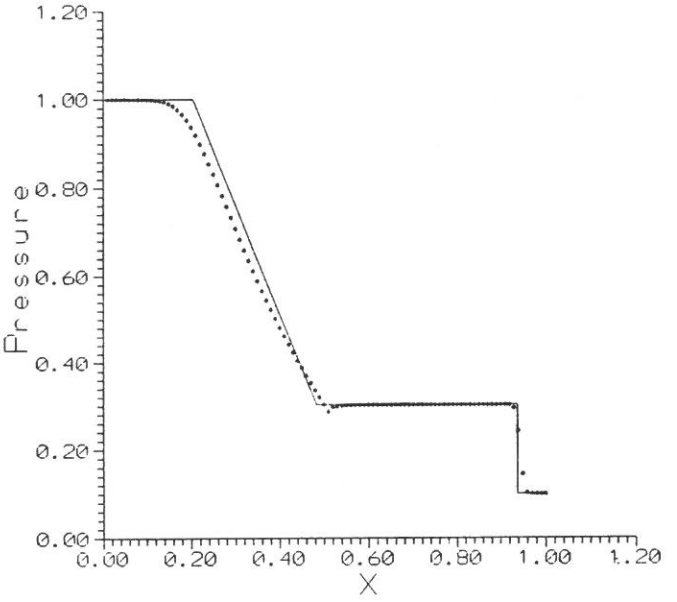

Fig. 6(c)

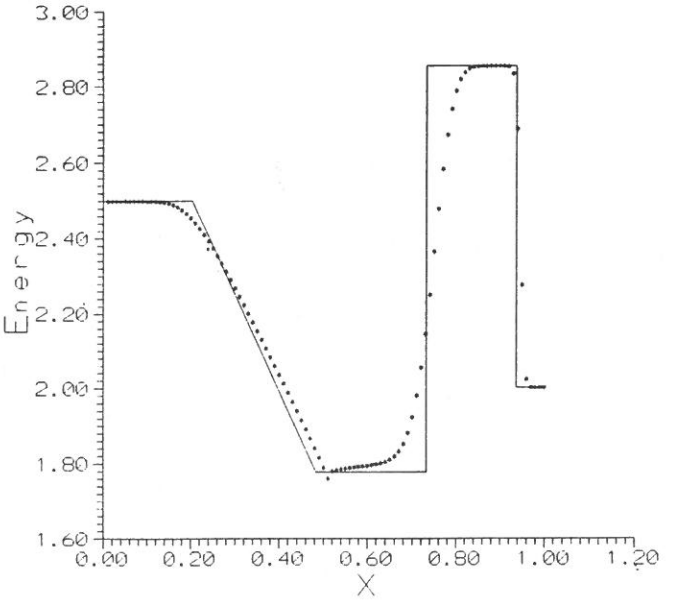

Fig. 6(d)

Fig. 6. Solution of the first Riemann solver ($\times\times\times$) and the exact solution ($---$).

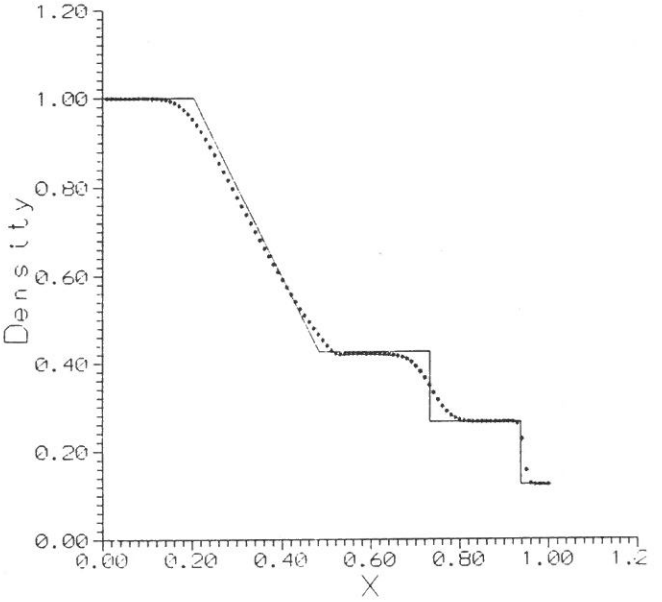
1.20
1.00
0.80
0.60
0.40
0.20
0.00
Density
0.00
0.20
0.40
0.60
0.80
1.00
X

Fig. 7(a)

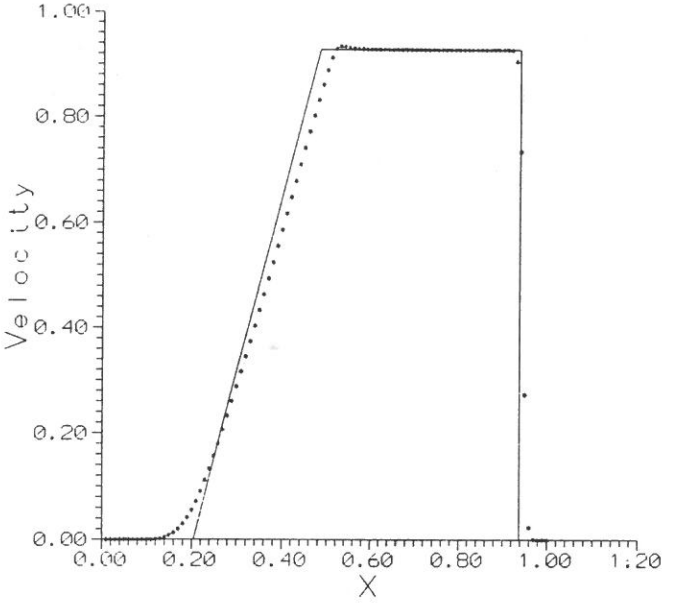
1.00
0.80
0.60
0.40
0.20
0.00
Velocity
0.00
0.20
0.40
0.60
0.80
1.00
X

Fig. 7(b)

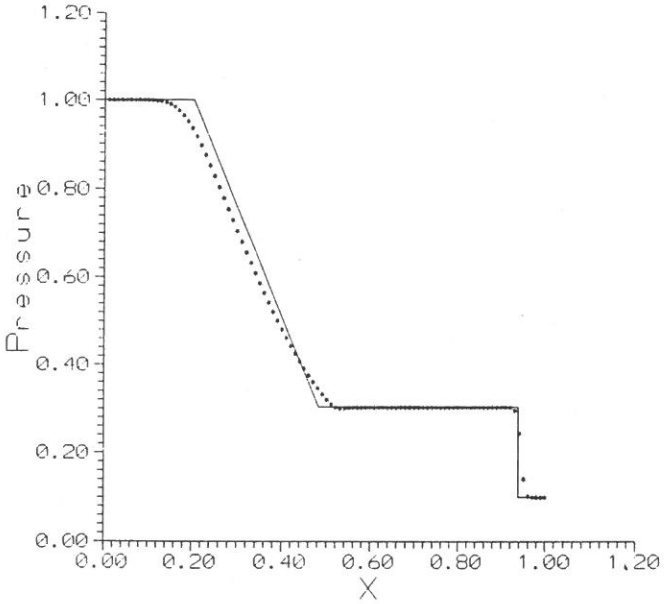

Fig. 7(c)

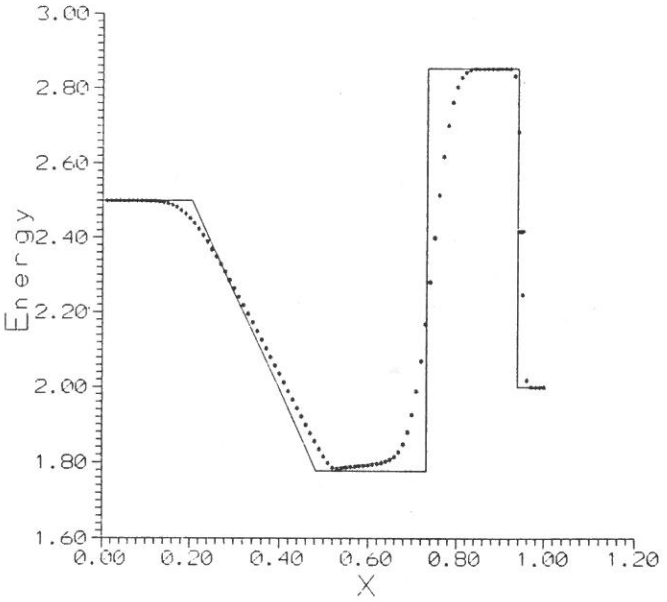

Fig. 7(d)

Fig. 7. Solution of the second Riemann solver (×××) and the exact solution (———).

The results in Figs. 6 and 7 compare well with most of the results surveyed by Sod. The advantage of Roe's method is to simplify Godunov's method when solving the Riemann problem. It provides an efficient and flexible numerical scheme.

REFERENCES

(1) J.D. Anderson, Jr., "Modern Compressible Flow with Historical Perspective", McGraw-Hill, New York (1982).

(2) R. Courant and P.D. Lax, "The Propagation of Discontinuities in Wave Motion", *Proc. Nat. Acad. Sci.*, **42**(11), 872-876 (1956).

(3) Parvir Dutt, "A Riemann Solver Based on a Global Existence Proof for the Riemann Problem", ICASE report No. 86-3 (1986).

(4) S.K. Godunov, "A Difference Scheme for Numerical Computation of Discontinuous Solutions of Equations of Fluid Dynamics", *Math Sbornik*, **47**, 271-306 (1959).

(5) Jen-Ing G. Hwang, Charlie H. Cooke and Tze-Jang Chen, "Roe's Scheme Revisited: A Weak-Derivative Form for Linear Hyperbolic Systems,,, Submitted.

(6) P.D. Lax, "Hyperbolic Systems of Conservation Laws and the Mathematical Theory of Shock Waves", CBMS Regional Conference Series in Applied Mathematics 11, Society for Industrial and Applied Mathematics, Philadelphia (1972).

(7) P.L. Roe, "The Use of the Riemann Problem in Finite Difference Scheme", Proceedings 7th International Conference on Numerical Methods in Fluid Dynamics, Springer-Verlag, New York/Berlin (1981).

(8) P.L. Roe, "Approximate Riemann Solvers, Parameter Vectors, and Difference Schemes", *J. Comp. Phys.*, **43**, 357-372 (1981).

(9) J. Smoller, "Shock Waves and Reaction-Diffusion Equations", Springer-Verlag, New York (1983).

(10) Gary A. Sod, "A Survey of Several Finite Difference Methods for Systems of Nonlinear Hyperbolic Conservation Laws", *Journal of Computational Physics*, **27**, 327-360 (1978).

衝擊管之洛氏里曼解與真解之完整程式碼

黃貞瑛　藍仁志

輔仁大學資訊工程系

摘　要

Sod 於 1978 年探討了若干有關於非線性，符合保守定律之雙曲線偏微分方程式之有限差分法，並利用標準之衝擊管問題 (shock tube problem) 評估各方法。Roe 於 1981 年提出一個近似里曼值解法 (approximate Riemann solver) 以取代 Godunov 方法中之里曼眞解 (Riemann solution)。本文將描述 Roe 之里曼解法應用於衝擊管問題中，並提出一完整程式碼。Roe 採用「性質 U」構造一流量函數 (flux function) 之近似 Jacobian 矩陣。此種處理將提供一有效率之計算方式。另外，本文也提出衝擊管眞解之完整程式碼。本文之探討，有助於對 Roe 之里曼解法與衝擊管問題之瞭解。

早期營養修飾與成長後膽固醇恒常性之關係

盧義發　　陳慧環

輔仁大學食品營養學研究所

摘　　要

本綜論在討論從嬰幼期到成熟期的有關膽固醇代謝與代謝記憶。迄今由於實驗數據仍不完全，無法由提供資料中獲得一滿意的結論。如果早期的一些營養修飾可促進膽固醇代謝，那麼異化的烙印效果可能影響其後膽固醇代謝。實驗設計、飼料組成和動物品種的不同，可能可以解釋動物實驗的矛盾點。曾以膽固醇生合成及異化的速率決定酵素、肝臟灌流實驗、LDL 受器與異化等參數來解釋代謝記憶的現象。然而，遺傳基因、膽固醇或其代謝物及特別是激素也許對膽固醇恒常性具有長遠的影響。

一、前　　言

根據行政院衛生署公布臺灣地區近五年的十大死因中腦血管及心血管疾病分別佔第二、第四位[1]；而高膽固醇血症乃動脈硬化，甚至於是心臟血管疾病的主要危險因子之一[2]。根據流行病學的研究顯示：動脈粥狀硬化症乃朔自嬰幼兒期而發展於其後數十年的生命裏[3,4]。近年來較年輕世代的高膽固醇血症及早熟性動脈粥狀硬化症 (premature-atherosclerosis) 日趨嚴重，所以儘早預防動脈粥狀硬化症乃成爲重要課題。有關嬰幼兒期的飲食修飾對成長後，脂質及脂蛋白的代謝會給予怎樣的影響，迄今仍在檢討中。根據動物實驗顯示早期經營養修飾 (modification) 後，即使其後改爲普通飲食，對成長以後的脂質代謝之影響仍會顯現出來，此現象稱爲「代謝記憶 (metabolic memory)」或烙印效果 (printing effect)。但此種現象之矛盾點仍然很多，至今並沒有一致的結論。表一爲早期經各種飲食修飾後的動物，於成熟期對血膽固醇濃度影響的一些代表作。本文乃針對此現象作一綜合論述。

二、產後修飾

動物早期以各種營養因子修飾，以活化其膽固醇異化途徑，其後經過一段時間的普通飲食，待成長後再給予 atherogenic diet，觀察其與血膽固醇濃度的相關性，分述如下：

表一 早期營養修飾對成熟期血膽固醇濃度之影響

Animals	Pretreated conditions		Serum CHOL in adult life	Reference
	Stimuli	Periods		
Rats	CHOL	18 days G→30 days L	↓	(5)
Rats	CHOL	18 days G→30 days L	↑	(21)
Rats	CHOL	14 days G→30 days L	—	(16)
Rats	CHOL	15 days BG→21 days L	—	(29)
Rats	CHOL	28 days PN→56 days PN	—	(30)
ExHC rats	CHOL	17 days PN→35 days PN	↓	(14)
Guinea-pigs	CHOL	1 week PN→13 weeks PN	—	(27)
Baboons	CHOL	birth→4 months PN	—	(31)
Baboons	CHOL	birth→14 weeks L	—	(35)
Rats	CY	28 days→56 days PN	—	(30)
Rats	CY	4 days BG→14 days L	↑	(41)
Pigeons	CY	6 weeks PN→14 weeks PN	↓	(10)
Guinea-pigs	CY	1 week PN→7 weeks PN	↓	(8)
Guinea-pigs	CY	3 weeks PN→7 weeks PN	↓	(13)
Guinea-pigs		2 days PN→10 days PN	—	(58)
Guinea-pigs		1 week PN→7 weeks PN	↓	(27)
Guinea-pigs	CY+ β-sitosterol	2 days PN→37 days PN	↑	(24)
Rats	HF or HC	15 days PN→30 days PN	↑ in HC	(6)
Rats	HF or HC	15 days PN→30 days PN	HF<HC	(7)
Rats	HF or HC	70 days PN→149 days PN	—	(32)
Rats	HF	18 days G→30 days L	↑	(22)
Rabbits	CY	6 weeks PN→12 weeks PN	↓	(53)
Rabbits	CY	4 weeks PN→10 weeks PN	—	(28)

CHOL: cholesterol, CY: cholestyramine, HF: high-fat, HC: high-carbohydrate, BG: before gestation, G: gestation, L: lactation, PN: postnatal, ↑: increased, ↓: decreased, —: no effect.

1. 負相關

已有很多實驗室證明在新生期經由飲食攝取的修飾可以永久地改變膽固醇恒常性的發展。1972 年 Reiser 和 Sidelman[5] 最早指出以飲食來修飾母奶，當攝取含高膽固醇母奶 (40 mg/dl) 的幼鼠，於成長後攝取含 10% 豬油和 0.5% 膽固醇飼料時，其血膽固醇濃度要比對照組（攝取低膽固醇母奶，24 mg/dl）者低；他們認爲長大後大白鼠血清中膽固醇濃度與早期所提供的母乳中膽固醇含量

呈負相關。於是提出假設：幼鼠於哺乳期攝取膽固醇可活化膽固醇之代謝酵素，使其於成熟後再攝取含高膽固醇之飲食時，可維持較低的血清膽固醇濃度。隨後 Hahn 和 Kirby[6] 也指出提早斷奶的幼鼠比正常斷奶者具有較高的血膽固醇濃度，而這種修飾對成長後的血膽固醇濃度有持續性的影響。於斷奶期餵高脂肪飲食者，成長後其血膽固醇濃度並不會增加，反而是原先餵食高醣類者，於成熟後膽固醇挑戰 (cholesterol challenge) 時，明顯增加血膽固醇濃度[7]；因此，他們提出斷奶期的血中膽固醇濃度愈高，於成長後接受膽固醇挑戰時，血膽固醇濃度愈低。

Li 等[8,9] 和 Subbiah 等[10] 分別以新生的天竺鼠和幼鴿子作爲實驗動物，餵以含 cholestyramine (CY，一種鹽基性離子交換樹脂，在腸道中與膽汁酸結合，促進膽汁酸異化，降低血膽固醇濃度[11]，可用以治療家族性第二型的高脂蛋白血症[12]) 的飼料，當成熟期給予高膽固醇挑戰時，皆比對照組 (未給予 CY) 有較低的血膽固醇濃度；對天竺鼠而言，即使在斷奶後進行 CY 修飾，成長後仍能有效改善對膽固醇的處理能力[13]。

這種所謂代謝記憶或烙印效果究竟於高膽固醇挑戰後能持續多久？最近我們以 ExHC (exogenous hypercholesterolemic) 大白鼠作爲實驗動物，於斷奶後餵高膽固醇飲食，成熟期再給予膽固醇挑戰，發現早期膽固醇的代謝記憶，在膽固醇挑戰的初期會降低血清 β-VLDL (極低密度脂蛋白) 之膽固醇濃度，而且抑制肝臟分泌 LDL (低密度脂蛋白) 中膽固醇的能力[14]。如果早期以不同蛋白質修飾後，於成熟期接受高膽固醇飲食挑戰的話，兩星期內大豆蛋白組的酸性固醇排泄量仍大於酪蛋白組[15]。至於何時給予飲食刺激 (修飾) 才能達到此種記效果呢？於懷孕期及哺乳期餵以高膽固醇飲食時，對斷奶的老鼠及成鼠而言，會顯著抑制肝臟中 HMG-CoA reductase (3-hydroxy-3-methylglutaryl-CoA reductase) 的活性，而增加 cholesterol 7α-hydroxylase 的活性[16]。而 HMG CoA reductase 的活性於懷孕期比哺乳期更易受到飲食的調節，cholesterol 7α-hydroxylase 的活性則較易受到哺乳期飲食的調節[17~19]。Hassan 等[20]認爲對超過三個月大的天竺鼠再給予飲食刺激，則這種記憶效果便消失。可見飲食修飾愈早實施，愈能改變成長後膽固醇代謝的恒常性。

2. 正相關

相對於 Reiser 和 Sidelman[5] 的假記，Green 等[21]發現幼鼠攝取經高脂肪、高膽固醇修飾的母乳，於成長後的膽固醇挑戰，其血膽固醇濃度反而高於普通飲食者。Coates 等[22]也認爲早期餵食高脂肪飲食者，於成長後較具高膽固醇血症性應答 (response)[23]；且這種現象在高脂肪挑戰的初期尤爲顯著，同時指出對成長後膽固醇代謝而言，懷孕期間開始的營養修飾要比從哺乳期者有效[23]。

前已述及早期經 CY 活化膽固醇異化途徑的話，於成長後對高膽固醇飲食之挑戰具有抑制血膽固醇濃度上升的作用。但是，當 CY 和 β-sitosterol 同時加到幼天竺鼠之飼料中時，成長後受到膽固醇挑戰時會增加血清膽固醇濃度[24]。

Lu 等[25]的膳食纖維實驗顯示，幼鼠經水溶性纖維（pectin，polydextrose）修飾者，當長大後受膽固醇挑戰時，其血膽固醇濃度比經非水溶性纖維（cellulose）修飾者更容易增加，同時減低糞便中 primary bile acid/secondary bile acid，sterols/stanols 之比例，此顯示早期膳食纖維修飾，對成熟期脂質代謝或腸道菌叢的改變皆有烙印效果。

3. 無 關

由於膽汁酸之異化途徑在出生前或剛出生後的老鼠乃處於未發育狀態[26]，此時藉營養因子來活化其代謝途徑，而有利成長後的膽汁酸代謝。其結果會使血膽固醇濃度下降，但也有使膽固醇濃度上升者，而認爲不影響的報告也有。

例如天竺鼠[27]、大白鼠[28~30]、狒狒[31]實驗中皆發現早期給予高膽固醇飲食，在受到膽固醇挑戰時對血清膽固醇濃度、cholesterol 7α-hydroxylase 活性或糞便排泄量與對照組比較，皆無顯著差異。Beynen 等[32]認爲早期給予高脂肪或高醣類飲食，並不影響其後膽固醇挑戰時血清膽固醇濃度；他們也認爲早期的餵食 CY 並不影響其後大白鼠之血膽固醇濃度[30]；但 Lu 等[33]以 ExHC rats 的實驗顯示，既使不影響血清及肝臟膽固醇濃度，卻會減少 cholesterol 7α-hydroxylase 活性或糞便固醇排泄量。

最近，Lewis 等[34]發現出生時餵母乳（含膽固醇 30 mg/dl），斷奶後餵高膽固醇飲食的狒狒，青春期時的血膽固醇濃度與早期餵食配方乳（含膽固醇 1 mg/dl）者無差異，但有較高 VLDL-C+LDL-C/HDL-C（高密度脂蛋白）。Mott 等[35~37]將新生的狒狒分別餵母乳（膽固醇含量 20-30 mg/dl）及配方奶（膽固醇含量分別爲 2、30 及 60 mg/dl），14 週斷奶後，各分成兩組改飼以含高（1.0 mg/kg）或低（0.01 mg/kg）膽固醇，同時配合飽和脂肪（P/S=0.37）或不飽和脂肪（P/S=2.1）之飲食，一直餵到青春期（7-8 歲）；結果發現不論斷奶前餵母乳或膽固醇配方乳，對斷奶時血清膽固醇、脂蛋白濃度皆無顯著差異。但斷奶後，若飲食中添加高膽固醇，則原先餵母乳者比餵配方者有較低 HDL-C 及較高 VLDL-C+LDL-C/HDL-C 比例，同時降低膽固醇生成速率、中性固醇排泄；而在相同的膽固醇含量下，含飽和脂肪者比含不飽和脂肪者更有此現象。由此可知不同哺育的方式（母乳或配方乳），會使青春期的脂蛋白濃度受油脂種類的影響；同時，飲食中膽固醇對膽汁酸推泄和膽固醇轉移速率也受到哺育方式的影響。

三、產前修飾

我們知道胎兒體內膽固醇的一部分乃經由母體而來[38,39]，因此，經由食物及藥物所給予母體而達到膽固醇代謝的產前修飾是另一種可行的方式。Hassan 等[40]指出懷孕期給予含膽固醇飽料，會使新生的天竺鼠有較低的膽汁酸池（bile acid pool）。Nassem 等[17,18]給予懷孕中的母鼠高膽固醇-高脂肪飲食，於新生期的幼鼠會有較高的血膽固醇濃度，此時也增加 cholesterol 7α-hydroxylase 活性而抑制 HMG-CoA reductase 活性。此顯示增加的胎兒膽固醇池可能促進膽汁酸生合成途徑；若於斷奶後給予同樣高膽固醇-高脂肪飲食挑戰，則實驗組有較高的血膽固醇濃度[19]。

懷孕期給予含 CY 的飼料，其子代成長後再給予相同飼料，雖然增加 cholesterol 7α-hydroxylase 活性和糞便固醇類排泄量，但血膽固醇濃度卻較高[40]。Innis[41] 也認爲懷孕期的大白鼠給予 CY，於懷孕的第 20 天，母體與胎兒的肝臟 HMG-CoA reductase 活性分別爲對照組的 2.4 與 1.9 倍，但不影響 cholesterol 7α-hydroxylase 活性；當雄性子代餵以高膽固醇-高脂肪飲食，實驗組有較高的血膽固醇濃度。

四、流行病學研究

基於早期接觸外因性膽固醇可預防成熟期的飲食性誘導高膽固醇血症的假設，其爭議不只在動物模型實驗，在人類也有同樣的困擾。對成年的女性而言，其血清膽固醇濃度以早期攝取母乳者比吃嬰兒配方者低[42]。Shaefer[43] 也認爲原始部落以含高膽固醇的母乳餵嬰兒 2-3 年，結果幼兒的血膽固醇濃度較低，且可減少成年期的動脈粥狀硬化症；然而 Hodgson 等[44]的調查顯示新生兒前三個月餵食低膽固醇（2-4 mg/dl）配方的 7-12 歲幼童，比餵食高膽固醇（20 mg/dl）配方者有較低的血膽固醇濃度。其他臨床研究顯示，早期的膽固醇飲食與其後血膽固醇應答之間並沒有相關性[45~47]。Stein 等[48]認爲給 1-6 個月大的嬰兒含粗纖維的配方食品時，於 12-15 個月大若給予含較高膽固醇飲食的話，會有較低的血膽固醇濃度及較低的 LDL-C。

五、代謝記憶之可能機轉

有關飲食與代謝記憶的諸報告中，仍無法獲得定論，造成這些結果的差異不外與動物種類、品種、實驗設計與飼料組成有關。而這種記憶的機轉究竟是什麼？Reiser 等[49] 指出早期的營養修飾會改變 HMG-CoA reductase 活性，而這種改變可能持續許久或永久。早期經膽固醇修飾的 ExHC rats，於膽固醇挑戰

初期會增加灌流肝臟分泌 VLDL，減少 LDL 的分泌[14]，顯示可能促進 VLDL 的異化。以 CY 刺激新生的天竺鼠，會增加 cholesterol 7α-hydroxylase 活性，而且單離肝的細胞也分泌較多量的膽汁酸[50]，當成長後接受膽固醇挑戰時，其 cholesterol 7α-hydroxylase 仍維持在較高的活性[9]。在兎子，CY 會促進 LDL 的異化[51]，同時會顯著增加 LDL receptor 活性[52]；當 CY 停止修飾之後，對某些酵素仍具遲延作用[53]。

據報告指出由胎兒期到出生、生長的所謂分化、發育期裏，在一些酵素、蛋白質中產生急激的遺傳基因的表現及修飾，這種情形追根究底乃是染色質構造的變化，或與特異的遺傳基因 DNA 的甲基化有關。例如 in vitro 以雌性激素 (17β-estradiol) 刺激人類肝癌細胞 HepG2，而後於無激素培養基中經 10 次細胞分裂增殖後，再以雌激素刺激時，其對 Apolioprotein B 和 E 的分泌促進仍表現出記憶效果 (memory effect)[54,55]，而其對 Apolipoprotein 的促進分泌乃在轉譯 (translation) 之前[56]。因此，於飲食與代謝記憶表現之際，在發育中的斷乳期，營養修飾可能對與脂蛋白的合成、異化途徑有關的諸遺傳基因的構造產生變化，於遺傳基因表現的容量 (capacity)，對成熟期大量的膽固醇負荷表現出種種的應答。正如 Mott[57] 指出新生期給予哺乳或嬰兒配方食品，對膽固醇代謝所造成的長期效應，不可能是因攝取膽固醇量的不同，母乳中的其他成分，如脂肪酸組成、免疫球蛋白，特別是激素可能影響發育的膽固醇代謝，致可能造成膽固醇恒常性的長期效應。從這樣的觀點，今後明瞭激素、膽固醇及其代謝產物與遺傳基因構造的關係，確定本現象的實際內容也許是有必要的。

六、結　　論

以上綜論了有關由胎兒、新生期到成熟期的有關膽固醇代謝記憶之種種報告，因資料仍有限，我們很難由這些報告獲致一滿意的結論。但無論如何，如果早期的一些營養修飾會促進膽固醇異化，那麼這種效果可能影響其後膽固醇代謝。實驗設計、飼料組成、動物品種的不同也許可以解釋這些矛盾點，正如 Jensen 等[59]提出：除非有理想的動物配合適當的研究，否則報告不完備，爭論仍會繼續存在。因此，在研究飲食與代謝記憶之前，需建立更多有關脂質與蛋白質代謝的資料，特別是在胎兒及初生期膽汁酸的合成，以及激素對 Apoprotein 合成之記憶效果，才能解開這些爭論。

參考文獻

(1) 行政院衞生署，臺灣省衞生處，臺北市衞生局，高雄市衞生局，「中華民國 79 年衞生統計，生命統計」，行政院衞生署 (1991)。

(2) W.B. Kannel, "Lipid Profile and Potential Coronary Victim", *Am. J. Clin. Nutr.*, **24**, 1074-1081 (1972).
(3) R.L. Holman, H.C. Mcgill, J.P. Strong and J.C. Geer, "The Natural History of Atherosclerosis: The Early Aortic Lesions as Seen in New Orleans in the Middle of the 20th Century", *Am. J. Pothol.*, **34**, 209-235 (1958).
(4) M.D. Haust, "The Morphogenesis and Fate of Potential and Early Atherosclerotic Lesions in Man", *Hum. Pathol.*, **2**, 1-9 (1971).
(5) R. Reiser and Z. Sidelman, "Control of Serum Cholesterol Homeostasis by Cholesterol in the Milk of the Suckling Rat", *J. Nutr.*, **102**, 1009-1016 (1972).
(6) P. Hahn and L. Kirby, "Immediate and Late Effects of Premature Weaning and of Feeding a High Fat or High Carbohydrate Diet to Weaning Rats", *J. Nutr.*, **103**, 690-696 (1973).
(7) P. Hahn and O. Koldousky, "Late Effect of Premature Weaning on Blood Cholesterol Level in Adult Rats", *Nutr. Rept. Int.*, **13**, 87-91 (1976).
(8) J.R. Li, L.K. Bale and M.T.R. Subbiah, "Effect of Enhancement of Cholesterol Degradation During Neonatal Life of Guinea Pig on Its Subsequest Response to Dietary Cholesterol", *Atherosclerosis*, **32**, 93-98 (1979).
(9) J.R. Li, L.K. Bale and B.A. Kottke, "Effect of Neonatal Modulation of Cholesterol Homeostasis on Subsequent Response to Cholesterol Challenge in Adult Guinea Pig", *J. Clin. Invest.*, **65**, 1060-1068 (1980).
(10) M.T.R. Subbiah, D. Deitemeyer and R.L. Yunker, "Decreased Atherogenic Response to Dietary Cholesterol in Pigeons After Stimulation of Cholesterol Catabolism in Early Life", *J. Clin. Invest.*, **71**, 1509-1513 (1983).
(11) C.J. Packard and J. Shepherd, "The Hepatobiliary Axis and Lipoprotein Metabolism: Effects of Bile Acid Sequestrants and Ileal Bypass Surgery", *J. Lipid Res.*, **23**, 1081-1098 (1982).
(12) S.A. Hashim and T.B. Van, "Cholestyramine Resin Therapy for Hypercholesterolemia", *J. Am. Med. Assoc.*, **192**, 89-92 (1965).
(13) A.S. Hassan, L.S. Gallon, R.L. Yunker and M.T.R. Subbiah, "Effect of Enhancement of Cholesterol Catabolism in Guinea Pigs After Weaning on Subsequent Response to Dietary Cholesterol", *Am. J. Clin. Nutr.*, **35**, 546-550 (1982).
(14) Y.F. Lu, A. Nagatomi, K. Imaizumi and M. Sugano, "Transient Control of Serum Cholesterol Homeostasis in Adult ExHC (Exogenous Hypercholesterolemic) Rat by Dietary Cholesterol During Weaning Period", *J. Nutr. Sci. Vitaminol.*, **35**, 463-474 (1989).
(15) 盧義發、陳慧環，「早期蛋白質修飾對田鼠成熟後脂質代謝之影響」，中華營誌，**17** 39-54 (1992)。
(16) P.M. Kris-Etherton, D.K. Layman, P.V. York and I.D. Frantz, Jr., "The Influence of Early Nutrition on the Serum Cholesterol of the Adult Rat", *J. Nutr.*, **109**, 1244-1257 (1979).
(17) S.Y. Naseem, M.A. Khan, F.P. Heald and P.O. Nair, "The Influence of Cholesterol and Fat in Maternal Diet of Rats on the Development of Hepatic Cholesterol Metabolism in the Offspring", *Atherosclerosis*, **36**, 1-5 (1980).

(18) S.Y. Naseem, M.A. Khan, M.S. Jacobson, P.O. Nair and F.P. Heald, "The Influence of Dietary Cholesterol and Fat on the Homeostasis of Cholesterol Metabolism in the Rat", *J. Nutr.*, **111**, 276-286 (1980).

(19) S.Y. Naseem, M.A. Khan, M.S. Jacobson and P.O. Nair, "The Influence of Dietary Cholesterol and Fat on the Homeostasis of Cholesterol Metabolism in Early Life in the Rat", *Pediatr. Res.*, **14**, 1061-1066 (1973).

(20) A.S. Hassan, L.S. Gallon, R.L. Yunke and M.T.R. Subbiah, "Effect of Enhancement of Cholesterol Catabolism in Guinea Pigs After Weaning on Subsequent Response to Dietary Cholesterol", *Am. J. Clin. Invest.*, **35**, 546-550 (1982).

(21) M.H. Green, E.L. Dohner and J.B. Green, "Influence of Dietary Fat and Cholesterol on Milk Lipids and on Cholesterol Metabolism in the Rat", *J. Nutr.*, **111**, 276-286 (1981).

(22) P.M. Coates, S.A. Brown, B.R. Sonawane and O. Koldovsky, "Effect of Early Nutrition on Serum Cholesterol Levels in Adult Rats Challenged with High Fat Diet", *J. Nutr.*, **113**, 1045-1050 (1983).

(23) S.A. Brown, L.K. Rogers, J.K. Dunn, A.M. Gotto, Jr. and W. Patsch, "Development of Cholesterol Homeostatic Memory in the Rat is Influenced by Maternal Diets", *Metabolism*, **39**, 468-473 (1990).

(24) A.S. Hassan, L.S. Gallon, R.L. Yunker and M.T.R. Subbiah, "Effect of Feeding β-Sitosterol During Early Life on Subsequent Response to Cholesterol Challenge in Adult Life in Guinea Pigs", *Br. J. Nutr.*, **48**, 443-450 (1982).

(25) Y.F. Lu, K. Imaizumi, M. Sakono and M. Sugano, "Effects of Dietary Fibers in Early Weaning on Later Response of Serum and Fecal Steroid Levels to High Cholesterol Dield in Rats", *Nutr. Res.*, **9**, 345-352 (1989).

(26) M.T.R. Subbiah and A.S. Hassan, "Deveolpment of Bile Acid Biogenesis and Its Significance in Cholesterol Homeostasis", *Adv. Lipid Res.*, **19**, 137-161 (1982).

(27) J.R. Li, B.A. Kottke and M.T.R. Subbiah, "Effect of Neonatal Modulation of Cholesterol Homeostasis on Subsequent Response to Cholesterol Challenge in Adult Guinea Pig", *J. Clin. Invest.*, **65**, 1060-1068 (1980).

(28) A.S. Hassan, "Effect of Treating Neonatal Rabbits with Cholestyramine on the Response to Dietary Casein in Adult Rabbits", *Nutr. Rept. Int.*, **36**, 281-290 (1987).

(29) G. Hulbron, R. Aubert, F. Bourgeois and D. Lemonnier, "Early Cholesterol Feeding: Are There Long-Term Effects in the Rat?", *J. Nutr.*, **112**, 1296-1314 (1982).

(30) A.C. Beynen, J.J. Bruijne and M.B. Katan, "Treatment of Young Rats with Cholestyramine of a Hypercholesterolemic Diet Does Not Influence the Response of Serum Cholesterol to Dietary Cholesterol in Later Life", *Atherosclerosis*, **58**, 149-157 (1985).

(31) R. Reiser, B.C. O'Brien, G.R. Henderson and R.W. Moore, "Studies on a Possible Function for Cholesterol in Milk", *Nutr. Rept. Int.*, **19**, 835-849 (1979).

(32) A.C. Beynen and M.B. Katan, "Previous High Fat or a High Carbohydrate Intake and the Subsequent Cholesterolemic Response to a High Cholesterol Diet in Rats", *Nutr. Rept. Int.*, **30**, 545-552 (1984).

(33) Y.F. Lu, K. Imaizumi and M. Sugano, "Effect of Cholestyramine in Early Weaning on Later Response of Serum and Fecal Steroids Levels and Cholesterol 7α-Hydroxylase Activity to High Cholesterol Diet in ExHC Rats", *J. Nutr. Sci. Vitaminol.*, **36**, 131-140 (1990).

(34) D.S. Lewis, G.E. Mott, C.A. McMahan, E.J. Masori and K.D. Carey, "Deferred Effects of Preweaning Diet on Atherosclerosis in Adolescent Baboons", *Atherosclerosis*, **8**, 274-280 (1988).

(35) G.E. Mott, C.A. McMahan, J.L. Kelley and C.M. Farley, "Influence of Infant and Juvenile Diet on Serum Cholesterol, Lipoprotein Cholesterol and Apolipoprotein Concentration in Juvenile Baboons", *Atherosclerosis*, **45**, 191-202 (1982).

(36) G.E. Mott, C.A. McMahan, J.L. Kelley and C.M. Farley, "Cholesterol Metabolism in Juvenile Baboons: Influence of Infant and Juvenile Diets", *Arteriosclerosis*, **5**, 347-354 (1985).

(37) G.E. Mott, C.A. McMahan, J.L. Kelley and C.M. Farley, "Cholesterol Metabolism in Adult Baboons is Influenced by Infant Diet", *J. Nutr.*, **120**, 243-251 (1990).

(38) W.E. Connor and D.S. Lin, "Placental Transfer of Cholesterol-4-^{14}C into Rabbit and Guinea Pig Fetus", *J. Lipid Res.*, **8**, 558-564 (1967).

(39) R.M. Pitkin, W.E. Connor and D.S. Lin, "Cholesterol Metabolism and Placental Transfer in the Pregnant Rhesus Monkey", *J. Clin. Invest.*, **51**, 2584-2592 (1972).

(40) A.S. Hassan, J.J. Hackley and L.L. Johnson, "Cholestyramine Treatment During Pregnancy in the Rat Results in Hypercholesterolemia", *Atherosclerosis*, **57**, 139-148 (1985).

(41) S.M. Innis, "Influence of Maternal Cholestyramine Treatment on Cholesterol and Bile Acid Metabolism in Adult Offspring", *J. Nutr.*, **113**, 2464-2470 (1983).

(42) M.G. Marmot and C.M. Pose, "Effect of Breast-Feeding on Plasma Cholesterol and Weight in Young Adults", *J. Epidem. Comm. Health.*, **34**, 164-167 (1980).

(43) O. Shaefer, "When the Eskimo Comes to Town", *Nutr. Today*, **6**, 8-12 (1971).

(44) P.A. Hodgon, R.D. Ellefson and R.A. Nelson, "Comparison of Serum Cholesterol in Children Feed High, Moderate, or Low Cholesterol Milk Diets During Neonatal Period", *Metabolism*, **25**, 739-746 (1976).

(45) C.J. Glueck, R. Tsang, W. Balistreri and R. Fallat, "Plasma and Dietary Cholesterol in Infancy: Effects of Early Low or Moderate Dietary Cholesterol Intake on Subsequent Response to Increased Dietary Cholesterol", *Metabolism*, **21**, 1181-1192 (1972).

(46) G. Friedman and S.J. Goldberg, "Concurrent and Subsequent Serum Cholesterol of Breast- and Formula-Fed Infants", *Am. J. Clin. Nutr.*, **28**, 42-45 (1975).

(47) J.K. Huttunen, U.M. Saarinen, E. Kostiainen and M.A. Simes, "Fat Composition of the Infant Diet Does Not Influence Subsequent Serum Lipid Levels in Man", *Atherosclerosis*, **46**, 87-94 (1983).

(48) E.A. Stein, C. Gapen and C.J. Glueck, "A Conditioning Effect in Early Infancy of Dietary Fiber or Cholesterol on Plasma HDL and LDL Cholesterol at Age 15 Months", *Am. J. Clin. Nutr.*, **39**, 669A (1984).

(49) R. Reiser, G.R. Henderson and B.C. O'Brien, "Persistence of Dietary Suppression of 3-Hydroxy-3-Methylglutaryl Coenzyme A Reductase During Development in Rats", *J. Nutr.*, **107**, 1131-1138 (1977).

(50) A.S. Hassan, L.S. Gallon, L.A. Zimmer, W.F. Balistrer and M.T.R. Subbiah, "Perisistent Enhancement of Bile Acid Synthesis in Guinea Pigs Following Stimulation of Cholesterol Catabolism in Neonatal Life", *Steroids*, **38**, 477-484 (1981).

(51) H.R. Slater, C.J. Packard, S. Bicker and J. Shepherd, "Effects of Cholestyramine on Receptor-Mediated Plasma Clearance and Tissue Uptake of Human Low-Density-Lipoproteins in the Rabbit", *J. Biol. Chem.*, **255**, 10210-10213 (1980).

(52) J. Shepherd, C.J. Packard, S. Bicker, T.D. Veitch-Lawrie and C.H.G. Morgan, "Cholestyramine Promotes Receptor Mediated Low-Density-Lipoprotein Catabolism", *New. Engl. J. Med.*, **302**, 1219-1222 (1980).

(53) Z. Rymaszewski, D.J. Sprinkle, R.L. Yunker, C.A. Stevens and M.T.R. Subbiah, "Cholestyramine Treatment in Early Life Immediate and Delayed Effects on Arterial Cholesterol Ester Metabolizing Enzymes in Rabbit", *Atherosclerosis*, **63**, 27-32 (1986).

(54) S.P. Tam, T.K. Archer and R.G. Deeley, "Biphasic Effects of Estrogen on Apolipoprotein Synthesis in Human Hepatoma Cells: Mechanism of Antagonism by Testosterone", *Proc. Natl. Acad. U.S.A.*, **83**, 3111-3115 (1986).

(55) S.P. Tam, R.J.G. Hache and R.G. Deeley, "Estrogen Memory Effect in Human Hepatocytes During Repeated Cell Division Without Hormone", *Science*, **234**, 1234-1237 (1986).

(56) T.K. Archer, S.P. Tam and R.G. Deeley, "Kinetics of Estrogen-Dependent Modulation of Apolipoprotein A-I Synthesis in Human Hepatoma Cells", *J. Biol. Chem.*, **261**, 5067-5074 (1986).

(57) G.E. Mott, "Deferred Effects of Breast Feeding Versus Formula Feeding on Serum Lipoprotein Concentrations and Cholesterol Metabolism in Baboons", In: The Breastfed Infant: A Model of Performance. Report of the 91st Ross Conference on Pediatric Research 1986. Columbus, OH: Ross Laboratories, pp. 144-149 (1986).

(58) M.T.R. Subbiah, R.L. Yunker, A. Menkhaus and B. Poe, "Premature Weaning-Induced Changes of Cholsterol Metabolism in Guinea Pigs", *Am. J. Physiol.*, **249**, E251-E256 (1985).

(59) R.G. Jensen, M.M. Hagerty and K.E. McMahan, "Lipids of Human Milk and Infant Formulas: A Review", *Am. J. Clin. Nutr.*, **31**, 990-1016 (1978).

Relationship Between Early Nutritional Manipulations and Cholesterol Homeostasis in Later Life: A Review

YI-FA LU AND HUEY-HWAN CHEN

Institute of Nutrition and Food Sciences
Fu Jen University

ABSTRACT

A short review about cholesterol metabolism and metabolic memory from early life to adulthood was discussed. We could not have received a satisfactory conclusion from available information, because the experimental data were still incomplete so far. If some nutritional modulations early in life could enhance cholesterol metabolism, catabolic imprinting might influence cholesterol metabolism in the later life. So far, the difference in experimental designs, dietary compositions, species and strains of animals may all be considered in explaining the confliciting results from animal experiments. For elucidation of metabolic memory, some studies including the rate-limiting enzyme of cholesterol biosythesis and catabolism, liver perfusion, LDL rectptor and catabolism were undertaken. However, genetic factors, cholesterol or its metabolites, and especially hormones that might affect cholesterol metabolism during early development, might have a long-term effect on cholesterol homeostasis.

玉米澱粉與明膠複合膠體系統之不相容性

陳炯堂　陳佳祺　吳曉霞　李正雲

輔仁大學理工學院食品營養研究所

摘　要

添加澱粉於明膠／羧甲基纖維複合膠體系統中，由於彼此分子在水溶液中之不相容性，澱粉分子會局部破壞複合膠體之結構，藉此不相容程度可間接由含澱粉之混合膠體物性改變情況加以評估。隨著澱粉添加量增加，複合膠體之流體行爲係數 (folw behavior index)、彈性係數 (modulus of elasticity) 及硬度皆明顯下降，其中，除了硬度之外，其他兩者下降程度均不受複合膠體強度、鈣離子濃度之影響。複合膠體在形成時，相分離所造成各層溶液體積比亦會受不相容澱粉之存在所影響。隨著澱粉添加量的增加，上層澄清膠體體積下降。而中層膠體體積及下層沈澱膠體體積皆明顯上升。

一、前　言

兩種食品成分於水溶液中，依兩者親水性及所存在交互作用之不同，可呈現共溶、相容及不相容現象[1,2]。兩種不相容物質混合於水溶液中，會導致彼此分子相斥而造成黏稠度下降及高溫失水速率增加[1,3]。嚴重時，不相容物質更促進相分離之沈澱現象[4~6]。此不相容現象的產生對於加工後產品之物性變化及品質影響顯著[7]，評估兩物質相容性大多以複合物形成之狀態及相分離程度來加以說明[8~11]，僅少部分對膠體結構變化來加以探討[1]。故本研究之目的在於了解添加不相容物質於複合物系統中，所導致物性變化的結果，以期進一步確立不相容性之評估方法。

二、材料與方法

1. 材　料

(1) 原　料

食品級之羧甲基纖維 (carboxylmethylcellulose)、明膠 (gelatin，type A)、黏質玉米澱粉 (waxy corn starch)，由臺灣振芳香料公司分別自日本 Daicel Ltd. 公司及法國 Roquette Freres 公司進口，實驗其他化學試劑均購自美國 Sigma 公司。

(2) 羧甲基纖維之處理

將 3 g 羧甲基纖維溶於 70°C，50 ml 蒸餾水中，待呈凝膠狀態後，冷卻至室溫。經 0.2 N NaOH 滴定至 pH 9.5 後，再以 pH 9.5 之 5 ℓ 稀鹼溶液於 40°C 透析 6 h 後稀釋成 100 ml。羧甲基纖維由以下透析處理後，其視黏稠度較未透析者低，顯示所購買之羧甲基纖維含有架橋之金屬離子，需以透析方法去除。稀鹼溶液透析後，再以 5 ℓ 去離子水透析 3 h 兩次，以去除游離鈉鹼離子。羧甲基纖維在稀鹼溶液中，透析一次 6 h 與透析三次 18 h，其視黏稠度皆未有顯著差異，可進一步證明透析一次 6 h，已充分去除架橋之金屬離子。

(3) 玉米澱粉之糊化

配製不同濃度之黏質玉米澱粉水溶液 75 ml。攪拌加熱至 60°C 爲預糊化玉米澱粉。再將糊化黏質玉米澱粉與單酸甘油脂以 100：3 (w/w) 混合均勻。冷卻後，若澱粉水溶液中含有氣泡，需以離心方法去除。使用前再以 700 w (Panasonic microwave oven (2,450 MHz) equiped with Fluroptic Thermometer MDL-755，U. S. A.) 微波加熱控制升溫至 95°C 之樣品卽爲糊化玉米澱粉。

(4) 明膠／羧甲基纖維複合膠體之製備

加入 1 ml 2 N NaOH 於 100 ml 9% 明膠溶液中，於 40°C 鹼處理一段時間。鹼處理後加入 20 ml 之 0.3 M Tris-Maleate (pH 7.3) 緩衝溶液及 100 ml 已透析之 3% 羧甲基纖維溶液。經 2 N HCl 中和後，加入不同濃度之乳酸鈣及糊化澱粉溶液並稀釋至 300 ml，加熱至 70°C 混勻後，卽爲複合膠體[12]。

2. 方 法

(1) 反應平面法

固定複合膠體之濃度，再以三因子反應平面法，探討明膠鹼處理時間、澱粉及鈣離子濃度，對混合水溶液之物性變化及相分離之影響。實驗並假設混合水溶液之各項測定值爲二次多項關係式，實驗所採用三因子之條件列於表一。重複試驗測得數據以統計分析系統軟體 (statistical analysis system，SAS) 進行變異分析及回歸分析，再以該分析系統軟體繪製反應平面圖。

表一 反應平面設計因子

實驗次數	分析代碼			實驗條件		
	X_1	X_2	X_3	X_1	X_2	X_3
1	−1	−1	−1	12	0.06	2.4
2	−1	−1	1	12	0.06	9.6
3	−1	1	−1	12	0.26	2.4
4	1	−1	−1	48	0.06	2.4
5	1	−1	1	48	0.06	9.6
6	−1	1	1	12	0.26	9.6
7	1	1	−1	48	0.26	2.4
8	1	1	1	48	0.26	9.6
9	−1.682	0	0	0	0.16	6
10	1.682	0	1	60	0.16	6
11	0	−1.682	0	30	0	6
12	0	1.682	0	30	0.32	6
13	0	0	−1.682	30	0.16	0
14	0	0	1.682	30	0.16	12
15	0	0	0	30	0.16	6
16	0	0	0	30	0.16	6
17	0	0	0	30	0.16	6

X_1=鹼處理的時間 (min)
X_2=%鈣離子濃度 (w/v)
X_3=%澱粉濃度 (w/v)

(2) 黏度分析

測量澱粉／複合膠體水溶液之視黏稠度 (apparent viscosity) 之前，pH 值需以稀鹽酸調至 7.0 後靜置隔夜，且溶液中若有相分離所形成之沈澱物或氣泡，亦需以 3,000×g 離心 10 分鐘後，取上澄液再以 Brookfield viscometer (LVF 型) 分析之。依 Toledo[12,26] 計算黏度係數 (μ)，流體行爲係數 (n)，及視黏稠度如下：

$$T_w=\mu R_w^n \qquad \text{Apparent viscosity}=\mu R_w^{n-1}$$

式中

T_w=Sheer stress (dyne/cm)=673.7×(% Full scale)/$2\pi LR^2$
R_w=Sheer rate (1/s)=$2\pi RN$/gap

μ=Consistency index
n=Flow behavior index
R, L: radius and length of the spindle
N: rotational speed of the spindle in rpm
gap: gap between the spindle and the outer beaker

(3) 物性儀測定

實驗採用物性測定儀 (NRM-2020 型 RHEO METER, Fudoh kogyo Co. Ltd., Tokyo, Japan) 進行壓縮測試以分析澱粉複合膠體之硬度及彈性係數。以底部 (20 mm) 平滑，塑膠製圓柱狀的 adaptor，使用 2 kg 感測器，進行膠體壓縮反應測試。測量時，載物台上升速度 (table speed) 及記錄器掃動速度 (sweep speed) 皆爲 6 cm/min。樣品溫度均控制在 28±0.5°C。

(4) 相分離測定

將 12 g 澱粉／複合膠體溶液與 8 ml 蒸餾水混合均勻，以 10,086×g 於 25°C 離心 20 min 後，測各層之體積。上層爲透明之澄清膠體，中層爲乳白膠體，而下層是白色沈澱膠體，經稀釋 5～15 倍後，以雙脲試劑在 540 nm 測定蛋白質含量。

三、結果與討論

1. 物性分析

明膠與羧甲基纖維在 pH 高於明膠等電點且有鈣離子存在時，會形成離子架橋之複合物[12]。複合物離子鍵之強度部分取決於蛋白質分子表面羧基數目及分子構形。增加前者方法之一，則可藉由鹼處理反應，使醯胺基 (amide group) 轉變成羧基[13]。倘若完全去醯胺，明膠約含有 18% 含羧基之胺基酸[14]，此含量應可與羧甲基纖維及鈣離子有效地形成離子架橋之複合物。一般而言，物化特性相近之食品成分，如親水性於適合濃度比及適當之 pH、離子強度時，可形成交互作用[15]，此現象不但可形成相容複合物且可提高有效水合體積 (effective hydrodynamic volume)[2,11,16] 而使膠體黏稠度、硬度及彈性係數上升[12,17]。反之，物化特性廻異之食品成分混合於水溶液中，高親水性成分會排斥低親水性成分，而導致低親水性分子有自分子凝聚現象[2,5,18]，進而使膠體之視黏稠度、硬度及彈性係數下降[1,17]。食品中普遍含有澱粉成分，糊化澱粉與明膠或與三仙膠在水溶液中之不相容性已由老化程度增加的現象加以證實[17]。故本研究嘗試進一步研究澱粉與明膠複合膠體之相容程度。本研究實驗設計均採取反應平面法

(response surface methodology)，實驗基本假設含澱粉複合膠體之物性變化及相分離現象均爲三因子：澱粉濃度、鈣離子濃度及明膠鹼處理時間等之函數。

添加不同濃度糊化黏質玉米澱粉於複合膠體中經流變性分析發現，除了澱粉濃度增加會導致流體行爲係數的下降之外，其餘兩因子皆無顯著影響（圖 1）。流變行爲係數的下降意謂複合膠體僞膠特性（pseudoplasticity）之上升，亦即複合膠體離子鍵結強度之下降。倘若進一步以物性測定儀直接分析此複合物膠體結構之強度，當明膠鹼處理時間爲 30 分時，隨澱粉添加量的增加，複合膠體硬度急遽下降至幾乎爲零（圖 2）。圖 3 與圖 4 分別表示在 0.16% 乳酸鈣及 6% 澱粉濃度時所測得之膠體硬度值。離子濃度（圖 2）及明膠鹼處理時間（圖 3）均較澱粉濃度之因子對膠體硬度影響之程度爲小。由圖 2 至圖 4 得知；複合膠體在 0.19% 乳酸鈣、明膠於 40°C 鹼處理時間爲 30 分且無澱粉存在時，硬度最高。

根據 Bagley[19] 之理論，彈性係數（modulus of elasticity）一般可應用於測量食品組織結構承受外力（stress）變形後，可回覆應力（strain）之指標；反之黏度係數（modulus of viscosity）爲不可回覆應力之表現，而根據 RHEO METER（Model：NRM-2020J-CW）操作手册指出可回覆鬆弛比（% recoverable relaxation ratio）即爲前兩者之比值百分比[19]。目前多數文獻常以貯存係數（storage modulus）及損失係數（loss modulus）來評估食品結構承受外力的變化[20,21]。在明膠鹼處理時間爲 30 分時，複合膠體之可回覆鬆弛比，亦即變形

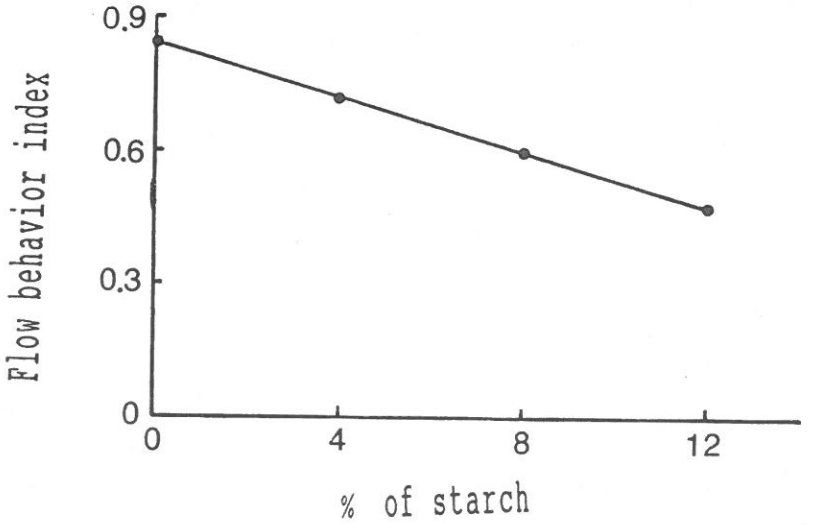

圖 1 澱粉濃度對膠體模式系統流體行爲係數的影響。

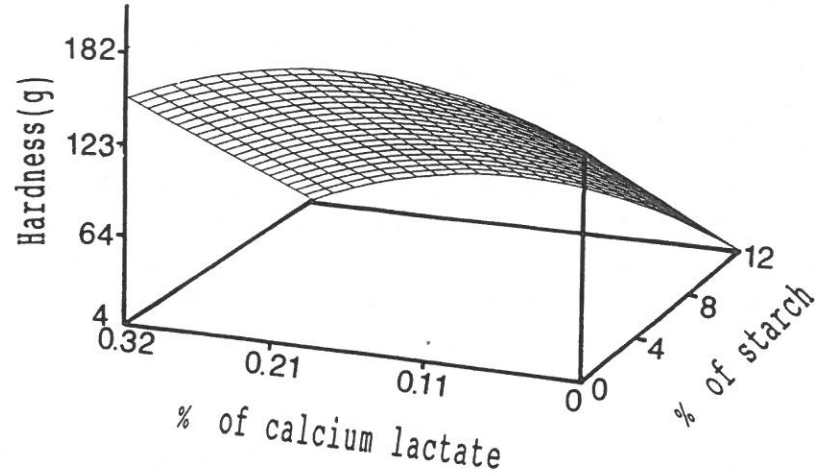

圖 2 鈣離子及澱粉濃度影響膠體模式系統硬度的反應曲面圖。

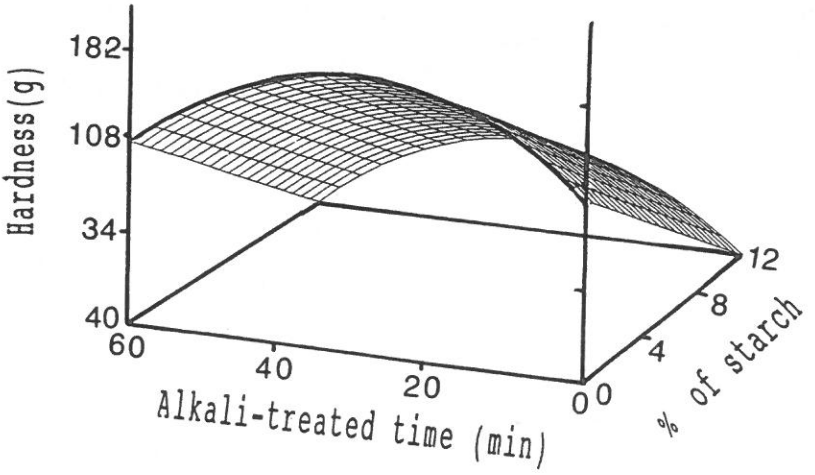

圖 3 動物膠鹼處理時間及澱粉濃度影響膠體模式系統硬度的反應曲面圖。

後回覆原形狀之比例較高（圖 5），這個結果與最佳硬度條件相同。但是依照理論，鈣離子濃度因子應對離子複合物之可回覆鬆弛比有直接的影響，但是結果卻顯示沒有影響，關於此點仍需進一步研究，最可能的原因是明膠與羧甲基纖維在 pH 7.3 且無鈣離子時，存在靜電交互作用力。圖 5 中亦可發現糊化澱粉之添加量在 4% 時，可回覆鬆弛比達最高。若進一步測試時複合膠體之彈性係數隨糊

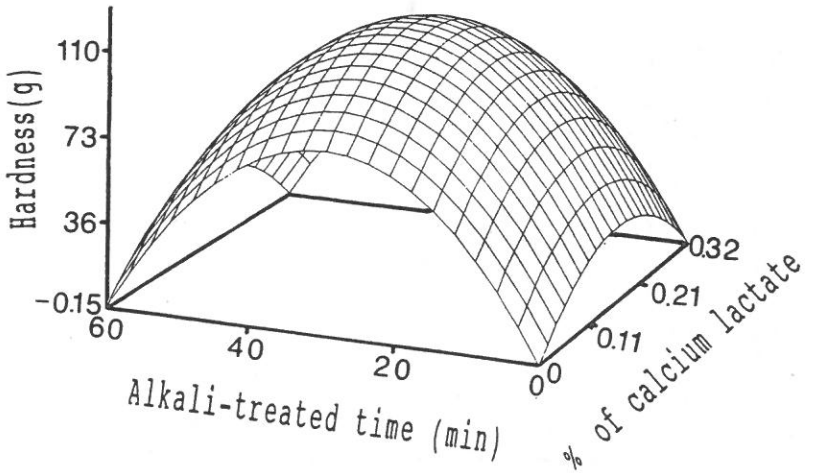

圖 4 動物膠鹼處理時間及鈣離子濃度影響膠體模式系統硬度的反應曲面圖。

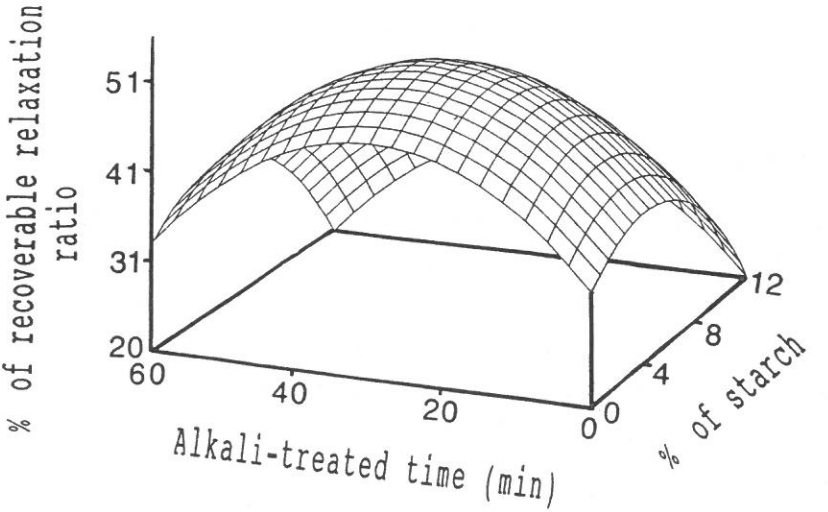

圖 5 動物膠鹼處理時間及澱粉濃度影響膠體模式系統 Relaxation ratio 的反應曲面圖。

化澱粉濃度的增加而急遽下降至零（圖 6）。比較兩圖結果可得黏度係數之變化情形。在糊化澱粉濃度小於 4% 時，隨澱粉濃度之增加黏度係數下降之速率大於彈性係數之下降速率；反之，當糊化澱粉濃度大於 4% 時，則隨澱粉濃度之增加彈性係數因而下降之速率較大。

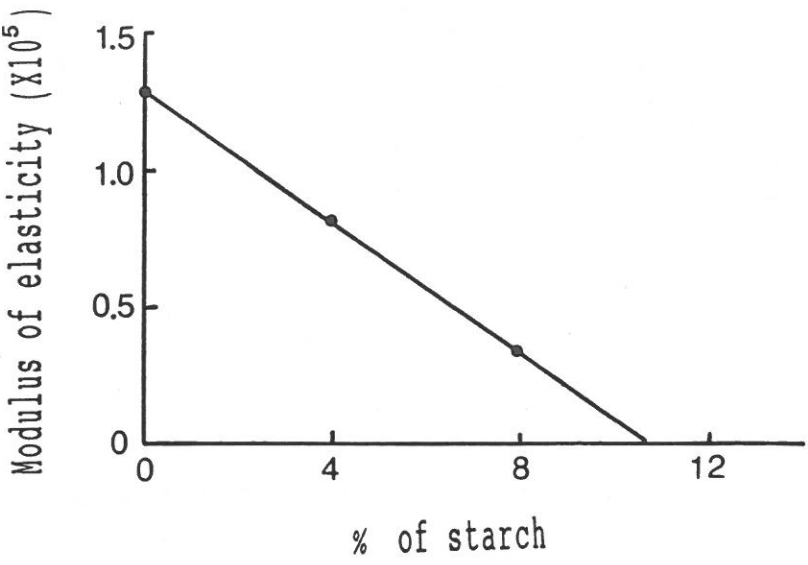

圖 6 澱粉濃度對膠體模式系統彈性的影響。

2. 相分離

食用成份於水溶液中形成複合物之溶解度變化與不相容成份之相互排擠程度常用比濁度滴定法 (nephelometric titration method)[22,23] 及光分散技術 (light scattering techniques)[3,5,6] 探討相平衡狀態 (phase equilibrium) 及相分離 (phase separation) 情形。複合物凝聚現象與最佳濃度比值亦可用相分離技術加以評估[24,25]。添加糊化澱粉於複合膠體中，會導致上層澄清膠體體積百分比下降（圖 7），而中層可溶乳白膠體體積百分比（圖 8）及下層沈澱膠體體積比（圖 9）上升。除了圖 9 顯示明膠鹼處理時間對下層體積比有影響之外，其他各層體積比均不受鈣離子濃度及明膠鹼處理時間之因子所影響。未添加糊化澱粉時，複合膠體爲透明狀態（圖 7），但是隨澱粉添加量增加而較高密度之中層乳狀膠體及下層白色膠體漸增（圖 8及圖 9）。倘若進一步分析各層中蛋白質含量，由雙脲試劑測定的結果顯示上、中、下層均含有明膠，其濃度約爲 5.8、2.2 及 4.6% (w/v)。上層透明膠體之蛋白質濃度接近所添加之量而中、下兩層均遠低於原來所添加之量。由此可知，較低親水性糊化澱粉分子被複合膠體排擠而自分子凝聚於複合膠體之網狀結構中，進而破壞複合膠體結構[1]。

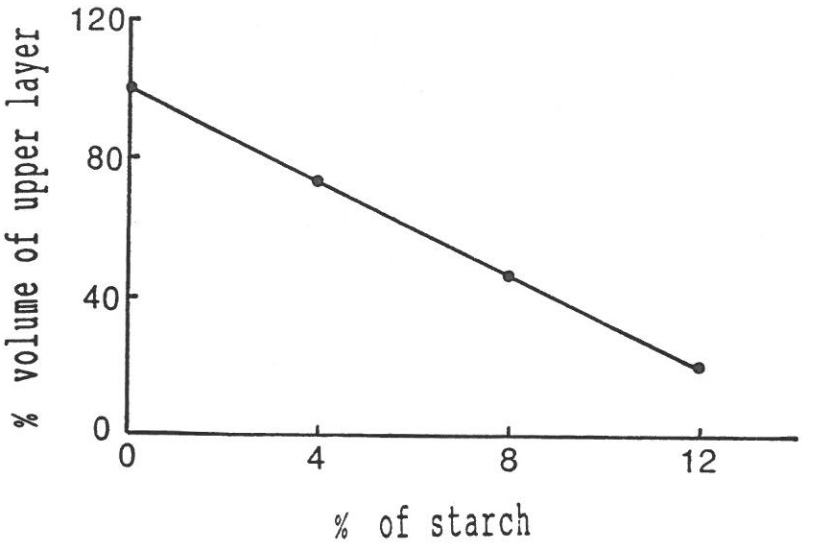

圖 7 澱粉濃度對膠體模式系統相分離之上層澄清液體積的影響。

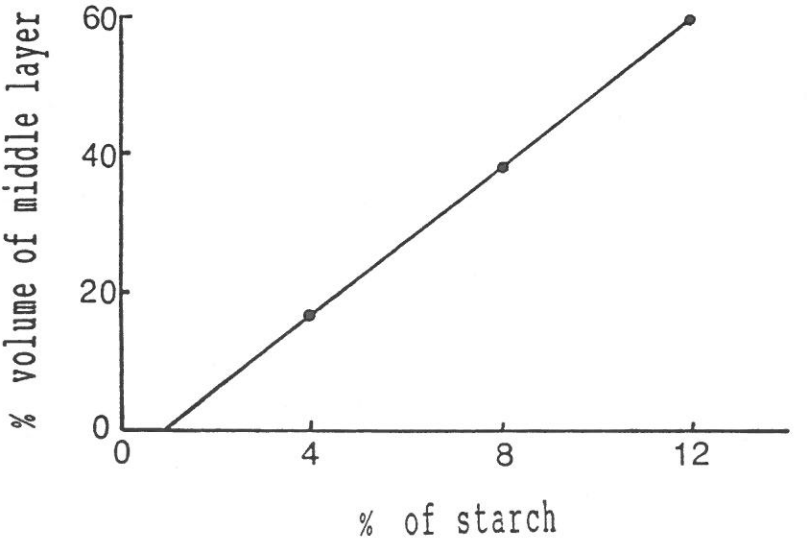

圖 8 澱粉濃度對膠體模式系統相分離之中層膠體體積的影響。

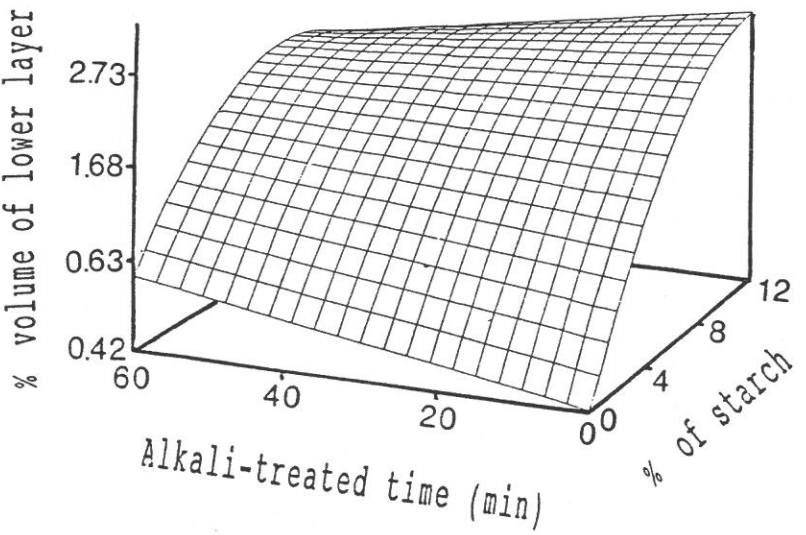

圖 9 動物膠鹼處理時間及澱粉濃度影響膠體模式系統相分離之下層沉澱膠體體積的反應曲面圖。

四、誌　　謝

本研究承蒙輔仁大學聖言會及行政院農委會（81 農建-12.2 糧 17(12)）經費補助，謹致最高謝意。

參考文獻

(1) 陳炯堂，「蛋白質與多醣類水溶液之不相容性」，將刊登於食品科學第一期（1993）（將於 1993 年發表）。

(2) V.B. Tolstoguzov, "Functional Properties of Food Proteins and Role of Protein-Polysaccharide Interaction", *Food Hydrocolloids.*, **4**, 429 (1991).

(3) V.B. Tolstoguzov, In J.R. Mitchell and D.A. Ledward, eds.: "Functional Properties of Food Micromolecules", Elsevier Applied Science Publishers, London, U.K., P. 385 (1986).

(4) V.B. Tolstoguzov, "Concentration and Purification of Proteins by means of Two Phase Systems. Membraneless Osmosis Process", *Food Hydrocolloids.*, **2**, 195 (1988).

(5) V.B. Tolstoguzov, In G.O. Phillips, P.A. Williams and D.J. Wedlock, eds.: "Gums and Satabilizers for The Food Industry", Vol. 5, IRL Press, Oxford, U.K., P. 157 (1990).

(6) M.G. Semenova, V.S. Bolotina, V.Y. Grinberg and V.B. Tolstoguzov, "Thermodynamic Compatibility of The 11s Fraction of Soybean Globulin and Pectinate in Aqueous Medium", *Food Hydrocolloids.*, **3**, 447 (1990).
(7) V.B. Tolstoguzov, "Some Physico-Chemical Aspects of Protein Processing into Food Stuffs", *Food Hydrocolloids.*, **2**, 339 (1988).
(8) A.V. Gurov, N.A. Gurova, A.L. Leontiev and V.B. Tolstoguzov, "Equilibrium and Nonequilibrium Complexes between Bovine Serum Albumin and Dextran Sulfate-1 Complexing Condictions and Composition of Nonequilibrium Complexes", *Food Hydrocolloids.*, **2**, 267 (1988).
(9) A.N. Gurov and V.B. Tolstoguzov, "Equilibrium and Nonequilibrium Complexes between Bovine Serum Albumin and Dextran Sulfate-2 Equilibrium Complexes in Solution", *Food Hydrocolloids.*, **2**, 285 (1988).
(10) A.N. Gurov, P.V. Nass, N.A. Gurova and S.H. Dotdaev, "Equilibrium and Nonequilibrium Complexes between Bovine Serum Albumin and Dextran Sulfate-3. Methylene Blue Binding by Equilibrium Complexes", *Food Hydrocolloids.*, **2**, 297 (1988).
(11) A.Y. Sherys, A.N. Gurov and V.B. Tolstoguzov, "Water-insoluble Triple Complexes: Bovine Serum Albumin-bivalent Metal Cation-alginate", *Carbohydr. Polymers.*, **10**, 87 (1989).
(12) 陳炯堂、杜宏文，「動物膠與陰電性多醣類複合物之流變性與熱性質」，食品科學，**19**(3)，397 (992)。
(13) 何慧如、詹朝閔、馬美蓉、陳炯堂，「鹼處理麵筋功能性之探討」，食品科學，**19**(2)，141 (1992)。
(14) R.E. Neumann, "The Amino Acid Composition of Gelatin, Collagens, and Elastins from Different Sources", *Arch. Biochem.*, **24**, 289 (1949).
(15) N. Sharon and H. Lis, "Carbohydrate-protein Interactions", *Chem. Br.*, **26**(7), 679-82 (1990).
(16) J. Menjivar and C.K. Rha, In G. Astarita, G. Marrucci and S. Nicholai, eds: "Rheology", *Plenum Press.*, New York, U.S.A., Vol. 2, p. 293 (1980).
(17) 黃正忠，「直鏈澱粉含量及不相容物質對玉米澱粉老化變化之探討」，輔仁大學食品營養研究所碩士論文 (1992)。
(18) V.P. Yuryev, I.G. Plashchina, E.E. Braudo and V.B. Tolstoguzov, "Structural Study of The Solutions of Acidic Polysaccharides-1, Study of The Solutions of Acidic Polysaccharides by Measuring The Activity of Coefficients of Counterions", *Carbohydr. Polymers.*, **1**, 139 (1981).
(19) E.B. Bagley, In M. Peleg and E.B. Bagley, eds.: "Physical Properties of Foods", AVI Publishing Co. Inc. Westport, Conneticut, P. 325 (1983).
(20) J.L. Doublier and L. Choplin, "A Rheological Description of Amylose Gelation", *Carbohydr. Res.*, **193**, 215 (1989).
(21) C.G. Biliaderis and J. Zawistowski, "Viscoelastic Behavior of Aging Starch Gels: Effects of Concentration, Temperature, and Starch Hydrolyzates on Network Properties", *Cereal Chem.*, **67**(3), 240 (1990).
(22) A.N. Gurov, E.S. Wajnerman and V.B. Tolstoguzov, "Interaction of Proteins with Dextransulfate in Aqueous Medium. Part 2, Nonequilibrium Phenomena", *Stark.*, **29**(6), 186 (1977).
(23) R.C. Randall, G.O. Phillips and P.A. Williams, "The Role of The Proteinaceous Component on The Role on The Emulsifying Porperties of Gum Auabic", *Food Hydrocolloids.*, **2**(2), 131 (1988).

(24) S.A.M. Mortada, A.M. Egaky, A.M. Motawi and K.A. Khodery, "Preparation of Microcapsules from complex Coacervation of Gantrezgelation. I. Development of The Technique", *J. Microencapsulation.*, **4**(1), 11 (1987a).
(25) S.A. Mortada, A.M. Egaky, A.M. Motawi and K.A. Khodery, "Preparation of Microcapsules from Complex Coacervation of Gantrezgelation. II. In vitro Dissolution of Nitrofurantoin Microcapsules", *J. Microencapsulation*, **4**(1), 23 (1987b).
(26) R.T. Toledo, In R.T. Toledo, eds.: "Fundamentals of Food Process Engineering", AVI Publish Co., Connecticult, U.S.A. P. 168 (1980).

Incompatibility Between Corn Starch and The Gelatin-containing Gum Complex

JOHN-TUNG CHIEN, CHIA-CHI CHEN,
SHEAU-SHYA WU AND JENG-YUNE LI
Graduate Institute of Nutrition and Food Sciences

ABSTRACT

Addition of starch into the complexed gum system of gelatin/carboxylmethylcellulose would cause a partial destruction of its gel network due to the existence of mutual molecular incompatibility in an aqueous solution. Thereby, degree of incompatibility between both molecules could be evaluated by the changes of their physical properties. Flow behavior index, modulus of elasticity and hardness of the complexed gum were decreased with increase of starch concentration. The extend of decrease in above properties except hardness was not affected by strength of the complexed gum and concentration of calcium cation. Moreover, addition of incompatible starch would change the volume ratio of the complexed gum after phase separation was occurred. Increase of starch concentration in the complexed gum decreased the volume of upper clear gum layer and increased volumes of both middle gum layer and lower precipitated gum layer.

市售運動襪標示與品質功能之調查研究

樂以媛　　荊淑華

輔仁大學織品服裝系

摘　　要

在一般人注重健康休閒生活的臺灣社會中，一般性運動襪已成爲日常服飾用品之一。各廠商紛紛在品牌、款式、功能、美學設計上各顯神通，輔以强勢的名人廣告攻勢，爲其品牌塑造名牌的「高品質」、「高價值」形象，以獲得消費者之青睞。然而這些市售「名牌」一般性運動襪是否眞能在其品質功能或洗滌保養上提供消費者與價格相符的品級或足够資訊，使其能在正常使用情況下維持一個令人滿意之「穿着，使用水準」，引發了研究者的興趣，而設計本次調查與比較研究。

本研究特色在於首次採用「穿着測試 (wear trial)」及實驗室清洗之混合方法，得以兼顧實際穿着時各種穿者與環境變數之綜合影響，以及實驗室統一標準之清洗乾燥方法之可控制性。

結果顯示除少數品牌外，大部份品牌之樣品均無法提供消費者正確充分的標示作爲選購與洗滌參考，其綜合性品質功能也無法符合價格所應提供的品質水準。

一、研究動機與目的

近年來，隨著政府大力提倡「全民運動」，「體育是外交的延伸」，「運動健身」，以及大量興建各類綜合體育場，強調運動休閒的重要性後，運動風氣逐漸在此忙碌的工商業社會中擴展開來。具有生意眼光，腦筋動的快的製造、銷售業者，便看準這個具有潛力的市場，卯足了勁在運動用品、器材上不斷地推陳出新，投入這個市場中競爭。

在這一波運動風潮中，運動襪也不例外。各廠商紛紛在品牌、款式、功能、美學設計乃致於價格上各顯神通，輔以大筆的金錢及強勢的名人廣告攻勢，爲其產品塑造名牌的「高品質」，「高價值」形象，以獲得消費者之青睞。然而，與所有的織品服裝一樣，運動襪終究也是要經過穿著、換洗的過程，這些標榜「高品質」，「高價值」的名牌運動襪，是否眞的在其功能、品質，或是洗滌保養上，提供給消費者與價格相符的品級或足够的資訊，使其能在正常的使用狀況下，維持一個令人滿意的「穿著 、 使用水準」，凡此種種 ， 都引發了我們研究的興趣。

故著眼於此，我們特別設計了這個國內首次進行的實驗方法，對一般市售的「名牌運動襪」，讓試驗者個別實際穿著以後，在實驗室統一洗滌，並加以測試

及評估，耗時數月，完成此份報告。希望借此提供一些經驗與建議給生產製造廠商及消費者，了解目前市售運動襪之概況，一方面有助於業者生產製造合於消費者需求的運動襪，另一方面也同時教育消費者，使其了解其本身應享有的，而應該積極爭取維護的「穿」的權益。

歸納起來，本實驗的目的在於探討下列數項內容：

(1) 市售各種進口或本國製造的有品牌運動襪，除了使消費者滿足品牌忠誠度及優越感外，是否眞能帶給消費者使用功能上的各種舒適性及耐久性？

(2) 運動襪上所標示的成份、產地及洗滌方法，是否代表正確無誤的訊息？文字圖案能否易於瞭解？有無錯誤地引導消費者做出不正確的購買決定或使用錯誤的洗滌方法？

(3) 市售運動襪價格的高低是否充分反應其品質水準？高價位產品眞的有好品質？而低價位產品有無好品質的可能？

二、研究方法與步驟

1. 實驗用品

(1) 實驗用襪

本研究針對市售知名品牌共 14 種，每個品牌各 14 雙運動襪共計 154 雙，分成三組如下：

(A) 一組爲標準對照組：每個品牌各 1 雙，共 14 雙，作爲實驗時對照比較之用。

(B) 一組爲烘乾組：每品牌各 5 雙，共 70 雙，洗滌後採用烘乾機，以 80°C 加以烘乾，歷時約 1 小時。

(C) 一組爲掛乾組：每品牌各 5 雙，共 70 雙，洗滌後用曬衣夾在室溫中掛乾，隔天以烘乾機，輔以約 15 分鐘之再乾燥，已確保其乾燥。

品牌分別爲：

愛迪達 (Adidas)	TS-2435
亞瑟士 (Asics)	No. 9101
Avia	A0311 RB
Converse	SM 9620
迪亞多納 (Diadora)	SK 03064
宜加跑 (Icasport)	ID 23102
肯尼士 (Kennex)	KYA-6415R
Lotto	K 771
美津濃 (Mizuno)	No. 54UM-J1762

耐	吉 (Nike)	No. 183403
花花公子	(Playboy)	PPS 31404
彪	馬 (Puma)	PE 0049T
銳	步 (Reebok)	GS 05207
三	花 (Sunflower)	

包裝後外觀如圖 1。

(D) 一組爲纖維成份定性定量分析，每品牌各三雙，每雙各一隻，每隻兩小塊進行包裝標示成份之比對分析。

圖 1

(2) 試穿人員

由輔仁大學織品服裝系二、三、四年級學生中，徵求 70 位男同學，以隨機抽樣之方式，每人分配一雙烘乾，一雙掛乾處理的襪子，按照穿著日檢核表，定時定日穿著及繳回洗滌，如此每雙襪子共穿著及洗滌 15 次。

(3) 洗滌設備

(A) Kenmore Heavy Duty 洗衣機：選擇 "normal" 的洗衣程序，採用低水位之冷水洗滌，其洗滌過程如下：自開始進水至第二次清水並脫水的過程時間約 35 分鐘，其中洗滌時間 14 分鐘，清洗兩次。

(B) 使用清潔劑：

(a) Charmantée 清洗劑 23～24 雙襪子，加入 18 g 清洗劑。

(b) 潔豔（含過氧化氫 NaOH（酸素系）界面活性劑）23～24 雙襪子，加入 5 cc，作爲消毒之用。

(C) 洗衣網：避免襪子糾纏，約 5～6 雙一袋。

(4) 乾燥設備

(A) 烘乾組：以 Kenmore 的烘乾機，"normal cycle"，正常織物，高溫 "high temperature" 的烘乾條件，特別厚的 Diadora 襪子，另外再續烘約 5 至 10 分鐘。

(B) 掛乾組：以普通曬衣架及衣夾掛乾於通風的室溫。

(5) 其他用具

籤標筆、布尺、照相設備、ASTM 毛毯評級板、中國國家標準總號第 2339 號「纖維混用率試驗法」及美國 AATCC 手册第 20 及 20a 方法，AATCC 褪色染污評級灰色標。

2. 實驗步驟

(1) 使用者穿着試驗部份

(A) 將各品牌的襪子隨機抽樣 1 雙，作標準組，無需編號。將各品牌的襪子隨機抽樣 5 雙，作烘乾組，依次編上品牌代號，烘乾代號 (D) 及編號，如 AvD-3。將各品牌的襪子隨機抽樣 5 雙，作掛乾組，依次編上品牌代號，掛乾代號 (L) 及編號，如 MiL-3。

(B) 在襪子上以籤標筆做數點記號，如圖 2 所示。並定義：(a) 襪筒寬，在筒身長 (b) 減鬆緊帶寬度之一半處測量，(b) 筒身長，(c) 襪長，(d) 襪身寬。

(C) 對 70 位穿著襪子之同學進行編號，二年級有 50 人，編號由 2-1 至 2-50。三年級有 6 人，編號由 3-1 至 3-6。四年級有 14 人，編號由 4-1 至 4-14。並以隨機抽樣的方式，每人分配不同品牌，已編好號的烘乾及掛乾襪子各一雙。

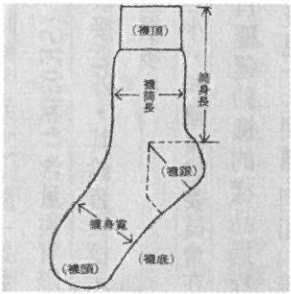

圖 2　襪上測量各部份之圖解。

(D) 爲學生們製作實驗記錄表格，其式樣如表一。分別記錄穿著者的姓名、編號、體重，及穿著襪號，同時做第零次的測試。卽：就外觀的整體現象，以及於步驟 (B) 定義之 (a)、(b)、(c)、(d) 四個數據進行測試，並塡寫於表格上。

(E) 準備塑膠袋，每人 30 個，及足够之標籤，以做爲學生穿著後回收及洗淨發還之用。

(F) 製作穿著日檢核表，以備學生自我檢測是否依其上規定，準時穿著，繳交並拿回洗淨襪子之依據。

(G) 舉行一次實驗的說明會，在會中對學生們說明實驗的動機、目的、方法，以及他們參與本實驗的全部流程，請他們確實依檢核表上之時間，穿著、繳交並拿回洗淨之襪子，以協助本實驗順利進行。

(H) 依穿著日檢核表上之日子回收襪子，並進行洗滌，將襪子 5～6 雙，正面朝外，分置於 4 個洗衣網內，放入洗衣機中。選擇 "normal" 的洗衣流程，採低水位之冷水洗，加入 18 g 的 Chamantée 洗衣劑與 5 g 的潔豔一併清洗，每次洗滌過程約 35 分鐘。

(I) 若襪子標明爲烘乾處理者，則於步驟 (H) 完畢後，除去洗衣網，放入烘乾機內烘乾，烘乾歷時約 60 分鐘。

(J) 若襪上標明爲掛乾處理者，則於步驟 (H) 完畢後，除去洗衣網，以曬衣夾一隻一隻地掛在空室內，保持室內的通風，掛乾一晚上，隔天早上再輔以烘乾 15 分鐘，以確保襪子乾燥完全。

(K) 將洗淨之襪子以編好號之塑膠袋包好，交由學生領回，以供下一次的穿著之用。

(L) 重覆 (H)、(I)、(J)、(K) 四步驟，使每雙襪子都經過 15 次之穿著，洗滌及乾燥。

表 一

襪號		乾燥法		姓名		編號	
10/29	11/02	11/06	11/09	11/15	11/19	11/21	11/23
11/27	11/30	12/04	12/07	12/11	12/14	12/18	

	第零次	第一次	第五次	第十次	第十五次
染汚					
褪色					
起球					
鬆緊帶斷紗					
變形性					
尺寸安定性：					
(a) 襪筒寬					
(b) 筒身長					
(c) 襪長					
(d) 襪身寬					
磨損性					
整體外觀描述					
穿者感覺及意見					

體重		襪號		乾燥法	
10/30	11/05	11/08	11/14	11/16	11/20	11/22	11/26
11/29	12/03	12/06	12/10	12/13	12/17	12/19	

	第零次	第一次	第五次	第十次	第十五次
染汚					
褪色					
起球					
鬆緊帶斷紗					
變形性					
尺寸安定性：					
(a) 襪筒寬					
(b) 筒身長					
(c) 襪長					
(d) 襪身寬					
磨損性					
整體外觀描述					
穿者感覺及意見					

(M) 在第一、五、十、十五次穿著，並經過步驟 (H)～(K) 的處理後，要進行評級，評級的項目包括：襪子汚染、褪色、起毛毬、變形等現象，做一對照之記錄，最後將這些資料加以彙總，製作成總表。

(N) 穿著體重的計算以評級次數及有效數據次數來計算，將各穿著者體重乘以其有效評級次數後相加；再除以總有效數據次數。

(O) 尺寸安定性之評級按照筒身長及襪長第 0 次與第 15 次平均長度之差距爲依據來做評級。

(2) 纖維成份標示測試部份

根據中國國家標準總號第 2339 號「纖維混用率試驗法」及美國 AATCC 試驗手册第 20 及 20a 方法，將三雙襪子中每雙各抽一隻，取兩小塊，按規定方法，分別以不同溶劑溶解襪子包裝上所標示之成份，並利用反覆乾燥及秤重方法分別求出襪中各成份之含量後求取平均值，成爲各品牌襪子試驗數據。以與標示重量百分比作比較。若按正常方法無法溶解其中某些成份，表示實際所含成份種類與標示成份種類不同，則再購買同型號襪子，重新測試。

三、文 獻 探 討

1. 織品舒適性

織品的舒適性，是一種人人都有親身體驗，但卻難以言語或文字描述出清晰輪廓的織品特性 (K. Slater，1977)。它牽涉的範圍甚廣，由最基本的纖維種類、紗線、布料結構、其後的染整加工、最終消費產品的製程、使用者本身的身心狀況、主觀感覺乃至與其周遭環境的交互關係等複雜構面均會影響舒適性，但均不足以完全描述舒適性。

儘管衆說紛云，但一般人普遍同意，對使用者而言，織品服裝舒適性中最重要的兩類特性就是：(a) 熱及水蒸氣在織品中的傳導狀態，以及 (b) 服裝產品的尺寸及合身性 (K. Slater，1977)。此兩大類因素格外影響使用者對織品服裝的舒適感受。

一般人在衡量衣著舒適性時，常以此兩大因素來探討；但目前研究人員爲了能客觀評量織物的舒適性及手感，常以 Kawabata 所發明的織物客觀手感評估系統 (KBS-FB，Kawabata Evaluation System for Fabric)* 測量織物的各種物理性質，這些物理性質過去都是消費者以手觸摸布料的感覺，作主觀的判斷，

* 另有一套較簡單的織物客觀測試儀器，謂之 FAST (Fabric Assurance by Simple Testing)，是由 CSIRO (Common-Wealth Scientific and Industrial Research Organization of Australia) 發展出來的。

現在則是以客觀數據顯示各種特性，而得到一個綜合的舒適性的指標（R. Postle、S. C. Harlock、J. I. Curiskis、Wolfgang A. Strahl，1989）。

熱及水蒸氣在織品中傳導狀態的優劣，取決於上游的紡織業，諸如：新纖維、紗線、布料等新素材的開發，及染整加工技術的提昇改良，以生產兼具天然材質高透氣性、高吸溼性、良好手感及人纖易處理保養，有光澤性的新產品，使消費者在穿著衣服時所產生的體熱、汗液能自然地被吸收或傳導至空氣中，而沒有不適之感。至於服裝產品的尺寸及合身性，則有賴於製造各類成衣、用品之製造廠商，重視各類衣服的設計、打版，良好精確之剪裁，適當之車縫縫線張力，以及縫合強度等製出有適量鬆份，合身而易於穿著的衣物。例如：運動襪類由紗的纖維成份決定水蒸氣及熱的傳導性，而織造能否合於人體工學，則決定穿著運動時的合脚性。此兩種特性綜合決定襪類的舒適性。

2. 耐久性

織品的耐久性，是指在正常的使用狀況下，該產品使用壽命的長短。它會因織品在使用、洗滌等過程中的耗損而遞減，直至該產品不堪使用爲止（Fabric Science，1984）。

一般織品的耐久性，非常不容易由日常的使用狀況下得知。故在實驗室中的測度，多採用「加速」實驗，也就是以機器模擬各種實際穿著使用狀況，在相同實驗狀況、短時間內，加壓力、重量，將其破壞，並以一公定標準評比之。

在實驗室普遍採用的方法，有取自 AATCC 各種耐水洗、乾洗、氯漂、汗液、耐候……的耐久測試；也有取自 ASTM 的撕裂強度、爆破強度、各種磨擦測試、抗起毬性測試等。

洗滌是衣物耐久性的致命傷，通常最受影響的就是對染色或印花的堅牢度及尺寸的安定性。洗滌的過程也常使布料織紋歪斜的衣物產生扭曲變形的現象（Elson，1992），衣著的耐久性，除了決定於車縫製程中針步、合縫種類及強度外，還包括副料材質的品質，因此也是一種綜合的特性。

3. 穿著測試

一般織品服裝的多項測試，都設定在實驗室內，標準狀況下，以標準測試方法及一定規格之機器爲之。雖然符合「客觀」的測試及評量標準，但似乎因爲「標準化」而過簡，忽略了使用者在實際穿著時，可能發生的複雜情況，對衣著是一種綜合的影響效果。故近年來，除了一貫的實驗室標準測試外，有人提倡以使用者直接穿著使用織品服裝的情況，從事實驗以作爲參考之佐證，此種方法即稱爲穿著測試（Wear trial）。英國 Marks and Spenscer 公司在新款衣種或新材質的開發時，多採用穿著測試的方法，實際觀察新產品在各種可能的使用環境內所實際產生的變化，以確保新產品的品質水準（Elson，1992）。

4. 橡膠纖維與彈性纖維

(1) 橡膠纖維 (rubber)

爲由天然或人造橡膠所製成的纖維，依材料成份可分爲天然橡膠、含 acrylonitrile 10～50% 及含 Chloroprene 35% 以上等三類 (FTC，1984)。在 1930 年由 U.S. Rubber Company 生產上市，現今要求高伸拉性的產品，已不太使用橡膠纖維，而改以彈性纖維取代之。這是因爲彈性纖維有較優異的延伸度及伸拉性、高回復力，以及較佳的抗老化等特性所致 (Fabric Science，1984)。

(2) 彈性纖維 (spandex)

爲含至少 85% 以上的 polyurethane 所製成的人造纖維，於 1959 年由杜邦公司開發成功，商品名爲 Lycra，是一種高伸拉性的纖維。特點爲：質輕、伸拉性極佳，可耐乾、水洗（氯漂會造成黃化但卻不致想影響其伸拉性），沒有靜電及起毛毬的問題。雖然其強力比一般人纖差，但由於其高伸拉性，故此點不成問題。且較橡膠纖維的強力大，故取代了絕大部份橡膠纖維的使用。有疏水性，在空氣中會黃化，若有需要，只能用熨斗以低溫快速熨燙 (Fabric Science，1984)。

目前一般襪類主要部位的彈性除了由針織結構來形成外，最主要就是將彈性纖維混合織入，或以其他纖維包覆於彈性纖維外形成彈性紗再織造。襪頭部份則多採用橡膠纖維以降低成本。

四、結果與討論

1. 成份含量

一般市售運動襪標示的成份，以棉纖維 (cotton fiber)、尼龍纖維 (nylon fiber)、聚酯纖維 (polyester fiber)、亞克立纖維 (acrylic fiber) 以及彈性紗 (spandex、Lycra 或 rubber) 爲主，當然各廠牌生產的運動襪成份比例並不盡相同。

以本研究實測的 14 種廠牌的運動襪樣品而言，除「花花公子 (Playboy PPS 31404)」沒有標示成份含量之外，其餘 13 種都有標示成份以及重量百分比，參見表二。

爲了解各樣品成份標示實不實在，本研究根據中國國家標準總號第 2339 號「纖維混用率試驗法」，及 AATCC (美國織品化學及染色專家協會) 的測試方法，實測 14 種廠牌樣品的成份含量。所得結果，請參見表三，除「迪亞多納 (Diadora SK 03064)」含量與實際標示較接近外，其餘皆與標示含量差距甚多。

表二 市售運動襪成份含量實測結果

廠牌	型號	價格(元/雙)	運動襪型式	商標標示及實測結果 % 棉(Cotton)	尼龍(Nylon)	聚酯纖維 Polyester	聚丙烯腈纖維 Acrylic fiber	彈性紗(Spandex、Lycra或Rubber)	標示 產地標	洗標
1.愛迪達 Adidas	TS-2435	95	厚/二						O	O
2.亞瑟士 Asics	No3101	125	厚/中						O	O
3.Avia	A0311 RB	130	厚/中						O	O
4.Converse	SM 9620	170	厚/短						O	●
5.迪亞多納 Diadora	SK 03064	130	厚/二					—	O	⊕ O
6.宜加跑 Icasport	ID 23102	80	薄/中					—	O	●
7.肯尼士 Kennex	KYA-6415 R	125	厚/二						O	●
8.Lotto	K 771	100	厚/中					—	O	O
9.美津濃 Mizuno	No54 UM J 1762	180	薄/中	+ +	+ —	+		+	O	O
10.耐吉 Nike	No183403	95	薄/中					—	O	O
11.花花公子 Playboy	PPS 31404	260	薄/中	+	+			+	O	O
12.彪馬 Puma	PE 0049 T	160	薄/二		—	D			O	●
13.三花 Sunflower	無	200	薄/二						O	O
14.銳步 Reebok	GS 05207	125	厚/二						O	●
15.銳步 Reebok	GS 05207	125	厚/二		+			+	O	●

註：1.「美津濃(Mizuno)」之外包裝所貼的成份標示，與其鞋牌上所印之成份標示不同，而本次實測結果，有三雙符合外包裝所貼之成份標示，僅含棉、尼龍及彈性紗，另外有一雙則多測出含有聚酯纖維之成份。
2.「銳步(Reebok)」前後兩次購買同型號之襪子，其中，測試第一次所購買的兩雙編號第[illegible]號及第二次編號第15號所購買三雙，但其成份標示略有不同，而測試結果顯示，成份及成份含量也不相同。
3.成份標示測試結果中，[illegible]為襪上標示，而[illegible]為實測結果。「-」表示該廠並無此標示成份；「+」表示只標示有此成份，但並無標示成份含量。
4.「迪亞多納(Diadora)」雖無洗標之標示，但在襪子上則以英文標示「Machine Washable And Dryable」之字樣。
5.「 」表無標示，「 」表有標示。

此外，本研究在實測 14 種運動襪的樣本過程中，還發現一些問題，例如「美津濃 (Mizuno No. 54UM-J1762)」的包裝袋上黏貼與商標上印刷的成份標示略有不同，參見圖 3，而且經取同型號四雙運動襪測試結果，其中一雙的成份內容與其他三雙不同，顯示該公司品管不穩定。

而「銳步 (Reebok GS 05207)」前後二次採樣的相同型號樣品，卻有不同的成份標示及測試結果，參見圖 4。

另外，「彪馬 (Puma PE 0049T)」則並未測出成份標示上所標示的聚酯織維成份，反而測出成份標示上並無註明的尼龍成份。

表三 市售運動襪各項功能評估結果

品牌及型號	褪色染污情形	起毛毬情況	鬆緊帶斷紗情形	收縮情況	有無磨損	變形情形	綜合評語
1. 愛迪達 Adidas TS-2435	可	好	可	劣—差	無	劣	1.經洗滌之後，扭曲變形。 2.顏料印花易剝落。
2. 亞瑟士 Asics No. 9101	差	差	劣—差	劣—差	無	好	1.顏料印花品質不良。 2.易生毛毬。 3.鬆緊帶會斷紗。
3. Avia A0311 RB	無商標	差	差—可	劣—差	無	可	1.起毛毬之狀況很嚴重。
4. Converse SM 9260	差	差	可	好	紗環鉤紗	差—可	1.襪筒反摺縫合處易脫線。 2.穿者不適應短襪之設計。
5. 迪亞多納 Diadora SK 03064	好—佳	差—可	差	可	無	好	1.襪筒反摺處易脫線。 2.因襪子較厚，故需較長時間來烘乾。
6. 宜加跑 Icasport ID 23102	劣	可	差	劣—差	無	可	1.易磨擦脚底，而穿著會有不適之感。
7. 肯尼士 Kennex KYA-6415R	差	差	差	差	無	好	1.起毛毬之情形很嚴重，多集中於襪跟及襪頭處。 2.鬆緊帶有斷裂情形產生，且易與襪筒中所織商標之紗線糾結成團。
8. Lotto K 771	劣	差	劣	差	無	好	1.新襪卽有黃色汚點存在。 2.洗淨力差，但易乾。 3.易藏臭味。 4.透氣性差。 5.襪筒上商標處之纖維易鬆散。
9. 美津濃 Mizuno No. 54UM-J1762	差	可	好	可	無	可—好	1.穿者反應透氣性佳。
10. 耐吉 Nike No. 183403	差	可	劣	差	無	差	1.襪筒商標處之藍色紗線有鬆浮現象。 2.合脚性差，故影響穿著之舒適性。
11. 花花公子 Playboy PPS 31404	好	差	好	劣①	無	可	1.透氣性佳。 2.合脚性佳。
12. 彪馬 Puma PE 0049T	差	可	劣—差	差	無	劣—差	1.洗淨力差，汚垢很難清洗乾淨。 2.手感差，有僵硬感。
13. 三花 Sunflower	無商標	差—可	可	劣—差①	無	差—可	1.合脚性佳，穿著性佳。 2.易透氣。
14. 銳步 Reebok GS 05207	差	差	劣—差	差	無	差—可	1.襪底成形不良，在穿著時，筒身易滑入鞋內。

註：1.「花花公子 (PPS 31404)」及「三花」的織法合乎人體脚形工學，故雖有嚴重的收縮情形，但不影響穿著性。

2. 評級用語：依實驗結果評級，表現最好至最差，依序爲「佳」、「好」、「可」、「差」、「劣」。

圖 3 「美津濃 (Mizuno)」包裝袋上與商標上印刷的成份標示不同。

圖 4 兩雙相同型號的「銳步 (Reebok) 運動襪」，成份標示却不同。

2. 褪色染汚情形

襪子上，如果使用品質不良的顏料印花商標，經水洗後，極易產生褪色染汚現象。襪上商標的印刷主要爲銷售目的，不會增加品質功能。但若因爲顏料品質不佳造成水洗後汚染或褪色情形，反而破壞該襪子整體外觀及品質形象。

本次 14 種測試樣品中，除「Avia A0311 RB」及「三花 (Sunflower)」因爲襪底無顏料印花商標，無法觀察褪色染汚情形外，其餘皆有印刷商標。

實測結果，以「迪亞多納 (Diadora SK 03064)」的表現最佳，襪底印刷字樣經洗滌後不會產生染汚情形。但洗滌多次後，印刷字樣還是會逐漸剝落。

另外「宜加跑 (Icasport ID 23102)」及「Lotto K 771」則表現較差，洗滌後，顏料印花處不僅會褪色，並擴散於襪底，且經多次洗滌，仍無法洗淨，參見圖 5。

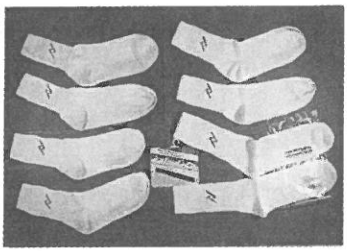

圖 5

一般襪類產品對塵土的可洗淨性均不佳「Lotto K 771」及「彪馬 (Puma PE 0049T)」則更差。

運動襪常因鞋兩側襯布及鞋底的染色堅牢度不良，不耐汗液及水洗，當其有褪色狀況發生時，即會染汚襪子，除非漂白，很難以一般方法洗淨。

但所有洗滌處理標示均註明「禁止使用含氯漂白劑漂白」，不知業者是否明確做過試驗，肯定不能使用含氯漂白劑漂白，才會如此標示。

3. 起毛毬情形

運動襪洗後產生毛毬，不僅會影響織物的外觀及穿著，日後洗滌時，也易與其他衣物纖維糾纏在一起。

本次實驗，經評級結果，以「愛迪達 (Adidas TS-2435)」表現最佳，洗滌後產生的毛毬較少。

其餘樣品則表現平平。

厚襪子，毛紗毛羽長之襪子較易起毬，嚴重影響外觀，也易藏汚納垢。

纖維成份中，若人造纖維的含量較多，也較容易起毛毬。

4. 鬆緊帶斷紗情形

襪頂的鬆緊帶萬一斷紗的話，就會鬆垮脫落，影響穿著舒適性及外觀。

經試驗後，以「花花公子 (Playboy PPS 31404)」表現最佳，在多次穿著及洗滌後，僅發現紗線自襪筒處突出的現象。

而「Lotto K 771」及「耐吉 (Nike No. 183403)」表現最差，分別發生襪筒內緣鬆緊帶處彈性紗逐漸鬆弛，及其外包紗線斷裂突出等現象。

5. 收縮情形

14 種運動襪樣品水洗後，都有變短變鬆的現象，其中表現最差的是「花花公子（Playboy PPS 31404）」，但值得注意的是「花花公子（Playboy PPS 31404)」及「三花 (Sunflower)」這兩種品牌之織法較特殊，雖經水洗後會嚴重收縮，但第二次穿著時仍可以撐開，並不影響穿著性。

就整體而言，以「Converse SM 9620」表現最佳，較不會收縮，但相對地，在經十五次穿著洗滌後，襪身卻變鬆了。

此外，本項實驗也發現：不論採用烘乾或掛乾的方式來乾燥襪子，對襪子的收縮程度並無太大差異。

6. 磨損情形

根據消費者使用經驗，品質不良的運動襪穿著日久，會有磨損破洞的情形。

經本研究實驗發現，易起毛毬或易褪色的運動襪，都較易磨損。本次所試驗之樣品中，除「Converse SM 9620」之襪底內的長紗環發現有鉤紗情形外，其餘樣品都沒有明顯的磨損。

7. 變形情形

品質較差的襪子多次穿著洗滌後，極易扭曲變形，不但影響美觀，且亦影響穿著舒適性。

測試結果，以「愛迪達 (Adidas TS-2435)」的表現最差，多次穿著洗滌後，襪筒及襪身已扭曲變形，而「亞瑟士 (Asics No. 9101)」、「迪亞多納 (Diadora SK 03064)」、「肯尼士 (Kennex KYA-6415R)」、「Lotto K 771」等四種品牌則較無變形。

舒適性除了受襪子纖維成份影響外，織造方法及組織結構亦有影響。襪身處、襪筒處以及兩者交接處是否合於人體工學、脚形，即會影響其合脚性及形狀穩定性。組織表面紋路、紗環或毛羽也會影響襪底與皮膚的磨擦情況，進而影響穿著舒適性。

8. 價格與品質功能及標示完整性的關係

價格最高的「花花公子 (Playboy PPS 31404)」、「三花 (Sunflower)」以及「美津濃 (Mizuno No. 54UM-J1762)」在各項品質功能評估中，均有較佳的表現（請見表三）。但似乎「美津濃 (Mizuno)」，就價格與品質而言，最能使消費者有划算之感。

「Converse SM 9620」、「彪馬 (Puma PE 0049T)」兩品牌之價格亦不低，但就各項品質功能評估，表現不良（請見表三），因此有價格與品質不符的現象。

其他品牌就品質功能評估的表現均不良，但若與價格相比較沒有顯著的優劣之別。

五、結論與建議

綜合七十位實際穿著運動襪樣品的使用者的意見，在穿著舒適方面，評語較佳者有「美津濃 (Mizuno No. 54UM-J1762)」透氣性佳，「花花公子 (Playboy PPS 31404)」的透氣性佳，以及「三花 (Sunflower)」的合脚性佳，穿著性佳，易透氣。一般而言，使用者較喜愛襪子筒身較長及襪跟部位符合人體工學者。

此外，使用者測試結果也發現，各品牌樣品運動襪都不太容易洗乾淨，尤以「彪馬 (Puma PE 0049T)」及「Lotto K 771」的表現最差。

另外，「迪亞多納 (Diadora SK 3064)」，由於襪底較厚，加上含棉量不低，因此比起其他品牌的運動襪，需要較長的烘乾時間。

綜合本次實測14種運動襪樣品的結果，我們針對政府、廠商和消費者有以下建議：

1. 對廠商之建議

(1) 本次實測各樣品的成份含量，顯然與標示含量有差距，呼籲運動襪製造廠商誠實正確地標示。

(2) 目前市售運動襪皆是取材各種纖維混合紡織，但穿著運動襪時，廠商考慮消費者的使用需求，如脚底易出汗，所以襪底需採用較易吸汗的棉纖維來織成。但由於棉易縮水，不妨添加適量的尼龍纖維，則可降低棉纖維的縮水程度。而襪頭及襪跟是最容易產生磨擦之處，若加入適量的尼龍或聚酯纖維，可提高耐磨性。爲防止襪子穿著時恐滑落鞋底，製造時，於運動襪頂處可加入適量的彈性紗或橡膠，以增加襪頂彈性。另外，壓克力纖維的保暖性佳，強力也大，若襪子以保暖爲主，可多添加此成份，與毛紗混紡。因此，建議業者應針對販售襪子的功能，來做不同部位成份的標示，以方便消費者購買。

(3) 以本次試驗的 14 種品牌的運動襪樣品而言，大多數品牌皆沒有洗滌處理的標示，樣品也欠缺產地標，至於成份標示則各廠商互異，有些清楚標示成份含量的百分比，也些僅以「＋」字符號表示有某種成份，令消費者購買時無所遵循，有待各廠商改善。

(4) 襪跟處應有足量之加放針，使此部位合於人體脚跟形狀，避免走路時滑落鞋內，增加穿着的舒適性，且運動襪長度以中統爲宜，較適應穿者穿着運動的習慣。

(5) 建議使用 spandex (Lycra) 彈性紗，因爲此種材質性能較佳，壽命較長，較耐汗水，不易生臭味。

(6) 建議業者在襪上以綉花的方式綉上商標而避免顏料印花，或根本不必標明商標以免因水洗或磨擦堅牢度不佳發生染污或褪色現象，破壞外觀。

2. 對消費者之建議

(1) 建議消費者選購時以品質爲優先考慮，而勿以品牌取向。消費者在選購時唯有依據標示上纖維成份及其重量百分比作客觀判斷，再以織紋設計及價格作主觀判斷。因此包裝上之標示能否正確至爲重要。不應僅以品牌的「名氣」作爲品質好壞的依據。

(2) 消費者洗滌襪子時，置於洗衣網內，可免拉扯變形。

3. 對政府之建議

經濟部商業司正研擬織品成衣標示法，建議將襪類標示納入該法管理。廠商亦應參考統一標準的標示制度來作正確標示。

參考資料

(1) AATCC Test Method 20-1985.
(2) ASTM D 3512-82.
(3) D. Elson, Unpublished Seminar Handout on "Quality Control Mangement", in the Department of Textiles and Clothing, Fu-Jen University (1992).
(4) Federal Trade Commerce, U.S.A., *Textile Fiber Praducts Indentification Act*, September 2, (1958), *Amended*, June 5 (1965), and September 24 (1984).
(5) Josepf J. Pizzuto, *Fabric Science*, Fifth Edition (1984).
(6) J.I. Curiskis, "Fabric Objective Measurement: 5. Production Control in Textile Manufacture", *Textile Asia*, October (1986).
(7) K. Slater, M. Sc., Ph.D., F.T.I., Comfort Properties of Textiles (1977).
(8) R. Postle, "Fabric Objective Measurement: 1. Historical Backgroung and Development", *Textile Asia*, July (1986).
(9) R. Postle, "Fabric Objective Measurement: 3. Assessment of Fabric Quality Attributes", *Textile Asia*, July (1986).
(10) R. Postle, "Fabric Objective Measurement: 6. Product Development and Implementation", *Textile Asia*, October (1986).
(11) S.C. Harlock, "Fabric Objective Measurement: 2. Principles of Measurement", *Textile Asia*, July (1986).
(12) S.C. Harlock, "Fabric Objective Measurement: 4. Production Control in Apparel Manufacture", *Textile Asia*, July (1986).
(13) 中國國家標準 CNS No. 2339。
(14) 中國紡織工業研究中心，紡織期刊目錄。

Survey Investigation on the Labclling and Performance of Locally Marketed Socks in Taiwan

YIIYWIEN YWEI
Lecturer, Department of Textile and Clothing

ABSTRACT

Sporting sock are one of apparel items for active wear. Since there are so many brand names including imports in the local market, the strong competition sometimes forces producers/retailers reduce costs in a way of sacrificing users' welfare. Besides, the labilling and regalation has not yet been legitimated, many a marketed socks contains no accurate labels, or even has no labels.

These researchers derived a method of wear trial to test various performances of fourteen locally marketed well-known brands of active wear socks. Results show that a high percentage of samples cannot be qualified in terms of the ratio of value over price.

18 歲至 26 歲年齡層大專女學生之人體尺碼調查與基本樣版之研究

傅 美 玲

輔仁大學織品服裝學系

摘 要

以輔仁大學 18-26 歲年齡層之女學生 301 人實施人體量身計測調查，其中 108 人並輔以體型分析調查。研究工具爲採卷尺實量調查及以體型輪廓攝影機拍攝調查，將統計資料整理規劃成 18-26 歲年齡層之成衣尺碼系統，並歸納出 18-26 歲年齡層之代表性尺寸及代表性體型，再以此代表性尺寸之人體樣本實驗，制定出基本樣版。

人體量身計測調查有：圍度 16 項、垂直高度 1 項、長／寬度 25 項及體重等共計 43 項。人體體型分析調查有：體重、體表傾斜角度、前後投影寬、垂直投影長、水平投影寬等共計 22 項。

一、前 言

成衣工業的發展，建立在產品設計、製作技術與品質水準的提昇，但在傳統接單照抄的生產模式下，我國一直沒有建立自身的基礎系統，既無國人量身計測之調查，亦沒尺碼系統之規劃；成衣生產更是沒有以國人體型爲依據之人臺設備製作，也沒有以國人體型爲對象之基本樣版，均直接抄襲外國資料、設備，照單自用。

成衣工業所涉及之範圍極廣，本研究係針對 18-26 歲年齡層女性，以人體量身計測調查與體型輪廓攝影調查，將統計資料整理分析，規劃成此年齡層之成衣尺碼分類系統，並以此年齡層之代表性尺寸及代表性體型，界定出基本樣版。

二、研 究 目 的

由於國內成衣界普遍缺乏國人人體量身計測資料，亦沒有以國人體型、尺寸爲依據之基本樣版，故本研究之目的如下：

㈠建立統一之計測方法以符合國際化與科學化之標準。

㈡分析國人人體量身計測統計資料，並制定 18-26 歲年齡層之代表尺寸。

㈢歸納 18-26 歲年齡層之體型，並制定此年齡層之代表性體型。

㈣調查資料經分析整理後，規劃成 18-26 歲年齡層女性之成衣尺碼系統。

㈤界定 18-26 歲年齡層女性適體性基本樣版之定義範圍與製圖。

三、研 究 方 法

1. 研究對象

民國七十九年，本研究開始進行人體量身計測調查，以就讀於輔仁大學織品服裝學系之女學生爲主；至民國八十年，並加上其他學系之女學生爲輔，受測樣本總人數共計 301 人。民國八十年並同時進行體型分析調查，受測樣本女學生總人數爲 108 人。受測者年齡均以調查日期止之 $n \pm 0.5$ 歲爲 n 歲，受測樣本之出生地分佈全臺灣十七縣市。

2. 研究工具

人體量身計測調查之測量儀器、配備有：直尺、卷尺、馬丁式身高計器、體重計器、量身用針織服裝（圖 1）、金屬細環項圈（圖 2）、水解筆、腰圍標示帶、記錄表等；體型分析調查之測量儀器及配備有：日製 System 10 Silhouetter 自動體型攝影器、體型輪廓照片、量身用針織服裝、描圖紙、直尺、量角尺、記錄表等；基本樣版實驗之工具有：方格胚布、樣版製圖用紙、方格尺、縫製機器、照相機、負片、正片等。

圖 1　量身用服裝。

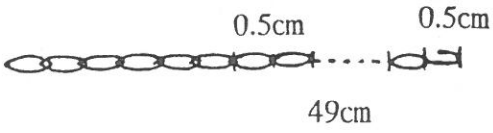

圖 2　量身用細頸圈。

3. 實施程序

本研究係以製作外用服（非內衣）之需爲目的，故受測者均著基本內衣（胸罩、內褲）調查，外再著統一量身用服裝，不穿鞋、襪，以自然常態之站姿，兩眼平視前方，腰圍繫標示帶，以皮下骨骼爲基礎，先記號測定點位置如圖 3，有：(1) 頸圍前中心點、(2) 頸圍後中心點、(3) 乳尖點、(4) 側頸點、(5) 肩點、(6) 前腋點、(7) 後腋點、(8) 臀圍點、(9) 膝點等。頸圍用金屬細環之項圈輔助畫頸圍線。計測之對稱部位均以量受測者之右側爲原則。

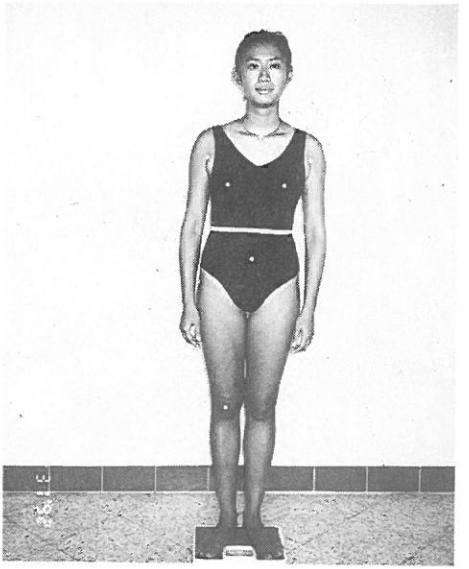

圖 3 受測者姿勢。

(1) 人體量身計測調查

人體量身計測調查之計測項目有 43 項，由 8 名計測人員分項計測之，以照片輔助，說明如下：

①頭圍 (Head Girth) 圖 4：由額頭中央環繞腦後最突出部分，計量由環繞頭部一圈的尺寸。

②頸根圍 (Neck Base Girth) 圖 5：將布尺沿頸圍後中心點、側頸點、前鎖骨上緣及頸圍前中心點等，將卷尺立起，計量由環繞頸圍一圈的尺寸，可由戴細項圈爲標示。

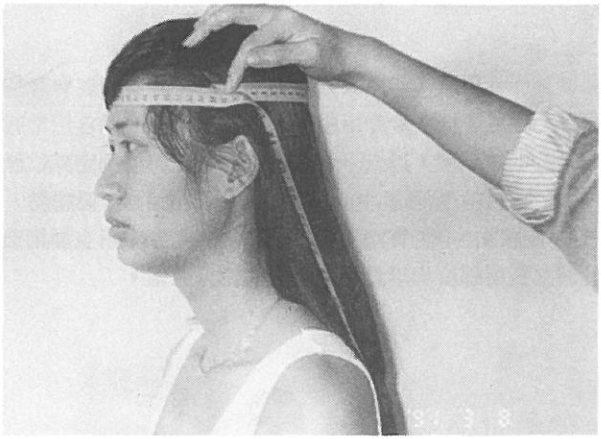

圖 4 頭圍。

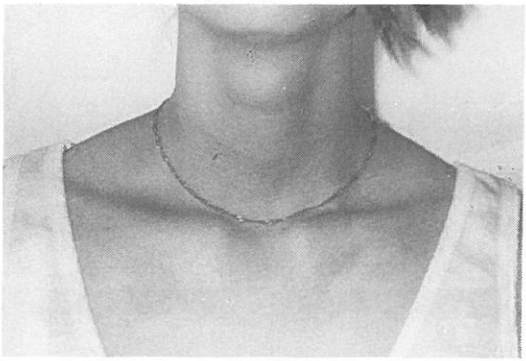

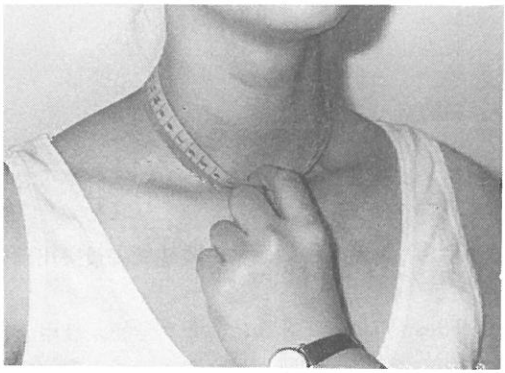

圖 5 頸根圍。

③胸圍 (Bust Girth) 圖 6：水平經乳尖點，計量由水平環繞胸部最寬部分一圈之尺寸。

④乳下圍 (Underbust Girth) 圖 7：水平經乳房下緣位置，計量由水平環繞胸部一圈之尺寸。

⑤腰圍 (Waist Girth) 圖 8：水平經腰圍點，計量由水平環繞腰部最小部位一圈之尺寸。

⑥臀圍 (Hip Girth) 圖 9：水平經臀圍點，計量由水平環繞臀部一圈之尺寸。

⑦大腿圍 (Max Thigh Girth) 圖 10：在腿上半部靠襠處，大腿最粗部位，水平環繞計量一圈之尺寸。

⑧膝圍 (Knee Girth) 圖 11：經過膝蓋骨中央，水平環繞計量一圈的尺寸。

⑨小腿圍 (Calf Girth) 圖 12：膝部以下之腿下半部，腿圍最粗部位，水平環繞計量一圈的尺寸。

⑩踝圍 (Ankle Girth) 圖 13：經過脚踝點最粗處，水平環繞計量一圈的尺寸。

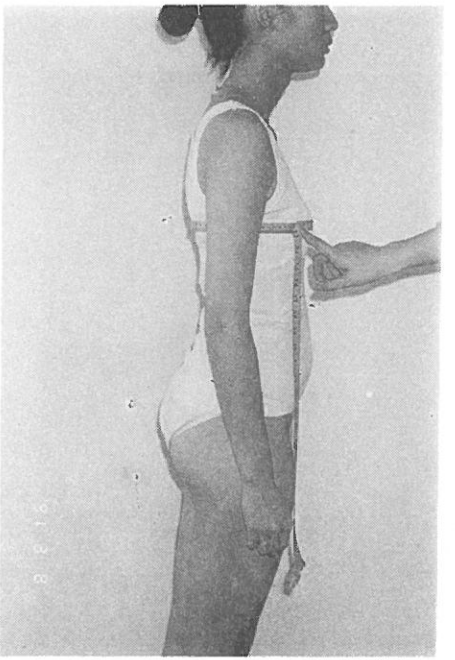

圖 6 胸圍。

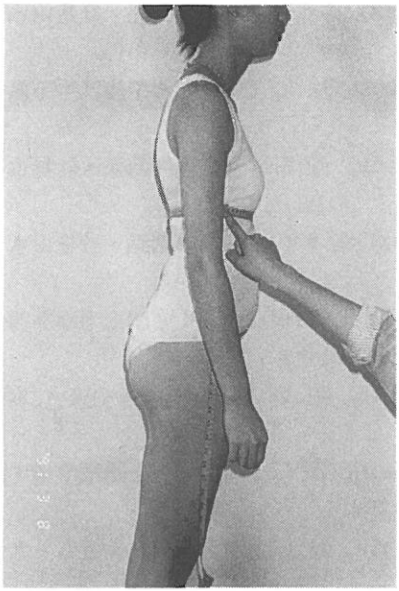

圖 7 乳下圍。

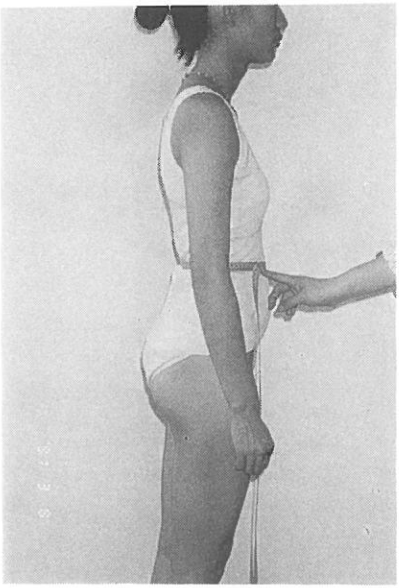

圖 8 腰 圍。

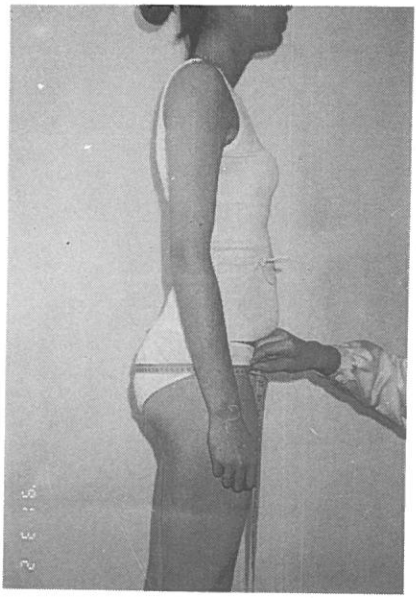

圖 9 臀 圍。

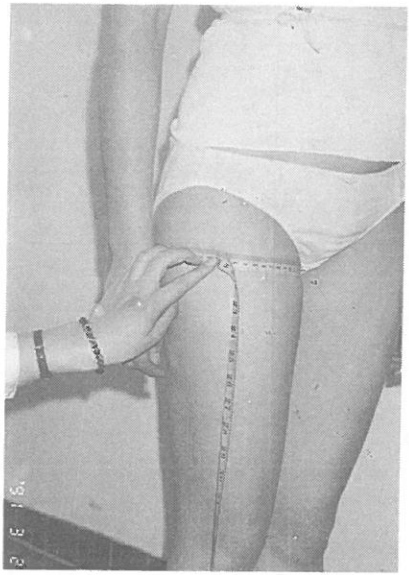

圖10 大腿圍。

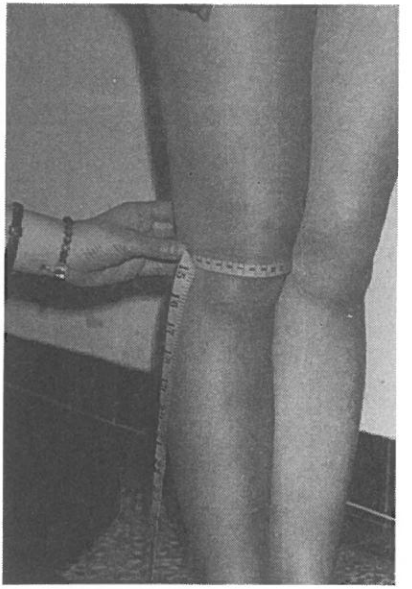

圖11 膝 圍。

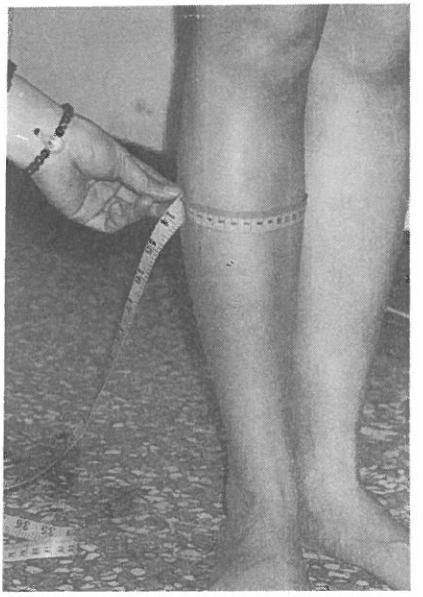

圖12 小腿圍。

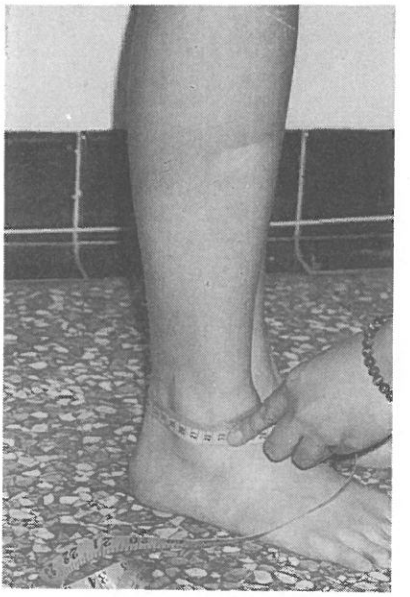

圖13 踝 圍。

⑪臂根圍 (Armscye Girth) 圖 14：經肩端點、肩峰點、鎖骨外端突起處及前、後腋點、腋窩等，環繞手臂根部計量一圈的尺寸。

⑫上臂圍 (Upper Arm Girth) 圖 15：在手臂根部，水平環繞手臂最粗部位，計量一圈的尺寸。

⑬肘圍 (Elbow Girth) 圖 16：肘彎曲，經肘點，環繞手臂計量一圈的尺寸。

⑭下臂圍 (Forearm Girth) 圖 17：在肘部以下之手臂下半部，於臂長約一半處，水平環繞手臂最粗部位，計量一圈的尺寸。

⑮腕圍 (Wrist Girth) 圖 18：經手腕點，環繞手臂計量一圈的尺寸。

⑯掌圍 (Hand Girth) 圖 19：將大姆指貼手掌，環繞手掌最寬部位，計量一圈的尺寸。

⑰背肩寬 (Across Shoulder) 圖 20：計量經頸圍後中心點而量左右肩端點間之寬度。

⑱手臂長 (Arm Length) (C. B. to Wrist) 圖 21：計量自頸圍後中心點，經肩點而順沿手臂外側經肘點，量至手腕點之長度。

⑲手臂長 (Arm Length) (N. P. to Wrist) 圖 22：計量自側頸點，經肩點而順沿手臂外側經肘點，量至手腕點之長度。

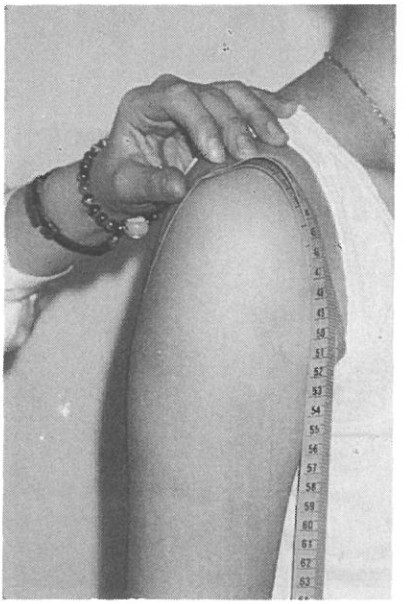

圖14 臂根圍。

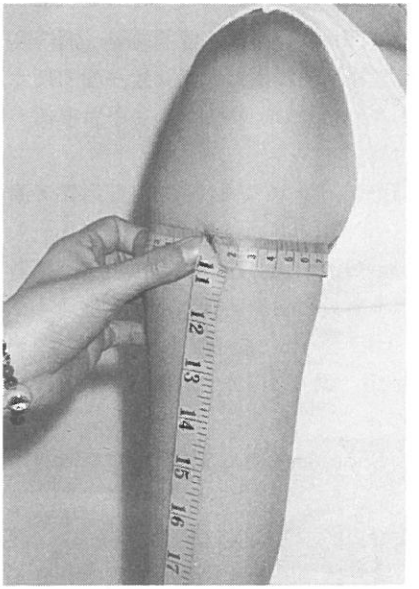

圖15 上臂圍。

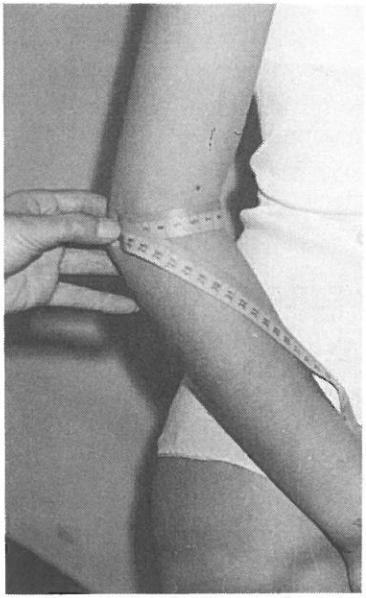

圖16 肘 圍。

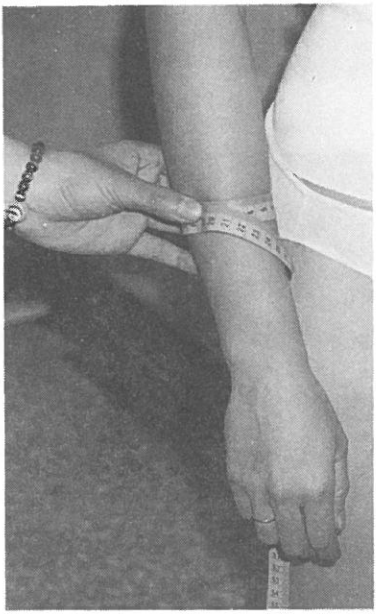

圖17 下臂圍。

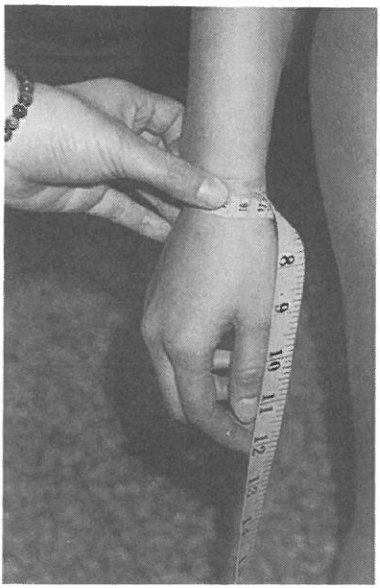

圖18 腕 圍。

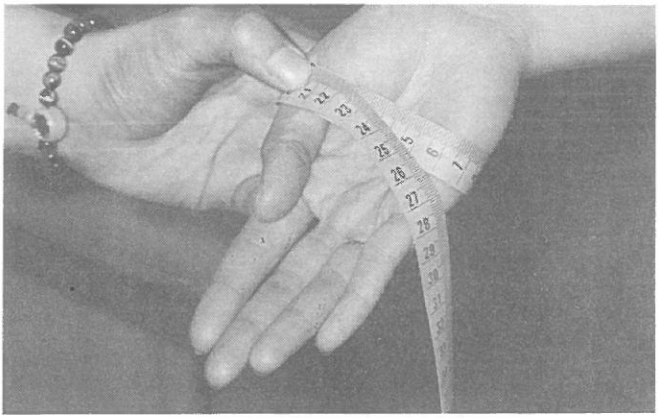

圖19 掌 圍。

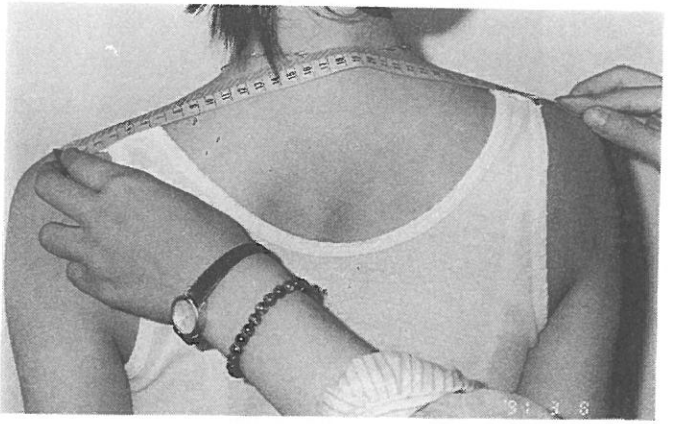

圖20 背肩寬。

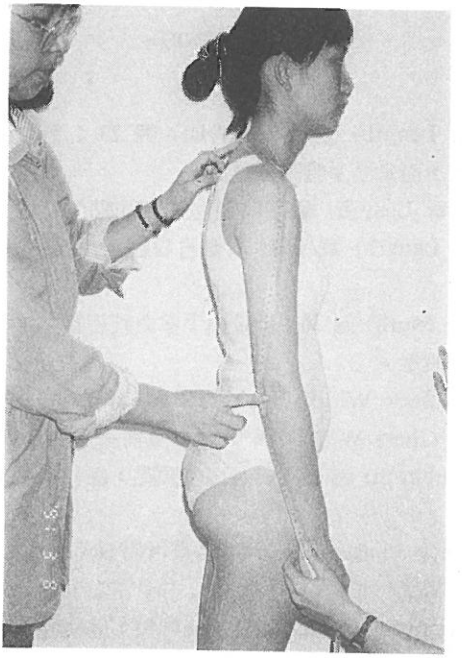

圖21 手臂長 (CB)。

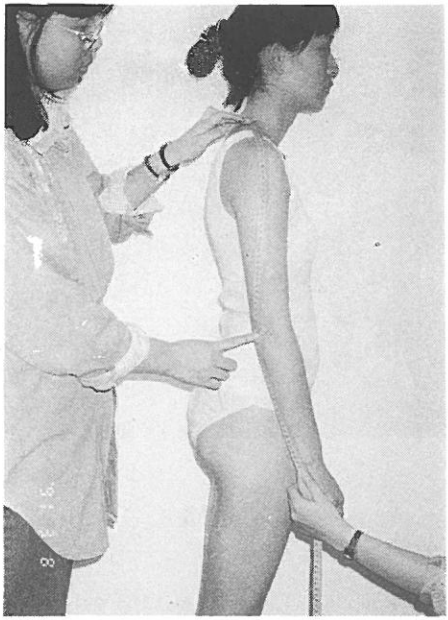

圖22　手臂長 (NP)。

⑳手臂長 (Arm Length) (S. P. to Wrist) 圖 23：計量由肩點而順沿手臂外側，經肘點，而量至手腕點之長度。

㉑肩寬 (Shoulder Length) 圖 24：計量由側頸點至肩點間距離之長度。

㉒肘長 (Elbow Length) 圖 25：計量自肩點，輕彎肘部，量至肘點之尺寸。

㉓手長 (Hand Length) 圖 26：計量由手掌與腕相接之第一條橫紋中央至第三指指尖點之長度。

㉔背寬 (Across Back Width) 圖 27：計量後背左右後腋點間之寬度。

㉕胸寬 (Across Chest Width) 圖 28：計量前胸左右前腋點間之寬度。

㉖前長 (Front Length) 圖 29：計量由側頸點，經乳尖點，垂直量至腰圍線之長度。

㉗乳尖點長 (Neck to Bust) 圖 30：計量由側頸點量至乳尖點之長度。

㉘乳尖點間距 (Nipple Breadth) 圖 31：計量左右乳尖點之間水平的距離。

㉙後長 (Back Length) 圖 32：計量由側頸點，經肩胛骨，垂直量至腰圍線之長度。

㉚背長 (Posterior Waist Length) 圖 33：計量由頸圍後中心點，量至腰圍後中心點間之長度。

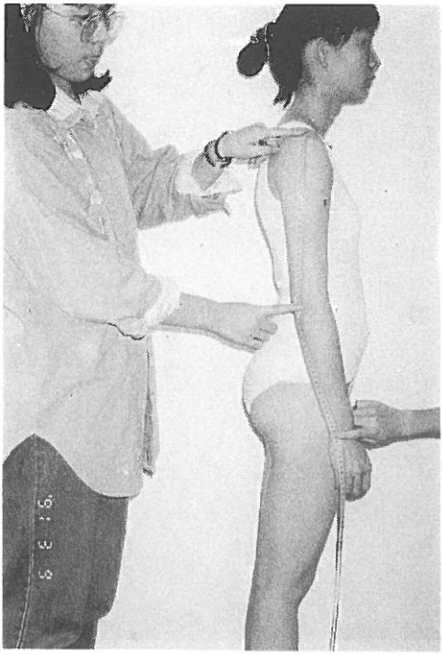

圖23 手臂長 (SP)。

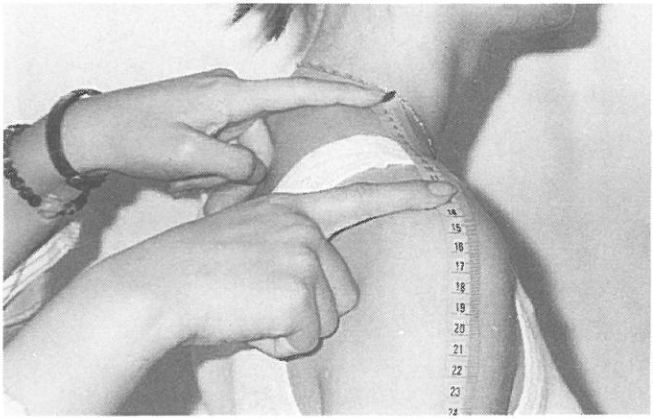

圖24 肩 寬。

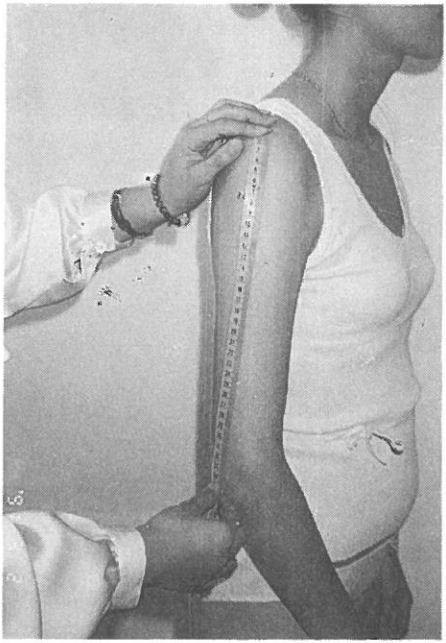

圖25 肘 長。

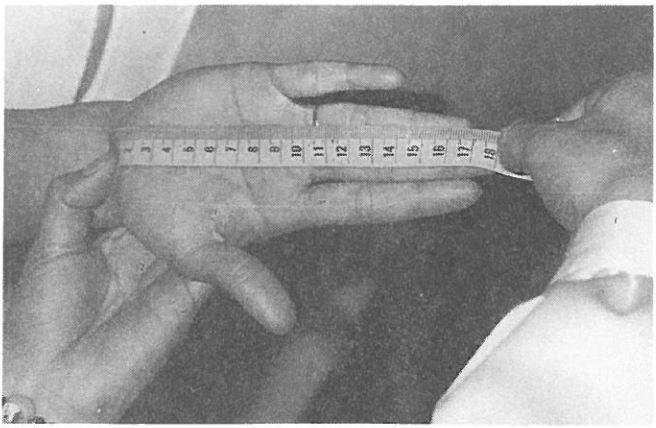

圖26 手 長。

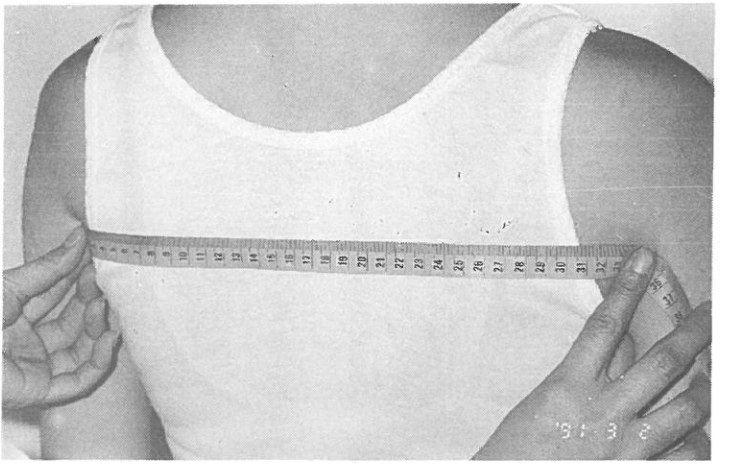

圖27 背寬。

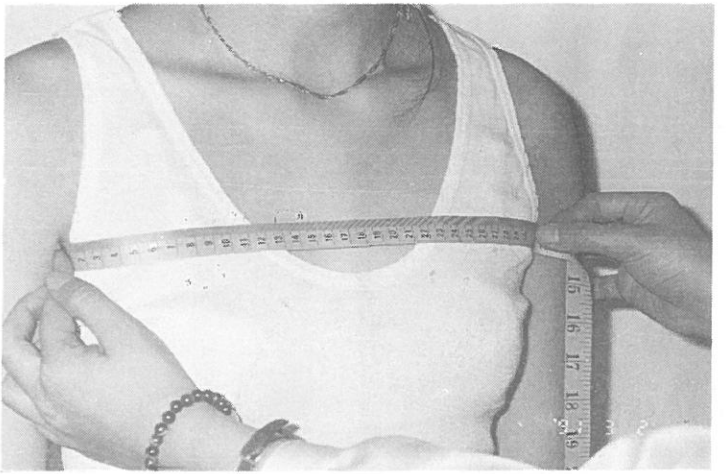

圖28 胸寬。

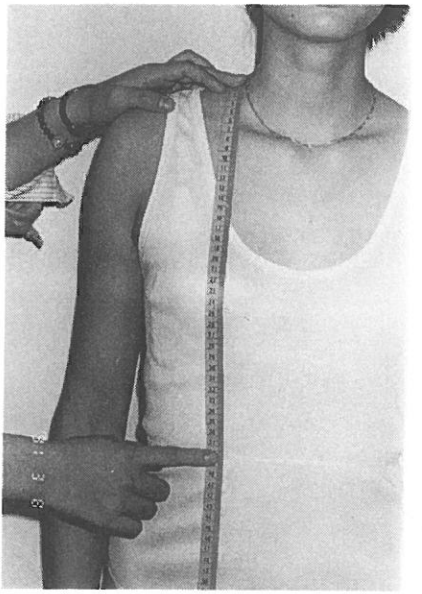

圖29　前 長。

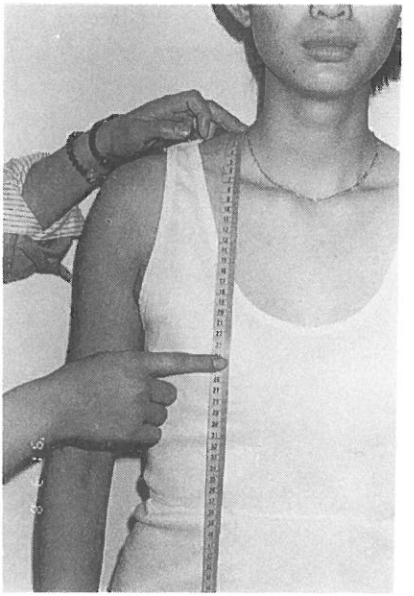

圖30　乳尖點長。

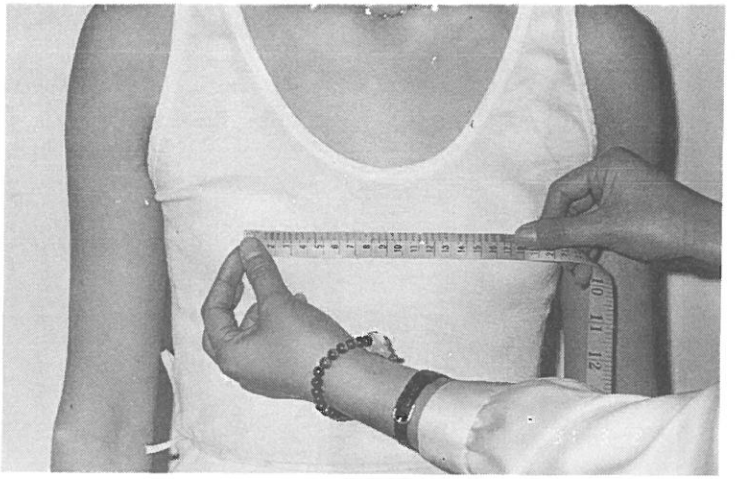

圖31 乳點間距。

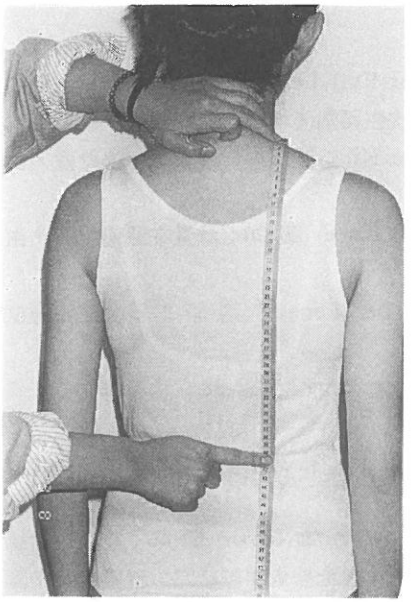

圖32 後 長。

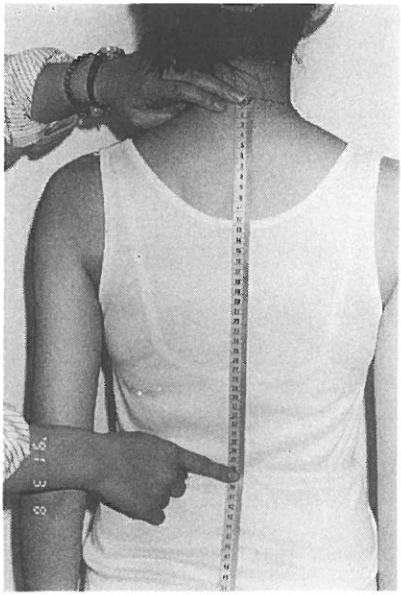

圖33　背 長。

㉛總長 (Posterior Full Length) 圖 34：計量由頸圍後中心點，垂直量至腰圍後中心，按住腰圍後中心點，再繼續一直量至地板的長度。

㉜腰長 (Waist to Hip) 圖 35：計量在胁邊位置，由腰圍線量至臀圍線間距離之長度。

㉝膝長 (Waist to Knee) 圖 36：計量在胁邊位置，由腰圍線量至膝點線之長度。

㉞外長 (Outside Leg Length) 圖 37：計量在胁邊位置，由腰圍線量至脚踝點之長度。

㉟內長 (Inside Leg Length) 圖 38：由軀幹之基底（卽襠處）計量至脚踝線之長度。

㊱直襠長 (Body Rise) 圖 39：受測者以坐姿，從體側計量由腰圍線至坐面的垂直距離。

㊲軀幹圍 (Vertical Trunk Girth) 圖 40：計量由肩線中點，經前身乳尖點，再經股襠處，由後身續量回原始點，環繞軀幹一圈之尺寸。

㊳全襠長 (Total Crotch Length) 圖 41：計量由腰圍前中心點，經股襠處，不緊繃，再續量至腰圍後中心點之長度。

㊴身高 (Stature)：計量由地面至頭頂點之垂直距離。

圖34 總 長。

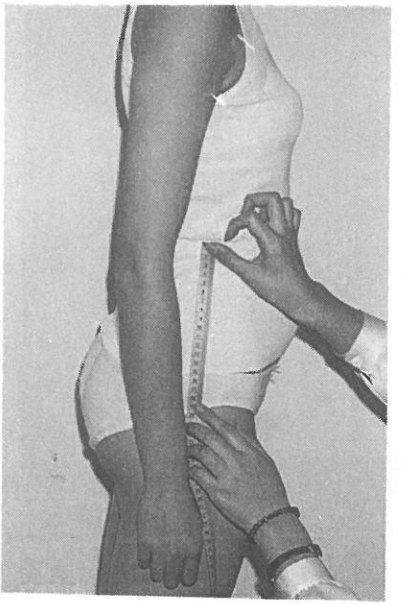

圖35 腰 長。

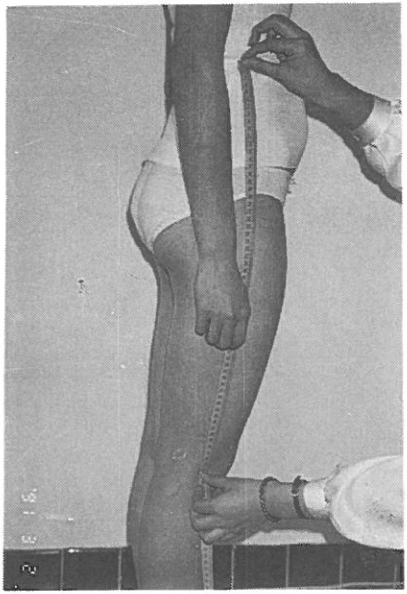

圖36 膝 長。

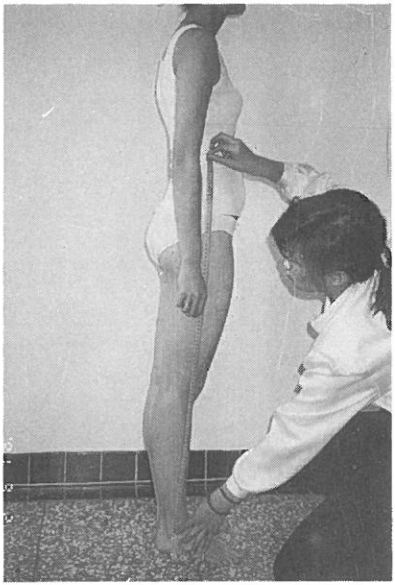

圖37 外 長。

圖38 內 長。

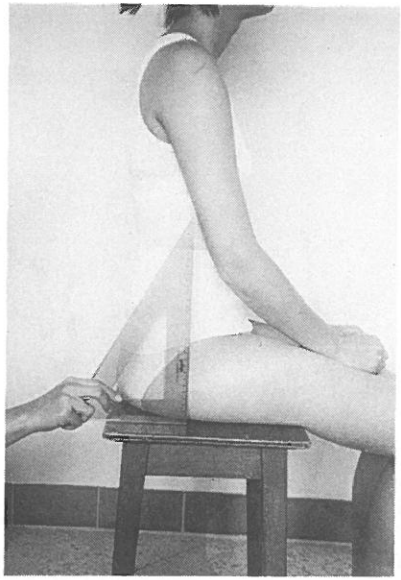

圖39 直襠長。

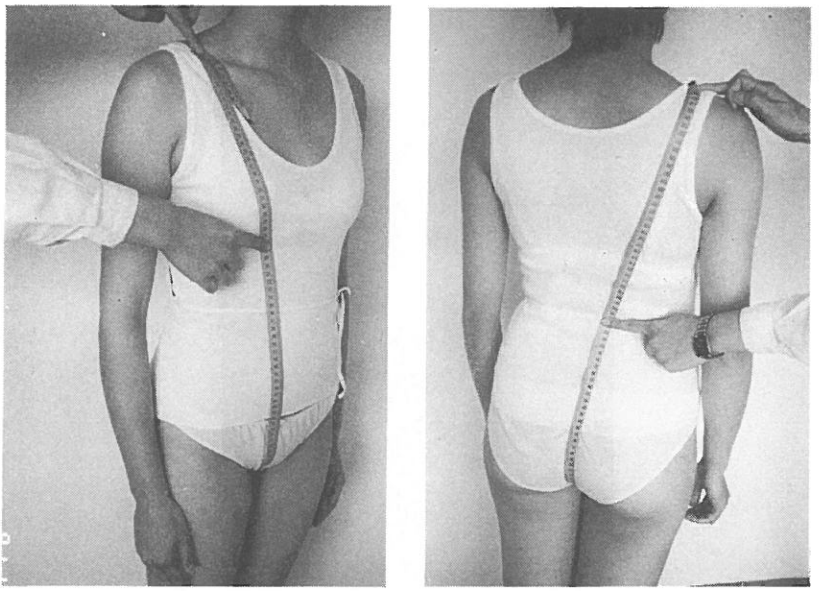

圖40　軀幹圍。

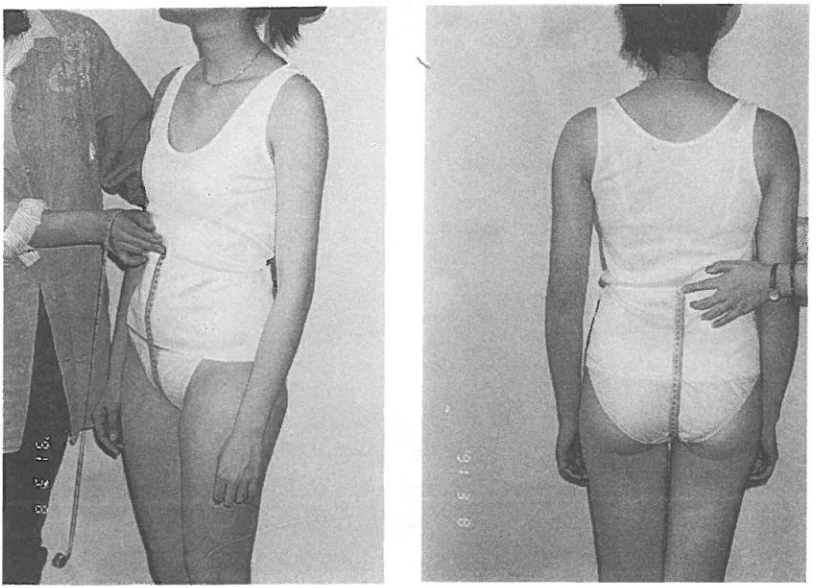

圖41　全襠長。

㊵體重 (Weight)：計量直立於磅秤台上，所秤得之重量。
㊶頭長 (Head Length)：由頭部側量，自頭頂點量至下顎點之垂直距離。
㊷脚寬 (Foot Girth) 圖 42：計量脚掌最寬部分一圈之尺寸。
㊸脚長 (Foot Length) 圖 43：計量由脚跟後端至最長足指前端之長度。

(2) 體型分析調查

人體體型分析調查是以體型輪廓攝影器，分別拍攝受測樣本之正面與側面之體型輪廓，再依體表傾斜角度、前後投影寬、垂直投影長、水平投影寬等分類，測量值共計 22 項，如圖 44，說明如下：

體表傾斜角度

①乳尖點至腰圍線之體表角度：在側面輪廓，由腰圍線前端點做地面垂直線及與乳尖點之連線，測二直線間之角度。
②胸部之傾斜角度：在側面輪廓，由領圍線前端點做地面垂直線及與乳尖點之連線，測此二直線間之角度。
③背頸處之傾斜角度：在側面輪廓，由領圍線後端點做地面垂直線，及與背面之切線，測此二直線間之角度。
④背腰處之傾斜角度：在側面輪廓，由腰圍線後端點做地面垂直線，及與背面之切線，測此二直線間之角度。
⑤體脇之傾斜角度：在正面輪廓，由腰圍線側端點做地面垂直線，及與體側脇邊切線，測此二直線間之角度。
⑥肩線之傾斜角度：在正面輪廓，由側頸點做地面水平線，及與肩端點之連線，測此二直線間之角度。
⑦臀部側面之傾斜角度：在側面輪廓，由腰圍線後端點做地面垂直線，及與臀面之切線，測此二直線間之角度。
⑧臀部正面之傾斜角度：在正面輪廓上，由腰圍線側端點做地面垂直線，及與臀側面之切線，測此二直線間之角度。
⑨腹部傾斜角度：在側面輪廓，由腰圍線前端點做地面垂直線，及與腹部之切線，測此二直線間之角度。

前、後投影寬

⑩胸圍厚度：在側面輪廓，計量在前、後水平胸圍線上，體型輪廓線內之橫寬距離。
⑪腰圍厚度：在側面輪廓，計量在前、後水平腰圍線上，體型輪廓線內之橫寬距離。

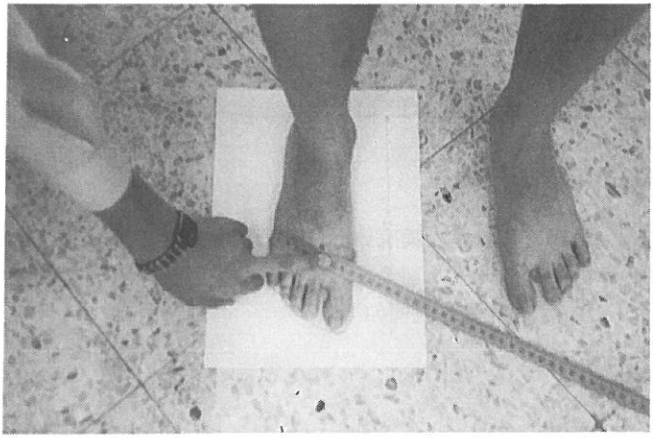

圖42 脚 寬。

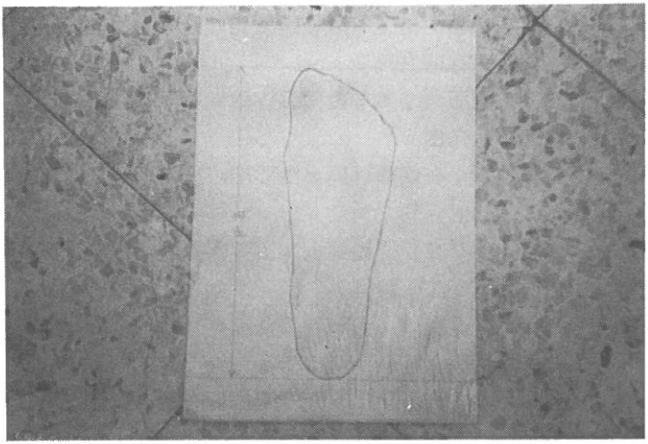

圖43 脚 長。

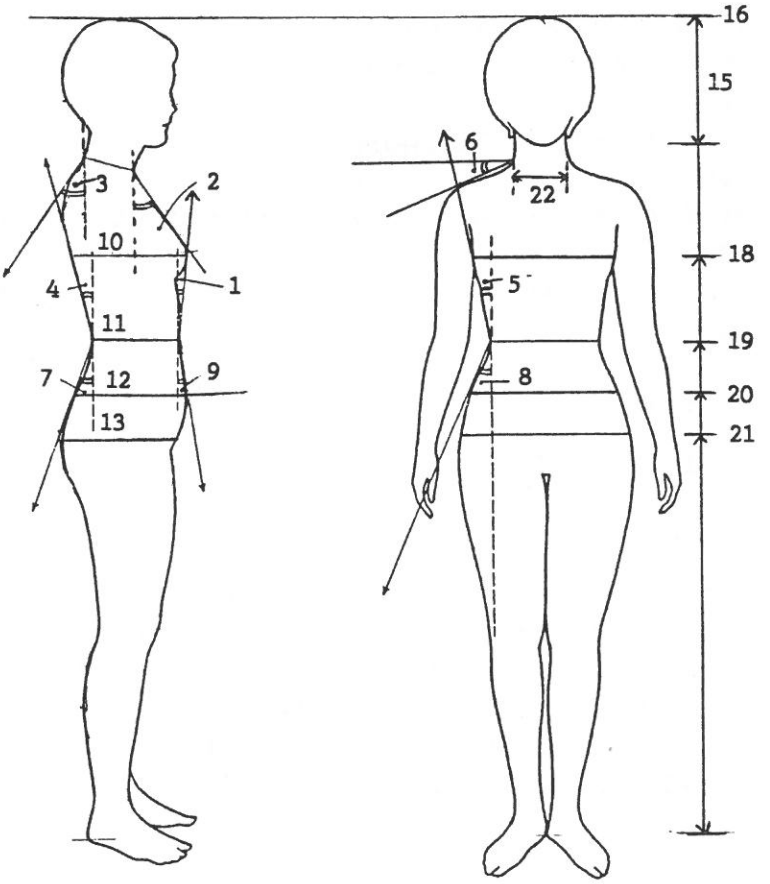

圖44　體型輪廓計測。

⑫腹圍厚度：在側面輪廓，計量在前、後水平腹圍線上，體型輪廓線內之橫寬距離。

⑬臀圍厚度：在側面輪廓，計量在前、後水平臀圍線上，體型輪廓線內之橫寬距離。

⑭臂根圍厚度：在側面輪廓，計量在前、後腋點間，手臂輪廓線內之橫寬水平距離。

垂直投影長

⑮頭長：在側面輪廓，計量由頭頂點水平線至下巴點水平線間之垂直距離。

⑯身長：在側面輪廓，計量由頭頂點水平線至脚底（地面）間之垂直距離。
⑰頭身指數：計算頭長與身高間之比例稱之。
⑱胸線垂直高度：在側面輪廓之中心線上，計量由胸圍水平線至地面之垂直距離。
⑲腰線垂直高度：在側面輪廓之中心線上，計量由腰圍水平線至地面之垂直距離。
⑳腹圍垂直高度：在側面輪廓之中心線上，計量由腹圍水平線至地面之垂直距離。
㉑臀圍垂直高度：在側面輪廓之中心線上，計量由臀圍水平線至地面之垂直距離。

水平投影寬

㉒頸寬：在正面輪廓，計量頸項基處水平線間之橫寬距離。

(3) 基本樣版制定

依人體量身計測調查及體型分析調查之結果，歸納出 18-26 歲年齡層之代表性尺寸及代表性體型。將此代表性尺寸與歐式 38 號人台尺寸，以日、美、英、德及紡研中心所研發之各基本樣版分別製圖，再以歐式 38 號人台及 18-26 歲年齡層代表性尺寸之人體樣本做實驗，比較由不同代表性尺寸所製出領圍、背寬、胸寬、肩斜、肩寬、及袖圈等主要尺寸之差異，再根據分析之結果，加上本研究之定義範圍，制定出 18-26 歲年齡層女性適體性基本樣版。

四、結果與討論

1. 人體量身計測調查

(1) 重要部位平均值

由 301 名 18-26 歲女學生之受測樣本爲研究對象之計測調查結果，由表一顯示了水平測度及垂直測度共 43 項之各項計測平均值。本研究參考陶嘉菊（民 62，P. 53）研究及國外日本、德國、美國、英國等之尺碼規劃，將最具人體代表性尺寸，且與服裝製作尺寸有密切相關之身高、胸圍、腰圍、臀圍等，選定爲重要部位尺寸，其平均值分別爲身高：159.64 cm、胸圍：81.61 cm、腰圍：64.85 cm、臀圍：90.37 cm。此結果與國內相關研究中（表二），相當時期之鄭國彬（民 80）研究結果非常接近。

表一 女生人體計測平均值

項目	樣本數	缺失值	有效值	平均值	標準差	變異數
身高	301	1	300	159.64	5.20	27.03
體重	301	4	297	50.23	6.12	37.44
頭圍	301	0	301	55.38	1.59	2.52
頭長	301	166	135	21.23	1.23	1.51
頸根圍	301	0	301	38.05	2.23	4.96
胸圍	301	3	298	81.61	4.89	23.92
乳下圍	301	1	300	71.52	4.38	19.19
腰圍	301	1	300	64.85	4.52	20.43
臀圍	301	1	300	90.37	4.97	24.74
大腿圍	301	1	300	53.98	4.15	17.26
膝圍	301	0	301	34.91	2.15	4.61
小腿圍	301	0	301	34.48	2.33	5.45
踝圍	301	1	300	22.99	1.64	2.69
臂根圍	301	0	301	39.34	3.05	9.29
上臂圍	301	0	301	26.58	2.39	5.73
肘圍	301	0	301	22.28	1.55	2.42
下臂圍	301	0	301	20.02	1.64	2.69
腕圍	301	0	301	14.67	0.82	0.67
掌圍	301	1	300	20.20	1.15	1.31
背肩寬	301	0	301	36.83	2.66	7.09
手臂長 (CB)	301	5	296	73.43	2.79	7.79
肩寬	301	23	278	13.02	1.18	1.39
手臂長 (NP)	301	3	298	67.46	2.84	8.05
手臂長 (SP)	301	6	295	54.78	2.85	8.12
肘長	301	9	292	31.69	3.00	8.98
手長	301	4	297	17.46	1.10	1.21
背寬	301	0	301	33.13	2.31	5.32
胸寬	301	0	301	31.62	1.94	3.75
前長	301	6	295	40.64	2.35	5.54
乳尖點長	301	3	298	25.27	2.09	4.37
乳點間距	301	1	300	17.73	1.29	1.67
後長	301	0	301	40.49	2.03	4.13
背長	301	0	301	38.17	2.19	4.78
總長	301	2	299	136.57	5.12	26.26
腰長	301	11	290	19.57	2.02	4.08
膝長	301	6	295	57.78	3.00	9.03
外長	301	5	296	95.59	4.13	17.05
內長	301	9	292	67.03	4.11	16.93
直襠長	301	7	294	26.24	1.55	2.42
軀幹圍	301	2	299	147.38	5.65	31.88
全襠長	301	7	294	68.99	4.15	17.24
脚寬	301	6	295	22.37	1.09	1.19
脚長	301	8	293	23.11	1.01	1.02

註：頭長計測部分由體型輪廓調查執行

表二　女性各重要部位之計測值比較

計測項目 / 統計量數	身高	胸圍	腰圍	臀圍
1. 輔大 1990-1991 年 18-26 歲之大學女生人體計測調查				
中位數	159.50	81.00	64.00	90.00
衆數	158.00	81.00	63.00	90.00
平均值	159.64	81.61	64.85	90.37
2. 紡研中心 1972-1973 年 19-23 歲之大專女生人體計測調查				
中位數	—	79.83	61.82	88.28
衆數	155.24	77.80	60.35	90.50
平均值	155.58	79.92	62.07	88.26
平均值增加(%)	2.61	2.11	4.48	2.39
3. 屏東農專 1983-1986 年 18-23 歲之大專女生人體計測調查				
平均值	157.76	79.61	60.60	88.02
平均值增加(%)	1.19	2.51	7.01	2.67
4. 臺北工專 1986-1991 年臺灣地區 18-26 歲女性人體計測調查				
平均值	157.37	81.64	64.70	89.72
平均值增加(%)	1.44	−0.04	0.23	0.72

(2) 尺碼間距 (Size Intervals)

尺碼間距之制定要依各國之體型狀況及該國成衣業之實際情形而選定。本研究參考各成衣工業先進國家之尺碼系統，將身高以 8 cm 爲間距，並由 18-26 歲年齡層之身高平均值 160 cm 爲一般中等身材，矮、中、高三組身高分別爲 152、160、168 cm。胸圍尺碼間距，在各國均依該國之成衣市場傳統規格而沿襲之，本研究參考德、日之尺碼系統，將胸圍分別以 3、4、6 cm 爲間距，加以統計調查之結果，胸圍平均值在 73-88 cm 間，以 3 cm 爲間距；平均值在 88-100 cm 間，以 4 cm 爲間距；平均值爲 100 cm 以上，以 6 cm 爲間距。臀圍尺碼間距，則依全部 18-26 歲年齡層樣本，以身高 8 cm 爲間距，胸圍 3、4 cm 爲間距之統計調查結果，臀圍平均值在 84-94 cm 間，以 2 cm 爲間距；平均值在 94-103 cm 間，以 3 cm 爲間距；平均值在 103 cm 以上，以 6 cm 爲間距。腰圍尺碼各國則均以參考性尺寸視之，本研究，依統計調查之結果，腰圍平均值在 59-65 cm 間，以 2 cm 爲間距；平均值在 65-71 cm 間，

以 3 cm 爲間距；平均值在 71-83 cm 間，以 4 cm 爲間距；平均值在 83 cm 以上，以 6 cm 爲間距。

(3) 重要部位次數分佈及頻率分佈

重要部位之尺寸與尺碼分類系統之制定有極密切之關係，故將身高、胸圍、腰圍、臀圍等尺寸，分別以次數分佈及頻率分佈（即確率密度分佈）來表示，用以觀察 18-26 歲體型分佈之情形，亦可預測成衣市場之人口分佈狀況。

① 次數分佈

由身高次數分佈圖（圖 45），顯示若將全部 18-26 歲年齡層之樣本，以身高 4 cm 爲間距，則平均值 160 cm 之人數最多，佔總人數之 29.0%；其次爲平均值 156 cm 之人數，佔總人數之 27.67%；再其次爲平均值 164 cm 之人數，佔總人數之 19.0%，故身高在 154-166 cm 間之人數，已佔總人數之 75.67%。

由胸圍次數分佈圖（圖 46），顯示若將全部 18-26 歲年齡層之樣本，平均值在 73-88 cm 間，以 3 cm 爲間距；平均值在 88-100 cm 間，以 4 cm 爲間距；平均值爲 100 cm 以上，以 6 cm 爲間距，則平均值 79 cm 之人數最多，佔總人數之 26.17%；其次爲平均值 82 cm 之人數，佔總人數之 24.83%；再其次爲平均值 76 cm 及平均值 85 cm 之人數，各佔總人數之 15.10%，故胸圍在 74.5-86.5 cm 間之人數，已佔總人數之 81.2%。

由腰圍次數分佈圖（圖 47），顯示若將全部 18-26 歲年齡層之樣本，平均值在 59-65 cm 間，以 2 cm 爲間距；平均值在 65-71 cm 間，以 3 cm 爲間距；平均值在 71-83 cm 間，以 4 cm 爲間距；平均值在 83 cm 以上，以 6 cm 爲間距，則平均值 65 cm 之人數最多，佔總人數之 23.33%；其次爲平均值 63 cm 之人數，佔總人數之 22.67%；再其次爲平均值 61 cm 之人數，佔總人數之 15.67%，故腰圍在 60-66.5 cm 間之人數，已佔總人數之 61.67%。

由臀圍次數分佈圖（圖 48），顯示若將全部 18-26 歲年齡層之樣本，平均值在 84-94 cm 間，以 2 cm 爲間距；平均值在 94-103 cm 間，以 3 cm 爲間距；平均值在 103 cm 以上，以 6 cm 爲間距，則平均值 88 cm 之人數最多，佔總人數之 19.67%；其次爲平均值 90 cm 之人數，佔總人數之 17.00%；再其次爲平均值 86 cm 之人數，佔總人數之 15.33%，故臀圍在 85-91 cm 間之人數，已佔總人數之 52.0%。

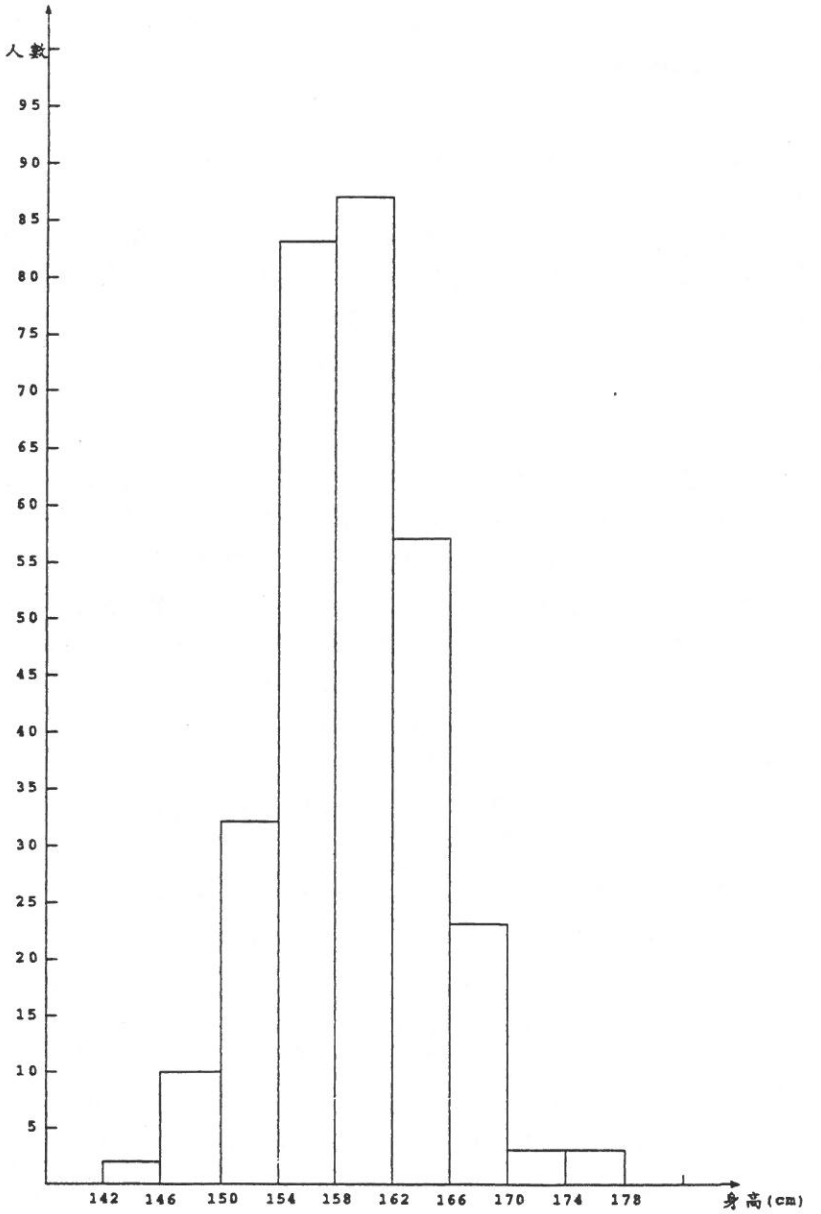

總人數：300 人

圖45 身高次數分佈圖。

註：平均值以 4 cm 爲間距

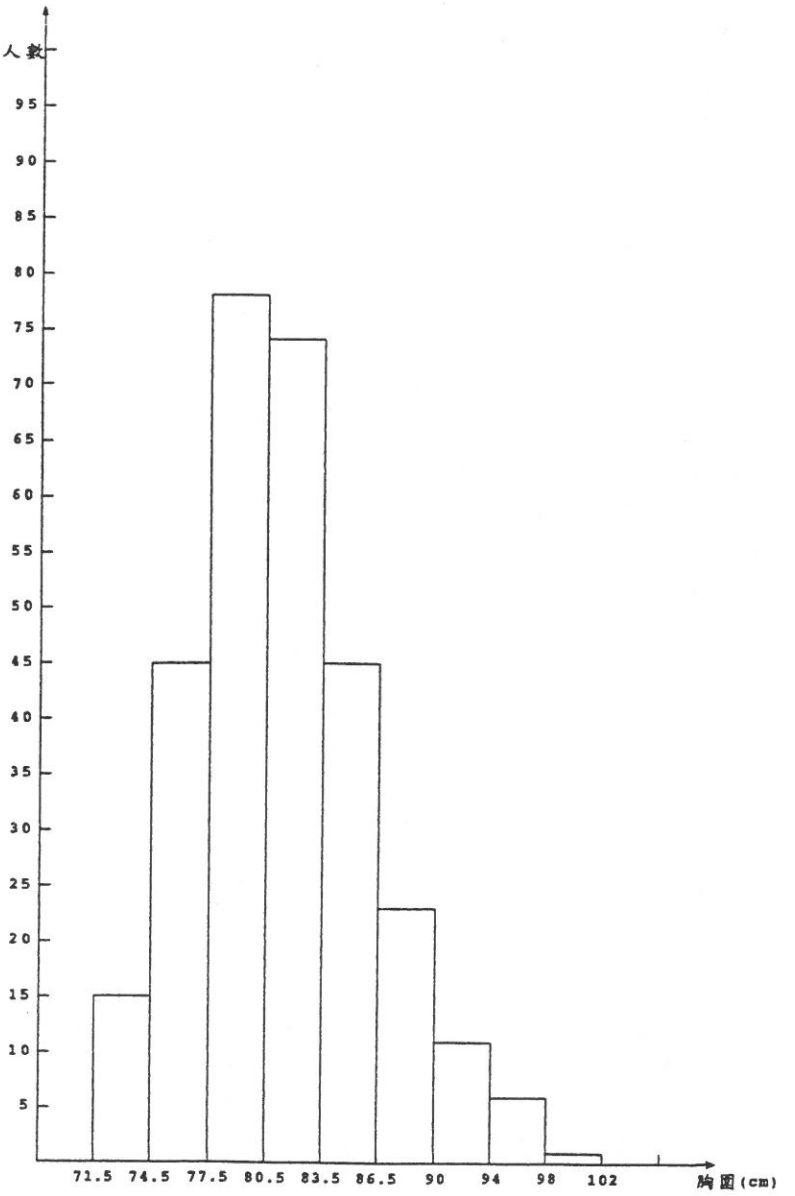

總人數：298 人

圖46 胸圍次數分佈圖。

註：平均值 73- 88 cm 以 3 cm 爲間距
平均值 88-100 cm 以 4 cm 爲間距
平均值 100 cm 以上以 6 cm 爲間距

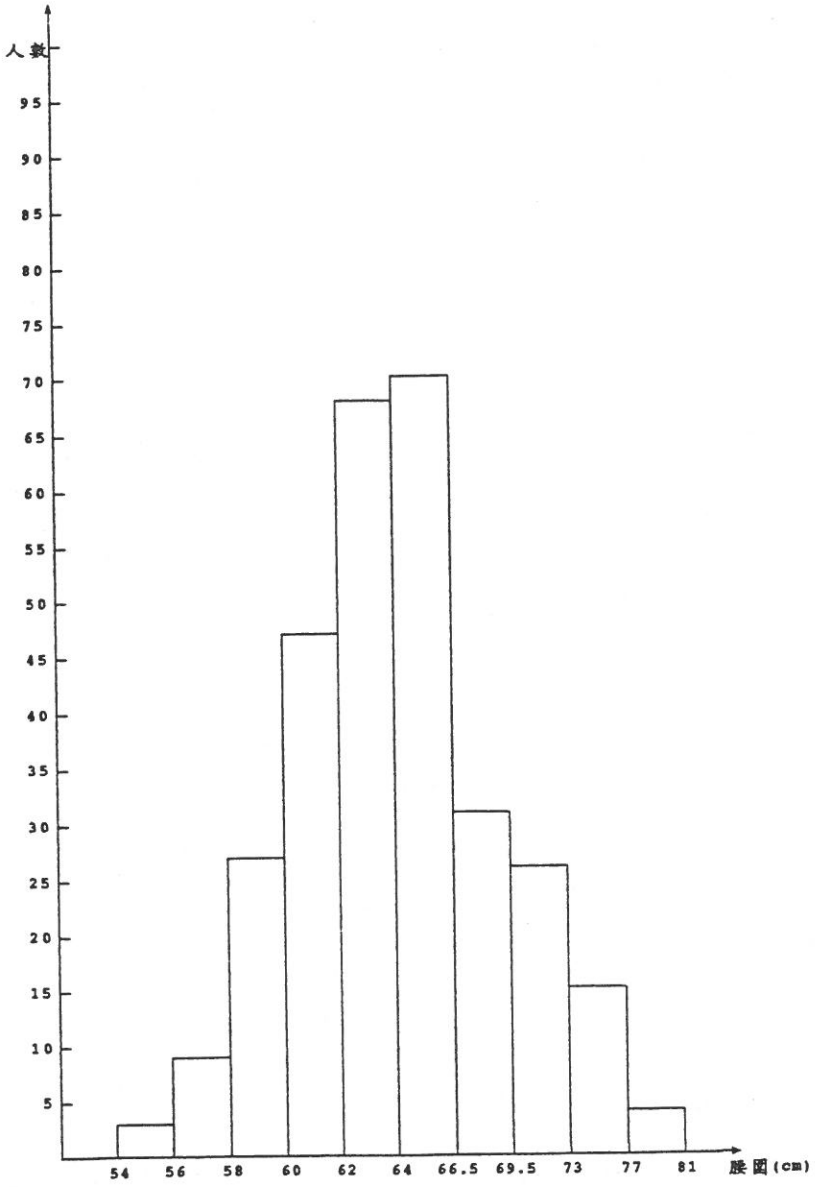

總人數：300 人

圖47 腰圍次數分佈圖。

註：平均值 59-65 cm 以 2 cm 爲間距
平均值 65-71 cm 以 3 cm 爲間距
平均值 71-83 cm 以 4 cm 爲間距
平均值 83 cm 以上以 6 cm 爲間距

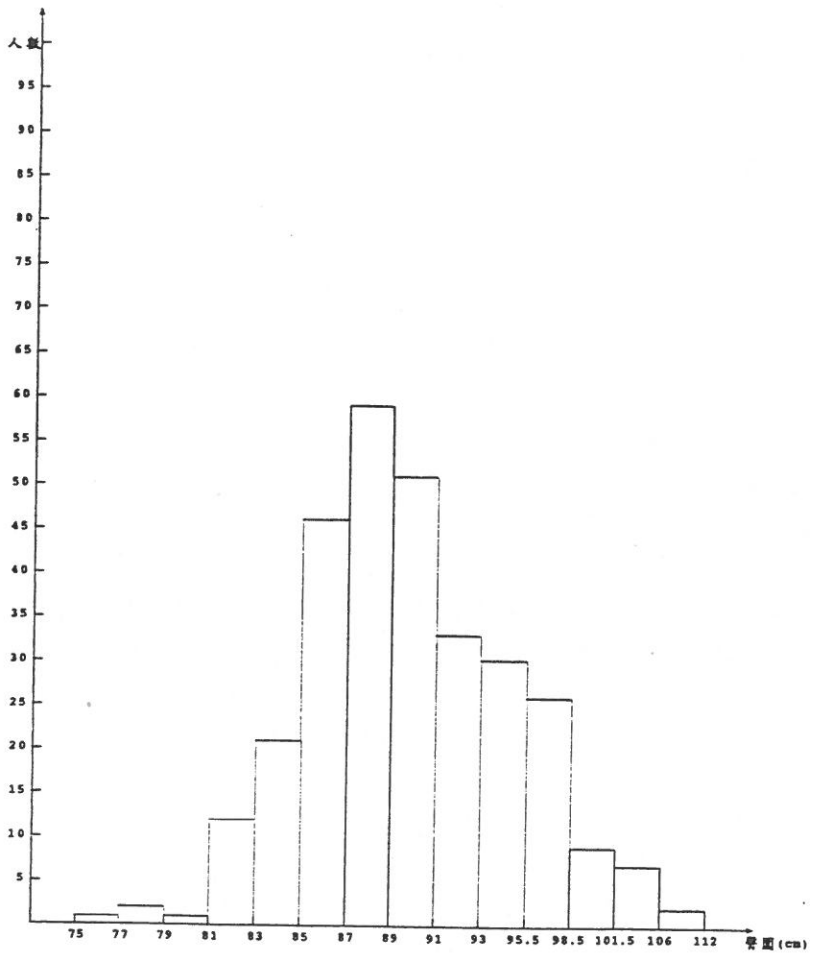

總人數：300 人

圖48 臀圍次數分佈圖。
註：平均值 84- 94 cm 以 2 cm 爲間距
平均值 94-103 cm 以 3 cm 爲間距
平均值 103 cm 以上以 6 cm 爲間距

② **頻率分佈**

由身高人數分佈百分比（表三）中，顯示若將全部 18-26 歲年齡層之樣本，以身高 8 cm 爲間距，則以身高平均值 160 cm 之人數佔最多，爲總人數之 58.0%；其次爲平均值 152 cm 之人數，佔總人數之 23.67%；再其次爲平均值 168 cm 之人數，佔總人數之 15.33%，此三組已佔總人數之 97.0%，即已涵蓋大部分之市場人口。

表三　受測者身高人數分佈百分比

統計量數 / 身高分類	平均值 (cm)	人數	百分比 (%)
矮	148 以下	5	1.67
	152 (148～156)	71	23.67
中	160 (156～164)	174	58.00
高	168 (164～172)	46	15.33
	172 以上	4	1.33
總人數		300	100.00

由胸圍頻率分佈表（表四）中，顯示若將全部 18-26 歲年齡層之樣本，胸圍以 3、4 cm 爲間距，則以胸圍平均值 79 cm 之人數佔最多，佔總人數之 26.26%，其次爲平均值 82 cm 之人數，佔總人數之 24.58%，以上二者已涵蓋總人數之 50.84%；再其次爲平均值 76 cm 之人數及平均值 85 cm 之人數，各佔總人數之 15.10%，以上四者共已涵蓋總人數之 81.04%。若再將身高以 8 cm 爲間距之因素一併考慮，則身高平均值在 160 cm，胸圍平均值在 79 cm 之人數佔最多，佔總人數之 16.84%，其次爲身高平均值在 160 cm，胸圍平均值在 82 cm 之人數，佔總人數之 14.81%，以上二者已涵蓋總人數之 31.65% 了。

表四　胸圍頻率分佈表

身高 (cm) / 胸圍 (cm)	148 以下	152 (148～156)	160 (156～164)	168 (164～172)	172 以上	總人數	百分比 (%)
73 (71.5～74.5)		6	8	1		15	5.05
76 (74.5～77.5)	2	17	23	3		45	15.15
79 (77.5～80.5)	1	17	50	10		78	26.26
82 (80.5～83.5)		17	44	9	3	73	24.58
85 (83.5～86.5)	1	5	28	10	1	45	15.15
88 (86.5～90.0)		6	9	8		23	7.74
92 (90.0～94.0)	1	1	6	3		11	3.70
96 (94.0～98.0)		1	3	2		6	2.02
100 (98.0～102.0)			1			1	0.34
總人數	5	70	172	46	4	297	100.00
百分比 (%)	1.68	23.57	57.91	15.49	1.35	100.00	

由臀圍頻率分佈表（表五）中，顯示若將全部 18-26 歲年齡層之樣本，身高以 8 cm 爲間距，胸圍以 3、4 cm 爲間距，臀圍以 2、3 cm 爲間距，則以身高平均值 160 cm，胸圍平均值 79 cm，臀圍平均值 88 cm 的人數爲最多，佔總人數之 6.08%，其次爲身高平均值 160 cm，胸圍平均值 79 cm，臀圍平均值 90 cm 之人數，佔總人數之 4.39%。若不考慮身高因素，則人數均集中在胸圍平均值 76-85 cm 間，臀圍平均值 86-90 cm 間，有 141 人，佔總人數之 47.64%；若將範圍縮小至胸圍平均值 79-82 cm，臀圍平均值 86-90 cm，則人數有 108 人，佔總人數之 36.49%。

以上各百分比，均可視產品性質、消費對象等因素，提供生產單位在產量比例分配時，作爲預估參考之用。

2. 尺碼系統規劃

本研究之尺碼系統規劃以身高、胸圍爲劃分基礎，再以臀圍做體型分類的依據，將主要尺寸尺碼表（表六）分類如下：

身高以 8 cm 爲間距，分高、中、矮三組高度，平均值分別爲 152、160、168 cm。胸圍平均值在 73-88 cm 間，以 3 cm 爲間距，平均值在 88-100 cm 間，以 4 cm 爲間距，平均值在 100 cm 以上，以 6 cm 爲間距。臀圍依體型可分成：一般體型、臀大體型、臀小體型三種。臀大體型之臀圍比一般體型大 4 cm，臀小體型之臀圍比一般體型小 4 cm。一般體型臀圍平均值在 84-94 cm 間，以 2 cm 爲間距，平均值在 94-103 cm 間，以 3 cm 爲間距，平均值在 103 cm 以上，以 6 cm 爲間距。但身高在「高」組（即平均值 168 cm）比其他「中」「矮」二組之臀圍，平均值均多 2 cm。

18-26 歲年齡層之主尺碼表(表七)，是以身高平均值之人數最集中的 160cm 爲主。

3. 人體體型分析調查

由 108 名 18-26 歲女學生之受測樣本爲研究對象之體型輪廓攝影調查結果，顯示了此年齡層之四項體型分析：(1) 體重，(2) 體表角度，(3) 軀幹各部分之厚度（投影前後寬），(4) 垂直高度等，並以各體型人數分佈，用以觀察 18-26 歲各體型分佈之情形，亦可預測成衣市場之人口分佈狀況。

(1) 體 重

依李維指數，指數值在 22.0-24.0 間者爲適中體型，指數值小於 22.0 者爲瘦長體型，指數值大於 24.0 者爲肥胖體型。本研究調查全部 18-26 歲年齡層之樣本，結果顯示適中體型佔總人數之 85.19%；肥胖體型佔總人數之 11.11%；瘦長體型佔總人數之 3.70%。

表五　臀圍頻率分佈表

總人數：296 人

身高 (cm)	胸圍 (cm) ＼ 臀圍 (cm)	76	78	80	82	84	86	88	90	92	94	97	100	103	109	合計人數
148 以下	73.0															—
	76.0					1			1							2
	79.0						1									1
	82.0															—
	85.0						1									1
	88.0															—
	92.0												1			1
152 (148.1 ～ 156)	73.0	1	1				1	2	1							6
	76.0		1		3	4	6	2		1						17
	79.0					1	5	10	1							17
	82.0					2	7	6	1	1						17
	85.0							1	1	2	1					5
	88.0									2	3		1			6
	92.0								1							1
	96.0										1					1
160 (156.1 ～ 164)	73.0			1	2	2	2	1								8
	76.0				4	4	6	5	3	1						23
	79.0				2	4	7	18	13	3	1	1				49
	82.0				2	2	6	12	11	8	1	3				44
	85.0								4	7	12	3	2			28
	88.0								2		1	2	2	2		9
	92.0								2			2	2			6
	96.0													2	1	3
	100.0										1					1
168 (164.1 ～ 172)	73.0								1							1
	76.0					1		1		1						3
	79.0						1	1	6	1		1				10
	82.0						1			2	4	2				9
	85.0								2	3		5				10
	88.0										2	4		2		8
	92.0											1	1	1		3
	96.0											1			1	2
172 以上	73.0															—
	76.0															—
	79.0															—
	82.0								1	1		1				3
	85.0										1					1

註：胸圍間距 3 cm，表中 b 值之範圍爲 $(b-1.4)\sim(b+1.5)$；88 cm 以上爲 4 cm，表中 b 值之範圍爲 $(b-1.9)\sim(b+2.0)$

臀圍間距 2 cm，表中 h 值之範圍爲 $(h-0.9)\sim(h+1.0)$；94 cm 以上爲 3 cm，表中 h 值之範圍爲 $(h-1.4)\sim(h+1.5)$；103 cm 以上爲 6 cm，表中 h 值之範圍爲 $(h-2.9)\sim(h+3.0)$

表六 尺碼表（主要尺寸）

1. 一般體型

尺碼	3	5	7	9	11	13	15	3	5	7	9	11	13	15
身高	152，160							168						
胸圍	73	76	79	82	85	88	92	73	76	79	82	85	88	92
臀圍	84	86	88	90	92	94	97	86	88	90	92	94	96	99
腰圍	59	61	63	65	68	71	75	61	63	65	67	70	73	77

* 尺碼編號暫以日本制代替

2. 臀大體型（臀圍比一般體型大 4 cm 者）

尺碼	3L	5L	7L	9L	11L	13L	15L	3L	5L	7L	9L	11L	13L	15L
身高	152，160							168						
胸圍	73	76	79	82	85	88	92	73	76	79	82	85	88	92
臀圍	88	90	92	94	96	98	101	90	92	94	96	98	100	103

3. 臀小體型（臀圍比一般體型小 4 cm 者）

尺碼	3S	5S	7S	9S	11S	13S	15S	3S	5S	7S	9S	11S	13S	15S
身高	152，160							168						
胸圍	73	76	79	82	85	88	92	73	76	79	82	85	88	92
臀圍	80	82	84	86	88	90	93	82	84	86	88	90	92	95

(2) 體表角度

由體型輪廓攝影，於兩測定點連線與地面垂直線或水平線所呈角度之大小，將體型分類。由表八顯示，18-26 歲年齡層之胸部傾斜角度平均值爲 28.75°，故胸部之傾斜角度在 33° 以上者爲厚胸體型。背頸處傾斜角度平均值爲 25.65°，故背頸處之傾斜角度在 30° 以上者爲駝背體型，20° 以下者爲後仰體型。肩線傾斜角度平均值爲 23.07°，故肩線傾斜角度在 28° 以上者爲斜肩體型，18° 以下者爲平肩體型。本研究調查全部 18-26 歲年齡層之樣本，結果顯示厚胸體型佔總人數之 10.19%；駝背體型佔總人數之 22.22%，後仰體型佔總人數之 20.37%，居間一般體型者佔總人數之 57.41%；斜肩體型佔總人數之 9.26%，平肩體型佔總人數之 13.89%，居間一般體型者佔總人數之 76.85%。

表七　主尺碼表（18-26 歲女性量身尺寸）

尺　碼	3	5	7	9	11	13	15
身　高	160.0						
胸　圍	73.0	76.0	79.0	82.0	85.0	88.0	92.0
臀　圍	84.0	86.0	88.0	90.0	92.0	94.0	97.0
腰　圍	59.0	61.0	63.0	65.0	68.0	71.0	75.0
背　寬	30.5	31.0	32.0	33.0	34.0	35.0	36.0
胸　寬	29.0	30.0	31.0	32.0	33.0	34.0	35.0
前　長	39.5	40.0	40.5	41.0	41.5	42.0	42.5
後　長	39.0	39.5	40.0	40.5	41.0	41.5	42.0
背　長	37.0	37.4	37.8	38.2	38.6	39.0	39.5
背肩寬	35.0	36.0	36.5	37.0	37.5	38.0	38.5
手臂長	54.3	54.5	54.8	55.0	55.3	55.5	55.8
上臂圍	24.0	25.0	26.0	27.0	28.0	29.0	30.0
腕　圍	14.0	14.3	14.6	15.0	15.3	15.6	16.0
外　長	95.4	95.6	95.8	96.0	96.2	96.4	96.6
直襠長	25.0	25.5	25.5	26.0	26.0	26.5	26.5
手　長	17.0	17.0	17.0	17.5	17.5	17.5	17.5
膝　長	57.0	57.0	57.0	58.0	58.0	58.0	58.0
膝　圍	33.0	34.0	34.5	35.0	36.0	37.0	38.0
大腿圍	50.0	51.0	53.0	54.0	56.0	57.0	59.0
頭　長	20.5	20.5	21.0	21.0	21.5	21.5	22.0
頭　圍	54.1	54.4	54.7	55.0	55.3	55.6	55.9
全襠長	67.0	67.5	68.0	69.0	70.0	71.0	72.0

* 尺碼編號暫以日本制代替

(3) 軀幹各部分之厚度（投影前後寬）

由體型輪廓攝影、胸線、腰線、腹圍線、臀線與地面之垂直高度平均值分別爲：胸圍厚度 21.90 cm，腰圍厚度 17.99 cm，腹圍厚度 21.01 cm，臀圍厚度 22.53 cm，臂根圍厚度 10.71 cm（表八）。

(4) 垂直高度

由體型輪廓攝影，胸線、腰線、腹圍線、臀線與地面之垂直高度平均值分別爲：胸線垂直高度 114.99 cm，腰線垂直高度 99.86 cm，腹圍線垂直高度 89.25 cm，臀線垂直高度 79.65 cm。而頭身指數在本研究之調查結果，頭身比例爲 6.88（表八）。

表八 女性人體體型計測統計值

項目	樣本數	缺失值	有效值	最大值	最小值	平均值	標準差	變異數
乳尖點至腰線之體表角度	108	0	108	16.0	0.0	4.71	3.19	10.20
胸部之傾斜角度	108	0	108	40.0	20.0	28.75	4.03	16.28
背部頸處之傾斜角度	108	0	108	42.0	14.0	25.65	6.40	40.98
背部腰處之傾斜角度	108	1	107	25.0	3.0	11.55	3.46	12.00
體脇之傾斜角度	108	1	107	22.0	1.0	7.52	3.42	11.68
肩線之傾斜角度	108	0	108	32.0	12.0	23.07	4.33	18.72
臀部側面之傾斜角度	108	0	108	27.0	6.0	15.83	4.35	18.89
臀部正面之傾斜角度	108	0	108	27.0	5.0	16.03	3.40	11.54
腹部之傾斜角度	108	0	108	18.0	0.0	6.56	4.04	16.35
胸圍厚度	108	0	108	29.5	18.0	21.90	1.72	2.97
腰圍厚度	108	1	107	25.5	14.0	17.99	2.53	6.41
腹圍厚度	108	0	108	31.0	17.0	21.01	2.26	5.10
臀圍厚度	108	0	108	30.0	17.0	22.53	2.04	4.16
臂根圍厚度	108	1	107	15.0	8.0	10.71	1.64	2.70
頭長	108	0	108	26.5	19.0	23.38	1.41	1.98
身長	108	0	108	175.0	150.0	160.11	4.65	21.62
頭身指數	108	0	108	7.9	5.7	6.88	0.41	0.17
胸線垂直高度	108	0	108	129.0	103.5	114.99	4.40	19.32
腰線垂直高度	108	0	108	113.0	89.0	99.86	3.99	15.96
腹圍垂直高度	108	0	108	100.0	82.0	89.25	3.75	14.05
臀線垂直高度	108	0	108	90.5	73.0	79.65	3.25	10.53
頸寬	108	0	108	14.0	9.0	10.98	1.21	1.46
身高	108	1	107	175.0	151.0	160.14	4.58	20.96
體重	108	0	108	70.0	39.0	50.53	6.38	40.65

綜合以上結果，18-26 歲女性代表性體型輪廓爲圖 49。

4. 基本樣版

(1) 基本樣版之尺寸比較

本研究依人體量身計測調查及體型分析調查之結果，歸納出 18-26 歲年齡層之代表性尺寸及代表性體型。將此歸納之代表性尺寸與歐式 38 號人台尺寸，以日、美、英、德及紡研中心所研發之各基本樣版分別製圖，再以歐式 38 號人臺及 18-26 歲年齡層代表性尺寸之人體樣本做實驗，比較由不同代表性尺寸所製出之領圍、背寬、胸寬、肩斜、肩寬及袖圈等主要尺寸之差異。

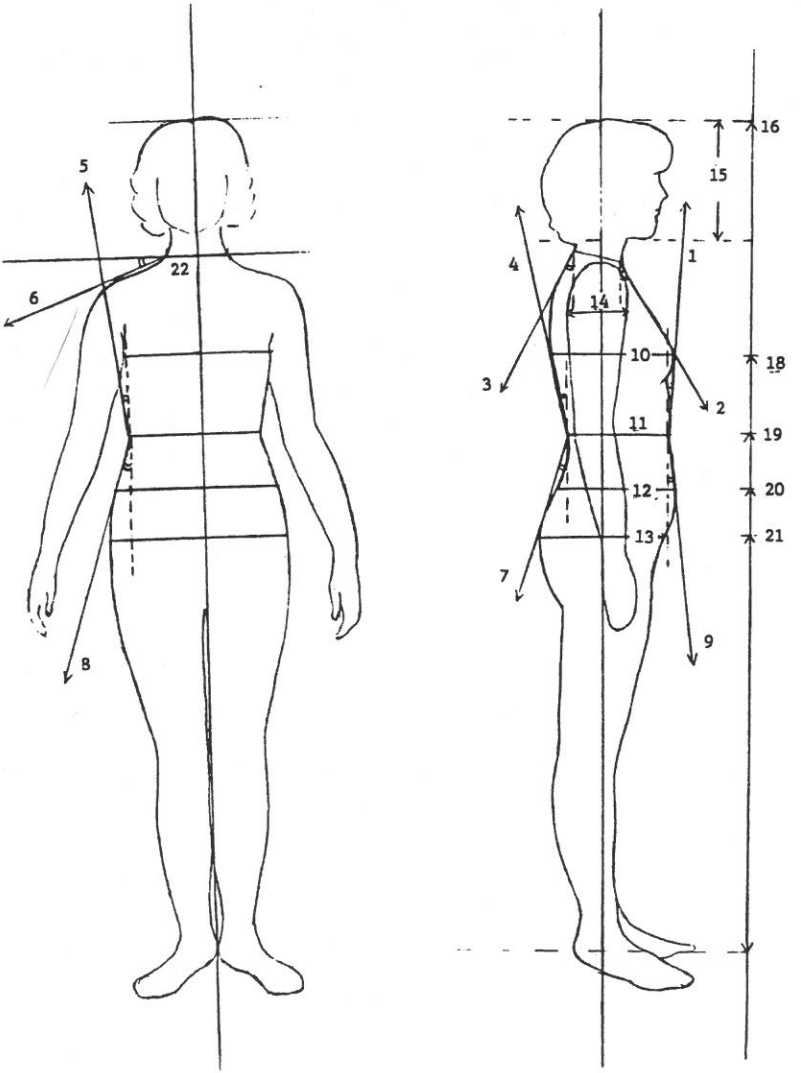

圖49 18-26 歲女性代表性體型輪廓。

由表九顯示，分別由人台尺寸與代表性尺寸，以日、美、英、德及紡研中心所研發之各基本樣版實驗，比較所製出之領圍尺寸差異。

由表十顯示，分別由人台尺寸與代表性尺寸，以日、美、英、德及紡研中心所研發之各基本樣版實驗，比較所製出之背寬、胸寬尺寸差異。

表九 各國基本樣版領圍尺寸差異比較

(單位：cm)

基本樣版 \ 位置		胸圍	1/2 領寬		領深		1/2 領圍		
			後	前	後	前	後	前	全 (1/1)
日本	文化式	82	7.0	6.8	2.3	7.5	7.7	11.2	37.8
		88	7.3	7.1	2.4	7.8	8.0	11.6	39.2
	登麗美式	82	6.8	6.8	1.8	7.5	7.2	11.2	36.8
		88	6.8	6.8	1.8	7.5	7.2	11.2	36.8
美國	F.I.T.式	82	8.3	5.6	2.5	8.0	9.0	10.8	39.6
		88	8.0	6.3	3.5	7.5	9.2	11.0	40.4
	F.D.式	82	8.75	6.0	2.5	8.0	9.3	10.7	40.0
		88	8.75	6.3	3.5	8.5	10.0	11.6	43.2
英式		82	6.5	6.5	2.0	7.5	7.0	11.0	36.0
		88	7.0	7.0	2.0	7.5	7.6	11.4	38.0
德式		82	6.4	6.4	3.0	6.4	8.0	9.8	35.6
		88	6.7	6.7	3.0	6.7	8.3	10.3	37.2
紡研中心計測式		82	5.9	6.4	2.5	8.4	7.0	12.0	38.0
		88	7.3	5.2	3.6	7.7	8.75	10.25	38.0

表十 各國基本樣版背寬、胸寬尺寸差異比較

(單位：cm)

基本樣版 \ 位置		胸圍	1/2 背寬	1/2 胸寬
日本	文化式	82	18.2	16.7
		88	19.2	17.7
	登麗美式	82	16.5	16.0
		88	16.5	16.0
美國	F.I.T.式	82	16.5	16.0
		88	17.0	16.5
	F.D.式	82	17.5	16.75
		88	17.5	16.75
英式		82	17.5	17.5
		88	17.5	17.5
德式		82	17.5	18.0
		88	18.5	19.5
紡研中心計測式		82	17.0	16.0
		88	17.0	16.0

由表十一顯示，分別由人台尺寸與代表性尺寸，以日、美、英、德及紡研中心所研發之各基本樣版實驗，比較所製出之肩斜尺寸與角度差異、肩寬尺寸差異及袖圈尺寸差異。

表十一　各國基本樣版肩寬、肩斜、袖圈尺寸差異比較

(單位：cm)

基本樣版 \ 位置		胸圍	肩寬		肩斜		袖圈		
			後	前	後	前	後	前	全
日本	文化式	82	14.1	12.3	4.6 (19.0°)	4.1 (20.0°)	20.5	20.0	40.5
		88	14.8	13.0	4.8 (19.0°)	4.3 (19.0°)	21.8	21.2	43.0
	登麗美式	82	13.0	13.0	6.0 (25.0°)	3.5 (15.0°)	18.8	22.7	41.5
		88	12.0	12.0	6.0 (27.0°)	3.5 (16.0°)	21.0	25.7	46.7
美國	F.I.T.式	82	13.5	13.0	6.0 (26.5°)	4.5 (20.0°)	18.8	17.0	35.8
		88	12.5	12.0	6.0 (28.5°)	3.3 (16.0°)	22.5	21.4	43.9
	F.D.式	82	14.25	13.0	6.4 (26.0°)	4.7 (21.5°)	18.1	21.5	39.6
		88	13.25	12.0	6.7 (30.5°)	3.3 (16.0°)	17.8	23.3	41.1
英式		82	14.0	13.0	5.0 (21.0°)	4.5 (19.0°)	19.9	19.4	39.3
		88	13.6	12.0	5.0 (22.0°)	4.5 (17.0°)	20.2	21.9	42.1
德式		82	13.0	13.0	4.5 (16.0°)	4.0 (21.5°)	22.1	18.0	40.1
		88	12.8	12.0	4.5 (15.0°)	3.8 (23.0°)	22.5	19.0	41.5
紡研中心計測式		82	13.2	12.8	3.5 (15.0°)	4.0 (18.0°)	22.3	18.4	40.7
		88	12.2	11.8	4.8 (22.5°)	2.5 (12.5°)	22.9	21.4	44.3

由表九至表十一結果顯示，由於每個國家均是基於其本身地區內之條件及標準而制定其代表性尺寸，故基本樣版亦須配合其特定條件而制定；且每個國家量身尺寸計測點之定義並非全然一致，故各國基本樣版若以他國代表性尺寸換算代入，則常有矛盾之情形發生。

(2) 基本樣版之穿著實驗

綜合穿著分析結果，直接以胸圍推算之日本文化式，最爲寬鬆，但以人體量身計測平均值所製之肩寬過小。以直接量身計測尺寸製圖之美國 F.I.T. 式、F.D. 式最緊身，但製圖時，若代表性尺寸變更，則製圖就產生問題；此外，後肩斜製圖角度均超過量身肩斜角度平均值，故實驗時亦顯太緊。以肩斜爲固定性尺寸製圖之日本登麗美式及英式、德式中，登麗美式以代表性尺寸換算後，袖圈會太寬，英式則沒影響，且尺寸相當吻合臂根圍尺寸。德式亦吻合臂根圍尺寸，但德式之肩寬需做適度修正。故整體以英式基本樣版在肩寬、肩斜、袖圈線之製圖上，與各代表性尺寸較能配合。

(3) 基本樣版之制定

本研究將基本樣版之定義界定於下：(1) 年齡層：18-26 歲，(2) 性別：女性，(3) 人體部位：上半身至腰，(4) 服裝種類：基本服裝項，(5) 目的：成衣量產之用，(6) 外形輪廓：半寬鬆適體合腰型。製圖方式：依據 18-26 歲女性人體量身計測統計值及體型分析計測統計值製圖（圖 50）。

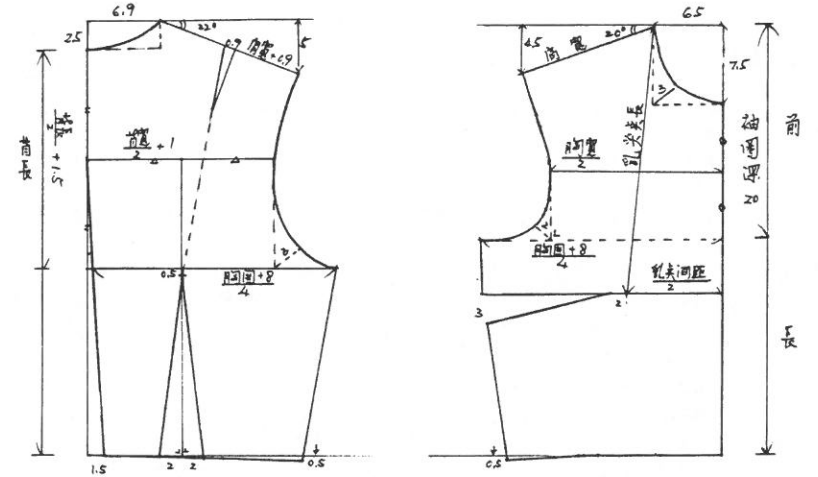

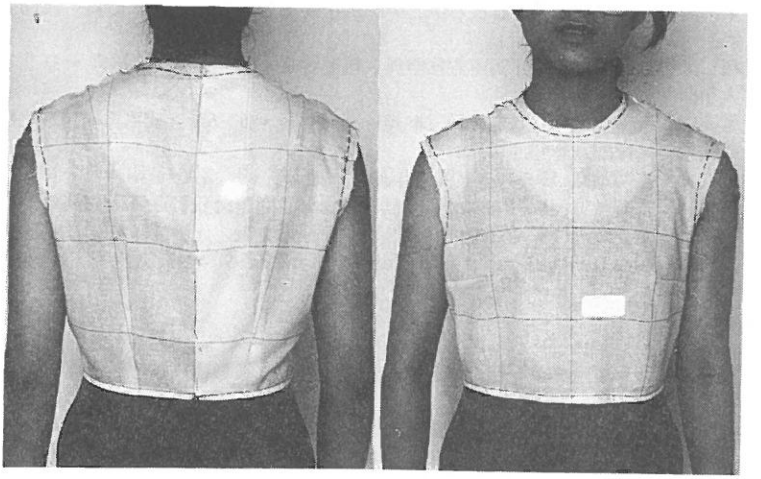

圖50 18-26 歲女性適體性基本樣版。

五、誌　　謝

本研究之完成，承蒙輔仁大學聖言會七十九學年度經費補助，及八十學年度中國紡織研究中心提供之經費，謹致最誠摯之謝意。

參考資料

中文部分

(1) 日本文化女子大學文化服裝學院編：婦女服①，實踐管理學院服裝設計系譯。臺北：影清出版部。民國七十七年。
(2) 中國紡織工業研究中心：女裝打樣之基本原理。中國紡織工業研究中心印製。民國六十六年。
(3) 中國紡織工業研究中心：女裝基本原型之研究。臺北：中國紡織工業研究中心。民國八十年。
(4) 李玉龍：人體工學概論。臺北：六合出版社。民國七十九年。
(5) 李俊格、楊翠竹：服飾經銷。臺南：國友文化出版股份有限公司。民國七十九年。
(6) 邱魏津：臺灣地區女子（6-18 歲）人體計測調查之研究。技術學刊，民國七十七年，第三卷，第一期，81-100 頁。
(7) 邱魏津：臺灣地區女子（19-23 歲）人體計測調查之研究。技術學刊，民國七十七年，第四卷，第三期，民國七十八年，291-300 頁。
(8) 邱魏津：日本新 JIS 成人女子用衣料尺寸規格之分析。
(9) 教育部體育司編印：臺閩地區各級學校學生身高、體重、胸圍測量報告書。民國七十九年，第二十五期，8-9 頁。
(10) 陶嘉菊：成衣製作之體型資料分析。高級紡織品與成衣製作之技術研究，專題研究報告。臺北：中國紡織工業研究中心，民國六十二年。
(11) 葉玲玲等，輔大織品系流行展示中心中山區市場研究。臺北：輔仁大學。民國七十五年。
(12) 輔仁大學織品服裝學系「圖解服飾辭典」編委會編、繪、圖解服飾辭典。臺北：輔仁大學織品服裝學系，(1985)。
(13) 鄭國彬：臺灣地區 6-17 歲、18-34 歲、35-51 歲、52-65 歲成衣標準尺碼之擬訂，成果報告。民國八十年。
(14) 鄭國彬：臺灣地區 18-34 歲女性各年齡之分組資料。民國八十年。
(15) 鄭國彬：臺灣地區 18-34 歲女性身高以 5 公分爲間距之分組資料。民國八十年。
(16) 鄭國彬：臺灣地區 18-34 歲女性胸圍以 5 公分爲間距之分組資料。民國八十年。
(17) 縫製專業綜合月刊 P.I. Journal。Tokyo: Feb.，1990，p. 14。

日文部分

(1) 文化女子大學被服構成學研究室，三吉滿智子等編：被服構成學，理論編。東京：文化出版局，(1985)。
(2) 日本規格協會：日本人の體格調查報告書。東京：日本規格協會，(1970)。
(3) 近藤れん子：近藤れん子の立體裁斷と基礎知識。東京：株式會社モードエモード社，(1988)。
(4) 近藤れん子：計測原理システム基礎と應用。東京：建帛社，(1989)。
(5) JIS：L0111 衣料のための身體用語。

(6) JIS 衣料サイズ推進協議會：女子用衣料のサイズシステム。東京：JIS 衣料サイズ推進協議會，(1987)。

德文部分

(1) Forschungsinstitut Hohenstein: DOB-Grössentabellen. Köln: Verband der Damenoberbekleidungsindustrie e.v. (1983).

英文部分

(1) Aldrich, W., Metric Pattern Cutting for Menswear. 2nd. ed. London: BSP Professional Books (1990).
(2) Armstrong, H.J., Patternmaking for Fashion Design. New York: Harper & Row, Publishers, Inc. (1987).
(3) Bray, Natalie. Dress Pattern Designing. London: BSP Professional Books (1986).
(4) BS: British Standard 5511: Definitions and Body Measurement Procedure.
(5) C & A Handbook (1985).
(6) Coats & Clark's Sewing Books. New York: Western Publishing Co. (1976).
(7) Cooklin, Gerry. Pattern Grading for Women's Clothes. London: BSP Professional Books (1990).
(8) Debbie A. Gioello and B. Berke, Figure Types & Size Ranges. New York: Fairchild Publications (1979).
(9) Elizabeth G., Liechty, Della N. Pottberg and Judith A. Rasband, Fitting & Pattern Alteration: A Multi-Method Approach. New York: Fairchild Publications (1986).
(10) Hackler, Nadine. Fitting Guide in AAMA Consumer Affairs Committee, 1984, 2, (1), Line Apparel 25 Vol.
(11) I.S.O.: Standard 3635: 1981, Size Designation of Clothes-Definitions and Body Measurement Procedure.
(12) Kunick, Philip. Modern Sizing and Pattern Making for Women's and Children's Garment. London: Philip Kunick Publications (1984).
(13) Lynn C. Ferrari, Vogue Easy Sewing. New York: Harper & Row, Publishers (1987).
(14) Marion S. Hillhouse and Evelyn. A. Mansfield, Dress Design. Boston: Houghton Mifflin Co. (1948).
(15) P.J. Taylor and M.M. Shoben, Grading for the Fashion Industry. London: Stanley Thornes Ltd. (1990).
(16) Sears Handbook (1988).
(17) Smith, Patricia Burkhart. Making Your Clothes Fit. New York: Doubleday & Co., Inc. (1979).
(18) U.S. Department of Commerce. Body Measurements for the Sizing of Women's Patterns and Apparel, PS 42-70. Washington D.C.: Government Printing Office.

A Study of Sizing Survey and Bodice Block of Female Students from 18 to 26 Years Old

MEI-LIN FU

Textile and Clothing Department
Fu-Jen University

ABSTRACT

The scientific study of women's measurements, range of ages from 18 to 26 years, was taken in Fu-Jen University. The body measurement survey taken with a measuring tape, covered a sample of 301 female students and the figure type analysis survey, taken with silhouetter, covered a sample of 108 female students. In this study statistical average measurements were used to produce a sizing system and a bodice block.

The investigation of body measurement survey, using 43 measurements which included 16 girth measurements, 1 vertical measurement, 25 width/length measurements and weight. The investigation of figure type analysis survey, using 22 measurements which included body surface angles, body diameters, vertical measurements, and horizontal measurements.

兒童青少年性別角色刻板印象之探討

林 惠 雅

生活應用科學系

摘 要

本研究主要目的是探討兒童、青少年在人格特質、職業工作、家庭事務和玩具與活動的刻板印象以及性別、年齡間的差異。

依據父母教育程度、年齡與性別選取 360 名兒童、青少年爲對象，以自編「性別、角色刻板印象問卷」進行調查。結果的主要發現爲：㈠兒童、青少年對於男性化刻板印象的看法較爲一致；㈡一般而言，國小兒童比其餘年齡組受試者的性別角色刻板印象稍爲强烈，然而達顯著差異者不多；㈢男生在男性化刻板印象較女生强烈，而女生則在女性化刻板印象部份較男生爲强烈。但性別差異達顯著的部份多半屬於男性化刻板印象。

一、前 言

近年來有關性別角色 (sex role) 的課題逐漸受到重視。其原因可能是由於社會變遷、家庭與經濟結構亦有所改變，再加上教育程度普遍提高，以及婦女投入工作者愈衆等因素之影響，致使原有「男主外、女主內」等性別角色分配受到挑戰，於是性別角色有重新討論之必要。除此之外，對兒童、青少年而言，性別角色發展乃是社會化過程中相當重要的一環，藉由性別角色的發展，個體學得社會化所特定之適合自己性別的行爲，相對地，社會亦藉此來衡量其行爲是否合宜。故性別角色發展爲社會適應重要指標之一。

一般而言，性別角色可分爲三個層面：㈠性別概念 (gender concept)：指的是對性別的瞭解；㈡性別角色刻板印象 (sex role stereotype)：指的是社會大部份成員認爲比較適合男/女性或典型的男/女性的特質、行爲或動機等(Shaffer[1])；㈢性別角色行爲：實際表現行爲符合性別角色期望的程度 (Bee[2])。

國外有關性別角色發展的研究文獻相當豐富。就性別角色刻板印象發展的層面來看，許多研究指出在學齡前兒童時期即已形成 (Issacks[3]；Reis 和 Weight[4]；Suter、Seegmiller 和 Dunivant[5])。當孩子知道自己性別之後，性別角色刻板印象就開始逐漸形成，例如二歲半左右的男女孩均同意女孩愛說話，不打人、尋求協助、喜歡洋娃娃、幫媽媽做家事等；而男女孩也都認爲男孩喜歡玩汽車、建構組合東西、幫爸爸的忙，常說「我打你」(Hutson[6]；Weinraub[7])。而 Best 等人[8] 研究英、美、愛爾蘭四、五年級學生的性別角色刻板印象，結果顯示男女受試者都同意女生較情緒化、心地善良、富情感與乖巧世故；而同意男生

較有野心、肯定、攻擊、支配與冷酷。

許多研究發現五至十一歲兒童的性別角色刻板印象持續增加，且國小兒童的刻板印象最爲強烈（Best 等人[8]；Ullian[9]；Williams 等人[10]）。從學齡兒童至青少年階段，性別角色刻板印象則漸趨彈性（Carter 和 Patterson[11]；Emmerich 和 Shepard[12]）。至於性別角色刻板印象的性別差異，研究通常顯示男孩較女孩強烈（Fagot[13]），其可能的原因之一是父母要求男孩表現適合的性別角色行爲較女孩嚴格，而男孩承受這方面的壓力也比較大，所以男孩性別角色刻板印象會比較強烈。

國內以性別角色爲主題的研究也不少，研究趨向一來是以成人爲對象探討性別角色的類型（如李美枝[14]）。二來是研究性別角色和其他變項的關係，例如性別角色和自我防衛、生活適應、認知能力的關係（林邦傑[15]）；和數學成就的關係（材默英[16]；和價值觀念與人際吸引之相關（沈姍姍[17]）；和生活適應、學習成就的關係（何金針[18]）；和生活滿意度的關係（李蔚虹[19]）等。三來是以學前幼兒爲對象探討性別角色發展（李然堯[20]），或父母教養態度與幼兒性別角色發展的關係（王雪貞[21]），或兒童讀物對性別角色態度之影響（黃玉梅[22]）等。在這些研究趨向下，國內較缺乏探討由幼兒至青少年之性別角色刻板印象發展。本研究之主要目的有三：㈠探討兒童、青少年在人格特質、職業工作、家庭事務和玩具與活動四方面之性別角色刻板印象的內容；㈡不同年齡組受試者在上述四方面性別角色刻板印象的差異；㈢不同性別的受試者在上述四方面性別角色刻板印象的差異。

二、研究方法

1. 預備研究

預備研究的目的在於發展研究工具，即「性別角色刻板印象問卷」。

2. 研究對象

依據父母教育程度（上、中、下）、子女年齡（高中一年級、國中一年級、國小一年級與幼稚園中班）及子女性別選取父母 274 位。

父母教育程度分類標準如下：研究所 5 分；大專 4 分；高中 3 分，國中 2 分，小學及以下 1 分。以父母教育程度之得分總和劃分爲上 8 至 10 分；中 4 至 7 分；下 1 至 3 分。

3. 研究工具

本研究工具爲「性別角色刻板印象問卷」，主要是以人格特質、職業工作

、家庭事務及玩具與活動作爲調查性別角色刻板印象的層面。工具編擬的步驟如下：

(1) 參考國內外相關文獻，如 Fagot[13,23]、Newson 和 Newson[24]、李然堯[20]、王雪貞[21] 等，收集合適的題項。

(2) 設計開放式問卷，調查 54 位擁有幼稚園大班、國小一年級、國中一年級、高中一年級子女之父母，詢問父母對適合男、女孩的人格特質、職業工作、家庭事務與玩具與活動等方面的看法與項目。

(3) 綜合 (1) 與 (2) 編擬初步問卷，包括人格特質形容詞 48 題，職業工作 50 題，家庭事務 17 題，玩具與活動 44 題。每一題均有三個選項：適合（或形容）男孩（性）、適合（或形容）女孩（性）、適合（或形容）男女孩（性）。依據個人對一般男、女孩的看法選擇其中一項。

(4) 選取研究對象。

(5) 進行初步問卷調查。

(6) 參考 Fagot[23] 分析性別角色刻板印象的方法，選答「適合（或形容）男孩（性）」者以 +1 分計算，選答「適合（或形容）女孩（性）」者以 −1 分計算，選答「適合（或形容）男女孩（性）」者以 0 分計算。

(7) 計算每一題的平均數，平均數 ≥ 0.5 者爲男性化刻板印象之題項，平均數 ≤ -0.5 者爲女性化刻板印象之題項；以此選取題項的理由是若該題項的平均數 ≥ 0.5，則表示該題項有一半以上的人數認爲該項適合（或形容）男孩（性），反之，若該題項的平均數 ≤ -0.5，則表示有一半以上人數認爲該題適合（或形容）女孩（性）。故依此來作爲男性化刻板印象或女性化刻板印象題項的依據 (Fagot[23])。

(8) 依照 (7) 的計算方式，共選取男性化人格特質刻板印象 7 題，女性化人格特質刻板印象 7 題，男性化職業工作刻板印象 11 題，女性化職業工作刻板印象 9 題，男性化家庭事務刻板印象 3 題，女性化家庭事務刻板印象 4 題，男性化和女性化玩具與活動刻板印象各 7 題，共計 55 題（表一至表四）。

(9) 以 Cronbach α 求取上述各部份之內部一致性爲 0.810-0.747 之間。

(10) 完成問卷之編製。

4. 正式研究

(1) 研究對象

依據父母教育程度（上、中、下）、年齡（高中一年級、國中一年級、國小一年級及幼稚園中班）和性別選取受試者 360 名，其中每一年齡組各 90 名，

表一 男性化、女性化人格特質刻板印象各題項的平均數

男性化刻板印象		女性化刻板印象	
題項	$\bar{X}$	題項	$\bar{X}$
有力量	0.83	溫柔	−0.79
調皮	0.83	害羞	−0.76
膽大	0.79	漂亮	−0.71
隨便	0.65	細心	−0.67
愛好運動	0.55	順從	−0.60
粗魯	0.94	愛哭	−0.87
愛打架	0.93	愛計較	−0.64

表二 男性化、女性化職業工作刻板印象各題項的平均數

男性化刻板印象		女性化刻板印象	
題項	$\bar{X}$	題項	$\bar{X}$
消防隊員	1.00	褓姆	−0.93
漁夫	1.00	護士	−0.89
工人	0.97	家務管理者	−0.83
船員	0.96	車掌	−0.77
司機	0.92	秘書	−0.68
軍人	0.90	模特兒	−0.64
農夫	0.82	幫傭者	−0.64
工程師	0.73	店員	−0.58
電機設計者	0.71	舞蹈家	−0.50
運動員	0.55		
商人	0.55		

表三 男性化、女性化家庭事務刻板印象各題項的平均數

男性化刻板印象		女性化刻板印象	
題項	$\bar{X}$	題項	$\bar{X}$
修理電燈	0.89	煮飯	−0.77
修理器具	0.81	買菜清洗	−0.74
洗車	0.62	洗衣服	−0.73
		洗碗碟	−0.53

表四 男性化、女性化玩具與活動刻板印象各題項的平均數

男性化刻板印象		女性化刻板印象	
題項	$\bar{X}$	題項	$\bar{X}$
刀槍棒棍	0.94	刺繡	−0.96
木匠工具	0.88	洋娃娃	−0.94
爬樹	0.85	化粧工具	−0.92
機器人	0.77	裁縫	−0.81
釣魚	0.65	烹飪	−0.75
飛盤飛靶	0.55	舞蹈	−0.66
交通工具	0.55	扮家家酒	−0.61

男女各半。父母教育程度的分類標準和預備研究階段相同。

(2) 研究工具

本研究採用上述預備研究階段所編製完成的「性別角色刻板印象問卷」。問卷分爲人格特質、職業工作、家庭事務和玩具與活動四部份，每一部份均有男性化和女性化刻板印象的題項，共計 55 題。每一題有三個選項：適合（或形容）男孩（性）、適合（或形容）女孩（性）、適合（或形容）男女孩（性）。受試者依其對一般男女孩的看法加以選答。在男性化刻板印象題項部份，若選答適合（或形容）男孩（性）的選項，則在男性化刻板印象分數計算 1 分。而女性化刻板印象題項部份，選答適合（或形容）女孩（性）的選項，則在女性化刻板印象分數計算 1 分，否則均以分 0 計算。

(3) 進行步驟

(a) 選取臺北市／縣的幼稚園、國小、國中、高中各二至四所。
(b) 於各校選取男／女生各一班。
(c) 抄寫學生之父母教育程度、職業與學生出生日期等基本資料。
(d) 依據父母教育程度、學生性別以分層隨機方式選取受試者。
(e) 幼稚園大班幼兒、國小一年級學生由訪員至學校以一對一訪問方式進行，詢問受試者對每一題項的答案。而國中、高中受試者的進行方式則是由該班老師選擇某一段時間，研究者在該段時間將問卷發予受試者自行填寫，並加以收回。

三、結果與討論

1. 全體受試者在人格特質、職業工作、家庭事務和玩具與活動之性別角色刻板印象的內容

若以百分之七十五受試者的看法爲基準，受試者認爲常用來形容男孩的人格特質形容詞有調皮的 (79.2%)、粗魯的 (83.6%)、愛打架的 (90.0%)、有力量的 (91.9%)；常用來形容女孩的人格特質形容詞只有漂亮的 (85.8%)。受試者認爲適合男孩從事的職業工作爲船員 (92.8%)、軍人 (87.2%)、工程師 (78.1%)、消防隊員 (93.1%)、司機 (77.5%)、漁人 (88.1%) 及工人 (89.2%)；而適合女孩的職業工作爲保姆 (83.6%) 一項。受試者認爲適合男性的家庭事務爲修理器具 (88.6%)、洗車 (81.4%)、修理電燈 (90.6%)；至於女性化家庭事務刻板印象，沒有任何一項有百分之七十五以上受試者認爲是適合女性。最後，受試者認爲適合男孩的玩具與活動是機器人 (83.3%)、刀槍棒棍 (89.7%)、木匠工具 (85.8%)、爬樹 (81.7%)；適合女孩者則爲舞蹈 (75.6%)、裁縫 (83.9%)、洋娃娃 (94.2%)、化粧工具 (92.0%)、刺繡 (82.8%)。

由以上結果顯示，除了玩具與活動刻板印象之外，兒童、青少年對於男性化刻板印象的看法來得比女性化刻板印象一致。換言之，兒童、青少年具有較強烈的男性化刻板印象，對於女性化刻板印象則較爲彈性。這結果或許和一般社會或父母較嚴格要求男孩符合男性化刻板印象有關 (Fagot[25])。

2. 年齡差異

表五列出不同年齡組受試者在男性化、女性化人格特質、職業工作、家庭事務和玩具與活動刻板印象的平均數和標準差。

至於不同年齡組的差異，經單因子變異數分析後達顯著水準者有下列部份：(1) 女性化人格特質刻板印象 ($F_{(3,356)}=18.901$，$p<0.001$) (表六)，由薛費氏事後比較，高中組和國中組的刻板印象顯著高於國小組和幼稚園組。(2) 女性化職業工作刻板印象 ($F_{(3,356)}=4.379$，$p<0.01$) (表七)，事後比較發現高中組和國中組的平均數顯著高於幼稚圖組。(3) 男性化家庭事務刻板印象 ($F_{(3,356)}=3.6579$，$p<0.05$) (表八)，而國小組的刻板印象顯著高於國中組。(4) 女性化家庭事務刻板印象 ($F_{(3,356)}=30.981$，$p<0.001$) (表九)，薛費氏事後比較顯示國小組和幼稚園組的刻板印印高中組和國中組。(5) 女性化玩具與活動刻板印象 ($F_{(3,356)}=6.1878$，$p<0.001$) (表十)，國中組和國小組刻板印象高於幼稚園組。

表五 不同年齡組在各性別角色刻板印象部份的平均數和標準差

年齡 / $\bar{X}$ 與 SD / 刻板印象	高中		國中		國小		幼稚園		合計	
	$\bar{X}$	SD	$\bar{X}$	SD	$\bar{X}$	SD	$\bar{X}$	SD	$\bar{X}$	SD
男性化人格特質刻板印象（7）	5.53	1.30	5.52	1.55	5.62	1.18	5.10	1.71	5.44	1.46
女性化人格特質刻林印象（7）	5.44	1.37	5.13	1.56	4.53	1.36	3.97	1.43	4.77	1.53
男性化職業工作刻板印象（11）	8.47	1.54	8.29	1.92	8.90	1.84	8.23	2.45	8.47	1.97
女性化職業工作刻板印象（9）	5.91	1.75	5.79	1.91	5.71	1.68	4.99	2.16	5.60	1.91
男性化家庭事務刻板印象（4）	2.51	0.81	2.48	0.88	2.81	0.54	2.62	0.71	2.61	0.75
女性化家庭事務刻板印象（3）	2.01	1.46	2.21	1.43	3.43	0.81	3.24	1.06	2.73	1.37
男性化玩具與活動刻板印象（7）	5.40	1.44	5.31	1.63	5.14	1.48	4.82	1.82	5.17	1.61
女性化玩具與活動刻板印象（7）	5.49	1.32	5.79	1.25	5.93	1.08	5.12	1.74	5.58	1.40

註：（ ）內數字表示該部份刻板印象之總分。

表六 不同年齡組在女性化人格特質刻板印象的單因子變異數分析摘要表

變異來源	離均差平方和	自由度	均方	F 值
組間	115.9417	3	38.6472	18.901***
組內	727.9222	356	2.0447	
全體	843.8639	359		

*** $p<0.001$

表七 不同年齡組在女性化職業工作刻板印象的單因子變異數分析摘要表

變異來源	離均差平方和	自由度	均方	F 值
組間	46.6444	3	15.5481	4.379**
組內	1,263.7556	356	3.5449	
全體	1,310.4000	359		

** $p<0.01$

表八 不同年齡組在男性化家庭事務刻板印象的單因子變異數分析摘要表

變異來源	離均差平方和	自由度	均方	F 值
組間	6.1000	3	2.0333	3.6579*
組內	197.8889	356	0.5559	
全體	203.9889	359		

* $p<0.05$

表九 不同年齡組在女性化家庭事務刻板印象的單因子變異數分析摘要表

變異來源	離均差平方和	自由度	均方	*F* 值
組間	139.0750	3	46.3583	30.9810***
組內	532.7000	356	1.4963	
全體	671.7750	359		

*** $p<0.001$

表十 不同年齡組在女性化玩具與活動刻板印象的單因子變異數分析摘要表

變異來源	離均差平方和	自由度	均方	*F* 值
組間	34.7667	3	11.5889	6.1878***
組內	666.7333	356	1.8728	
全體	701.5000	359		

*** $p<0.001$

由表五的結果顯示國小組受試者在男性化人格特質、男性化職業工作、男性化和女性化家庭事務以及女性化玩具與活動五部份刻板印象的平均數是爲四組受試者中最高者。這或許反映國小兒童在上述刻板印象比其他年齡組來得稍微強烈一些。這與一些研究發現國小兒童的刻板印象較爲強烈，而青少年則較具彈性(如 Best 等人[8]；Carter 和 Patterson[11]；Emmerich 和 Shepard[12]；Meyer[26]；Ullian[9]；Williams 等人[10]) 的結果大致符合。

不過，在上述五部份刻板印象中，國小兒童顯著高於國中組或高中組的只有男性化和女性化家庭事務刻板印象。因此國小組的性別角色刻板印象和國中組、高中組比較下達顯著差異的部份不多。

有趣的是，在女性化人格特質、女性化職業工作及男性化玩具與活動三部份刻板印象，高中組受試者的平均數最高，且在女性化人格特質刻板印象的平均數顯著高於國小組。

至於幼稚園組在人格特質、職業工作和玩具與活動刻板印象的平均數均是四組受試者最低的。其原因可能是幼兒，尤其是四歲幼兒，其性別角色刻板印象才逐漸形成，另一種可能是幼兒對上述刻板印象的題項並不十分明瞭而導致這種結果。

3. 性別差異

表十一列出男女受試者在各刻板印象部份的平均數和標準差。

表十一 男女受試者在各性別角色刻板印象部份的平均數和標準差

性別 / $\bar{X}$ 與 SD / 刻板印象	男		女		合計	
	$\bar{X}$	SD	$\bar{X}$	SD	$\bar{X}$	SD
男性化人格特質刻板印象	5.64	1.50	5.25	1.39	5.44	1.46
女性化人格特質刻板印象	4.74	1.58	4.80	1.49	4.77	1.53
男性化職業工作刻板印象	8.65	1.97	8.29	1.96	8.47	1.97
女性化職業工作刻板印象	5.36	2.03	5.84	1.76	5.60	1.91
男性化家庭事務刻板印象	2.73	0.61	2.48	0.85	2.61	0.75
女性化家庭事務刻板印象	2.74	1.36	2.71	1.38	2.73	1.37
男性化玩具與活動刻板印象	5.45	1.57	4.89	1.60	5.17	1.61
女性化玩具與活動刻板印象	5.48	1.49	5.69	1.30	5.58	1.40

由表十一發現除了女性化家庭事務刻板印象之外，其餘在男性化刻板印象，男生的平均數高於女生；在女性化刻板印象，則是女生的平均數高於男生。經 t 考驗後，男女受試者在刻板印象達顯著差異者有男性化人格特質刻板印象（$t=2.55$，$p<0.05$）；女性化職業工作刻板印象（$t=2.44$，$p<0.05$）；男性化家庭事務刻板印象（$t=3.11$，$p<0.01$）及男性化玩具與活動刻板印象（$t=3.36$，$p<0.01$）。

上述結果顯示受試者對於符合自己性別的性別角色刻板印象持比較強烈的看法，而對於異性的刻板印象則較有彈性，這可能的原因之一是對自己性別的性別角色認同有關。不過，男女孩在刻板印象達顯著差異者多半屬於男性化刻板印象部份，因此，這或許仍反映男孩的刻板印象比女孩顯得強烈些。這和 Fagot[25] 的研究結果相似，如前所述，其可能的原因是父母對男孩的性別角色發展予以較大的壓力，致使男孩形成較強烈的性別角色刻板印象。

四、結　　論

綜合本研究結果可以發現：

(1) 百分之七十五以上的兒童、青少年認爲常用來形容男孩的人格特質有調皮的、粗魯的、愛打架的、有力量的；常用來形容女孩的人格特質爲漂亮的。而適合男孩從事的職業工作爲船員、軍人、工程師、消防隊員、司機、漁人和工人，適合女孩的職業工作只有保姆。至於家庭事務，適合男性的有修理器具、洗車、修理電燈，適合男孩的玩具的活動是機器人、刀槍棒棍、木匠工具、爬樹，適合女孩的則爲舞蹈、裁縫、洋娃娃、化粧工具、刺繡。

(2) 國小兒童在男性化人格特質、男性化職業工作、男性化和女性化家庭事務及女性化玩具與活動刻板印象的平均數最高，而其餘三部份的刻板印象以高中生的平均數較高，幼稚園幼兒的平均數則是最低。唯年齡差異在家庭事務刻板印象與女性化人格特質刻板印象達顯著水準。

(3) 一般而言，男生在男性化刻板印象比女生强烈，反之，女生在女性化刻板印象比男生强烈。而性別差異較顯著者多半爲男性化刻板印象，如男性化人格特質，男性化家庭事務及男性化玩具與活動刻板印象，女性化刻板印象只有職業工作一項。

參考文獻

(1) D.F. Shaffer, *Developmental Psychology* (2nd ed.), Belmont, CA: Brooks/cole Publishing Company (1989).

(2) H. Bee, "The Developing Child", N.Y.: Harper and Row (1985).

(3) L.A. Issacks, "Sex Role Sterotyping as it Relates to Ethnicity, Age and Sex in Young Children", *Dissertation Abstracts International*, **41**(10), 4276-A (1981).

(4) H.T. Reis and S. Wright, "Knowledge of Sex-Role Stereotype in Children Aged 3 to 5", *Sex Roles*, 8(10), 1049-1056 (1982).

(5) B. Suter, B.R. Seegmiller and N. Dunivant, "Effects of Age, Sex, and Income Level on Sex-Role Differentiation in Preschoolers", *The Journal of Psychology*, **104**, 217-220 (1980).

(6) A.C. Hutson, *Sex Typing*, In P.H. Mussen (Ed.), Handbook of Child Psychology: Socialization, Personality and Social Development, Vol. 4, 387-467, N.Y.: John Wiley and Sons (1983).

(7) M. Weinraub, L.P. Clemens, A. Sockloff, T. Ethridge, E. Gracely and B. Myers, "The Development of Sex-Role Stereotypes in Third Year: Relationships to Gender Labeling, Gender Identity, Sex-Typed Toy Preferences, and Family Characteristics", *Child Developmeht*, **55**, 1493-1503 (1984).

(8) D.L. Best, J.E. Williams, J.M. Cloud, S.W. Davis, L.S. Robertson, J.R. Edwards, H. Giles and J. Fowels, "Development of Sex-Trait Stereotypes Among Young Children in the United States", *England and Ireland, Child Development*, **48**, 1375-1384 (1977).

(9) D.Z. Ullian, "The Child's Construction of Gender: Anatomy as Desting", In E.K. Shapiro and E. Weber (Eds.), Cognitive and Affective Growth, Hillsdale, N.J.: Erlbaum (1981).

(10) J.E. Williams, S.M. Bennett and D.L. Best, "Awareness and Expression of Sex Stereotypes in Young Children", *Developmental Psychology*, **11**, 635-642 (1975).

(11) D.B. Carter and C.J. Patterson, "Sex Roles as Social Conventions: The Development of Children's Conceptions of Sex-Role Stereotypes", *Developmental Psychology*, **18**, 812-824 (1982).

(12) W. Emmerich and K. Shepard, "Development of Sex Differentiated Preferences During Late Childhood and Adolescence", *Developmental Psychology*, **18**, 406-417 (1982).
(13) B.I. Fagot, "Sex Differences in Toddlers' Behavior in Preschool Children", *Child Development*, **48**, 902-907 (1974).
(14) 李美枝，「女性心理學」，臺北：大洋出版社 (1984)。
(15) 林邦傑，「性別角色與自我防衛、生活適應、認知能力的關係」，中華心理學刊，**23**(2)，187-199 (1981)。
(16) 李默英，「性別、年級、數學學習態度、性別角色和數學成就之關係」，政治大學教育研究 (1983)。
(17) 沈姍姍，「性別角色、價值觀念與人際吸引之相關研究」，政治大學教育研究所 (1984)。
(18) 何金針，「國中學生性別角色與生活適應、學習成就之關係」，師範大學教育研究所 (1986)。
(19) 李蔚虹，「已婚婦女的現代化程度、性別角色與生活滿意度之研究」，師範大學社會教育研究所 (1988)。
(20) 李然堯，「中國兒童性別角色發展之研究」，師範大學教育研究所 (1983)。
(21) 王雪貞，「父母之性別角色教養態度、性別特質對學前兒童性別角色之影響」，師範大學家政教育研究所 (1985)。
(22) 黃玉梅，「兒童讀物對兒童性別角色態度之影響研究」，中國文化大學家政研究所 (1989)。
(23) B.I. Fagot, "The Influences of Sex of Child on Parental Reactions to Toddler Children", *Child Development*, **49**, 459-465 (1978).
(24) J. Newson and E. Newson, "Family and Sex Roles in Middle Childhood", In D.J. Hargreaves and A.M. Colley (Eds.), The Psychology of Sex Roles", 142-158, N.Y.: Harper and Row (1986).
(25) B.I. Fagot, "Consequences of Moderate Cross-Gender Behavior in Preschool Children", *Child Development*, **48**, 902-907 (1977).
(26) B. Meyer, "The Development of Girls' Sex-Role Attitudes", *Child Development*, **51**, 508-514 (1980).

Sex-Role Development of Children and Adolescents in Taiwan

HUEY-YA LIN
Department of Applied Life Science

ABSTRACT

This study has two main goals: (1) to investigate sex-role stereotypes of children and adolescents in the areas of personality characteristics, vocations, family matters and toys and activities; (2) to examine the differences among various age-groups as well as the differences between boys and girls. Three hundred and sixty subjects of both sexes were divided into four age groups (4. 7. 13. 16). Within groups, they were equally divided among parents' educational levels. Results showed the following: (1) In general, first-grade children had stronger sex-role stereotypes than the other three age-groups. (2) When questioned how they felt about traditional male stereotypes, most of boys agreed that these stereotypes are the truth. When girls were questioned how they felt about traditional female stereotypes, most girls agreed that these stereotypes are the truth.

ABSTRACTS OF PAPERS BY FACULTY OF THE COLLEGE OF SCIENCE AND ENGINEERING THAT APPEARED IN OTHER REFEREED JOURNALS DURING THE 1992 ACADEMIC YEAR

Gevrey Property of Formal Solutions of a Differential System

CHING-HER LIN (林清河)

Bulletin of the Institute of Mathematics Academia Sinica,
Volume 19, Number 4, December (1991)

In this paper, a nonlinear differential system with a parameter is investigated. It is shown that the system admits a unique formal solution. Furthermore this series is of Gevrey order 1 uniformly on a domain.

Robust Tests in Statistical Quality Control

PAUL J. SMITH AND SY-MIEN CHEN (陳思勉)

Joint Statistical Meetings, August 8-13 (1992)

In this paper, we construct robust hypothesis testing procedures for acceptance sampling by variables. Here, one wishes to control the proportion of a lot in which a quality characteristic X falls below a lower specification limit LSL. Hence we wish to test hypothesis that X falls below LSL with probability at most p_0. The usual plans, which assume normality and are based on thenoncentral t distribution, are not robust when the data is not normal. We construct robust procedures by extending Huber's robust minimax tests to composite hypotheses. We study the performance of our procedures by simulation and establish their approximate distribution and robustness.

SERS in Sandblast Roughened Metal Surface

K. J. LING (凌國基), W. S. TSE, P. PENG, S. H. SHEN,
K. T. SUN AND S. J. LIN

Phys. Stat. Sol., **128**, K123 (1991)

The discovery of surface enhanced Raman scattering (SERS) in 1974 /1/ has generated considerable excitement in the physics and chemistry communities. In this note a more detailed experiment on crystal violet (tri-*p*-dimethylamino phenylcarboniumion ion) and TCNQ (7, 7, 8, 8, tetracyanoquinodimethane) in sandblast roughened metal surfaces (Ag, Au, Al, Pt, Cu) is presented. Usually a silver-coated substrate has an interface between the silver film and the base material. Atmospheric moisture or water can penetrate into the interface and spoil the silver-coated substrate /2/. But with the sandblast method, because the roughened surface is made by removing part of the silver surface, there is no interface. The substrate should be able to last much longer than those prepared by vacuum coating. Furthermore, because the roughness is almost only dependent on the size and speed of the abrasive, the roughness of the surface is more reproducible. With some improvement in the future this kind of substrate making method may also becomes an alternative candidate for SERS measurement in chemical analysis.

A Study of Velocity Fluctuation Spectra in the Troposphere and Lower Stratosphere Using MU Radar

F. S. KUO (高士達), H. Y. LUE (呂秀鏞), C. M. HUANG,
C. L. LO, C. H. LIU, S. FUKAO AND Y. MURAOKA

Journal of Atmospheric and Terrestrial Physics, **54**(1), 31-48 (1992)

We present an anlysis of the vertical wave number and frequency spectra of atmospheric motions in the height ranges between 5 and 25 km observed using the Shigaraki, Japan, MU radar during a 4-day period in January 1988. The vertical wave number spectrum of the horizontal velocity fluctuation is found to saturate at large wave numbers satisfying power law $\sim N^2/2K^3$, while departing from this -3 power law at small

wave numbers. Frequency spectra of the oblique radial velocity fluctuations can be fitted by a Garrett-Munk gravity wave model spectrum. However, the vertical velocity fluctuation cannot be fitted simultaneously. The observed spectra are too steep and their energy levels are too low compared with the results from model prediction. Also, the vertical profiles of the energy densities of the horizontal velocity fluctuations are found to be positively correlated to the background wind velocity profile. These characteristics of the observed spectra are satisfactorily explained by dynamic instability and wave-wave interactions in the regions below the critical layer through nonlinear numerical simulations. The correlation between the background wind and the horizontal velocity fluctuations is shown to result from wave-shear interaction.

Numerical Simulations of the Saturated Gravity Wave Spectra in the Atmosphere

C. M. HUANG, F. S. KUO (高士達), H. Y. LUE (呂秀鏞) AND C. H. LIU

Journal of Atmospheric and Terrestria Physics, 54(2), 129-142 (1992)

A two dimensional numerical model is used to compute the saturation of small scale gravity waves in the region uear the critical level. The vertical wave number spectrum of horizontal velocity fluctuations in the unstable region (USR) where shear instability develops is found to be governed by wave-shear interaction and follows a theoretical saturation spectrum $\sim\omega_b^2/2m^3$. Wave-shear interaction is also found to be responsible for the observed fact that the variance of vertical velocity fluctuations is significantly lower than the level predicted by linear gravity wave theory. On the other hand, the corresponding spectrum in the stable region (SR) following a much shallower spectJum $\sim m^{-2}$ is found to result from the combined effects of wave-wave interactions and eddy diffusion. The key step in our simulation is the separate parameterization of horizontal and vertical eddy diffusion coefficients instead of a constant molecular viscosity coefficient.

A Study of the Power Spectra of Scintillations in Taiwan and Implications Regarding the Mechanisms Involved

JOHN R. KOSTER (高士達), H. Y. LUE (呂秀鏞)
AND H. S. WU

Pacific Regional STEP Conference, pp. 132-151 (1991)

Most low latitude scintillations in the Asian sector seem to be due to the equatorial bubble (EB) mechanism, but doubt remains about the June scintillations, especially those occurring during low sunspot years. In an effort to resolve this question, over a thousand power spectra of Taiwan scintillations have been produced. A study of occurrence times, S4 values, asymptotic slopes and other characteristics of the spectra leads to the conclusion that only a small fraction of the Taiwan night-time scintillations during summer can be accounted for by equatorial bubbles. The remainder must arise from a different physical mechanism. They are similar in seasonal distribution to the midlatitude (ML) type of scintillations found in published Tokyo data. Most equinoctial scintillations in Taiwan are of the bubble type, and give convincing evidence of multiple scattering. At such times, the total received power decreases, scintillation frequency is high, and S4 values are relatively low. A search for a lunar monthly component in the probability of summer time scintillations is in progress, but the result is still inconclusive.

Light Scattering Studies in ZBLAN Glasses at High Temperature

J. SCHROEDER, L. G. HWA (華魯根), L. BUSSE
AND I. AGGARWAL

Material Science Forum, **67/68**, 471-476 (1991)

We studied the intrinsic light scattering behavior of a particular halide glass (ZBLAN) using the techniques of high temperature light scattering. The technique of high temperature light scattering allows us to determine the temperature and time dependence of the Landau-Placzek ratio of the ZBLAN glass up to and through the glass transition

temperature. The behavior of the Landau-Placzek ratio will then give indications as to the existence of critical demixing processes and also allow the calculations of the equilibrium compressibility. Mechanisms responsible for extrinsic scattering have also been probed by the high temperature light scattering techniques and interpreted in the light of existing theories.

Intramolecular Diels-Alder Reactions via 3-(Phenylthio)-4-(trimethylsilyl)-3-sulfolene

SHANG-SHING P. CHOU (周善行) AND CHIEN-MING LEE (李堅明)

Journal of the Chinese Chemical Society, 38, 491-496 (1991)

Deprotonation of the title compound 2 followed by treatment with 5-iodo-1-pentene or 6-iodo-1-hexene gave the alkylated products 3 and 4 which upon refluxing in toluene yielded the dienes 8a and 8b. Intramolecular Diels-Alder reactions were achieved by heating the dienes 8a and 8b in toluene in a sealed tube at 160-180°C to give bicyclo[4.3.0]nonene 9 and bicyclo[4.4.0]decene 10, respectively, in good yield. The stereochemistry of the cyclization products was determined, and was rationalized by comparison of the possible transition states involved.

Novel Nucleophilic Additions to [η^4-2-(Phenylsulfonyl)-1, 3-butadiene]tricarbonyliron(0) Complex

SHANG-SHING P. CHOU (周善行), CHIEN-HUNG HSU AND MING-CHANG P. YEH

Tetrahedron Letters, 33(5), 643-646 (1992)

Reactions of the title compound (1) with various nucleophiles give the addition products (2) regio- and stereospecifically in good yield.

Dialkylative Cyclization Reactions of 3-(Phenylthio)-3-sulfolenes

SHANG-SHING P. CHOU (周善行), CHIN-CHUNG SUNG (宋清泉) AND DER-JEN SUN (孫德崢)

Journal of the Chinese Chemical Society, **39**, 333-338 (1992)

3-(Phenylthio)-3-sulfolene (**4**) underwent bridged dialkylative cyclization with 2-methylene-1,3-diiodopropane to give the bridged bicyclic 3-sulfolene **23**, and spirodialkylation with 1,4-diiodobutane and 1,5-diiodopentane to give the spiro bicyclic 3-sulfolenes **15** as the major product. The reaction of **4** with 1,3-diiodopropane led to the fused bicyclic 2-sulfolene **12**. 3-(Phenylthio)-3-sulfolenes bearing an ω-iodoalkyl group at the C-2 position gave the fused bicyclic 2-sulfolenes **28** and/or the spiro bicyclic 3-sulfolene **29** depending on the chain length.

Reduction of $[Os(NH_3)_5(\eta^1\text{-}CH_3CN)]^{2+}$ to $[Os(NH_3)_5(\eta^2\text{-}CH_3CH{=}NH_2)]^{3+}$

TAI HASEGAWA, KEH SHIN KWAN (管克新) AND HENRY TAUBE

Inorganic Chemistry, **31**, 1331 (1992)

The reduction of $[Os(NH_3)_5(CH_3CN)](O_3SCF_3)_3$ or of $[Os(NH_3)_5(O_3SCF_3)](O_3SCF_3)_2$ in acetonitrile by zinc amalgam yields a product of composition corresponding to the formula $[Os(NH_3)_5(\eta^2\text{-}CH_3CH{=}NH_2)](O_3SCF_3)_3$ (**4**). Proton NMR spectroscopy shows a large splitting between cis and trans ammines and for the heteroligand shows a patten consistent with the structure proposed. In particular three equivalent protons and ane other proton are not exchangeable with desterium in methanol-d_4 while two protons, inequivalent as observed in acetonitrile-d_3, are. Although some **4** is formed also in dried CH_3CN, the yield is much increased when a small amount of water is added. Compound **4** is quite stable in solution in DME, but when Proton Sponge (1,8-bis(dimethylamine)naphthalene) is added, deprotonation to produce

$[Os(NH_3)_5(CH_3CH{=}NH)]^{2+}$ takes place, which then disproportionates to yield the acetonitrile complex as one of the products. The value of pK_a for the corresponding protonation-deprotonation equilibrium quotient, $[Os(NH_3)_5(\eta^2\text{-}(CH_3)_2C{=}NH_2)]^{3+} = [Os(NH_3)_5(\eta^1\text{-}(CH_3)_2C{=}NH)]^{2+} + H^+$, for the more stable analogue derived from acetone in water at room temperature was measured as 10.3 ± 0.2.

The 3-(3′-Pyridyl)Sydnone Complex of Pentacyanoferrate(II)

CHARNG-SHENG LIN, ANDREW YEH, TSUN-YANG LIU, KEH SHIN KWAN (管克新), DEREK J. HODGSON AND HSIEN-JU TIEN

Inorganica Chimica Acta, **192**, 81-86 (1992)

The 3-(3′-pyridyl)sydnone (3-PySd) complex of pentacyanoferrate(II) was prepared and characterized both in aqueous solution and in the isolated state. A comparison of ^1H NMR results between the free and the coordinated ligand indicates that the metal center is coordinated to the ligand through the pyridine nitrogen atom. A metal to ligand charge transfer band was observed at $\lambda_{max}=410$ nm and $\epsilon_{max}=3.20\times10^3\ m^{-1}\ cm^{-1}$. The rate constants of formation and dissociation of the complex were measured; the k_f and k_d values at $\mu=0.10$ M ($LiClO_4$), pH=5 and $T=25°C$ are $5.62\times10^2\ M^{-1}\ s^{-1}$ and $3.23\times10^{-3}\ s^{-1}$, respectively. A cyclic voltammetric study of the complex has shown that the Fe^{II}-Fe^{III} oxidation is a reversible one-electron process with $E_{1/2}=0.54$ V versus NHE. The strong electron withdrawing power of the sydnone is demonstrated by both the spectral and the electrochemical properties of the title complex in comparison with those of the pyridine and 3-substituted pyridine complexes. This result is consistent with the assignment of the sydnones to the family of non-benzenoid aromatic compounds.

Synthesis of Bi- and Tetranuclear Sulfur Ylide Complexes of Gold(I) by Phase-Transfer-Catalysis Techniques

IVAN J. B. LIN (林志彪), C. W. LIU, LING-KANG LIU AND YUH-SHENG WEN

Organometallics, 11, 2311 (1992)

The luminescent binuclear sulfur ylide gold compound $\{Au_2(dppm)[(CH_2)_2S(O)N(CH_3)_2]\}BF_4$ (**1**; dppm=$Ph_2PCH_2PPh_2$) and the tetranuclear sulfur ylide gold compound $\{Au_4(dppm)(Ph_2PCHPPh_2)[(\mu\text{-}CH)(CH_2)S(O)N(CH_3)_2]\}BF_4$ (**2**) have been synthesized by phase-transfer-catalysis techniques. Crystal structure studies show that the molecules of **1** are packed pairwise with shorter inter- than intramolecular Au···Au distances and that **2** has triply briding $Ph_2PCHPPh_2$- and $(CH)(CH_2)S(O)N(CH_3)_2^{2-}$ ligands.

Palladium-Catalyzed Hydroesterification of Alkenes in the Presence of Molecular Hydrogen

IVAN J. B. LIN (林志彪), J. C. LIAO (廖志成) AND C. C. CHUANG (鍾杞泉)

Journal of the Chinese Chemical Society, 38, 483-486 (1991)

The effects of molecular hydrogen on the palladium-catalyzed alkene-alcohol-carbon monoxide and alkene-formate reactions have been studied. Yields of esters were generally increased, especially in the alkene-formate reaction, in which an improvement up to 46% yield has been observed. A possible explanation is proposed in which the molecular hydrogen promotes the oxidative addition of formate to palladium. Decarbonylation of formate ester is unlikely to be the initial step.

Palladium-Catalyzed Formate-Nitrobenzene-Carbon Monoxide Reaction: Formation of Carbamate Ester

IVAN J. B. LIN (林志彪) AND CHING-SHENG CHANG

Journal of Molecular Catalysis, **73**, 167-171 (1992)

The catalyst $PdCl_2(PPh_3)_2$, together with $OP(n\text{-}Bu)_3$ and KBr, can promote the reaction of formate ester with nitrobenzene under carbon monoxide atmosphere to produce *N*-phenylcarbamate. This formate-nitrobenzene-carbon monoxide reaction did not involve the formation of aniline before the carbamate ester formation.

利用昆蟲細胞及幼蟲生產外源蛋白

王重雄　羅竹芳

有用昆蟲研討會　中華昆蟲特刊第五號　第 153-161 頁　(1990)

桿狀病毒 (baculovirus) 爲昆蟲主要病原體，可分成 A、B 及 C 群，其中 A 群病毒卽爲核多角體病毒 (nuclear polyhedrosis virus)。自 1983 年 Smith 等人將此病毒開發成眞核細胞表現載體 (eukaryotic expressing vector，EEV) 稱之爲桿狀病毒表現載體 (baculovirus E. V.)，以此載體生產外源蛋白，促使桿狀病毒的研究範圍除應用於生物防治外，另外再開拓了一條嶄新且頗具潛力的生物技術領域。核多角體病毒具有一些非必要基因 (nonessential genes)，病毒若缺乏這些基因，並不影響病毒在昆蟲細胞及幼蟲體內的複製與增殖，這些非必要基因中，有一主要的基因是形成多角體蛋白 (polyhedrin)，此蛋白可以和病毒粒子結晶成核多角體 (polyhedral inclusion body 稱之 PIB)，用以作爲蟲與蟲間的感染。將核多角體病毒的 DNA 純化後，選殖出非必要基因 (如多角體蛋白基因，polyhedrin gene 或 P 10 基因)，利用限制酶切割，將非必要基因之構造性基因 (structure gene) 之全部或部份切除，再銜接入外來基因 (foreign gene)，卽將外來基因接於此基因之強勢啓動子 (promotor) 之後，再與野生型 DNA 進行共轉染 (cotransfection) 於細胞株之細胞，而得到重組病毒 (recombinant virus)，將重組病毒感染細胞或幼蟲，則此病毒於細胞內或幼蟲體內進行病毒的複製 (replication)、轉錄 (Transcription) 及轉譯 (Translation) 過程中，連帶地產生大量的外源蛋白。目前已有 50 種以上的外源蛋白經此系統成功的表現，或外源蛋白包括的範圍甚廣，如干擾素 (α 或 β-interferon) 和疫苗 (vaccine，如 B 型肝炎表面抗原，愛滋病毒抗原等) 等，目前世界研究潮流除尋求更多的外源基因表現外，亦趨向於影響表現率之調節因子的研究。

Viral Polypeptides and RNA of Defective Interfering Particles of IPN Virus Generated by Serial Undiluted Passaging in TO-2 Cells

CHU-FANG LO AND CHUNG-HSIUNG WANG (王重雄)

Gyobyo Kenkyu, **26**(3), 119-125 (1991)

HB-1 virus, a strain of infectious pancreatic necrosis virus (IPNV), was isolated from hard clam, *Meretrix lusoria*, with TO-2 cell line derived from tilapia ovary. The defective interfering (DI) particles of HB-1 virus could be generated by serial undiluted passaging. The polypeptides and RNA in virus particles of diluted and undiluted virus preparations were compared in order to investigate the nature of defective interfering particles involved in viral interference of HB-1 virus. Cesium chloride density gradient centrifugation was applied to purify virus particles of diluted and undiluted virus preparations. By comparing the polypeptides and RNA in virus particles of diluted and undiluted virus preparations, it was revealed that (I) the virus particles of undiluted virus preparation had smaller β polypeptides than normal; (II) subgenomic RNA of large segment was found in virus particles of undiluted virus preparation. These two findings suggested that DI particles of HB-1 virus was a deletion mutant of standard virus.

This is the first report indicating the polypeptides and RNA possibly related to IPN virus DI particles.

The Characterization of Clonal Cell Strains Derived from Established IPLB-SF 21AE Insect Cell Line

CHUNG-HSIUNG WANG (王重雄), HSU-WEI HUNG, GUANG-HSIUNG KOU AND CHU-FANG LO

Acta Zoologica Taiwanica, **3**(1), 35-46 (1992)

By dilution plating, a total of fifty-four clonal cell strains were initially isolated from the established IPLB-SF 21AE cell line. Eleven clonal cell strains, 2-4G, 2-6G, 5-2E, 5-5C, 6-9B, 6-10A, 7-2G, 7-3C, **7-6H**, 8-3C, and 8-5D, were selected for further studies, on the basis of

their susceptibility to insect nuclear polyhedrosis virus (NPV). The clonal cell strains differed in their morphology, cell doubling time, and the susceptibility to *Autographa californica* nuclear polyhedrosis virus (Ac NPV) and NPV isolated from the moribund larvae of *Spodoptera exigua*. Comparisons of isozyme profiles of clonal cell strains with the parental cell line and four other insect cell lines, which were maintained routinely in our laboratory, were made for confirming their origin. With the present study, we provide IPLB-SF 21AE clonal cell strains that are more susceptible and produce more occlusion bodies upon infection with insect NPV of interest.

關渡自然公園解說設施整體規劃研究報告

林曜松　李瑞琪　陳擎霞

臺北市政府建設局　中華民國野鳥協會　共 300 頁　(1991)

關渡自然公園及其南面的沿澤區之自然解說資源相當豐富，無論其地理位置、地質、河域生態、鳥類及沼澤動植物，潮汐的升降、食物鏈、鳥類的遏徙、各種動物的適應、生物族群的變化、河川的汚染、沼澤區的價值等都是重要的環境教育資源。

由前面第四章遊客調查得知，目前基地上遊客對關渡地區的評價特別重視當地的生態價值與環境美質。他們來此目的爲了欣賞自然環境、看紅樹林、賞鳥、散散心及呼吸新鮮空氣者，乃佔全部遊客的 80%。至於潛在遊客群，則以賞鳥、認識沼澤動植物及生態、接受環境保育觀念、介紹公園等爲主要解說機會需求重點。因此就全案而言，遊客在自然公園內，接受外界環境刺激（解說資源或資訊）之反應有時是個別的，有時是整體的，個別的如地形（河口）、植物（如水筆仔）、動物（如候鳥、招潮蟹、彈塗魚），因此可分別介紹個別的靜態美質特性（如體態、季節之變化）。至於是整體印象，可以特別介紹關渡自然公園內環境生態保育的特性，並強調其與日常生活環境甚至都市公園等美感上之差異。若遊客爲賞鳥而來的，則可特別強調對鳥的美質介紹，諸如各種野鳥的體形、羽毛、體色、飛翔、行走、啄食、鳴聲等特性。

除此之外，自然公園在環境教育之推廣和配合學校教育等方面亦負有重大使命。有關詳節一併討論於後。

德基水庫集水區植被調查

陳　擎　霞
臺灣省政府經濟部德基水庫集水區管理委員會
德基水庫集水區第三期整體治理規劃報告

水庫集水庫集水區在雪山、品田、池有、桃山、南湖大山、中央尖山、畢祿、合歡，群山的環境下，不祇承受這些大山水資源的供應，也與大山上植被的狀況息息相關，由於集水區內群山起伏，山谷交錯、地形複雜，其植物社會也隨之變化，使此地區擁有暖溫帶、冷溫帶、亞寒帶各種植型，也包含了岩原、草原、森林等不同植相使該地區擁有一千零四十五種植種及五十種稀有植物，這些稀有植種絕大多與高山冰斗、冰岩地形有關，故此集水區應由國家公園管理處劃爲自然保留區，加強保護，以免有遺珠之憾。

太魯閣國家公園動物相及海拔高度、植被之關係研究

林曜松　盧堅富　梁輝石　陳擎霞
太魯閣國家公園管理處　共 59 頁　(1991)

本研究於太魯閣國家公園境內，由平地至高海拔選定樣區，並配合植被調查作有系統的探討動物與海拔高度及植被之關係。研究區內之植被幾乎涵蓋臺灣各垂直帶之植被。植物種類至少有 294 種分別隸屬於 103 科 215 屬。動物方面則有 13 種兩棲類、28 種爬蟲類、31 種哺乳類及 139 種鳥類。其中兩棲類之種數隨海拔之升高而遞減，而鳥類、哺乳類和爬蟲類則由低海拔往高海拔漸增，至海拔 2,000 公尺達到最高峰。至於優勢種動物則以分佈較局限之地區性優勢種爲主。另外，動物對棲地之使用上，鳥類、大型哺乳類以原始闊葉林爲主要棲息環境，其次爲次生闊葉林，而草原、崩塌地及破壞較嚴重之地區，其動物之種類及數量均不多。此外，對植相與動物、植層與動物及植物疏密與動物活動等各相關性，也都有詳細之探討。

宜蘭縣野生植物之調查

於幼華　駱尚廉　陳擎霞
宜蘭縣環境品質規劃研究案　宜蘭縣政府委託
財團法人馮繼華、林清涼環境　8，1-49 (1991)

宜蘭縣在雪山山脈北支稜及中央山脈北峰南湖大山的環境下、三面環山、一

面臨海。在 21 萬多公頃 (213,746) 的面積內，高山林立，三千公尺以上的高山就有 3 座。這些山區不但承受東北季風所帶來的大量雨量，同時也是供應蘭陽地區各溪流的主要水源。而整個蘭陽平原就在蘭陽溪、福德溪、得子口溪、大湖溪、寒溪、武荖坑溪、南澳溪的沖刷下，淤積而成。

在宜蘭縣十二個鄉鎮中，以大同鄉與南澳鄉面積最大，佔全縣之半，境內大都爲一千公尺以上的高山，是屬於高山針葉林及山地闊葉林區。臺灣有名的太平山林場就在境內。至於頭城鎮、礁溪鄉、員山鄉、三星鄉、冬山鄉與蘇澳鎮皆屬於丘陵與平原交合處。這些地區除部份丘陵地尚俱有溫帶闊葉雨林外，大都開闢爲果園及農田。而壯圍鄉、五結鄉、羅東鎮及宜蘭市之平原部份，除溪口少數沼澤地外，已極度開發。成爲人口滙集處。亦爲水稻、蔬、魚、蝦栽培養殖區。

預測狀態觀測器應用於直流伺服系統之研究

曾榮泰　潘純新

Journal of Electrical Engineering, **35**(1), 81-92 (1992)

本文提出預測狀態觀測器應用於以微處理器爲基礎之直流馬達速度控制系統之研究，目的是解決數位控制系統中所遭遇的兩大問題：截捨誤差與時間延遲，使系統在極短的取樣週期下能滿足暫態及準確性的要求，首先使用系統判別求得馬達參數值，再利用零差響應的控制法則設計數位控制器，並以預測狀態觀測器重建馬達的眞實速度而不是用編碼器回授信號爲眞實速度，且用其預測性質事先計算下一取樣週期的控制輸出以解決時間延遲問題，同時在硬體製作上以數學輔助處理器 INTEL 8087 作精確的實數運算以徹底解決截捨誤差問題，最後，再以相同法則建立傳統 PID 系統與本文預測狀態觀測器系統作一比較，並將兩系統建構於 IBM PC 電腦介面實際控制脈寬調變馬達系統，結果顯示含觀測器系統優於傳統 PID 系統。

Application of Superconducting Magnetic Energy Storage Unit to Improve the Damping of Synchronous Generator

CHI-JUI WU AND YUANG-SHUNG LEE (李永勳)

IEEE Transactions on Engrgy Conversion, **6**(4), 573-578 (1991)

A systematic approach is presented to design a controller for superconducting magnetic energy storage (SMES) unit to improve the dynamic stability of a power system. The developed scheme employs

a proportional-integral (PI) controller to enhance the damping of the electromechanical mode oscillation of synchronous generators. The parameters of the proposed PI controller are determined by pole assignment method based on modal control theory. Eigenvalues analysis and nonlinear computer simulations show that SMES with the PI controller can greatly improve the damping of system under various operating conditions.

The Minimum Storage Cascade Transformed Structure Fealization of the Filters Disigned by McClellan Transformations

BRIAN K. LIEN (連國珍)

Proceedings of the NSC—Part A: Physical Science and Engineering (1992)

The multidimensional finite impulse response (FIR) filters designed by the McClellan transform can be implemented efficiently by the direct transformed structure, transpose direct transformed structure, cascade transformed structure, Chebyshev structure and the reversed Chebyshev structure. In this paper, the minimum storage implementation of the cascade structures is presented. For a (2NP+1)*(2NP+1) filter, it is found that implementation of the cascade transformed structure requires only 2NP rows of storage, which is the minimum storage the FIR filter can reach.

On the Cascade Realization of 2-D FIR Filters Designed by McClellan Transformations

BRIAN K. LIEN (連國珍)

IEEE Trans. on Acoustics, Speech, Signal Processing, September (1992)

The multidimensional finite impulse response (FIR) filters designed by McCellan transform can be implemented efficiently by the direct transformed structur, transpose direct transformed structure, cascade structure, Chebyshev structure, and reversed Chebyshev structure. In this

correspondence, peak scaling and section reconfiguration are provided to modify the cascade structure realization. The modifications result in a reduction in the output roundoff noise power and the number of operations required.

Developing and Evaluating an Expert System to Support Media Selection

PING-CHENG CHAO (趙平正)

National Convention of the Technology and Innovations in Training and Education Conference (1991)

The purpose of this research was to develop and evaluate a Media Selection Expert System (MSES) to address four significant limitations common to existing media selection models and media selection expert systems. The four limitations are that existing systems: are too complicated to be effectively used by instructional designers, do not reference high technology media, do not consider viable and thorough media selection factors, and do not reflect the knowledge of multiple media specialists. A review of the literature provided the basis for constructing a media pool containing high technology computer-based media and frequently used traditional media. The review also provided a list of the most important media selection attributes. A survey was constructed to estimate the effectiveness of the media across the media selection attributes on the basis of the knowledge of nineteen media specialists. The survey data analyses indicate that a more accurate knowledge base was produced by incorporating the expertise of multiple experts. The MSES evaluation data demonstrate significant improvements in the quality of the recommendations produced by individuals when given access to the MSES. The results of the user acceptance questionnaire indicate that MSES users were satisfied in their overall acceptance of the program.

The Development and Evaluation of Media Selection Expert System: A Matrix Format Knowledge Base

PING-CHENG CHAO (趙平正)

National Convention of American Educational Research Assocation, Chicago, IL (1991)

The purpose of the research was to develop and evaluate a Media Selection Expert System (MSES) to address four significant limitations common to media selection models and media selection expret systems available today. These four limitations are as follows: First, manual media selection models are complicated and time consuming to use, the instructional designer may not have the time and desire to run through complicated flowcharts, matrices, or worksheets. Second, they do not reference high technology media. Third, they do not present viable and thorough media selection factors. Fourth, they do not reflect the knowledge of multiple media specialists.

The assumption was made that a MSES with a matrix format knowledge base would be a good starting point to address these issues. A review of the literature provided the theoretical basis for constructing a media pool that contains all currently available computer-based high technology media and includes all known critical media selection attributes.

A survey was constructed to acquire knowledge from multiple media specialists who were in either the U. S. Army training division or academic environments. An expert system was then developed to automate the media selection process. A four-stage process was followed to construct the MSES to ensure successful development. Finally, the MSES was thoroughly tested and evaluated by target users and domain experts. The performance of MSES was then compared to that of human experts.

The results of the data analysis demonstrated significant improvements in the quality of the recommendations produced by individuals when they are given access to the MSES. The results of the user acceptance questionnaire showed that domain experts and target users indicated a high satisfaction level concerning the overall user acceptance of MSES.

Based on the results of this study, three recommendations were made.

First, future studies be conducted which address the four significant limitations embedded in current media selection models and expert systems. Second, it may be worthwhile to assess the usefulness of all currently available media selection expert systems. Finally, comparative studies of rule-based approach and matrix format approaches will help lay the groundwork for more research in this important area.

Computing Supperquadics Using Binocular Stereo Sensor

LIANG-HUA CHEN (陳良華)

IEEE International Conference on Systems, Man, and Cybernetics, pp. 225-230 (1991)

Most of the previous research on superquadrics focus on recovering superquadrics using range image or synthetic depth data, and very little work has been done in developing complete recovery procedure for stereo images. This paper presents an integrated approach to recovering a superquadrical model of single object from stereo images. The algorithm combines the recovery processes of occluding contour, surface, and volumetric models in a cooperative and synergetic way. The aggregation of shape information is performed via model recovery. By integrating the depth information and orientation information from the respective surface and contour modules, the volumetric model based on superquadrics can be recovered robustly. This results in consistent interpretation of object and increase of system flexibility.

Part Segmentation for Object Recognition

LIANG-HUA CHEN (陳良華)

International Conference on Pattern Recognition (1992)

This paper addresses the problem of segmenting objects into parts using stereo images. There are three components in the part segmentation process: surface segmentation, region grouping, and volumetric models recovery/segmentation. The surface segmentation process segments the image into a set of regions such that each region represents a surface

smooth in depth. The region grouping process merges the segmented regions into meaningful part. Finally the process of volumetric model recovery/segmentation phase recovers the part model and segments that part into smaller parts if necessary. Since we use multi-shape models to drive the part segmentation process, we can capture more geometric properties of the object and the application domain of our approach is broader than that of the previous approaches.

鹼處理麵筋功能性之探討

何慧如 詹朝閔 馬美蓉 陳炯堂

食品科學 第十九卷 第二期 第 241-252 頁 (1992)

麵筋爲小麥蛋白質的主要成份，具良好延展性，唯水溶性差，限制了它在食品上的應用。然而，麵筋蛋白之胺基酸成分中，含有高比例的醯胺，若以 0.08 N 氫氧化鈉區分麵筋爲鹼溶性麵筋 (ASG) 與鹼不溶性麵筋，並於不同溫度下 (25°C、40°C、60°C) 加熱 30 分鐘進行去醯胺作用，以提高羧基含量，使麵筋之親水性、功能性增加即可提高其應用性，而且亦可應用於不同親水程度之食品蛋白質模式系統探討。鹼處理後之 ASG 於中和、透析及離心後，麵筋蛋白質之分子量於鹼處理溫度在 40°C 或以下不受影響。而且，高溫鹼處理所導致雙硫鍵斷裂及去醯胺百分率的增加，可增加水溶解度及吸水力。60°C 鹼處理 ASG 在吸水力及溶解度都優於在其他溫度鹼處理之 ASG。乳化性以 25°C 鹼處理 ASG，40°C ASG 較佳，而乳化安定性以 40°C 鹼處理 ASG 爲最高，至於吸油力則以 25°C 鹼處理 ASG 爲最佳。由統計分析得知，鹼處理溫度除了與親水性、水溶解度有關外，與其他功能性之間並無一定線性相關，但是蛋白質之某一最佳功能性皆可由鹼處理控制得到。故蛋白質須依其功能需要而做適當的鹼處理。

白蛋白輸液與營養支持對胃切除病患之血清白蛋白濃度的影響

蔡敬民 羅妲妤 張子明 丁海惠

Journal of Chinese Nutrition Society, **17**, 201-213 (1992)

本研究的目的在探討白蛋白輸液與營養支持對胃切除患者復原之影響。實驗共篩選出 24 位受試者，分成四組：(1) 加輸白蛋白液並給予足够的營養支持 (TN 組)；(2) 加輸白蛋白液但營養支持不足 (Tn 組)；(3) 未輸白蛋白液而營

養支持足够（*tN* 組）；(4) 未輸白蛋白液且營養支持不足（*tn* 組）。於手術後觀察病患每週血清白蛋白值的變化，來比較外輸白蛋白液與營養支持等因子對體內血清白蛋白值之影響。實驗結果顯示，手術後血清白蛋白總平均值 ≧3.0 g/dL 的病患比平均值 <3.0 g/dL 者有較好的腸道耐受性與較短的恢復期。接受白蛋白外輸液的兩組（*TN* 組和 *Tn* 組）在手術後前兩週的血清白蛋白平均值與後兩週並無顯著差異（$p<0.10$），而無外輸液兩組（*tn* 組和 *tn* 組）後兩週的血清白蛋白平均值卻比前兩週的值顯著上升（$p<0.05$）。在營養支持足够的狀況下（*TN* 組和 *tN* 組），患者的血清白蛋白平均值略有（$p<0.10$）上升的現象，但營養支持不足時（*Tn* 組和 *tn* 組），其血清白蛋白的平均值有下降的趨勢（$p<0.10$），而且比營養支持足够者有較長的住院天數。由此可以看出，血清白蛋白可以做爲臨床狀況的良好指標，而且足够的營養支持似乎比昂貴的白蛋白外輸液更能幫助患者血清白蛋白的回升。

比較不同膳食纖維來源對大白鼠脂質代謝之影響

楊佳玲　林子清　蔡敬民

食品科學　第十八卷　第四期　第 356-367 頁　(1991)

本實驗之研究目的在了解不同膳食纖維質來源，尤其米糠纖維是否有利於體內之脂質代謝？採用雄性 Wistar 大白鼠作爲實驗動物，先飼以含高脂肪之飼料一個月，而後分別餵予膳食纖維來源爲米糠、燕麥糠、大麥糠以及聚糊精之含膽固醇飼料，以纖維素作爲對照組，四週後取血漿與肝臟，測其中之總脂質、總膽固醇及三酸甘油酯，並收集最後三天之糞便，測中性及酸性固醇。結果顯示，與纖維素比較之下，添加米糠、燕麥糠、大麥糠及聚糊精，並不能更有效降低血漿與肝臟膽固醇，其中米糠組之血漿膽固醇比其他組高（$p<0.05$），其餘各組間無顯著差異（$p<0.05$）；聚糊精組之肝膽固醇較對照組高（$p<0.05$）；燕麥糠組之血漿三酸甘油酯較對照組及聚糊精組高（$p<0.05$）；而大麥糠對血與肝脂質之影響，與對照組無顯著差異（$p<0.05$）。綜合各項分析結果顯示，此 4 種膳食纖維來源對大白鼠之脂質代謝，並未顯示較纖維素有良好之影響。

比較不同油脂來源對大白鼠脂質代謝之影響

楊佳玲　楊淑貞　蔡敬民

食品科學　第十九卷　第一期　第 1-11 頁　(1992)

本研究之目的在探討不同脂肪酸組成之三種食用油脂對大白鼠質代謝之影響

。採用雄性 Wistar 大白鼠作爲實驗動物，以隨機取樣的方式分爲三組，每組七隻，餵飼高脂飲食一個月後，分別餵予油脂來源爲米糠油、棕櫚油及黃豆油之飼料，四週後取血漿與肝臟，測其中之總脂質、總膽固醇及三酸甘油酯，並集收最後三天之糞便，測中性及酸性固醇。結果顯示，血漿膽固醇以黃豆油組較其他兩組爲低（$p<0.05$），米糠油與棕櫚油組之間並無顯著差異；而三者於血漿及肝臟三酸甘油酯方面，無明顯之差異（$p<0.05$）；米糠油組之肝總膽固醇明顯低於棕櫚油及黃豆油組（$p<0.05$）；糞中性固醇排出量，米糠油組較棕櫚油組爲高（$p<0.05$）；糞酸性固醇排出量，三組之間無顯著差異。此外亦發現，三種食用油脂之飽和程度，P/S 及 (P+M)/S 與血漿脂質之反應並無一致性。而糞中性固醇排出量與肝膽固醇值呈逆相關性。因此可推論食用油脂之飽和程度非爲影響脂質代謝之主要因素。

以體外實驗法探討鋁對鐵吸收之影響

王果行　張明敏

中華營誌　第十七卷　第 137-145 頁　(1992)

以透析膜及大白鼠小腸模擬消化道酸鹼度之變化，觀察不同鋁濃度對鐵通過透析膜及大白鼠小腸壁的影響。結果顯示，鐵通過透析膜之量隨著反應液中鋁濃度（0、500、2,000 μg/ml）之增加而減少（$p<0.05$）。此種現象尤其是在酸鹼度變化模擬胃中狀況時（即 pH 由 2 變化至 pH 5）特別明顯。體外大白鼠小腸壁實驗結果顯示，在 pH 由 2 轉變至 5 的情況下，反應液中添加鋁（500、2,000 μg/ml）亦明顯的（$p<0.05$）抑制鐵通過小腸腸壁細胞的能力。

Studies on the Yield of Coupling Sugar from Starch Using Alkalophilic *Bacillus* CGTase

CHIHWEI P. CHIU (丘志威), YI-HSIN LEE,
HOANG-YUNG CHIANG AND HUNG-TSUNG TSAI

J. of Chin. Colld. and Intfac. Soc., **14**(2), 13-19 (1991)

Substrate containing 13% sucrose and 13% potato starch was treated with alkalophilic *Bacillus* CGTase at 85°C to liquefy the starch and subsequently at 55°C to proceed coupling reaction. The best conditions for starch liquefaction and coupling sugar formation were pH 7.5 and 8.5 respectively, same as the conditions used in the production of

cyclodextrins. Maximum yield of coupling sugar, about 10.5%, was attained after 30 hr reaction. In order to obtain the favorable formation of coupling sugar and the proper sucrose residue after coupling reaction, the optimal substrate concentration of starch ranges from 11% to 13%, and the ratio of sucrose to starch is 1.25.

Synthesis and Characterization of β-Cyclodextrin and Its Derivaties

I-Feng Wang, Chi-Feng Ko and Chihwei P. Chiu (丘志威)

J. of Chin. Colld. and Intfac. Soc., 14(2), 22-26 (1991)

The solubility of β-cyclodextrin is much lower than that of α- and γ-cyclodextrin. Therefore, β-cyclodextrin is easily crystallized and purified, making it much cheaper than the others. The low solubility limits the broad applications of β-cyclodextrin. *Bacillus acidopullulyticus* pullulanase catalyzed the reverse action in a mixture containing high concentration of β-cyclodextrn and maltose to produce branched cyclodextrin, such as maltosyl β-cyclodextrin. The solubility of maltosyl β-cyclodextrin is 151.6%, much higher then that of β-cyclodextrin, 1.85%. The yield of branched cyclodextrin with tharmostable debranched amylase was relatively low, and the enzyme should be used in a large quantity. About 50% of the products from the reaction of immobilized Pullulanase with substrate containing β-cyclodextrin and maltose was branched cyclodextrin. However, only 35% conversion of β-cyclodextrin was achieved when soluble pullulanase was employed. It is concluded that the application of immobilized pullulanase not only offers the repeated use of the enzyme but also enhances the yield of branched cycldoextrin.

Studies on the Stability of Carotenoids in Garland Chrysanthemum (*Ipomoea* spp.) as Affected by Microwave and Conventional Heating

B. H. Chen (陳炳輝)

Journal of Food Protection, 55(4), 296-300 (1992)

The effect of microwave and conventional heating on carotenoid

stability in garland chrysanthemum was studied. Each cooking treatment was conducted for 0, 2, 4, 8 and 16 min with two replications. The various carotenoids were analyzed by high-preformance liquid chromatography with photodiode-array detection. Experimental results suggested that microwave cooking could retain more β-carotene and less lutein than conventional cooking when the output power was 180 W. Epoxy-containing carotenoids were more susceptible to heat loss than othe carotenoids. Both *cis*-lutein and *cis*-β-carotene contents were higher with the increase of heating time. The increase of *cis*-β-carotene content also implied that the provitamin A activity would decrease.

An Improved Analytical Method for the Determination of Carotenes and Xanthophylls in Dried Plant Materials and Mixed Feeds

B. H. CHEN (陳炳輝) AND S. H. YANG

Food Chemistry, 44, 61-66 (1992)

Various experiments were performed to evaluate the current Association of Official Analytical Chemists (AOAC) method used for the determination of carotenes and xanthophylls in dried plant materials and mixed feeds. Incorporation of nitrogen gas and antioxidants such as BHT during extraction and saponification increased carotene and xanthophyll contents from 2 to 4% and from 19 to 30%, respectively. Combination of extraction time and saponification time for 16 h increased xanthophyll content by approximately 23%. Cold saponification also resulted in higher xanthophyll contents than hot saponification. A 1:1 mixture of MgO and diatomaceous earth was found suitable to replace silica gel as the adsorbent to separate major carotenoids by open-column chromatography. A binary solvent system of hexane-acetone and a ternary solvent system of hexane-acetone-methanol in different ratios were used to separate carotenes, monohydroxy pigments, dihydroxy pigments and polyoxy pigments. The amounts of β-carotene and lutein were also substantially increased by using the modified AOAC method.

Determination of Carotenoids and Chlorophylls in Water Convolvulus (*Ipomoea aquatica*) by Liquid Chromatography

B. H. CHEN (陳炳輝) AND Y. Y. CHEN

Food Chemistry, **45**, 129-134 (1992)

The carotenoids and chlorophylls present in water convolvulus (*Ipomoea aquatica*) were analyzed by high-performance liquid chromatography (HPCL) with photodiode-array detection and their identify confirmed by thin-layer chromatography (TLC). An HPLC quaternary solvent system of acetonitrile methanol chloroform hexane (75:12.5:7.5:7.5, v/v/v/v) resolved 14 peaks in 20 min by using a 25 cm reversed-phase column, of which 12 pigments were identified. These pigments include carotenoids, chlorophylls and their isomers. The coefficient of variation for pigment concentrations was less than 12% in five sample analyses. A TLC quaternary solvent system of hexane acetone chloroform methanol in different proportions also resolved 10 pigments on silica gel layers. In addition to *cis*-lutein and *cis*-β-carotene, all major pigments were adequately resolved by TLC.

早期蛋白質修飾對田鼠成熟後脂質代謝之影響

盧義發　陳慧環

中華營誌　第十七卷　第 39-54 頁　(1992)

出生三週剛斷奶的雄性田鼠，餵食含酪蛋白或大豆蛋白的半合成飼料四週（第一期），然後轉爲給予普通飲食（第二期）一週（實驗一）或四週（實驗二）；最後再經膽固醇挑戰二週（第三期），以瞭解早期不同蛋白質的攝取對成長後體內脂質代謝的影響。實驗一經普通飲食一週（第二期）後，兩組的血清、肝臟脂質及糞便酸性固醇排泄量皆無顯著差異；先前餵大豆蛋白的田鼠於膽固醇挑戰（第三期）的初期，其血清膽固醇濃度明顯低於酪蛋白組；但經過二週膽固醇挑戰結束後，血清膽固醇濃度的烙印效果消失，值得注意的是此時大豆蛋白組的糞便酸性固醇類排泄量明顯高於酪蛋白組，但兩組間的血清和肝臟脂質濃度卻無顯

著差異。實驗二經四週普通飲食（第二期）後，再給予膽固醇挑戰二週（第三期），發現大豆蛋白組的糞便酸性固醇排泄量明顯高於酪蛋白組，而此現象和實驗一相似，但血清膽固醇或其他血清、肝臟脂質濃度皆無烙印效果的反應。本研究證實早期以飲食蛋白質修飾的田鼠，其血清膽固醇濃度的烙印效果，暫時表現於膽固醇挑戰的初期。

微 波 食 品 之 開 發

蔣見美　陳炯堂　吳景陽　高馥君　葉安義　郭靜娟　張永欣

微波食品加工原理與應用　第 10 章　第 199-228 頁　(1992)

所謂微波菜餚是由食品工業界研究發展之食品，經微波加熱即可供食者，包括調理或半調理之菜餚，其保存方法有常溫流通、冷藏及冷凍三大類。適合於業者開發的菜餚可分兩種，一是屬於高價位，調理過程繁瑣、費時之款式，可替消費者省下不少時間和精力。另一種是具有普及性，薄利多銷，但仍以自己調理不易者屬之。

微波食品開發前與一般新產品相同，其所考慮之項目不外乎種類、對象、份量、營養、貯藏期限、產品形態、品質要求及價格等。但微波食品應特別注意的除需具備獨特配方外，同時應選擇適合之包裝內容，並配合最後微波加熱之正確操作方法及標示完整之使用說明。

微波加熱對食品物化特性的影響

陳炯堂　張永欣

微波食品加工原理與應用　第 4 章　第 79-88 頁　(1992)

微波加熱食品比傳統加熱方式，如煎、煮、烤、炸等皆來得快速而且簡便，不但沒有油煙，亦不需炊具，因此，近年來食品工業或家庭，應用微波加熱於解凍、烹調等皆有增加的趨勢。微波快速的加熱方式，卻造成食品有不同於傳統加熱的品質，例如微波加熱不易使食品如同高溫油炸、焙烤一樣，表面具有金黃色澤、酥脆及散發特殊香味之特性 (Ohlsson，1990)。目前僅利用微波加熱片 (microwave heat susceptor) 來局部解決此問題 (Lorenson，1989)。如欲達到完全解決問題的目的，需進一步研究。

微波食品之市場現況與發展趨勢

張永欣　陳建斌　張哲朗　蔣見美

微波食品加工原理與應用　第 11 章　第 231-249 頁　(1992)

我國的微波調理食品香度有規模地上市案例似應以龍鳳食品公司於 1989 年 9 月份一齊推出的冷凍香菇燒賣、冷凍海棠果、冷凍蟹黃燒賣、冷凍蝦飯、冷凍魚翅餃、冷凍椰蓉煎堆、冷凍芝麻球等八道港式點心爲代表，該公司當月份曾爲此案花費 400 餘萬元經費打電視廣告並辦理微波爐抽獎大贈送，強烈訴求調理冷凍食品以微波加熱食用的方便及可口。該公司當時辦理廣告及促銷的第一個月份，上列八項微波加熱冷凍點心的業績曾達三百餘萬元，而後卻業績略呈下退。該公司迅即檢討原因後，發現由於廣告訴求中太強調微波加熱的關係，使得家裏沒有微波爐的消費者卻步不敢購買。因此，該公司當即將強調的重點由「微波點心」，改爲微波爐及蒸鍋都適用的「港式點心」，爾後這些港式點心的每月銷售成績都有很緩慢但穩定的成長，現在約達每月 600 萬元的水準。

中國歷代服飾之蒐證與傳統服飾郵票繪製之研究

胡　澤　民

荆州博物館編　中國古代服飾國際學術會議論文　(1991)

從 1985 年元月開始，至 1991 年六月止，前後七年，完成「中華傳統服飾郵票」的蒐集與繪製之研究；共計發行 6 組 24 枚中國歷史男女服飾郵票與明信片，爲了使這一系列郵票更具客觀價值，筆者以文圖（幻燈片）說明，有關蒐證圖片、資料、出土地點、年代、時間、典藏處等，整合出各年代服飾的典型特徵，並將各朝代形制、色彩、圖紋等具體區割搭配不同人物情態，重新給予「打扮定裝」，使每組郵票皆具特色。

中國傳統增強體能飲食之研究

李寧遠　黃韶顏　巫錦霖　阮雅倩　陳淑娟

中華家政學會　第二十六期　第 60-63 頁　(1992)

本文探討中國之飲食文化，包括歷代飲食風俗、中國飲食療法發展史、食療、食療中常見強身保健的食物和中草藥、各種食物特殊療效，由文獻探討後發展出增強體能的菜單，由不同體質的人來品嚐看其身體變化來決定食物的食療效果，結果以人參與靈芝之療效對一般人增強體能最爲有效。

幼兒發展與遊戲

林 惠 雅

親子科學輯要 第七輯 第 33-37 頁 (1992)

幼兒的生活重心是遊戲，而遊戲對幼兒身心成長與學習亦扮演相當重要的角色。然而如何依據幼兒時期發展上的特色，提供適宜的遊戲和玩具以促進幼兒的成長乃成爲值得重視的課題。本文主要內容卽探討不同年齡階段幼兒發展與遊戲的關係。

個人現代性對婚姻滿意度之影響

利 翠 珊

中華家政 第二十期 第 67-75 頁 (1991)

本研究的目的，在探討夫妻雙方的個人現代性及其有關變項對婚姻滿意度的影響，受試爲 240 對留美學生夫妻。研究結果發現男性的個人現代性並未顯著地影響其婚姻滿意度，而女性的教育程度及個人現代性卻對婚姻滿意度有顯著的影響。教育程度越高的女性，個人現代性與婚姻滿意度都較高，但是當女性的現代性越高時，婚姻滿意度卻有相對下降的趨勢。在將夫妻雙方的資料合併處理時，則發現男性的個人現代性顯著地影響夫妻雙方的婚姻滿意度。現代型的丈夫，無論妻子爲傳統或現代，夫妻的婚姻滿意度均顯著地高於傳統型丈夫組成的家庭。作者根據研究發現，分別對未來研究及實務工作提出了建議。